The Dissertation Committee for Amit Vijay Kulkarni certifies that this is the approved version of the following dissertation:

Instant Center Based Kinematic and Dynamic Motion Synthesis for Planar Mobile Platforms

Committee:

Delbert Tesar, Supervisor

Alexis Kwasinski

Chetan Kapoor

Richard Crawford

Richard Hooper

Richard Neptune

S.V. Sreenivasan

Instant Center based Kinematic and Dynamic Motion Synthesis for Planar Mobile platforms

by

Amit Vijay Kulkarni, B.Eng., M.Tech.

Dissertation

Presented to the Faculty of the Graduate School of

The University of Texas at Austin

in Partial Fulfillment

of the Requirements

for the Degree of

Doctor of Philosophy

The University of Texas at Austin

December 2009

To my better half, Dipty

Acknowledgments

I am very thankful to my supervisor, mentor, and teacher, Prof. Del Tesar for his continuous guidance and mentorship throughout my doctoral studies. His vision in the area of Mechanisms, Robotic Systems and general Mechanical Engineering served as a “light house” for me through these years.

I am grateful to Dr. Chetan Kapoor for his constant encouragement and guidance. I am thankful to my colleagues at RRG, namely, Dr. Dinesh Rabindran, Mr. Ganesh Krishnamurthy, Dr. Pradeep Ashok, Dr. Oziel Rios, Dr. Mitch Pryor, Mr. Brian O’Neil, and Dr. Jagadish Janardhan who were my support system at RRG from a technical as well as personal standpoint.

I am grateful to my dissertation committee members, namely, Dr. S. V. Sreenivasan, Dr. Richard Neptune, Dr. Richard Hooper, Dr. Richard Crawford, Dr. Chetan Kapoor, and Dr. Alexis Kwasinski for their guidance and valuable suggestions.

My thanks are due to RRG administration staff, Mrs. Betty Wilson, Mrs. Malena Pomerleau-Petersen, and Mrs. Janie Terrel and to the Administrative Associate for Manufacturing & Design, Ms. Cindy Raman and the Mechanical Engineering Graduate Coordinator, Mr. David Justh for their administrative and logistical help.

I am thankful to the God for my health and well being through these years. I would also like to thank my parents, Mrs. Vinaya and Mr. Vijay Kulkarni and in-

laws, Dr. Shailaja and Mr. Pramod Maybhate for their love and belief in me. This endeavor would not have been successful without the encouragement and understanding of my loving wife and best friend, Dipty.

This work was supported by Department of Energy's University Research Program in Robotics (URPR Grant number DE-FG52-2004NA25591), Idaho National Lab (Grant number UTA08-039; SUBC# 0007245) and ConMediSys Inc.. I would specifically like to thank Mr. David Bruemmer and Dr. Curtis Neilson, Mr. Douglas Few, Mr. Robert Kinoshita from Idaho National Lab and Mr. Ralph Smucker from ConMediSys Inc.

Instant Center Based Kinematic and Dynamic Motion Synthesis for Planar Mobile Platforms

Publication No._____

Amit Vijay Kulkarni, Ph.D.

The University of Texas at Austin, 2009

Supervisor: Delbert Tesar

For a general *J* wheeled mobile platform capable of up to *3-Degrees-Of-Freedom* (DOF) planar motion, there are up to *2J* independent input parameters yet the output of the planar platform is specified with only three independent parameters. Currently, the motion synthesis for such platforms is done with a Jacobian based "pseudo" inverse that uses a rectangular matrix for Jacobian. However, a mobile platform is a parallel mechanism and has a more direct solution to the inverse kinematics problem. To this effect, we propose a physical methodology for kinematic modeling of multi-wheeled mobile platforms using Instant Centers (IC) to describe the kinematic state of all system points up to the k^{th} order using a generalized algebraic formulation. This is achieved by using a series of ICs (velocity, acceleration, jerk, etc.) where each point in the system has a time state with its magnitude proportional to the radial distance of the point from the associated IC and at a constant angle relative to that radius. The use of IC's for mobile platform

kinematics is not new, however we present a completely generalized and extensive formulation that also treats the higher order kinematics. *To the best of our knowledge, this is the first time the third and higher order ICs have been presented in the literature.*

The components of this research effort are: (i) extension of the theory of instantaneous invariants to the higher order motion by generalizing the theory to any order, (ii) studying some special case 1-DOF, 2-DOF motions to understand the physical nature of the higher order ICs, (iii) applying the results of (i) and (ii) to the motion synthesis of planar, wheeled mobile platforms by first categorizing them into four distinct categories, and (iv) studying the dynamic model of a representative mobile platform to emphasize the importance of wheel dynamics and traction parameters on the performance of the mobile platform. The IC based formulation presents a concise expression for a general order time state of a general point on the rigid body with the magnitude and direction separated and identified. We showed that the method based on instant centers provides a straightforward and yet physically intuitive way to synthesize a general k^{th} order planar motion of mobile platforms. The study of special case 1-DOF/2-DOF motions emphasized the geometric nature of the higher order ICs and also helped understand the influence of instantaneous kinematic states (such as angular velocity ω, angular acceleration, α, etc.) on the various ICs. The application of this theory to planar mobile platform allowed us to categorize the platforms based on their dexterity and to generalize the motion synthesis to some extent. The study of the dynamic model of a representative mobile platform showed us that the redundant inputs (*2J* inputs versus *3* outputs) in this case may be employed to sustain and manage the uncertainties and nonlinearities in the wheel ground interaction.

Table of Contents

List of Tables xiv
List of Figures xv

1 INTRODUCTION 1

1.1 Background 1
1.2 Research Outline 3
1.3 Scope of the Research 4
1.4 Outline of the Report 4

2 INSTANT CENTER BASED KINEMATIC FORMULATION FOR 3-DOF PLANAR MOTION 6

2.1 Introduction 6
2.2 Literature Review 6
2.3 Generalized Notation 10
2.4 First Order (Velocity) Planar Motion of a Rigid Body 12
2.4.1 First Order Instant Center Formulation: Special Cases 16
2.5 Second Order (Acceleration) Planar Motion of a Rigid Body 19
2.5.1 Directionality and Proportionality: Properties of the Acceleration IC 21
2.5.2 A Note on the Uniqueness of the Value of the Orientation Angle, β_2 23
2.5.3 Second Order Instant Center Formulation: Special Cases 24
2.6 Higher Order Planar Motion of a Rigid Body 27
2.7 Summary and Discussion 35

3 KINEMATIC FORMULATION USING INSTANT CENTERS: STUDY OF SPECIAL SCENARIOS 38

3.1 Introduction 38
3.2 Case 1: A Circle Rolling on a Straight Line without Slipping 39
3.2.1 Schematic Representation of the System 39
3.2.2 First Order Kinematics for A Circle Rolling on a Straight Line without Slipping 40
3.2.3 Second Order Kinematics for A Circle Rolling on a Straight Line without Slipping 41
3.2.3.1 Special Case Scenarios for the Second Order Motion for A Circle Rolling on a Straight Line without Slipping 44
3.2.3.2 Simulation Plot for Second Order Motion of A Circle Rolling on a Straight Line without Slipping 46
3.2.4 Third Order Kinematics for A Circle Rolling on a Straight Line without Slipping 48
3.2.4.1 Simulation Plot of the Third Order Motion of A Circle Rolling on a Straight Line without Slipping 49
3.2.4.2 Special Case Scenarios for the Third Order Motion of A Circle Rolling on a Straight Line without Slipping 50
3.2.4.3 Summary of the Third Order Motion of A Circle Rolling on a Straight Line without Slipping 52
3.2.5 Fourth Order Kinematics of A Circle Rolling on a Straight Line without Slipping 54
3.2.5.1 Simulation Plot for the Fourth Order Motion of A Circle Rolling on a Straight Line without Slipping 55
3.2.5.2 Special Case Scenarios for for the Fourth Order Motion of A Circle Rolling on a Straight Line without Slipping 56
3.2.5.3 Summary of the Fourth Order Motion of A Circle Rolling on a Straight Line without Slipping 62
3.3 Case 2: A Circle Rolling on another Circle 64
3.3.1 Kinematic Description of the System 64
3.3.2 First Order Kinematics of A Circle Rolling on another Circle 66
3.3.3 Second Order Kinematics of A Circle Rolling on another Circle 68

3.3.3.1 On the Radius of the Acceleration IC Locus Circle 70
3.3.3.2 Special Case Scenarios for Second Order Motion of A Circle Rolling on another Circle 74
3.3.4 Third Order Kinematics of A Circle Rolling on another Circle 76
3.3.4.1 Simulation Plot for the Fourth Order Motion of A Circle Rolling on another Circle 77
3.3.4.2 Special Case Scenarios for the Third Order Motion of A Circle Rolling on another Circle 78
3.3.5 Fourth Order Motion of A Circle Rolling on another Circle 84
3.3.5.1 Simulation Plot for Fourth Order Motion of A Circle Rolling on another Circle 85
3.3.5.1 Special Case Scenarios for Fourth Order Motion of A Circle Rolling on another Circle 86
3.3.5.2 Summary of Fourth Order Motion of A Circle Rolling on another Circle 93
3.4 Case 3: Circle Rolling with Slipping on a Straight Line 95
3.4.1 Wheel Slipping and Sliding 95
3.4.1.1 Definition of Slipping 96
3.4.1.2 Definition of Skidding 96
3.4.1.3 Definition of Sliding 97
3.4.2 The Slippage Factor 98
3.4.3 First Order Motion of Circle Rolling with Slipping on a Straight Line 99
3.4.4 Second Order Motion of Circle Rolling with Slipping on a Straight Line 100
3.4.4.1 Special Case Scenarios for the Second Order Motion of Circle Rolling with Slipping on a Straight Line 102
3.4.4.2 Simulation Plot 103
3.4.5 Third Order Motion of Circle Rolling with Slipping on a Straight Line 104
3.4.5.1 Simulation Plot for the Third Order Motion of Circle Rolling with Slipping on a Straight Line 104
3.4.5.2 Special Case Scenarios for Third Order Motion of Circle Rolling with Slipping on a Straight Line 105
3.4.6 Fourth Order Motion of Circle Rolling with Slipping on a Straight Line 107
3.4.6.1 Simulation Plot of Fourth Order Motion of Circle Rolling with Slipping on a Straight Line 107
3.4.6.2 Special Case Scenarios for Fourth Order Motion of Circle Rolling with Slipping on a Straight Line 108
3.5 Case 4: A Line Rolling without Slipping on a Circle 110
3.5.1 Schematic Representation of the System 110
3.5.2 First Order Motion of A Line Rolling without Slipping on a Circle 111
3.5.3 Second Order Kinematics of A Line Rolling without Slipping on a Circle 113
3.5.4 Third Order Kinematics of a Line Rolling without Slipping on a Circle 115
3.6 Summary and Discussion 117

4 MOBILE PLATFORM CONFIGURATIONS 120

4.1 Platforms with Fixed Wheels Mounted on a Common Rolling Axis on Either Side 120
4.1.1 Skid-Steer Platforms 121
4.1.1.1 Two Wheeled Platforms 122
4.1.1.2 Four Wheeled Platform 123
4.1.1.3 Six Wheeled Platform 124
4.1.1.4 Tracked Platform 124
4.1.2 Tricycle Platforms 125
4.1.3 Ackerman Steer Platforms 126
4.1.3.1 Ackerman-Steer Front Wheels with Two Passive Trailing Wheels 126
4.1.3.2 Ackerman Steered Front Wheels with Four Passive Trailing Wheels 127
4.1.3.3 Ackerman Steered Front Wheels with Passive /Active Trailing Tracks 128
4.1.4 Kinematic Formulation for the Platforms with Fixed Wheels 130
4.1.4.1 The First Order Motion Synthesis for the Platforms with Fixed Wheels 132
4.1.4.2 The Second Order Motion Synthesis for the Platforms with Fixed Wheels 136
4.1.4.3 Third Order Motion Synthesis for the Platforms with Fixed Wheels 140
4.1.5 Summary 144
4.2 Omnidirectional Platforms with Active Offset (Caster) Wheels 147
4.2.1 Kinematic Configurations for Mobile Platforms with Active Caster Wheels 149

4.2.1.1 Platform with Two Active caster Wheels 149
4.2.1.2 Platform with Three Active Caster Wheels 151
4.2.1.3 Platform with Four Active caster Wheels 151
4.2.1.4 A General Mobile Platform with *J* Active caster Wheels 152
4.2.2 Kinematic Formulation for a General Wheeled Mobile Platform with J Caster Wheels *154*
4.2.3 The Second Order Motion Synthesis for the Platforms with Active Caster Wheels *156*
4.2.3.1 Computation of Wheel Input Accelerations 161
4.2.3.2 Third Order Motion Synthesis for the Platforms with Active Caster Wheels 163
4.3 Platforms with Centered Wheels 167
4.3.1 Different Configurations for the Platforms with Active Centered Wheels *168*
4.3.1.1 Platform with Two Active Centered Wheels 169
4.3.1.2 Platforms with Three Active Centered Wheels 170
4.3.1.3 Platforms with Four Active Centered Wheels 171
4.3.2 Kinematic Description for the Platforms with Active Centered Wheels *172*
4.3.2.1 First Order Motion Synthesis for the Platforms with Active Centered Wheels 173
4.3.2.2 The Second Order Motion Synthesis for the Platforms with Active Centered Wheels 174
4.3.2.3 Third Order Motion Synthesis for the Platforms with Active Centered Wheels 179
4.4 Platforms with Omnidirectional Wheels 182
4.4.1 Different Configurations for the Mobile Platforms With Omni-Wheels *184*
4.4.1.1 Mobile Platform with Three Omni-wheels 184
4.4.1.2 Mobile Platform Configurations with Four Omni wheels 184
4.4.2 Kinematic Description for a General Platform with J Omni Wheels *185*
4.4.2.1 First Order Motion Synthesis for the Mobile Platform with Omni Wheels 187
4.4.2.2 The Second Order Motion Synthesis for the Mobile Platform with Omni Wheels 189
4.4.2.3 Third Order Motion Synthesis for the Mobile Platform with Omni Wheels 194
4.5 Summary and Discussions 197

5 DEMONSTRATIVE EXAMPLES OF THE MOTION SYNTHESIS FOR PLATFORMS WITH CONVENTIONAL WHEELS 199

5.1 Straight Line Motion of the Mobile Platforms 201
5.1.1 Straight Line Motion without Orientation Change *201*
5.1.2 Straight Line Motion with Orientation Change *202*
5.1.2.1 Motion Synthesis: The Platform with Three Centered Wheels 205
5.1.2.2 Motion Synthesis: The Platform with Three Caster Wheels 207
5.2 Circular Motion 210
5.2.1 Circular Motion when Platforms Face the Direction of Travel *210*
5.2.2 Platforms Traveling on a Circular Path with Fixed Orientation *214*
5.3 Discontinuous Path with Straight Lines 215
5.3.1 C^1 Discontinuous Path with Straight Lines with Orientation Control *216*
5.3.1.1 Motion Synthesis for the Tricycle Platform or the Platform with Three Active Centered Wheels 217
5.3.1.2 Motion Synthesis for the Platform with Three Active Caster Wheels 218
5.3.2 Platforms Traveling on a Straight Line Discontinuous Path with Fixed Orientation . *219*
5.3.2.1 Motion Synthesis for the Platform with Three Active Centered Wheels 220
5.3.2.2 Motion Synthesis for the Platform with Three Active Caster Wheels 221
5.4 Platforms Traveling on a Discontinuous, Curved Path 223
5.4.1 Platforms Traveling on a Discontinuous, Curved Path Facing Direction of the Travel *223*
5.4.1.1 Motion Synthesis for the Tricycle Platform or the Platform with Three Active Centered Wheels 224
5.4.1.2 Motion Synthesis for the Platform with Three Active Caster Wheels 225
5.4.2 Platforms Traveling on a Discontinuous Curved Path with Fixed Orientation *225*
5.5 Summary and Discussions 226

6 DYNAMICS OF MOBILE PLATFORMS 228

6.1 Introduction 228
6.2 Description of the Mobile Platform 229
6.3 Force/Moment Equilibrium Equations 232
6.3.1 Force and Moment Equilibrium for the Platform Body 233
6.3.2 Force and Moment Equilibrium for the j^{th} Wheel Subsystem 235
6.4 Wheel Dynamics 237
6.4.1 Ground Contact Forces 237
6.4.1.1 Longitudinal Friction Coefficient and Tractive (Braking) Force 238
6.4.1.2 Lateral Friction Coefficient and Lateral (Cornering) Force 241
6.4.1.3 Lateral (Cornering) Coefficient and Normal Load 241
6.4.1.4 Lateral (Cornering) Coefficient and Inflation Pressure 242
6.4.2 Rolling Resistance Moment 242
6.4.2.1 Tire Pressure 243
6.4.2.2 Temperature 243
6.4.2.3 Rolling Resistance Moment and the Vehicle Speed 244
6.4.2.4 Rolling Resistance Moment and the Ground Surface Quality 244
6.4.3 Actuator Limitations 245
6.4.4 Platform Performance Factors 245
6.5 Numerical Example 246
6.5.1 Dynamic Motion Programming 248
6.5.2 Kinematic Motion Synthesis 249
6.5.2.1 Operational Space Motion Description 249
6.5.2.2 Motion Synthesis for the Wheel Subsystems 250
6.5.3 Dynamic Motion Synthesis 254
6.5.3.1 Platform Body Forces 254
6.5.3.2 Wheel Subsystem Dynamics 257
6.5.4 Dynamic Synthesis Under Varying External Conditions 259
6.6 Summary 260

7 SUMMARY AND FUTURE WORK 262

7.1 Introduction 262
7.2 Research Summary and Conclusions 263
7.2.1 Research Objectives 263
7.3 Literature Review Summary 264
7.4 Research Results and Discussions 265
7.4.1 IC Based Formulation 266
7.4.1.1 General Discussions 269
7.4.1.2 Numerical Example of Motion Planning 271
7.4.1.3 Study of Classical Motions to Understand Physical Meaning of ICs 274
7.4.2 Mobile Platform Kinematics and Dynamics 281
7.4.2.1 Dynamic Motion Synthesis for Mobile Platforms 287
7.4.3 Primary Contributions 297
7.5 Recommendations and Future Work 298
7.5.1 Short Term Plan 298
7.5.1.1 Studying Wheel Dynamics 298
7.5.1.2 Wheel Dynamics Based Performance 301
7.5.1.3 Payload Interaction 302
7.5.1.4 Spatial Mobile Platforms 303
7.5.2 Long Term Plan 303
7.5.2.1 Uneven Terrain 303
7.5.2.2 Necessary Mobile Platform Decision Theory/Software Development 304
7.5.2.3 Development Forecast 306

APPENDIX **308**
Appendix A 308
REFERENCES **324**

List of Tables

TABLE 2.1: SUMMARY OF THE IC BASED KINEMATIC FORMULATION FOR MOBILE PLATFORMS 37
TABLE 3.1: SUMMARY OF THE THIRD ORDER MOTION PROPERTIES IN SPECIAL CASE SCENARIOS FOR A CIRCLE ROLLING ON A STRAIGHT LINE 53
TABLE 3.2: FOURTH ORDER MOTION FOR A CIRCLE ROLLING ON A STRAIGHT LINE: SPECIAL CASE SCENARIO WHEN $\boldsymbol{\alpha = 0, \text{and } \omega \neq 0 \text{ or } \alpha \neq 0}$. THE FOURTH ORDER IC IS AT POINT P [0, 0] 58
TABLE 3.3: SUMMARY OF THE FOURTH ORDER MOTION PROPERTIES IN SPECIAL CASE SCENARIOS FOR A CIRCLE ROLLING ON A STRAIGHT LINE 63
TABLE 3.4: THIRD ORDER MOTION FOR A CIRCLE ROLLING INSIDE ANOTHER CIRCLE: SUMMARY OF SPECIAL CASES 83
TABLE 3.5: SUMMARY OF THE FOURTH ORDER MOTION PROPERTIES FOR SPECIAL CASE SCENARIOS FOR A CIRCLE ROLLING INSIDE ANOTHER CIRCLE 94
TABLE 3.6: SUMMARY OF THE THIRD ORDER MOTION PROPERTIES IN SPECIAL CASE SCENARIOS FOR A CIRCLE ROLLING ON A STRAIGHT LINE WITH SLIPPING/SKIDDING 106
TABLE 3.7: SUMMARY OF THE FOURTH ORDER MOTION PROPERTIES IN SPECIAL CASE SCENARIOS FOR A CIRCLE ROLLING ON A STRAIGHT LINE 109
TABLE 3.8: SUMMARY OF THE IC LOCI FOR A CIRCLE ROLLING ON A STRAIGHT LINE..... 119
TABLE 4.1: QUALITATIVE COMPARISON OF THE FOUR CATEGORIES OF PLANAR MOBILE PLATFORMS 198
TABLE 6.1: GEOMETRIC AND MASS PROPERTIES OF THE MOBILE PLATFORM WITH THREE ACTIVE CASTER WHEELS 246
TABLE 7.1: RESEARCH OBJECTIVES 263
TABLE 7.2: LITERATURE REVIEW 264
TABLE 7.3: SUMMARY OF THE IC BASED KINEMATIC FORMULATION FOR MOBILE PLATFORMS 268
TABLE 7.4: SPECIAL CASE SCENARIOS FOR THE FIRST AND SECOND ORDER ICS 270
TABLE 7.5: SUMMARY OF THE NUMERICAL EXAMPLE RESULT 273
TABLE 7.6: THE FOURTH ORDER MOTION FOR A CIRCLE ROLLING ON A STRAIGHT LINE: SPECIAL CASE SCENARIO WHEN $\boldsymbol{\alpha = 0, \text{and } \omega \neq 0 \text{ or } \alpha \neq 0}$. THE FOURTH ORDER IC IS AT POINT P [0, 0] .. 276
TABLE 7.7: SUMMARY OF THE FOURTH ORDER MOTION PROPERTIES FOR SPECIAL CASE SCENARIOS FOR A CIRCLE ROLLING ON A STRAIGHT LINE 277
TABLE 7.8: SUMMARY OF THE IC LOCI FOR A CIRCLE ROLLING ON A STRAIGHT LINE..... 280
TABLE 7.9: QUALITATIVE COMPARISON OF THE FOUR CATEGORIES OF PLANAR MOBILE PLATFORMS 282
TABLE 7.10: GEOMETRIC AND MASS PROPERTIES OF THE MOBILE PLATFORM WITH THREE ACTIVE CASTER WHEELS 289
TABLE 7.11: PRIMARY CONTRIBUTIONS 297

List of Figures

FIG. 2.1: GENERALIZED NOTATION FOR THE K^{TH} ORDER 3-DOF PLANAR MOTION OF A RIGID BODY 11
FIG. 2.2: DESCRIPTION OF AN INSTANTANEOUS BODY FIXED FRAME {2} AT THE FIRST ORDER IC 14
FIG. 2.3: DESCRIPTION OF THE FIRST ORDER MOTION OF GENERAL POINTS IN THE RIGID BODY USING THE FIRST ORDER (VELOCITY) IC 16
FIG. 2.4: SPECIAL CASE FOR THE FIRST ORDER, 3-DOF, PLANAR MOTION OF A RIGID BODY WHEN THE VELOCITY OF POINT P IS ZERO. THE LOCATION OF THE VELOCITY IC IS COINCIDENT WITH POINT P. 17
FIG. 2.5: SPECIAL CASE FOR THE FIRST ORDER, 3-DOF, PLANAR MOTION OF A RIGID BODY WHEN THE ANGULAR VELOCITY OF THE BODY IS ZERO. THE LOCATION OF THE VELOCITY IC IS AT THE INFINITY. 18
FIG. 2.6: THE LOCATION OF THE VELOCITY IC FOR A TWO WHEELED DIFFERENTIALLY DRIVEN PLATFORM IS CONSTRAINED TO THE AXIS OF WHEEL ROTATION 18
FIG. 2.7: THE VELOCITY IC COINCIDENT WITH ONE OF THE WHEEL CENTER FOR A TWO WHEELED DIFFERENTIALLY DRIVEN PLATFORM 19
FIG. 2.8: DESCRIPTION OF THE SECOND ORDER MOTION OF A GENERAL POINT IN THE RIGID BODY USING THE ACCELERATION IC 22
FIG. 2.9: TANGENTIAL AND NORMAL COMPONENTS OF THE ACCELERATION OF A GENERAL POINT WITH RESPECT TO THE ACCELERATION IC 24
FIG. 2.10: SPECIAL CASE SCENARIO FOR THE SECOND ORDER, 3-DOF, PLANAR MOTION OF A RIGID BODY WHEN THE ANGULAR VELOCITY OF THE BODY IS ZERO 25
FIG. 2.11: SPECIAL CASE SCENARIO FOR THE SECOND ORDER, 3-DOF, PLANAR MOTION OF A RIGID BODY WITH ZERO ANGULAR ACCELERATION 26
FIG. 2.12: SPECIAL CASE SCENARIO FOR THE SECOND ORDER, 3-DOF, PLANAR MOTION OF A RIGID BODY WHEN THE ACCELERATION OF POINT P IS ZERO: ANGULAR ACCELERATION IC IS COINCIDENT WITH P 26
FIG. 2.13: SPECIAL CASE SCENARIO FOR THE SECOND ORDER, 3-DOF, PLANAR MOTION OF A RIGID BODY WITH ZERO ANGULAR VELOCITY AND ANGULAR ACCELERATION: ACCELERATION IC AT INFINITY 27
FIG. 2.14: THE THIRD AND FOURTH ORDER MOTION DESCRIPTION OF A RIGID BODY USING THE ICS .. 31
FIG. 2.15: K^{TH} ORDER KINEMATICS OF A GENERAL RIGID BODY 34
FIG. 3.1: KINEMATIC STATE DESCRIPTION OF A CIRCLE ROLLING ON A STRAIGHT LINE WITHOUT SLIPPING OR SKIDDING 39
FIG. 3.2: THE FIRST ORDER MOTION DESCRIPTION FOR A CIRCLE ROLLING ON A STRAIGHT LINE WITHOUT SLIPPING 40
FIG. 3.3: LOCATION OF THE ACCELERATION IC BASED ON THE VALUE OF CONSTANT ANGLE B_2 UNDER TWO DIFFERENT MOTION SCENARIOS: A) WHEN VALUES OF BOTH THE ANGULAR ACCELERATION AND ANGULAR VELOCITY OF THE CIRCLE ARE INSTANTANEOUSLY 1, AND B) WHEN VALUES OF BOTH THE ANGULAR ACCELERATION AND ANGULAR VELOCITY OF THE CIRCLE ARE INSTANTANEOUSLY -1 43
FIG. 3.4: ZERO ANGULAR ACCELERATION: LOCATION OF THE ACCELERATION IC IS AT THE CENTER OF THE CIRCLE 44
FIG. 3.5: ZERO ANGULAR VELOCITY: THE ACCELERATION INSTANT CENTER AT THE POINT OF CONTACT OF THE CIRCLE AND THE STRAIGHT LINE 45
FIG. 3.6: THE GENERAL LOCUS OF THE ACCELERATION IC FOR A CIRCLE ROLLING ON A STRAIGHT LINE WITHOUT SLIPPING IS A CIRCLE WITH DIAMETER OP 46
FIG. 3.7: SIMULATION PLOT FOR THE ACCELERATION IC FOR A CIRCLE (RADIUS = 1 FT) ROLLING ON A STRAIGHT LINE WITHOUT SLIPPING 47
FIG. 3.8: CIRCLE ROLLING ON A STRAIGHT LINE WITHOUT SLIPPING OR SKIDDING: THE LOCUS OF THE THIRD ORDER IC FOR A GENERAL MOTION 49

FIG. 3.9: CIRCLE ROLLING ON A STRAIGHT LINE WITHOUT SLIPPING: THE THIRD ORDER IC LOCATION WHEN $\boldsymbol{\alpha \neq 0, \omega = 0}$ 50
FIG. 3.10: A CIRCLE ROLLING ON A STRAIGHT LINE WITHOUT SLIPPING: THE THIRD ORDER IC LOCATION WHEN $\boldsymbol{\alpha = 0, \omega \neq 0, \text{and } \alpha = 0}$ 51
FIG. 3.11: A CIRCLE ROLLING ON A STRAIGHT LINE WITHOUT SLIPPING: THE THIRD ORDER IC LOCATION WHEN $\boldsymbol{\alpha \neq 0, \alpha = 0, \omega \neq 0}$ 52
FIG. 3.12: CIRCLE ROLLING ON A STRAIGHT LINE WITHOUT SLIPPING: THE LOCUS OF FOURTH ORDER IC FOR A GENERAL MOTION 56
FIG. 3.13: CIRCLE ROLLING ON A STRAIGHT LINE WITHOUT SLIPPING: THE FOURTH ORDER IC LOCATION WHEN $\boldsymbol{\alpha \neq 0, \alpha = \omega = 0}$ 57
FIG. 3.14: CIRCLE ROLLING ON A STRAIGHT LINE WITHOUT SLIPPING: THE FOURTH ORDER IC LOCATION WHEN $\boldsymbol{\alpha = 0, \text{and either } \omega \neq 0 \text{ or } \alpha \neq 0}$ 58
FIG. 3.15: THE CIRCLE ROLLING ON A STRAIGHT LINE: LOCUS OF THE FOURTH ORDER IC WHEN $\boldsymbol{\alpha \neq 0, \alpha \neq 0, \omega = 0}$ 60
FIG. 3.16: CIRCLE ROLLING ON A STRAIGHT LINE: THE LOCUS OF THE FOURTH ORDER IC WHEN $\boldsymbol{\alpha \neq 0, \alpha = 0, \omega \neq 0}$ 62
FIG. 3.17: KINEMATIC DESCRIPTION OF A CIRCLE ROLLING ON ANOTHER CIRCLE WITHOUT SLIPPING A) CIRCLE 1 ROLLS THE INSIDE OF CIRCLE 2; B) CIRCLE 1 ROLLS ON THE OUTSIDE OF CIRCLE 2 64
FIG. 3.18: THE LOCUS OF VELOCITY IC FOR THE GENERAL MOTION OF A CIRCLE ROLLING ON ANOTHER CIRCLE: CASE A) CIRCLE 1 ROLLS ON THE INSIDE OF CIRCLE 2, AND CASE B) CIRCLE 1 ROLLS ON THE OUTSIDE OF CIRCLE 2 67
FIG. 3.19: THE LOCUS OF ACCELERATION IC FOR THE GENERAL MOTION OF A CIRCLE ROLLING ON ANOTHER CIRCLE: CASE A) CIRCLE 1 ROLLS ON THE INSIDE OF CIRCLE 2, AND CASE B) CIRCLE 1 ROLLS ON THE OUTSIDE OF CIRCLE 2 69
FIG. 3.20: GENERAL LOCUS OF THE ACCELERATION IC FOR CIRCLE ROLLING ON THE OUTSIDE OF ANOTHER CIRCLE (NEGATIVE Λ) FOR DIFFERENT SCENARIOS: A) CIRCLE 2 (THE FIXED CIRCLE) IS A STRAIGHT LINE ($R2 = \infty$, THUS $\Lambda = \infty$) (SEC. 3.2), B) CIRCLE 2 IS LARGER THAN OR EQUAL TO CIRCLE 1 ($\boldsymbol{|\lambda| \geq 1}$), C) CIRCLE 2 IS SMALLER THAN CIRCLE 1 ($|\Lambda| < 1$), AND D) CIRCLE 1 (THE ROLLING CIRCLE) IS A STRAIGHT LINE ($R = \infty$, THUS $\Lambda = 0$) 72
FIG. 3.21: THE ACCELERATION IC LOCUS RADIUS FOR ROLLING CIRCLES, THREE SPECIAL CASES: 1) CIRCLE ROLLING ON A STRAIGHT LINE, 2) CIRCLE ROLLING ON THE INNER SIDE OF ANOTHER CIRCLE, AND 3) CIRCLE ROLLING ON THE OUTER SIDE OF ANOTHER CIRCLE 73
FIG. 3.22: A CIRCLE ROLLING ON ANOTHER CIRCLE: THE ACCELERATION IC LOCATION WHEN $\boldsymbol{\alpha \neq 0, \omega = 0}$: CASE A) CIRCLE 1 ROLLS ON THE INSIDE OF CIRCLE 2, AND CASE B) CIRCLE 1 ROLLS ON THE OUTSIDE OF CIRCLE 2 74
FIG. 3.23: THE ACCELERATION IC LOCATION WHEN $\boldsymbol{\alpha = 0, \omega \neq 0}$ FOR A CIRCLE ROLLING ON ANOTHER CIRCLE: CASE A) CIRCLE 1 ROLLS ON THE INSIDE OF CIRCLE 2, AND CASE B) CIRCLE 1 ROLLS ON THE OUTSIDE OF CIRCLE 2 75
FIG. 3.24: THE LOCUS OF THE THIRD ORDER IC FOR THE GENERAL MOTION OF A CIRCLE ROLLING ON ANOTHER CIRCLE WHEN A) ($\Lambda>0$) CIRCLE 1 ROLLS ON THE INSIDE OF CIRCLE 2, AND B) ($\Lambda<0$) CIRCLE 1 ROLLS ON THE OUTSIDE OF CIRCLE 2 77
FIG. 3.25: THE THIRD ORDER IC LOCATION WHEN $\boldsymbol{\alpha \neq 0, \omega = 0}$ FOR A CIRCLE ROLLING ON ANOTHER CIRCLE: CASE A) CIRCLE 1 ROLLS ON THE INSIDE OF CIRCLE 2, AND CASE B) CIRCLE 1 ROLLS ON THE OUTSIDE OF CIRCLE 2 79
FIG. 3.26: THE THIRD ORDER IC LOCATION WHEN $\boldsymbol{\alpha = 0, \alpha = 0, \text{and } \omega \neq 0}$ FOR A CIRCLE ROLLING ON ANOTHER CIRCLE: SHOWN HERE IS THE CASE WHEN CIRCLE 1 ROLLS ON THE INSIDE OF CIRCLE 2 80
FIG. 3.27: THE LOCUS OF THIRD ORDER IC FOR $\boldsymbol{\alpha = 0, \alpha \neq 0, \omega \neq 0}$ FOR A CIRCLE ROLLING ON ANOTHER CIRCLE: SHOWN HERE IS THE CASE WHEN CIRCLE 1 ROLLS ON THE INSIDE OF CIRCLE 2 81

FIG. 3.28: A CIRCLE ROLLING ON ANOTHER CIRCLE: THE THIRD ORDER IC LOCATION WHEN $\boldsymbol{\alpha \neq 0, \alpha = 0, \omega \neq 0}$ 82
FIG. 3.29: A CIRCLE ROLLING ON ANOTHER CIRCLE: THE LOCUS OF THE FOURTH ORDER IC LOCATION FOR GENERAL MOTION 85
FIG. 3.30: THE FOURTH ORDER IC LOCATION WHEN $\boldsymbol{\alpha \neq 0, \alpha = \alpha = \omega = 0}$ FOR A CIRCLE ROLLING ON ANOTHER CIRCLE: CASE A) CIRCLE 1 ROLLS ON THE INSIDE OF CIRCLE 2, AND CASE B) CIRCLE 1 ROLLS ON THE OUTSIDE OF CIRCLE 2 87
FIG. 3.31: THE FOURTH ORDER IC LOCATION WHEN $\boldsymbol{\omega \neq 0, \alpha = \alpha = \alpha = 0}$ FOR A CIRCLE ROLLING ON ANOTHER CIRCLE: SHOWN HERE IS THE CASE WHEN CIRCLE 1 ROLLS ON THE INSIDE OF CIRCLE 2 88
FIG. 3.32: THE FOURTH ORDER IC LOCATION WHEN $\boldsymbol{\omega \neq 0, \alpha \neq 0, \alpha = \alpha = 0}$ FOR A CIRCLE ROLLING ON ANOTHER CIRCLE: SHOWN HERE IS THE CASE WHEN CIRCLE 1 ROLLS ON THE INSIDE OF CIRCLE 2 89
FIG. 3.33: THE FOURTH ORDER IC LOCATION WHEN $\boldsymbol{\omega \neq 0, \alpha \neq 0, \alpha = \alpha = 0}$ FOR A CIRCLE ROLLING ON ANOTHER CIRCLE: SHOWN HERE IS THE CASE WHEN CIRCLE 1 ROLLS ON THE INSIDE OF CIRCLE 2 90
FIG. 3.34: THE FOURTH ORDER IC LOCATION WHEN $\boldsymbol{\omega \neq 0, \alpha \neq 0, \alpha = \alpha = 0}$ FOR A CIRCLE ROLLING ON ANOTHER CIRCLE: SHOWN HERE IS THE CASE WHEN CIRCLE 1 ROLLS ON THE INSIDE OF CIRCLE 2 91
FIG. 3.35: THE FOURTH ORDER IC LOCATION WHEN $\boldsymbol{\alpha \neq 0, \alpha \neq 0, \alpha = \omega = 0}$ FOR A CIRCLE ROLLING ON ANOTHER CIRCLE: SHOWN HERE IS THE CASE WHEN CIRCLE 1 ROLLS ON THE INSIDE OF CIRCLE 2 93
FIG. 3.36: A SCHEMATIC DIAGRAM DEPICTING SLIPPING OF A WHEEL 96
FIG. 3.37: THE SCHEMATIC REPRESENTATION OF WHEEL SKIDDING 97
FIG. 3.38: THE SCHEMATIC REPRESENTATION OF WHEEL SLIDING 97
FIG. 3.39: A CIRCLE ROLLING WITH SLIPPING ON A STRAIGHT LINE: FIRST ORDER IC LOCATION FOR A GENERAL MOTION OF THE CIRCLE 99
FIG. 3.40: CIRCLE ROLLING ON A STRAIGHT LINE WITH SLIPPING OR SKIDDING: THE GENERAL LOCUS OF THE SECOND ORDER IC 101
FIG. 3.41: LOCATION OF THE ACCELERATION IC FOR A CIRCLE ROLLING ON A STRAIGHT LINE WITH SLIPPING WHEN $\boldsymbol{\alpha = 0}$ 102
FIG. 3.42: LOCATION OF THE ACCELERATION IC FOR A CIRCLE ROLLING ON A STRAIGHT LINE WITH SLIPPING WHEN $\boldsymbol{\omega = 0}$ 103
FIG. 3.43: SIMULATION PLOT SHOWING THE GENERAL LOCUS OF THE ACCELERATION IC FOR A CIRCLE ROLLING ON A STRAIGHT LINE WITH SLIPPING/SKIDDING 103
FIG. 3.44: SIMULATION PLOT SHOWING THE LOCUS OF THE THIRD ORDER IC FOR A CIRCLE (R = 1FT) ROLLING ON A STRAIGHT LINE WITH SKIDDING (E = -0.2) 105
FIG. 3.45: SIMULATION PLOT SHOWING THE LOCUS OF THE FORTH ORDER IC FOR A CIRCLE ($R = 1FT$) ROLLING ON A STRAIGHT LINE WITH SKIDDING ($E = -0.2$) 108
FIG. 3.46: KINEMATIC STATE DESCRIPTION OF A STRAIGHT LINE ROLLING ON A CIRCLE WITHOUT SLIPPING OR SKIDDING 110
FIG. 3.47: LOCATION OF THE FIRST ORDER IC FOR A STRAIGHT LINE ROLLING ON A CIRCLE WITHOUT SLIPPING OR SKIDDING 112
FIG. 3.48: LOCUS OF THE SECOND ORDER IC FOR A STRAIGHT LINE ROLLING ON A CIRCLE WITHOUT SLIPPING OR SKIDDING IS A CIRCLE 115
FIG. 3.49: LOCUS OF THE THIRD ORDER IC FOR A STRAIGHT LINE ROLLING ON A CIRCLE WITHOUT SLIPPING OR SKIDDING IS A CIRCLE 117
FIG. 4.1: DIFFERENT KINEMATIC CONFIGURATIONS OF SKID-STEER PLATFORMS. (A) A PLATFORM WITH TRACKS (PACKBOT EOD FROM IROBOT CORPORATION, PICTURE REPRODUCED FROM WWW.IROBOT.COM), (B) A TWO WHEELED STATICALLY UNSTABLE PLATFORM (RMP200 FROM SEGWAY INC., PICTURE REPRODUCED FROM WWW.SEGWAY.COM), (C) A FOUR WHEELED, SKID-STEER PLATFORM (RMP400 FROM SEGWAY INC., PICTURE SHOWS THE MOBILE MANIPULATION

System at RRG), and (d) a Six Wheeled, Skid-Steer Platform (Crusher from NREC, CMU, Picture Reproduced from : http://www.rec.ri.cmu.edu/projects/crusher/photos/index.htm) 122
Fig. 4.2: Different Wheel Configurations for Skid-Steer Platforms: Two Wheeled Platform with Passive Caster Wheels 123
Fig. 4.3: Different Wheel Configurations for Skid-Steer Platforms: Four Wheeled Platform 123
Fig. 4.4: Different Wheel Configurations for Skid-Steer Platforms: Six Wheeled Platform 124
Fig. 4.5: Different Wheel Configurations for Skid-Steer Platforms: Platform with Tracks 125
Fig. 4.6: A Tricycle like Mobile Platform (Actively Steered and Driven front Wheel with Two Trailing Passive Fixed Wheels) 125
Fig. 4.7: Ackerman Steered Platform Schematic Diagram (A 2DOF Active Input System with Coordinated Steering and Driving for Front Two Wheels and Passive Trailing Fixed Wheels) 127
Fig. 4.8: Ackerman Steered Platform Schematic Diagram (A 2DOF Active Input System with Coordinated Steering and Driving for Front Two Wheels and Four Passive Trailing Fixed Wheels) 128
Fig. 4.9: Ackerman Steer Platform with Trailing Active/Passive Tracks 129
Fig. 4.10: An Example of Halftrack Vehicle [Wikimedia] 129
Fig. 4.11: Common Rolling Axis for the Class of Mobile Platforms with Fixed Wheels on Both Sides 130
Fig. 4.12: Kinematic Description for the Class of Mobile Platforms with Fixed Wheels on Either Side of the Platform, the First Order IC is Constrained on the Wheel Rolling Axis 131
Fig. 4.13: Motion Description of Operational Space in Terms of an End-Effector that is Offset from the Wheel Rolling Axis 133
Fig. 4.14: The First Order Motion Synthesis for a Skid-Steer Mobile Platform Based on the First Order IC Location 134
Fig. 4.15: The First Order Motion Synthesis for a Tricycle Like/Ackerman-Steer Mobile Platform Based on the First Order IC Location 135
Fig. 4.16: Tangential and Normal Components of the Acceleration of a General Point with respect to the Acceleration IC 136
Fig. 4.17: The Second Order Motion Synthesis for a Skid-Steer Mobile Platform Based on the Second Order IC Location 138
Fig. 4.18: The Second Order Motion Synthesis for a Tricycle Like/Ackerman-Steer Mobile Platform Based on the Second Order IC Location 139
Fig. 4.19: The Third Order Motion Synthesis for a Skid-Steer Mobile Platform Based on the Second Order IC Location 142
Fig. 4.20: The Third Order Motion Synthesis for a Tricycle Like/Ackerman-Steer Mobile Platform Based on the Third Order IC Location 144
Fig. 4.21: The Location of Various ICs for the Class of Mobile Platforms with Fixed Wheels on Either Side 145
Fig. 4.22: Mobile Platform Traversing Circular Trajectory 146
Fig. 4.23: Higher Order Properties for a Mobile Platform Traversing a Trajectory 146
Fig. 4.24: An Example of the Mobile Platform with Active Caster Wheels (Picture Reproduced from Low and Leow [2006a]) 147
Fig. 4.25: A Schematic Representation of the general J^{TH} Wheel Subsystem with an Active Caster Wheel 148
Fig. 4.26: Mobile Platform with Two Laterally Arranged, Independently Driven and Steered Caster Wheels with Passive Caster Wheels 150

FIG. 4.27: MOBILE PLATFORM WITH TWO INDEPENDENTLY DRIVEN AND STEERED CASTER WHEELS WITH PASSIVE CASTER WHEELS 151
FIG. 4.28: MOBILE PLATFORM WITH THREE INDEPENDENTLY DRIVEN AND STEERED CASTER WHEELS 151
FIG. 4.29: MOBILE PLATFORM WITH FOUR INDEPENDENTLY DRIVEN AND STEERED CASTER WHEELS 152
FIG. 4.30: GEOMETRIC DESCRIPTION OF A *J* WHEELED MOBILE PLATFORM WITH CASTER WHEELS ... 153
FIG. 4.31: VELOCITY OF WHEEL ATTACHMENT POINT, E_J, EXPRESSED IN TERMS OF THE FIRST ORDER IC. 155
FIG. 4.32: THE LOCI OF THE SECOND ORDER IC FOR A GENERAL *J* WHEELED MOBILE PLATFORMS ... 157
FIG. 4.33: EXAMPLE LOCATIONS OF THE SECOND ORDER IC FOR MOBILE PLATFORMS WITH *J* ACTIVE CASTER WHEELS 159
FIG. 4.34: THE LINEAR ACCELERATION OF A WHEEL SUBSYSTEM 161
FIG. 4.35: THE LOCI OF THE THIRD ORDER IC FOR A GENERAL *J* WHEELED PLATFORM WITH *J* ACTIVE CASTER WHEELS 164
FIG. 4.36: A NUMERICAL EXAMPLE FOR THE THIRD ORDER IC LOCATION 165
FIG. 4.37: AN EXAMPLE OF CENTERED WHEEL OMNIDIRECTIONAL ROBOT (SEEKUR FROM MOBILE ROBOTS INC., PICTURE REPRODUCED FROM HTTP://ROBOTIKA.CZ/COMPETITIONS/FIELDROBOT2009/CS). A MOBILE PLATFORM WITH FOUR ACTIVE CENTERED WHEELS 167
FIG. 4.38: A MOBILE PLATFORM WITH TWO ACTIVE CENTERED WHEELS PLACED LATERALLY 169
FIG. 4.39: A MOBILE PLATFORM WITH TWO INDEPENDENTLY DRIVEN AND STEERED WHEELS WITH CENTERED STEERING 170
FIG. 4.40: A MOBILE PLATFORM WITH THREE INDEPENDENTLY DRIVEN AND STEERED WHEELS WITH CENTERED STEERING 171
FIG. 4.41: A MOBILE PLATFORM WITH FOUR INDEPENDENTLY DRIVEN AND STEERED WHEELS WITH CENTERED STEERING 171
FIG. 4.42: SCHEMATIC REPRESENTATION OF A MOBILE PLATFORM WITH *J* ACTIVE CENTERED WHEELS 173
FIG. 4.43: THE LOCI OF THE SECOND ORDER IC FOR A GENERAL *J* WHEELED MOBILE PLATFORMS ... 176
FIG. 4.44: EXAMPLE LOCATIONS OF THE SECOND ORDER IC FOR MOBILE PLATFORMS WITH *J* ACTIVE CENTERED WHEELS 177
FIG. 4.45: LOCUS OF THE THIRD ORDER IC FOR A GENERAL MOBILE PLATFORM WITH *J* CENTERED WHEELS 179
FIG. 4.46: A NUMERICAL EXAMPLE FOR THE THIRD ORDER IC LOCATION 181
FIG. 4.47: AN ILLUSTRATIVE MECANUM WHEEL (PICTURE REPRODUCED FROM WIKIMEDIA COMMONS: HTTP://EN.WIKIPEDIA.ORG/WIKI/FILE:ILONWHEELCHAIR.JPG) 182
FIG. 4.48: AN OMNI-WHEEL DESIGN (PICTURE REPRODUCED FROM WIKIMEDIA COMMONS: HTTP://UPLOAD.WIKIMEDIA.ORG/WIKIPEDIA/COMMONS/D/D9/YHST-33833170891817_1977_3727729.JPG) 183
FIG. 4.49: A MOBILE PLATFORM WITH OMNI WHEELS 184
FIG. 4.50: A MOBILE PLATFORM WITH FOUR OMNI WHEELS: A) OBLIQUELY ARRANGED WHEELS, B) WHEELS ARRANGED IN PRINCIPAL DIRECTIONS 185
FIG. 4.51: THE SCHEMATIC REPRESENTATION OF A GENERAL MOBILE PLATFORM WITH *J* OMNI WHEELS 186
FIG. 4.52: MOTION SYNTHESIS FOR J^{TH} WHEEL 187
FIG. 4.53: THE FIRST ORDER MOTION SYNTHESIS FOR A MOBILE PLATFORM WITH FOUR OMNI WHEELS 188
FIG. 4.54: THE LOCI OF THE SECOND ORDER IC FOR A GENERAL *J* WHEELED MOBILE PLATFORMS ... 191
FIG. 4.55: EXAMPLE LOCATIONS OF THE SECOND ORDER IC FOR MOBILE PLATFORMS WITH *J* ACTIVE CENTERED WHEELS 192
FIG. 4.56: LOCUS OF THE THIRD ORDER IC FOR A GENERAL MOBILE PLATFORM WITH *J* CENTERED WHEELS 194

FIG. 4.57: A NUMERICAL EXAMPLE FOR THE THIRD ORDER IC LOCATION 196
FIG. 5.1: PLATFORM CONFIGURATIONS WITH CONVENTIONAL WHEELS: A) A TRICYCLE PLATFORM WITH A 2-DOF FRONT WHEEL AND TWO PASSIVE, TRAILING, FIXED WHEELS; B) A TRICYCLE PLATFORM WITH 3 ACTIVE (2-DOF) CASTER WHEELS, AND C) A TRICYCLE PLATFORM WITH 3 ACTIVE (2-DOF) CENTERD WHEELS 199
FIG. 5.2: COMMON GEOMETRIC DESCRIPTION OF THREE WHEELED PLATFORMS 200
FIG. 5.3: A STRAIGHT LINE MOTION OF THE PLATFORMS 201
FIG. 5.4: A STRAIGHT LINE MOTION OF THE PLATFORMS WITH ORIENTATION CONTROL 202
FIG. 5.5: COMPUTATION OF THE ANGULAR VELOCITY FOR THE STRAIGHT LINE MOTION WITH ORIENTATION CONTROL 203
FIG. 5.6: THE LOCUS OF THE VELOCITY IC FOR A MOTION OF A GENERAL PLATFORM ALONG A STRAIGHT LINE WITH ORIENTATION CONTROL 205
FIG. 5.7: MOTION SYNTHESIS FOR THE FRONT WHEEL OF THE MOBILE PLATFORM WITH THREE ACTIVE CENTERED WHEELS UNDERGOING A STRAIGHT LINE MOTION WITH ORIENTATION CONTROL .. 206
FIG. 5.8: VELOCITY OF WHEEL ATTACHMENT POINT, E_J, EXPRESSED IN TERMS OF THE FIRST ORDER IC. 208
FIG. 5.9: MOTION SYNTHESIS FOR THE FRONT WHEEL OF THE MOBILE PLATFORM WITH THREE ACTIVE CASTER WHEELS UNDERGOING A STRAIGHT LINE MOTION WITH ORIENTATION CONTROL: SIMULATION FOR INITIAL STEERING ANGLE $\Psi_1 = 225^o$ 209
FIG. 5.10: MOTION SYNTHESIS FOR THE FRONT WHEEL OF THE MOBILE PLATFORM WITH THREE ACTIVE CASTER WHEELS UNDERGOING A STRAIGHT LINE MOTION WITH ORIENTATION CONTROL: SIMULATION FOR INITIAL STEERING ANGLE $\Psi_1 = 135^o$ 210
FIG. 5.11: THE MOBILE PLATFORM WITH TRAVELING ALONG A CIRCULAR PATH 211
FIG. 5.12: MOTION OF A GENERAL PLATFORM ALONG A A CIRCULAR PATH WHEN THE MOBILE PLATFORM ALWAYS FACES THE DIRECTION OF THE MOTION 212
FIG. 5.13: THE MOBILE PLATFORM WITH FIXED WHEELS TRAVELING ALONG A CIRCULAR PATH 214
FIGURE 5.14: MOTION SYNTHESIS FOR THE FRONT WHEEL OF THE MOBILE PLATFORM WITH THREE ACTIVE CENTERED WHEELS UNDERGOING A CIRCULAR MOTION WITH FIXED ORIENTATION: SIMULATION 215
FIG. 5.15: THE MOBILE PLATFORM TRAVELING ALONG A CIRCULAR PATH 216
FIG. 5.16: MOTION SYNTHESIS FOR THE FRONT WHEEL OF THE TRICYCLE PLATFORM OR THE PLATFORM WITH THREE ACTIVE CENTERED WHEELS FOR A C_1 DISCONTINUOUS MOTION WHEN THE PLATFORM FACES THE DIRECTION OF TRAVEL 217
FIG. 5.17: LOCATION OF THE VELOCITY IC COINCIDENT WITH THE POI 218
FIG. 5.18: MOTION SYNTHESIS FOR THE FRONT WHEEL OF THE TRICYCLE PLATFORM OR THE PLATFORM WITH THREE ACTIVE CENTERED WHEEL FOR A C_1 DISCONTINUOUS MOTION WHEN THE PLATFORM FACES DIRECTION OF TRAVEL 219
FIG. 5.19: THE GENERAL MOBILE PLATFORM UNDERGOING THE DISCONTINUOUS PATH COMPOSED OF STRAIGHT LINES 220
FIG. 5.20: THE MOTION SYNTHESIS FOR A MOBILE PLATFORM WITH THREE CENTERED WHEELS 221
FIG. 5.21: THE MOTION SYNTHESIS FOR A MOBILE PLATFORM WITH THREE CENTERED WHEELS 222
FIG. 5.22: THE MOBILE PLATFORM WITH FIXED WHEELS TRAVELING ALONG A CIRCULAR PATH 224
FIG. 5.23: THE MOBILE PLATFORM WITH FIXED WHEELS TRAVELING ALONG A CIRCULAR PATH 226
FIG. 6.1: FRAME ASSIGNMENTS FOR DYNAMICS 229
FIG. 6.2: THE FREE-BODY DIAGRAM OF A GENERAL MOBILE PLATFORM WITH *J* ACTIVE 2-DOF CASTER WHEELS 230
FIG. 6.3:THE VARIATION OF LONGITUDINAL FRICTION COEFFICIENT M_X WITH RESPECT TO THE LONGITUDINAL SLIP Λ [WONG, 2001] 239
FIG. 6.4: THE MAGNITUDE OF BRAKING FRICTION COEFFICIENT M_X WITH RESPECT TO THE VEHICLE SPEED [WONG 2001] 240
FIG. 6.5: THE MAGNITUDE OF BRAKING FRICTION COEFFICIENT M_X WITH RESPECT TO THE TIRE INFLATION PRESSURE [WONG 2001] 241

FIG. 6.6: EFFECT OF THE NORMAL LOAD ON THE CORNERING COEFFICIENT M_Y WONG 2001] 242
FIGURE 6.7: EFFECT OF THE TIRE INFLATION PRESSURE ON THE CORNERING COEFFICIENT M_Y [WONG 2001] 242
FIG. 6.8: ROLLING RESISTANCE COEFFICIENT WITH RESPECT TO THE TIRE INFLATION PRESSURE ON VARIOUS SURFACES. (REPRODUCED FROM WONG (2001)) 243
FIG. 6.9: ROLLING RESISTANCE COEFFICIENT WITH RESPECT TO THE TIRE INTERNAL TEMPERATURE (REPRODUCED FROM WONG (2001)) 244
FIG. 6.10: ROLLING RESISTANCE COEFFICIENT WITH RESPECT TO THE VEHICLE SPEED (REPRODUCED FROM WONG (2001)) 244
FIG. 6.11: GEOMETRIC DESCRIPTION OF THE MOBILE PLATFORM WITH THREE ACTIVE CASTER WHEELS 246
FIG. 6.12: THE PATH OF THE MOBILE PLATFORM 247
FIG. 6.13: THE MOTION PLAN FOR SMOOTH PLATFORM MOTIONS 249
FIG. 6.14: SIMULATION SECOND ORDER INPUT MOTION SYNTHESIS FOR THE MOBILE PLATFORM WITH THREE CASTER WHEELS WHEN IT TRAVELS FROM CORNER 1 TO CORNER 2 AS SHOWN IN FIG. 6.12 251
FIG. 6.15: SECOND ORDER INPUT MOTION SYNTHESIS FOR THE MOBILE PLATFORM WITH THREE CASTER WHEELS WHEN IT TRAVELS FROM CORNER 2 TO CORNER 3 AS SHOWN IN FIG. 6.12. 252
FIG. 6.16: SECOND ORDER INPUT MOTION SYNTHESIS FOR THE MOBILE PLATFORM WITH THREE CASTER WHEELS WHEN IT TRAVELS FROM CORNER 1 TO CORNER 3 AS SHOWN IN FIG. 6.12 253
FIG. 6.17: FORCE EQUILIBRIUM FOR THE PLATFORM BODY 254
FIG. 6.18: WHEEL SUBSYSTEM FORCES DUE TO OPERATIONAL SPACE DYNAMIC REQUIREMENT WHEN THE MOBILE PLATFORM WITH THREE CASTER WHEELS TRAVELS FROM CORNER 1 TO CORNER 3 (τ = *0s* TO *20s*) 257
FIG. 6.19: THE TRACTIVE FORCE FXJ AND THE LATERAL FORCE FYJ FOR THE PLATFORM DYNAMIC MOTION FROM T= 0 TO 20(S) 258
FIG. 6.20: INPUT TORQUE CURVE FOR THE DYNAMIC MOTION OF THE MOBILE PLATFORM WITH THREE CASTER WHEELS FROM τ = *0 TO 20 (S)* 259
FIG. 7.1: K^{TH} ORDER KINEMATICS OF A GENERAL RIGID BODY 267
FIGURE 7.2: MOTION PLAN FOR A RIGID BODY USING THE FIRST AND SECOND ORDER ICS 269
FIG. 7.3: MOBILE PLATFORM TRAVERSING AN '*S*' SHAPED TRAJECTORY 271
FIG. 7.4: HIGHER ORDER MOTION PLANNING FOR THE MOBILE PLATFORM TRAVERSING THE *S* SHAPED TRAJECTORY 271
FIGURE 7.5: THE SCHEMATIC REPRESENTATIONS OF THE CLASSICAL MOTIONS. CLOCKWISE FROM TOP LEFT: (I) A CIRCLE ROLLING ON A STRAIGHT LINE (WITH OR WITHOUT SLIPPING), (II) A LINE ROLLING ON A CIRCLE WITHOUT SLIPPING, (III) A CIRCLE ROLLING OUTSIDE ANOTHER CIRCLE, AND (IV) A CIRCLE ROLLING INSIDE ANOTHER CIRCLE 274
FIGURE 7.6:THE SCHEMATIC REPRESENTATION OF WHEEL SLIPPING, SLIDING AND SKIDDING 278
FIGURE 7.7: EXAMPLES OF PLANAR MOBILE PLATFORMS. CLOCKWISE FROM TOP LEFT, (I) A FOUR WHEELED, SKID-STEER PLATFORM (RMP400 FROM SEGWAY INC., PICTURE SHOWS THE MOBILE MANIPULATION SYSTEM AT RRG), (II) AN EXAMPLE OF CENTERED WHEEL OMNIDIRECTIONAL ROBOT (SEEKUR FROM MOBILE ROBOTS INC., PICTURE REPRODUCED FROM HTTP://ROBOTIKA.CZ/COMPETITIONS/FIELDROBOT2009/CS). A MOBILE PLATFORM WITH FOUR ACTIVE CENTERED WHEELS, (III) A FORKLIFT WITH FOUR MECANUM WHEEL FROM AIRTRAX (PICTURE REPRODUCED FROM NEWS SITE HTTP://WWW.FORKLIFTACTION.COM/UPLOAD/NEWS/1913-1.JPG), AND (IV) AN EXAMPLE OF THE MOBILE PLATFORM WITH ACTIVE CASTER WHEELS (PICTURE REPRODUCED FROM LOW AND LEOW [2006A]) 281
FIG. 7.8: A STRAIGHT LINE MOTION OF THE PLATFORMS WITH ORIENTATION CONTROL 284
FIG. 7.9: MOBILE PLATFORM UNDERGOING THE DISCONTINUOUS PATH COMPOSED OF STRAIGHT LINES 285

FIGURE 7.10: ARRAY OF OPEN ARCHITECTURE MOBILE PLATFORMS ((EMPHASIS ON STEERABLE CENTERED/CASTER WHEELS)..... 286
FIG. 7.11: THE FREE-BODY DIAGRAM OF A GENERAL MOBILE PLATFORM WITH *J* ACTIVE 2-DOF CASTER WHEELS 287
FIG. 7.12: GEOMETRIC DESCRIPTION OF THE MOBILE PLATFORM WITH THREE ACTIVE CASTER WHEELS 289
FIG. 7.13: THE PATH OF THE MOBILE PLATFORM..... 290
FIG. 7.14: SECOND ORDER INPUT MOTION SYNTHESIS FOR THE MOBILE PLATFORM WITH THREE CASTER WHEELS WHEN IT TRAVELS FROM CORNER 1 TO CORNER 3 292
FIG. 7.15: SYSTEM OF FORCES AND MOMENTS FOR THE PLATFORM BODY 293
FIG. 7.16: THE TRACTIVE FORCE F_{xJ} AND THE LATERAL FORCE F_{yJ} FOR THE PLATFORM DYNAMIC MOTION FROM T= 0 TO 20(S) 293
FIG. 7.17: INPUT TORQUE CURVE FOR THE DYNAMIC MOTION OF THE MOBILE PLATFORM WITH THREE CASTER WHEELS FROM T = 0 TO 20 (S)..... 295
FIG. 7.18: NONLINEAR NATURE OF THE WHEEL-GROUND CONTACT (WONG, 2001) 296
FIG. 7.19: TIRE PERFORMANCE MAPS DEPICTING THE INFLUENCE OF WHEEL/GROUND CONTACT (EXTERNAL) PARAMETERS 300

1 INTRODUCTION

1.1 Background

A mobile platform should be considered as an open architecture system that uses a wide variety of steered/powered wheels, vector directed suspension axes with powered wheels, passive/active suspensions, etc., in many combinations. A generalized kinematic representation encompassing all the possible configurations is not available for mobile platforms. Also, the general approach to model mobile platforms on the lines similar to manipulators (Thomas and Tesar, 1982) as proposed by Muir and Newman (1989) uses the Jacobian to represent the forward kinematics of a mobile platform. For computing the inverse kinematics in order to compute the input DOF requirements, the Jacobian is needed to be inverted. For simpler mobile platforms such as a skid-steer platform, this results in a fixed Jacobian inverse. However for a general J wheeled planar mobile platform that uses 2-DOF wheel modules, the Jacobian becomes highly rectangular (thereby making the configuration a redundant configuration) even for a three wheeled platform (6x3) and thus poses problems in inversion. Various solutions have been offered in the literature to resolve this "redundancy" in the kinematic domain (Yi and Kim, 2002; Low and Leow, 2006a). However, a planar mobile platform is a parallel robotic system that should not have kinematic redundancy at the platform system level (kinematic redundancy may be present at the wheel subsystem level). The fact that parallel robotic systems have a straight forward (analytically direct with no uncertainty) inverse

kinematic solution is not exploited in the aforementioned papers (Yi and Kim, 2002; Low and Leow, 2006a). This research proposes such a solution by means of instantaneous invariants (Instant Centers (IC)) which also helps to describe the kinematic model at the platform system level. The method of instant centers provides a straightforward and yet physically intuitive way to synthesize (obtain the required input parameters) a general order planar motion of mobile platforms.

Also the operation of platforms demands considerable attention to input parameter choices to permit accurate trajectory following under various specific speeds, accelerations, ground surface quality, loading configuration, operation of active systems (manipulators) on the platform, etc. This leads to an input parameter resolution problem based on operational criteria which are in development for mobile platforms just as they have been developed for n input manipulator systems (Tisius et al., 2009; Kapoor and Tesar, 2006). These operational criteria often necessitate computation of higher order properties such as the jerk of points of interest (wheel attachment points, payload attachment point, etc.) for motion synthesis of the mobile platform. To this effect, the research presents the kinematic formulation for up to the fifth order of the mobile platform motions using corresponding ICs as the foundation.

In the past, instantaneous invariants have been used in a time independent basis for analysis and synthesis of constrained mechanisms (Pennock, 2008; Uicker et al., 2003; Cowie, 1961; Hirschhorn, 1962; Myklebust and Tesar, 1975; Oleska and Tesar, 1971; Lorenc et al., 1995; Goehler et al., 2004; Ambike and Schmiedeler, 2008; Soh and McCarthy, 2008). In the present paper, the emphasis is on time based control of the planar mobile platform with 3 outputs and multiple inputs at J wheels. This initial work is intended to present a firm analytical formulation for the motion specification and its physical meaning. The ICs for the first (velocity) and second (acceleration) order have

been extensively studied in the literature (Cowie, 1961; Hirschhorn, 1962; Bottema, 1961; Bottema and Roth, 1979; Veldkamp, 1963, 1967, 1969; Alleivi, 1895; Mueller, 1960; Ridley et al., 1992; Wang et al., 1997; Martinez and Duffy, 1998; Tesar, 1967, 1968, 1968; Gallardo-Alvarado, and Rico-Martínez, 2001); however the authors have not seen such a generalized and concise formulation for the third and higher order rigid body motion using instant centers. The generalized formulation also allows a straightforward extension to further higher order kinematics. It is shown with a systematic algebraic formulation, that the k^{th} order *(k = 1, 2, 3, …)* time state of a general point on a rigid body follows two properties, namely, vector directionality and proportionality with respect to the corresponding IC. The formulation presents a concise expression for the k^{th} order time state of a general point with the magnitude and direction separated and identified. *We believe that this is the first time the third and higher order instantaneous invariants have been studied for a time based motion of unconstrained, multi-input, planar 3-DOF platforms*.

1.2 Research Outline

The objective of the research was two-pronged, (i) to generalize the theory for the instant centers (also known as curvature theory (Bottema and Roth, 1979) to higher order motions (third and higher) and (ii) to study the mobile platforms in the light of the theory for ICs.

The IC based formulation presented in this research uses an algebraic formulation (Bottema, 1961) since it assisted in the generalization of the formulation when dealing with the higher order properties. It was observed that the expressions for the general (3-DOF) higher order properties was coupled and provided no physical meaning as to the influence of various kinematic terms on them. Thus, a study of special case 1-DOF and 2-

DOF motions was performed to understand the physical nature the higher order ICs. The theory that was developed was then applied to the class of planar mobile platforms which were categorized into four distinct categories based on the arrangements of the wheel subsystems as follows, (i) platforms with fixed wheels on both sides, (ii) platforms with active caster wheels, (iii) platforms with active centered wheels, and (iv) the platforms with omnidirectional wheels. The motion synthesis for each configuration was described for up to the third order motion. To compare the dexterity of various configurations, a representative set of mobile platforms was chosen. The motion synthesis for the set of mobile platforms was done for various motion scenarios to underscore the kinematic capabilities of each platform configuration. The redundancy of input DOF in the case of a general *J* wheeled platform influences the dynamic (rather than kinematic) capabilities of the platform. The significance lies in the fact that a mobile platform with redundant actuation provides redundancy in force domain (Yi and Freeman, 1993) just as a redundant manipulator provides redundancy in position domain. Thus the dynamics of mobile platform was studied for a representative configuration of a mobile platform where we showed the influence of wheel-ground interaction on the overall performance of the mobile platform.

1.3 Scope of the Research

This research was focused on wheeled mobile platforms traversing relatively flat and hard surfaces. The platform configurations that are capable of only 3-DOF planar motions were considered.

1.4 Outline of the Report[1]

The outline of the following report is as follows. Chapter 2 presents the development of

[1] A section on Contribution Summary will be added here.

the IC based formulation for up to the fourth order planar motion of a rigid body. The general properties of the ICs for up to the fourth order are studied in terms of some well understood 1-DOF/2-DOF planar motions in Chapter 3. Chapter 4 studies the kinematic motion synthesis of various planar mobile platform configurations. The representative platform configurations are evaluated for dexterity with the help of numerical examples in Chapter 5. Chapter 6 evaluates the dynamic motion synthesis with the help of a representative platform configuration with J active caster wheels. Chapter 7 summarizes the research with a conclusion and future work

2 INSTANT CENTER BASED KINEMATIC FORMULATION FOR 3-DOF PLANAR MOTION

2.1 Introduction

The following sections detail the IC based kinematic formulation for wheeled mobile platforms. The literature in the area of instantaneous invariants and platform kinematics will be reviewed in Sec. 2.2. A generalized notation that describes a general planar motion of a rigid body for the k^{th} order will be presented in Sec. 2.2. In Sec. 2.3, the first order (velocity) algebraic formulation for a general rigid body will be developed using the notation. Sec. 2.4 discusses the kinematic formulation that uses the IC for second order (acceleration). The higher order formulation is presented in Sec. 2.5 by first extending it to the third order (jerk) and the fourth order (time derivative of jerk) and generalizing it for the k^{th} order in the form of magnitude and direction of a general point in the body. The chapter concludes with a summary and discussions in Sec. 2.6.

2.2 Literature Review

Due to the wide variety of kinematic configurations for planar mobile platforms, a generic kinematic representation similar to the D-H parameters (Denavit and Hartenberg, 1955) is not available. However there have been various efforts to model mobile platforms (Sreenivasan and Nanua, 1999; Muir and Newman, 1987; Campion et al., 1996; Oetomo and Ang, 2008; Low et al., 2005; Alexander and Maddocks, 1989; Saha et al., 1995; Low and Leow, 2005; Gracia and Tornero, 2008; Yi and Kim, 2002;

Borenstein, 1995; Reister, 1991)[2]. Muir and Newman (1987) developed a method for kinematic modeling using individual transformations of components along the lines similar to manipulator modeling. Sreenivasan and Nanua (1999) employed a screw based kinematic model for analyzing dexterous wheeled vehicle systems for up to the second order. Campion et al. (1996) developed a method for kinematic modeling of mobile platforms using kinematic constraints on various wheel configurations by first categorizing wheel configurations into four basic types: conventional fixed wheel, conventional centered wheel, conventional off-centered (caster) wheel, and the Swedish wheel. Oetomo and Ang (2008) presented the singularity analysis of a general mobile platform with powered caster wheels. They showed that for singularity free workspace, the omnidirectional mobile platform with powered caster wheels should have a minimum of two wheels with full actuation (i.e. both steering and driving actuation). Low et al. (2005) studied the kinematics of an omnidirectional (with the 3-DOF planar output motion capability) step climbing robot that uses six Mecanum wheels. Papers by Saha et al. (1995) and Low and Leow (2005) systematically studied mobile platforms with Swedish wheels and conventional wheels, respectively. Gracia and Tornero (2008) presented the kinematic models for mobile platforms that use the four aforementioned wheel types (Campion et al., 1996; Yi and Kim, 2002) developed forward analysis based kinematics for a three wheeled omnidirectional mobile platform by identifying a set of independent input parameters equal to the number of output parameters so as to create a square Jacobian. The inverse kinematics is then computed by inverting the Jacobian. The dependent input parameters are computed using a higher order loop constraint method. However a mobile platform is a parallel mechanism and should have a more direct solution to the inverse kinematics problem. This research proposes one such solution

[2] This is a brief list. A detailed review can be found in these papers.

using the IC as the analytic foundation for the motion description of the rigid platform. The use of IC's for mobile platform kinematics is not new (Borenstein, 1995; Reister, 1991), however we present a completely generalized and extensive formulation that also treats the higher order kinematics.

The IC of velocity (velocity pole (Uicker et al., 2003) has been widely used in the analysis and synthesis of linkage mechanisms (Uicker et al., 2003: Cowie, 1961; Hirschhorn, 1962; Myklebust and Tesar, 1975; Oleska and Tesar, 1971; Lorenc et al., 1995; Goehler et al., 2004; Ambike and Schmiedeler, 2008; Pennock, 2008; Soh and McCarthy, 2008). This approach simplifies the platform motion synthesis problem since, as we will show, all wheel motion requirements can be computed directly (and similarly) because they act in parallel (i.e., the inverse problem instead of the normal forward analysis approach). The IC also provides physical information of the kinematic state of the platform. A popular method for the analysis using IC's uses a vector representation because of its intuitiveness and simplicity (Cowie, 1961, Hirschhorn, 1962; Tesar and Sparks, 1968; Beggs, 1983); however this paper uses an algebraic representation since it assists in the generalization of the formulation when dealing with the higher order properties. This algebraic formulation was initiated by Bottema in an NSF workshop at Yale University in 1961[3] (Bottema, 1961). Very extensive work followed in Bottema and Roth (1979), where they gave a preliminary algebraic approach up to the third order with respect to time (as reference parameter) without reducing it to practice. Veldkamp took this algebraic approach into planar (Veldkamp, 1963) and spatial (Veldkamp, 1967) kinematics giving extensive physical meaning to the instantaneous invariants of the motion based on a single reference input parameter. For example, in (Veldkamp, 1969), Veldkamp treats the problem of acceleration axes and acceleration distribution in spatial

[3] Tesar provided notes at the workshop based on the lectures by Bottema.

motion. Note that Alleivi (1895) provided an in-depth treatment on planar instantaneous invariants to support the extensive work on planar synthesis performed over 2 decades by Mueller[4] (Mueller, 1960). Ridley et al. (1992) used a screw and its time derivative to describe the spatial motion of a rigid body for up to the second order (velocity and acceleration). They then computed the inflection surfaces (three quadric ruled surfaces) and Bresse hyperboloid to describe the motion of the body in a time independent manner by eliminating the time from the analytics. Another interesting work by Wang et al. (1997) extended this screw based formulation to describe the characteristic lines' distribution in a rigid body spatial motion. Martinez and Duffy (1998) studied the acceleration center and acceleration field of the rigid body spatial motion with a study on special scenario.

The algebraic formulation enabled Tesar et al. (Tesar, 1967; Tesar, 1968; Tesar and Sparks, 1968) to compactly treat the synthesis of kinematic motion in terms of multiple separated positions, a generalization of the instantaneous formulations by Bottema and Veldkamp. This led to special cases treated in depth for Cardan (Spragg and Tesar, 1971) and Cycloidal (Tesar and Anderson, 1968) motion. Extensive work was performed on the synthesis of complex motions by Myklebust and Tesar (1975), where a principal objective was the synthesis of a point path kinematically timed to a remote geometric parameter. A unique synthesis formulation was achieved by Oleska and Tesar (1971) for a geared five bar path generator where the motion of two cranks had a fixed ratio provided by gears.

Recently, a move has been provided to generalize the concept of two coordinated inputs (λ, μ) for synthesis of planar mechanisms by Lorenc et al. (1995). This essentially sets up a two input kinematic synthesis problem which is a welcome/needed

[4] Translated by Tesar in 1961 under an Army Research Office grant

generalization of the previous one input problem. The theory was applied to the path tracking of 2-DOF robotic systems: a planar manipulator and an Ackerman steered mobile platform. Another interesting paper by Goehler et al. (2004) considers a special case motion of an Ackerman steered platform (using the 1-DOF theory) when the system experiences a dwell in its driving variable. Ambike and Schmiedeler (2008) present an algorithm for the path tracking problem of 2-DOF systems that addresses the dwell. A more recent study on 2-DOF curvature theory to not only define the geometry but also to begin the dynamic synthesis of the coordinated velocities of a dual input system was presented by Pennock (2008). Finally, significant work has been performed by McCarthy et al. (See (Soh and McCarthy, 2008) for an example) on the concept of coordinating local motions (by synthesis) by considering planar, spherical and spatial n DOF manipulator systems. The desired output (up to 6-DOF in space) specification is inverted to obtain the local joint motions (which are normally considered as independent inputs). They then obtain local constraints (say function generators) to tie two or more of the inputs together by synthesizing the dimensions of these local linkages to generate the complex motion such as the motion of the hood of an automobile, the motion of the opening of a folded bed etc. This has the very attractive feature of creating a combination of serial and parallel configurations with a reduced set of controllable inputs.

2.3 Generalized Notation

Fig. 2.1 shows a schematic of a mobile platform which is treated as a rigid body with a general shape. Frame *{1}* is a body fixed frame located at point *P*. Frame *{0}* is the inertial frame of reference. Point *P* can be a point of physical significance such as a manipulator attachment point or it can simply be the geometric center of the platform. The instantaneous angle made by frame *{1}* with frame *{0}* is Θ. Vector $R_P\ [X_P,\ Y_P]$ is the

position vector for point *P* in frame *{0}*. The pre-superscript indicates the frame of reference. If no pre-superscript is specified, the entity can be assumed to be expressed in frame *{0}*.

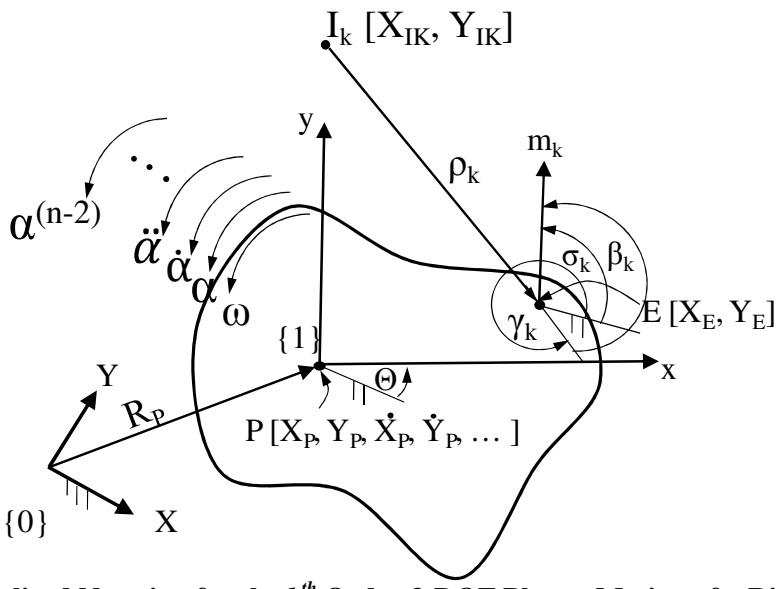

Fig. 2.1: Generalized Notation for the k^{th} Order 3-DOF Planar Motion of a Rigid Body

Point *E* is a general point on the body, described as *[x_E, y_E]* in frame {1} and as *[X_E, Y_E]* in frame {0}. The kinematic formulation is shown for the k^{th} order motion of the rigid body (for instance, $k = 1$, is the velocity formulation; $k = 2$ is the acceleration formulation, etc.). The kinematic state of point *E* for the k^{th} order is m_k. The location of the IC for the k^{th} order is I_k. Radius ρ_k is the radius of point *E* with respect to the corresponding IC, I_k. Angle γ_k is the angle made by the radius vector ρ_k with the *X* axis of frame *{0}*. Angle σ_k is the angle made by the time state m_k with the *X* axis of frame *{0}*. When dealing with more than one general point[5], E_j (j = 1, 2, 3…), the radius and the time state can be described as $\rho_{k(j)}$ and $m_{k(j)}$, respectively. Similarly the angles made by $\rho_{k(j)}$ and $m_{k(j)}$ with the *X* axis of frame *{0}* are described as $\gamma_{k(j)}$ and $\sigma_{k(j)}$, respectively. Angle

[5] In case of a *J* wheeled mobile platforms, E_j *(j = 1, 2, 3,..., J)* can represent *J* wheel attachment points.

β_k is the angle that the time state, m_k (or $m_{k(j)}$ in particular), makes with the radius vector, ρ_k (or $\rho_{k(j)}$),. It will be later shown that angle β_k is constant throughout the body at every instant of time. The planar motion of the rigid body in frame *{0}* is expressed in terms of motion of the point *P* (velocity, acceleration, jerk, etc.) and the rotation of the frame {1} (angular velocity, $\dot{\Theta}$, angular acceleration, $\ddot{\Theta}$, etc.).

With these notations, the algebraic formulation is developed starting with the first order formulation. Though the first and second order ICs have been well documented in the literature, their derivation here is necessary to build the foundation for the higher order formulation.

2.4 First Order (Velocity) Planar Motion of a Rigid Body

The velocity IC is defined (Uicker et al., 2003; Cowie, 1961; Hirschhorn, 1962; Bottema, 1961; Bottema and Roth, 1979) as a point in a moving body, which has zero velocity with respect to the inertial frame of reference, frame *{0}*. Its importance lies in the fact that a general planar motion of the body can be represented as an instantaneous rotation with the angular velocity (ω) around an axis passing through the velocity IC. The velocity m_1, is always proportional and perpendicular to the radius vector: $m_1 \propto \rho_1$; $\beta_1 = 90^o$.

With the known velocity of point *P*, the velocity of any point on the rigid platform body can be computed using the IC for velocity as follows.

The location of a general point E, expressed in frame {1} as show in Fig. 2.1, is transformed to frame *{0}* as (Bottema and Roth, 1979):

$$X_E = X_P + x_E \cos\Theta - y_E \sin\Theta$$
$$Y_E = Y_P + x_E \sin\Theta + y_E \cos\Theta \qquad \text{Eq. 2.1}$$

The velocity of point *E* can be computed by differentiating Eq. 2.1 w.r.t. time such that:

$$\dot{X}_E = \dot{X}_P - x_E sin(\Theta)\omega - y_E cos(\Theta)\omega$$
$$\dot{Y}_E = \dot{Y}_P + x_E cos(\Theta)\omega - y_E sin(\Theta)\omega \qquad \text{Eq. 2.2}$$

where: $\dot{\Theta} = \omega$.

In order to find the location of the IC for velocity, let the general point be the IC. Thus $x_E = x_{I1}$, and $y_E = y_{I1}$ Also it becomes necessary that $\dot{X}_{I1} = \dot{Y}_{I1} = 0$. Then Eq. 2.2 becomes:

$$0 = \dot{X}_P - x_{I1}\sin(\Theta)\omega - y_{I1}\cos(\Theta)\omega$$
$$0 = \dot{Y}_P + x_{I1}\cos(\Theta)\omega - y_{I1}\sin(\Theta)\omega \qquad \text{Eq. 2.3}$$

Eq. 2.3 can be considered as a set of two linear equations with two unknowns x_{I1}, and y_{I1} which can be inverted to give:

$$x_{I1} = \frac{\dot{X}_P}{\omega} sin\,\Theta - \frac{\dot{Y}_P}{\omega} cos\Theta$$
$$y_{I1} = \frac{\dot{X}_P}{\omega} cos\,\Theta + \frac{\dot{Y}_P}{\omega} sin\Theta \qquad \text{Eq. 2.4}$$

This is the location of the IC as expressed in frame *{1}*. It can be expressed in frame *{0}* using Eq. 2.1 as follows:

$$X_{I1} = X_P - \frac{\dot{Y}_P}{\omega}$$
$$Y_{I1} = Y_P + \frac{\dot{X}_P}{\omega} \qquad \text{Eq. 2.5}$$

Thus the operation of the platform as specified by the motion of reference point *P* yields a unique location for the velocity IC as long as the body has a finite angular velocity ω. On the other hand, when $\omega = 0$, the velocity IC lies at ∞ and the body is instantaneously in pure translation.

Eq. 2.1 can be rearranged to get:

$$x_E \cos\Theta - y_E \sin\Theta = X_E - X_P$$
$$x_E \sin\Theta + y_E \cos\Theta = Y_E - Y_P \qquad \text{Eq. 2.6}$$

Rearranging Eq. 2.2 using Eq. 2.6, we get the following:

$$\dot{X}_E = \dot{X}_P - (Y_E - Y_P)\omega$$
$$\dot{Y}_E = \dot{Y}_P + (X_E - X_P)\omega \qquad \text{Eq. 2.7}$$

We define frame *{2}* (Fig. 2.2) such that it is instantaneously located at I_1 and is parallel to frame *{1}*. Thus in Eq. 2.7, we replace point *P* with I_1. We can then simplify Eq. 2.7 as (since $\dot{X}_{I1} = \dot{Y}_{I1} = 0$):

$$\dot{X}_E = -Y_{\rho 1}\omega$$
$$\dot{Y}_E = X_{\rho 1}\omega \qquad \text{Eq. 2.8}$$

where $X_{\rho 1}$ and $Y_{\rho 1}$ are the *X* and *Y* components of the radius vector ρ_1 as follows:

$$X_{\rho 1} = X_E - X_{I1}$$
$$Y_{\rho 1} = Y_E - Y_{I1} \qquad \text{Eq. 2.9}$$

As stated earlier the velocity, m_1, of a general point *E* is perpendicular to the radius

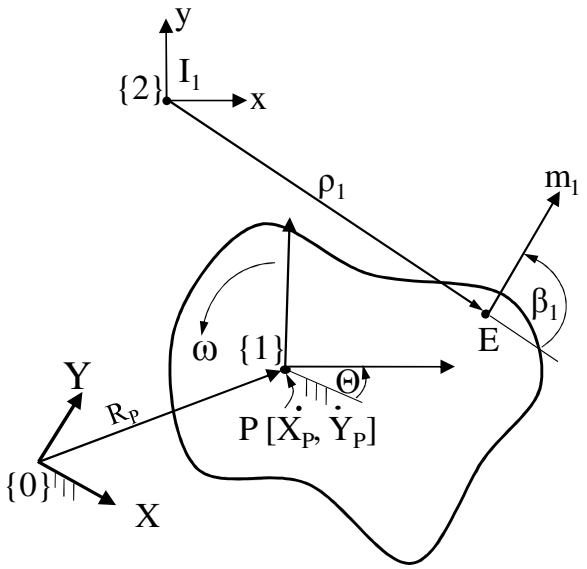

Fig. 2.2: Description of an Instantaneous Body Fixed Frame {2} at the First Order IC

vector, ρ_1 (Uicker et al., 2003; Cowie, 1961; Hirschhorn, 1962; Bottema, 1961; Bottema and Roth, 1979). We will show this analytically. Taking the dot product of m_1 (Eq. 2.8) and ρ_1 (Eq. 2.9), we get:

$$X_{\rho 1} \cdot \dot{X}_E + Y_{\rho 1} \cdot \dot{Y}_E = \left(-X_{\rho 1} Y_{\rho 1} \omega\right) + \left(Y_{\rho 1} X_{\rho 1} \omega\right) = 0 \qquad \text{Eq. 2.10}$$

Another property of the IC states that the velocity of any point on the body is proportional to its distance from the IC. To show this, consider the magnitude of total velocity of point *E*:

$$m_1 = \left|\sqrt{(\dot{X}_E)^2 + (\dot{Y}_E)^2}\right|$$
$$m_1 = \left|\sqrt{(-Y_{\rho 1} \cdot \omega)^2 + (X_{\rho 1} \cdot \omega)^2}\right| \qquad \text{Eq. 2.11}$$

Eq. 2.11 can be simplified to Eq. 2.12 which shows that the velocity of point E is proportional to its distance from the IC.

$$m_1 = |\rho_1 . \omega| \qquad \text{Eq. 2.12}$$

Fig. 2.3 demonstrates these properties (proportionality and perpendicularity) graphically. The location of the IC of velocity in case of a 1-DOF or 2-DOF motion is a geometric property. For instance, a wheel rolling on a flat ground without slipping (1-DOF motion) always has its velocity IC located at the point of contact of the wheel with the ground, whereas the IC of velocity for a differentially driven (such as a two wheeled platform or a four wheeled skid steered platform) mobile platform (2-DOF motion) lies along the common rolling axis. However for a 3-DOF motion, the location of the velocity IC is not completely geometric and depends on the instantaneous motion parameters (the three independent output parameters are: $\dot{X}_P$, $\dot{Y}_P$, and ω). Since we can arbitrarily choose the values of all three parameters, the location of the instant center can be placed anywhere instantaneously as evident from Eq. 2.5. However once the location of the velocity IC is

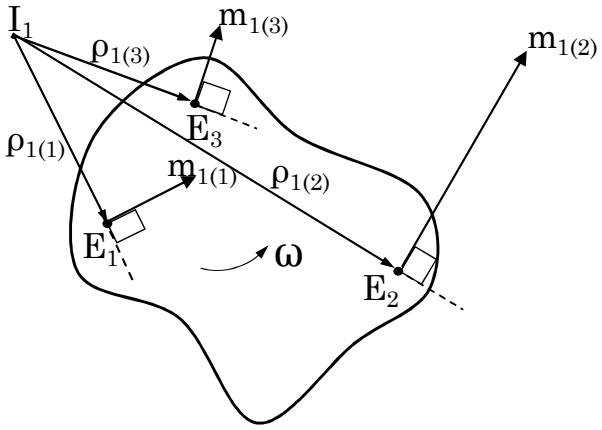

Fig. 2.3: Description of the First Order Motion of General Points in the Rigid Body using the First Order (Velocity) IC

known, the problem simplifies to a geometric nature in that, the velocity, m_1, of any point in the body is proportional and perpendicular to the radius, ρ_1, of itself with respect to the velocity instant center, I_1.

2.4.1 First Order Instant Center Formulation: Special Cases

The location of IC yields significant information about the state of the platform. The following are some of the special cases that can be used to better understand the physical nature of the platform motion.

Case: $\dot{X}_P = \dot{Y}_P = 0$

When the velocity of point P is zero; i.e., when $\dot{X}_P = \dot{Y}_P = 0$, and $\omega \neq 0$, Eq. 2.5 becomes:

$$X_{I1} = X_P$$
$$Y_{I1} = Y_P \qquad \text{Eq. 2.13}$$

Thus the IC is located at the reference point, P. This means that the body is under an instantaneous rotation around the axis passing through point P. This condition is shown in Fig. 2.4.

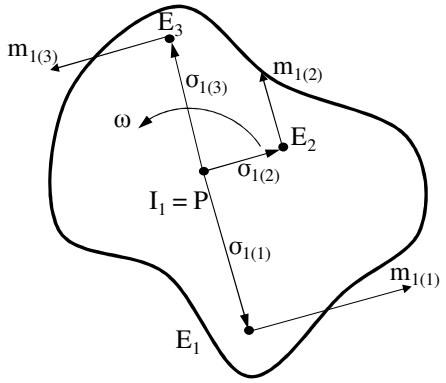

Fig. 2.4: Special Case for the First Order, 3-DOF, Planar Motion of a Rigid Body when the Velocity of Point P is zero. The Location of the Velocity IC is Coincident with Point P.

Case: ω = 0

If the body is under pure translation motion; i.e., ω = 0, Eq. 2.5 reduces to:

$$X_{I1} = \infty$$
$$Y_{I1} = \infty \qquad \text{Eq. 2.14}$$

With the IC at infinity, the velocity of a general point E cannot be defined using the Eq. 8. However using Eq. 7, we can see that $\dot{X}_E = \dot{X}_P$ and $\dot{Y}_E = \dot{Y}_P$. Also we know that the velocity of E is orthogonal to the radius vector between E and the IC. Thus for every point in the body, the IC is located at infinity along the vector orthogonal to the velocity of the point.

Thus when the angular velocity of the body is zero, there are an infinite number of ICs at infinity and every point in the body moves with the same linear velocity equal to the velocity of P, as shown in Fig. 2.5.

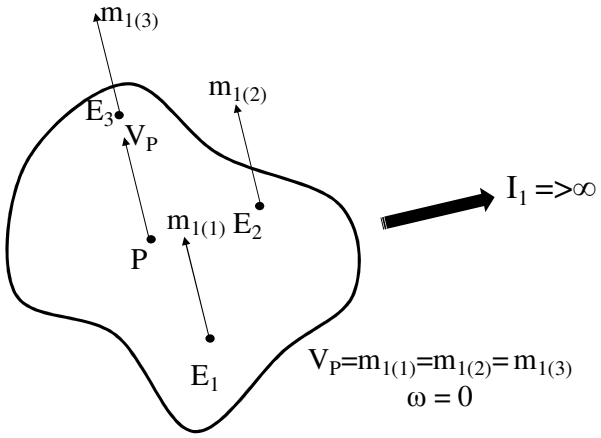

Fig. 2.5: Special Case for the First Order, 3-DOF, Planar Motion of a Rigid Body when the Angular Velocity of the body is zero. The Location of the Velocity IC is at the Infinity.

Other Cases

Other platform configuration specific cases may constrain the location of the velocity IC and we can quickly evaluate if the motion requirement can be achieved or not. For example, in case of a fixed wheel, we know that the IC always lies on the wheel rolling axis. Thus if the IC is away from the axis, we realize that the motion cannot be achieved without skidding. An example is a two wheeled platform such as shown in Fig. 2.6. The velocity IC is constrained to lie along the wheel rolling axis.

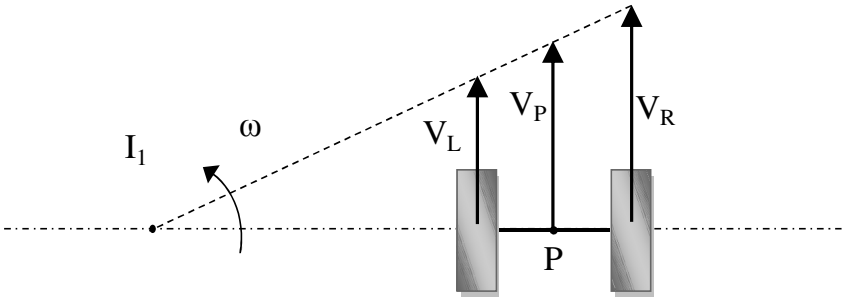

Fig. 2.6: The Location of the Velocity IC for a Two Wheeled Differentially Driven Platform is Constrained to the Axis of Wheel Rotation

Using the same platform configuration, we can consider another special case. When the velocity IC is coincident with one of the wheel attachment points, we can see that the whole platform revolves around that wheel as shown in Fig. 2.7. This information can then be used to evaluate the feasibility of the motion by computing wheel-ground

interaction forces.

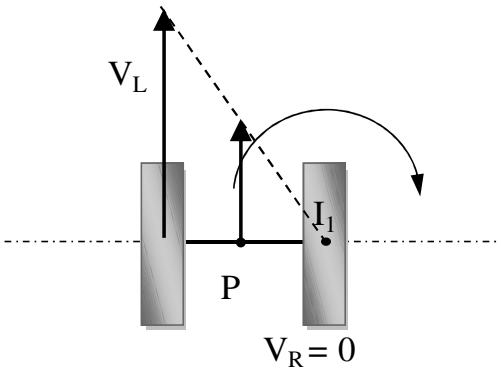

Fig. 2.7: The Velocity IC Coincident with One of the Wheel Center for a Two Wheeled Differentially Driven Platform

2.5 Second Order (Acceleration) Planar Motion of a Rigid Body

Using the vector method, we can locate the IC for velocity with the velocity directions of any two points on the body. However, to locate the IC for acceleration, we need to know both the magnitude and the direction of the two points (Uicker et al., 2003). However, the acceleration IC computation is useful for computing accelerations of a large number of points on a body (Cowie, 1961). A multi- wheeled mobile platform has a large number of points of interest (such as wheel attachment points, payload attachment points, etc.). Thus the acceleration IC is a useful tool for mobile platform synthesis. The acceleration center has been well documented in the literature (Bottema and Roth, 1979; Veldkamp, 1963, 1967; Ridley et al., 1992; Wang et al., 1997; Martinez and Duffy, 1998). Veldkamp's paper (1963) on the acceleration distribution with a discussion at the end by Skreiner and a paper by Martinez and Duffy (1998) studied the acceleration center and the acceleration field for a general rigid body under spatial motion with an emphasis on special case scenarios. Ridley et al. (1992) and Wang et al. (1997) used the screw theory to describe the spatial motion of a rigid body up to the second order.

Similar to the velocity IC, the acceleration IC is defined as the point on a rigid body in motion where the total acceleration with respect to the inertial frame of reference, frame *{0}*, is zero ($\ddot{X}_{I2} = \ddot{Y}_{I2} = 0$). The following section details the algebraic formulation to define the acceleration IC in order to compute the required acceleration of any point on the platform.

Acceleration of a general point *E* on the platform body is found by differentiating Eq. 2.2 as follows:

$$\begin{aligned} \ddot{X}_E &= \ddot{X}_P - x_E\, sin(\Theta)\,\alpha - x_E \cos(\Theta)\,\omega^2 - y_E\, cos(\Theta)\,\alpha + y_E sin(\Theta)\omega^2 \\ {}^0\ddot{Y}_E &= \ddot{Y}_P + x_E\, cos(\Theta)\,\alpha - x_E \sin(\Theta)\,\omega^2 - y_E\, sin(\Theta)\,\alpha - y_E cos(\Theta)\omega^2 \end{aligned} \qquad \text{Eq. 2.15}$$

The location of the acceleration IC, I_2, can be found by replacing point *E* with I_2. Thus $x_E = x_{I2}$, and $y_E = y_{I2}$. Also it becomes necessary that $\ddot{X}_{I2} = \ddot{Y}_{I2} = 0$. Then Eq. 2.13 becomes:

$$\begin{aligned} 0 &= \ddot{X}_P - x_{I2}\, sin(\Theta)\,\alpha - x_{I2}\, cos(\Theta)\,\omega^2 - y_{I2}\, cos(\Theta)\,\alpha + y_{I2}\, sin(\Theta)\,\omega^2 \\ 0 &= \ddot{Y}_P + x_{I2}\, cos(\Theta)\,\alpha - x_{I2}\, sin(\Theta)\,\omega^2 - y_{I2}\, sin(\Theta)\,\alpha - y_{I2}\, cos(\Theta)\,\omega^2 \end{aligned} \qquad \text{Eq. 2.16}$$

Eq. 2.14 is a set of two linear equations with two unknowns (x_{I2} and y_{I2}). Solving for the unknowns we get:

$$\begin{aligned} x_{I2} &= \frac{\ddot{X}_P(sin(\Theta)\alpha + cos(\Theta)\omega^2) - \ddot{Y}_P(cos(\Theta)\alpha - sin(\Theta)\,\omega^2)}{\alpha^2 + \omega^4} \\ y_{I2} &= \frac{\ddot{X}_P(\,cos(\Theta)\alpha - sin(\Theta)\omega^2) + \ddot{Y}_P(sin(\Theta)\,\alpha + cos(\Theta)\,\omega^2)}{\alpha^2 + \omega^4} \end{aligned} \qquad \text{Eq. 2.17}$$

This is the location of the IC for acceleration as expressed in frame {1}. Using Eq. 2.1 to transform it into the global frame {0} we get:

$$\begin{aligned} X_{I2} &= X_P + \frac{\ddot{X}_P\,\omega^2 - \ddot{Y}_P\alpha}{\alpha^2 + \omega^4} \\ Y_{I2} &= Y_P + \frac{\ddot{X}_P\,\alpha + \ddot{Y}_P\omega^2}{\alpha^2 + \omega^4} \end{aligned} \qquad \text{Eq. 2.18}$$

Thus with a known motion plan; i.e., with a known acceleration of point *P,* the angular velocity, ω, and the angular acceleration, α, we can uniquely locate the IC as long as either ω or α is nonzero.

Now Eq. 2.13 can be rearranged using Eq. 2.6 to give the following:

$$\ddot{X}_E = \ddot{X}_P - (X_E - X_P)\omega^2 - (Y_E - Y_P)\alpha$$
$$\ddot{Y}_E = \ddot{Y}_P + (X_E - X_P)\alpha - (Y_E - Y_P)\omega^2 \qquad \text{Eq. 2.19}$$

Angle β_2 in Fig. 2.1 is computed as follows (Bottema and Roth, 1979; Veldkamp, 1963, 1967).

$$\tan(\beta_2) = -\frac{\alpha}{\omega^2} \qquad \text{Eq. 2.20}$$

2.5.1 DIRECTIONALITY AND PROPORTIONALITY: PROPERTIES OF THE ACCELERATION IC

The value of β_2 is dependent on the angular velocity and angular acceleration of the rigid body which are constant entities at every instant in time for all points in the body. Though this is a well known result, it will be validated mathematically as this result will be used for higher order formulation in Sec. 2.6.

Eq. 2.17 can be rearranged using Eq. 2.18 as:

$$\ddot{X}_E = \ddot{X}_P - \omega^2[(X_E - X_P) - (Y_E - Y_P)\,tan(\beta_2)]$$
$$\ddot{Y}_E = \ddot{Y}_P - \omega^2[(X_E - X_P)tan(\beta_2) + (Y_E - Y_P)] \qquad \text{Eq. 2.21}$$

If we define a coordinate frame *{3}* such that it is located at the acceleration IC and is parallel to frame *{1}* similar to frame *{2}* (Fig. 2.2), we can simplify Eq. 2.19 to give:

$$\ddot{X}_E = -\omega^2\left[X_{\rho 2} - Y_{\rho 2} tan\,\beta_2\right]$$
$$\ddot{Y}_E = -\omega^2\left[X_{\rho 2} tan\beta_2 + Y_{\rho 2}\right] \qquad \text{Eq. 2.22}$$

where ρ_{2X} and ρ_{2Y} are the X and Y components of the radius vector ρ_2 (see Fig. 2.1) expressed in frame $\{0\}$ as follows:

$$X_{\rho 2} = X_E - X_{I2}$$
$$Y_{\rho 2} = Y_E - Y_{I2}$$
Eq. 2.23

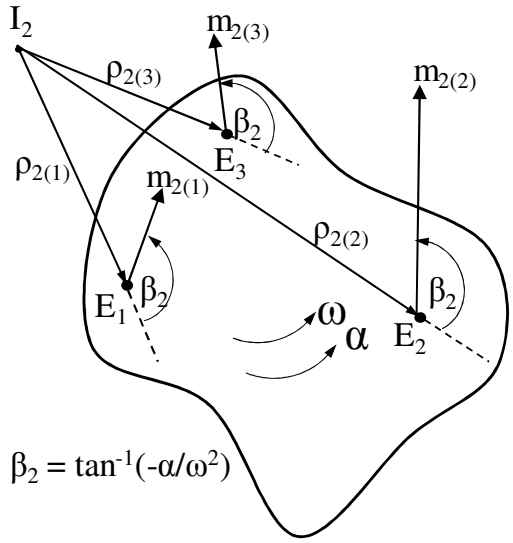

Fig. 2.8: Description of the Second Order Motion of a General Point in the Rigid Body using the Acceleration IC

From Fig. 2.1, we see for the second order formulation that:

$$\sigma_2 = \gamma_2 + \beta_2$$ Eq. 2.24

We will show that this expression can be validated using the instantaneously constant value of β_2 as defined in Eq. 2.18. The angle σ_2 can be computed as:

$$\sigma_2 = tan^{-1}\left(\frac{\ddot{Y}_E}{\ddot{X}_E}\right)$$ Eq. 2.25

Using expressions for $\ddot{X}_E$, and $\ddot{Y}_E$ from Eq. 2.20, we get:

$$\sigma_2 = tan^{-1}\left(\frac{-\omega^2\left[X_{\rho 2} tan\beta_2 + Y_{\rho 2}\right]}{-\omega^2\left[X_{\rho 2} - Y_{\rho 2} tan\beta_2\right]}\right)$$ Eq. 2.26

Dividing the numerator and denominator by$X_{\rho 2}$, we get:

$$\sigma_2 = tan^{-1}\left(\frac{tan\beta_2 + \frac{Y_{\rho 2}}{X_{\rho 2}}}{1 - (\frac{Y_{\rho 2}}{X_{\rho 2}}) tan\beta_2}\right)$$ Eq. 2.27

But $\frac{Y_{\rho 2}}{X_{\rho 2}} = tan\,(\gamma_2)$, the tangent of the angle made by the radius vector with *X* axis of the global frame *{0}*. Thus Eq. 2.25 can be written as:

$$\sigma_2 = tan^{-1}\left(\frac{tan\beta_2 + tan\gamma_2}{1 - tan\gamma_2 tan\beta_2}\right)$$

$$\sigma_2 = tan^{-1}(tan(\gamma_2 + \beta_2)) \qquad \text{Eq. 2.28}$$

$$\therefore \sigma_2 = \gamma_2 + \beta_2$$

Comparing Eq. 2.26 with Eq. 2.22, we can see that the value of β_2 as given by Eq. 2.18 provides the desired result.

Thus the angle between the total acceleration, m_2, and the radius vector, ρ_2, of a general point on the body is constant as shown in Fig. 2.8.

Thus by locating the IC for acceleration, we can compute both the magnitude and the direction for the total acceleration of any point on the body.

2.5.2 A NOTE ON THE UNIQUENESS OF THE VALUE OF THE ORIENTATION ANGLE, β_2

Note that the definition of angle β_2 given by Eq. 2.20 does not yield a unique value for β_2. For example, when α =1 and ω = 1; the Eq. 2.20 can yield two values, -45^o and 135 ^{o}, for β_2. Which of the two values is the correct one? This can be resolved by the following discussion. Fig. 2.9 shows an instantaneous motion of a rigid body that results in the acceleration IC located at I_2. A general point, E, is located at a radius ρ_2 w.r.t. the acceleration IC, I_2. The total acceleration of point E, m_2, can be separated into two orthogonal components, namely, the tangential component, m_{2t}, and the normal component, m_{2n} with respect to the radius, ρ_2. The magnitude (and direction) of the two components are dependent on the values of instantaneous angular velocity, ω, and angular acceleration, α, of the rigid body, and on the magnitude of the radius, ρ_2, as shown. Note that the normal component, which is also known as centripetal acceleration, is always directed towards the center, I_2. Thus the total acceleration will always make an

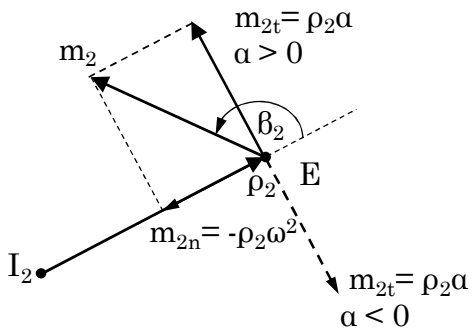

Fig. 2.9: Tangential and Normal Components of the Acceleration of a General Point with respect to the Acceleration IC

angle, β_2, such that its magnitude is greater than or equal to 90^o i.e. $|\beta_2| > \frac{\pi}{2}$. When, angular acceleration, α, has a negative value, $\beta_2 < -\frac{\pi}{2}$. This is summarized in Eq. 2.29:

$$|\beta_2| > \frac{\pi}{2}$$
$$\alpha > 0: \quad \beta_2 > \frac{\pi}{2}$$
$$\alpha < 0: \quad \beta_2 < -\frac{\pi}{2} \qquad \text{Eq. 2.29}$$

This information can be used to compute the unique value of angle, β_2.

Next, we study some special case scenarios that occur as instantaneous kinematic states of the rigid body. The study of special case scenarios (Veldkamp, 1969; Ridley et al., 1992; and Martinez and Duffy, 1998) for location of the acceleration pole gives physical insight into the state of the motion of the platform much as obtained using the velocity pole.

2.5.3 SECOND ORDER INSTANT CENTER FORMULATION: SPECIAL CASES

Case: $\omega = 0$

When the angular velocity of the platform is zero, the acceleration IC (Eq. 2.16) is located at:

$$X_{I2} = X_P - \frac{\ddot{Y}_P}{\alpha} \qquad \text{Eq. 2.30}$$

$$X_{I2} = Y_P + \frac{\ddot{X}_P}{\alpha}$$

Notice that this expression is a similar to the expression for velocity IC given by Eq. 2.5. The total acceleration for point E (Eq. 2.20) also takes a form identical to the velocity of a general point (Eq. 2.8) as follows:

$$\begin{aligned} \ddot{X}_E &= -Y_{\sigma 2} \cdot \alpha \\ \ddot{Y}_E &= X_{\sigma 2} \cdot \alpha \end{aligned} \qquad \text{Eq. 2.31}$$

Thus the location of acceleration IC and total acceleration assume a form identical to the first order formulation when ω = 0. This means that when the angular velocity of the body is zero, the acceleration of a general point becomes orthogonal to radius vector similar to the velocity pole as shown in Fig. 2.10, i.e., it has no normal acceleration component.

Case: α = 0

When the angular acceleration of the platform is zero, the acceleration of point E (Eq. 2.20) reduces to:

$$\begin{aligned} \ddot{X}_E &= -\omega^2 X_{\sigma 2} \\ \ddot{Y}_E &= -\omega^2 Y_{\sigma 2} \end{aligned} \qquad \text{Eq. 2.32}$$

Here the only nonzero component of acceleration is the centripetal acceleration which is

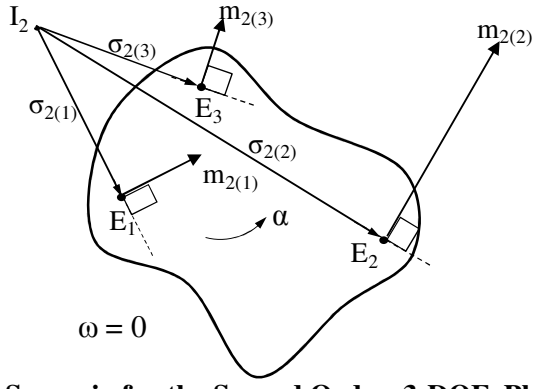

Fig. 2.10: Special Case Scenario for the Second Order, 3-DOF, Planar Motion of a Rigid Body when the Angular Velocity of the Body is Zero

always directed towards the center. Thus when angular acceleration of the body is zero, the total acceleration of every point on the body is directed towards the acceleration IC as shown in Fig. 2.11. In this case, $\beta_2 = 180$ and the first two ICs collide, i.e., $I_1 = I_2$.

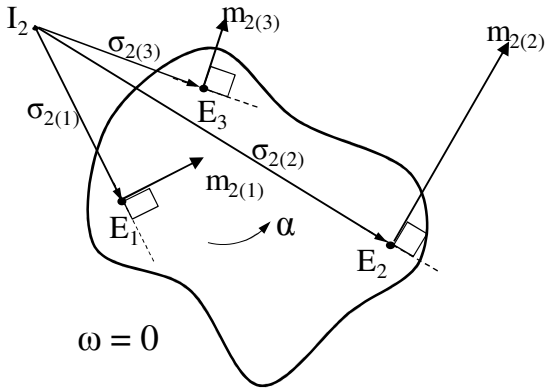

Fig. 2.11: Special Case Scenario for the Second Order, 3-DOF, Planar Motion of a Rigid Body with Zero Angular Acceleration

Case: $\ddot{X}_P = \ddot{Y}_P = 0$

When the acceleration of point P is zero; i.e., when $\ddot{X}_P = \ddot{Y}_P = 0$, Eq. 2.20 becomes:

$$X_{I2} = X_P$$
$$Y_{I2} = Y_P \qquad \text{Eq. 2.33}$$

Thus the IC is located at the reference point, P. This means that the body is under pure rotation up to the second order around an axis passing through the point P. This condition is shown in Fig. 2.12. The acceleration of a point on the body is dependent upon its

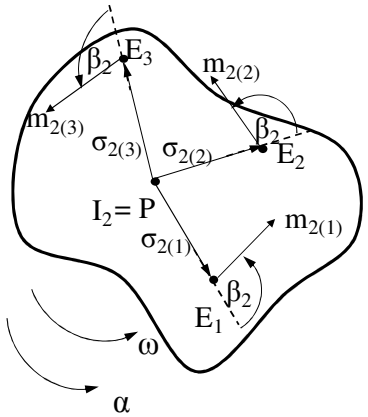

Fig. 2.12: Special Case Scenario for the Second Order, 3-DOF, Planar Motion of a Rigid Body when the Acceleration of Point P is Zero: Angular Acceleration IC is Coincident with P

distance from the point P and is at an angle β_2 with the radius vector.

Case: ω = α =0

When both the angular velocity, ω, and, angular acceleration, α, of the mobile platform are zero, the IC for acceleration goes to infinity (Eq. 2.16). The acceleration of Point E cannot be computed using the acceleration IC (i.e., using Eq. 2.22). However, using Eq. 2.17, we can see that the acceleration of point E is instantaneously equal to the acceleration of the point of reference, P. It means that all points in the body move with same linear velocity up to the second order as shown in Fig. 2.13.

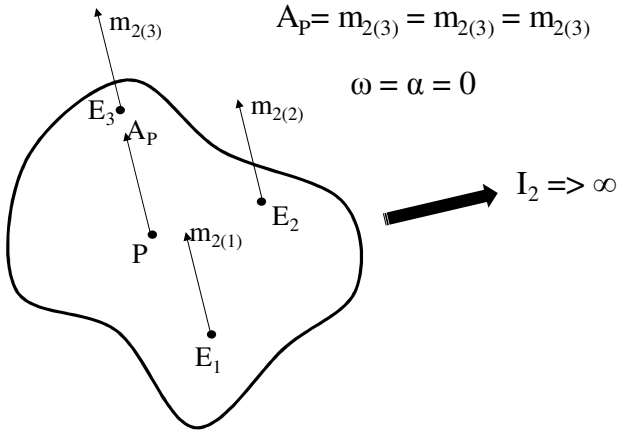

Fig. 2.13: Special Case Scenario for the Second Order, 3-DOF, Planar Motion of a Rigid Body with Zero Angular Velocity and Angular Acceleration: Acceleration IC at Infinity

2.6 Higher Order Planar Motion of a Rigid Body

A smooth motion plan in the operational space for robotic systems usually specifies a motion profile for the third order motion parameter known as jerk (Gallardo-Alvarado, and Rico-Martínez, 2001; Beggs, 1983) (or second acceleration (Bottema and Roth, 1979). Though the first order (velocity) and second order (acceleration) poles have been studied to some level of detail, the authors are not aware of a work on the third order (jerk) and further higher order ICs. Bottema and Roth (1989) provide a brief discussion on the jerk of a general point at time *t=0*, when the frames *{0}* and *{1}* coincide without

discussing the IC for jerk. Beggs (1983) uses a vector based formulation to derive the jerk of a general point in a rigid body under spatial motion without alluding to the properties of the IC for jerk.

The following section details the IC based algebraic formulation for third and higher order kinematics. The kinematic formulation is derived for the third and fourth order planar motion simultaneously while Table 2.1 shows the formulation for up to the fifth order. The expression for a general order formulation using the corresponding instant center is presented in a compact form for k^{th} order in terms of the magnitude and the direction of the time state of point *E*. The important result of the proposed formulation is that the location of the k^{th} order IC immediately determines the corresponding kinematic field of the rigid body.

Differentiating Eq. 2.13 with respect to time, we get the third order equation for a general point E on the platform

$$\begin{aligned} X_E^{(3)} &= X_P^{(3)} - x_E\, sin(\Theta)\,(\dot{\alpha} - \omega^3) - x_E\, cos(\Theta)\,(3\omega\alpha) - y_E\, cos(\Theta)\,(\dot{\alpha} - \omega^3) \\ &\quad + y_E \sin(\Theta)\,(3\omega\alpha) \\ Y_E^{(3)} &= Y_P^{(3)} + x_E\, cos(\Theta)\,(\dot{\alpha} - \omega^3) - x_E\, sin(\Theta)\,(3\omega\alpha) - y_E\, sin(\Theta)\,(\dot{\alpha} - \omega^3) \\ &\quad - y_E\, cos(\Theta)\,(3\omega\alpha) \end{aligned} \qquad \text{Eq. 2.34}$$

Note that the third derivative of X_E with time is denoted as $X_E^{(3)}$. Further, differentiating Eq. 2.34 with time, we get the fourth order equation for Point E.

$$\begin{aligned} X_E^{(4)} &= X_P^{(4)} - x_E\, sin(\Theta)\,(\ddot{\alpha} - 6\omega^2\alpha) - x_E\, cos(\Theta)\,(4\omega\dot{\alpha} + 3\alpha^2 - \omega^4) \\ &\quad - y_E\, cos(\Theta)\,(\ddot{\alpha} - 6\omega^2\alpha) + y_E sin(\Theta)(4\omega\dot{\alpha} + 3\alpha^2 - \omega^4) \\ Y_E^{(4)} &= Y_P^{(4)} + x_E\, cos(\Theta)\,(\ddot{\alpha} - 6\omega^2\alpha) - x_E\, sin(\Theta)\,(4\omega\dot{\alpha} + 3\alpha^2 - \omega^4) \\ &\quad - y_E\, sin(\Theta)\,(\ddot{\alpha} - 6\omega^2\alpha) - y_E\, cos(\Theta)\,(4\omega\dot{\alpha} + 3\alpha^2 - \omega^4) \end{aligned} \qquad \text{Eq. 2.35}$$

In order to simplify the Eq. 2.34 and Eq. 2.35, collecting terms with identical coefficients as follows:

$$
\begin{aligned}
X_E^{(3)} &= X_P^{(3)} - (x_E \sin(\Theta) + y_E \cos(\Theta))(\dot{\alpha} - \omega^3) \\
&\quad - (x_E \cos(\Theta) - y_E \sin(\Theta))(3\omega\alpha) \\
Y_E^{(3)} &= Y_P^{(3)} + (x_E \cos(\Theta) - y_E \sin(\Theta))(\dot{\alpha} - \omega^3)) \\
&\quad - (x_E \sin(\Theta) + y_E \cos(\Theta))(3\omega\alpha)
\end{aligned}
\qquad \text{Eq. 2.36}
$$

and,

$$
\begin{aligned}
X_E^{(4)} &= X_P^{(4)} - (x_E \sin(\Theta) + y_E \cos(\Theta))(\ddot{\alpha} - 6\omega^2\alpha) \\
&\quad - (x_E \cos(\Theta) - y_E \sin(\Theta))(4\omega\dot{\alpha} + 3\alpha^2 - \omega^4) \\
Y_E^{(4)} &= Y_P^{(4)} + (x_E \cos(\Theta) - y_E \sin(\Theta))(\ddot{\alpha} - 6\omega^2\alpha)) \\
&\quad - (x_E \sin(\Theta) + y_E \cos(\Theta))(4\omega\dot{\alpha} + 3\alpha^2 - \omega^4)
\end{aligned}
\qquad \text{Eq. 2.37}
$$

The location of the IC for the third and fourth order kinematics can be found by equating the right hand side of the Eq. 2.36 and Eq. 2.37 to zero, respectively. We get a set of two linear equations each similar to Eq. 2.3 and Eq. 2.14. The locations of ICs for the third and fourth order kinematics can then be computed by inverting the two sets of equations. The resulting ICs are expressed in local frame *{1}*. Transforming them into frame *{0},* we get the IC for jerk (Eq. 2.38) and the derivative of jerk (Eq. 2.39), respectively.

$$
\begin{aligned}
X_{I3} &= X_P + \frac{X_P^{(3)}(3\omega\alpha) - Y_P^{(3)}(\dot{\alpha} - \omega^3)}{(\dot{\alpha} - \omega^3)^2 + (3\omega\alpha)^2} \\
Y_{I3} &= Y_P + \frac{X_P^{(3)}(\dot{\alpha} - \omega^3) + Y_P^{(3)}(3\omega\alpha)}{(\dot{\alpha} - \omega^3)^2 + (3\omega\alpha)^2}
\end{aligned}
\qquad \text{Eq. 2.38}
$$

and,

$$
\begin{aligned}
X_{I4} &= X_P + \frac{X_P^{(4)}(4\omega\dot{\alpha} + 3\alpha^2 - \omega^4) - Y_P^{(4)}(\ddot{\alpha} - 6\omega^2\alpha)}{(\ddot{\alpha} - 6\omega^2\alpha)^2 + (4\omega\dot{\alpha} + 3\alpha^2 - \omega^4)^2} \\
Y_{I4} &= Y_P + \frac{X_P^{(4)}(\ddot{\alpha} - 6\omega^2\alpha) + Y_P^{(4)}(4\omega\dot{\alpha} + 3\alpha^2 - \omega^4)}{(\ddot{\alpha} - 6\omega^2\alpha)^2 + (4\omega\dot{\alpha} + 3\alpha^2 - \omega^4)^2}
\end{aligned}
\qquad \text{Eq. 2.39}
$$

To simplify Eq. 2.36, we can define an angle β_3 such that:

$$\beta_3 = tan^{-1}\left(-\frac{\dot{\alpha} - \omega^3}{3\omega\alpha}\right) \quad \text{Eq. 2.40}$$

Similarly we can define angle β_4 such that:

$$\beta_4 = tan^{-1}\left(-\frac{\ddot{\alpha} - 6\omega^2\alpha}{4\omega\dot{\alpha} + 3\alpha^2 - \omega^4}\right) \quad \text{Eq. 2.41}$$

Eq. 2.36 can then be simplified (on the lines similar to Eq. 2.19) to give:

$$\begin{aligned} X_E^{(3)} &= X_P^{(3)} - 3\omega\alpha[(X_E - X_P) - (Y_E - Y_P)tan\beta_3] \\ Y_E^{(3)} &= Y_P^{(3)} - 3\omega\alpha[(X_E - X_P)tan\beta_3 + (Y_E - Y_P)] \end{aligned} \quad \text{Eq. 2.42}$$

Similarly Eq. 2.37 is simplified to:

$$\begin{aligned} X_E^{(4)} &= X_P^{(4)} - (4\omega\dot{\alpha} + 3\alpha^2 - \omega^4)\,[(X_E - X_P) - (Y_E - Y_P)tan\beta_4] \\ Y_E^{(4)} &= Y_P^{(4)} - (4\omega\dot{\alpha} + 3\alpha^2 - \omega^4)\,[(X_E - X_P)tan\beta_4 + (Y_E - Y_P)] \end{aligned} \quad \text{Eq. 2.43}$$

We can define a coordinate frame each for the third order and fourth order formulation such that it is located at the third order IC and fourth order IC, respectively and is parallel to frame {1} similar to frame {2} (Fig. 2.2); then we can further simplify Eq. 2.42 and Eq. 2.43 to give:

$$\begin{aligned} X_E^{(3)} &= -3\omega\alpha\left[\left(X_{\rho 3}\right) - (Y_{\rho 3})tan\beta_3\right] \\ Y_E^{(3)} &= -3\omega\alpha\left[\left(X_{\rho 3}\right)tan\beta_3 + (Y_{\rho 3})\right] \end{aligned} \quad \text{Eq. 2.44}$$

where $X_{\rho 3}$ and $Y_{\rho 3}$ are the X and Y components of the radius vector ρ_3 expressed in frame {0} as follows:

$$\begin{aligned} X_{\rho 3} &= X_E - X_{I3} \\ Y_{\rho 3} &= Y_E - Y_{I3} \end{aligned} \quad \text{Eq. 2.45}$$

Similarly for the fourth order:

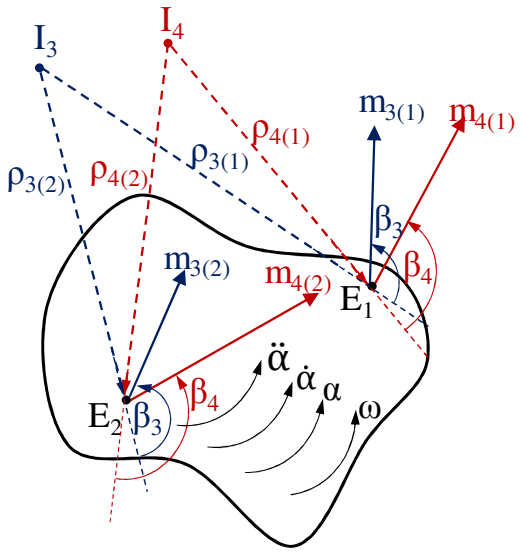

Fig. 2.14: The Third and Fourth Order Motion Description of a Rigid Body using the ICs

$$X_E^{(4)} = -(4\omega\dot{\alpha} + 3\alpha^2 - \omega^4)\left[(X_{\rho 4}) - (Y_{\rho 4})tan\beta_4\right]$$
$$Y_E^{(4)} = -(4\omega\dot{\alpha} + 3\alpha^2 - \omega^4)\left[(X_{\rho 4})tan\beta_4 + (Y_{\rho 4})\right] \quad \text{Eq. 2.46}$$

where $X_{\rho 4}$ and $Y_{\rho 4}$ are the X and Y components of the radius vector ρ_4 expressed in frame $\{0\}$ as follows:

$$X_{\rho 4} = X_E - X_{I4}$$
$$Y_{\rho 4} = Y_E - Y_{I4} \quad \text{Eq. 2.47}$$

Note that Eq. 2.44 and Eq. 2.46 take an identical form to Eq. 2.20. We showed using Eq. 2.22-Eq. 2.26 that the acceleration of a general point on the platform body makes a constant angle β_2 with the radius vector ρ_2. Note that the term ω^2 gets dropped during the computation and thus has no effect on the final outcome.

We can show using the same procedure as in Eq. 2.22-Eq. 2.26 that the jerk, m_3, of point E (a general point in the body) makes a constant angle β_3 with the radius vector ρ_3. Similarly the jerk derivative, m_4, of point E makes a constant angle β_4 with the radius vector ρ_4. Fig. 2.14 shows these properties of the third and fourth order formulation. The

third order and fourth order entities are shown in blue and red color respectively for better visualization. The IC locations dictate the kinematic requirements from every point of the body. This is demonstrated by two general points on the body, E_1, and E_2. Obviously a lot of interesting special cases exist for the third and fourth order properties.

We can start to see that there is a general form for the expression for the time state of point E in the body which can be written as:

$$X_E^{(k)} = M_k\left[(X_{\rho k}) - (Y_{\rho k})tan\beta_k\right]$$
$$Y_E^{(k)} = M_k\left[(X_{\rho k})tan\beta_k + (Y_{\rho k})\right] \qquad \text{Eq. 2.48}$$

The term M_k can be viewed as the scaling factor that depends on the the k^{th} order instantaneous kinematic state for of the mobile platform. For instance $M_2 = -\omega^2$, $M_3 = -3\omega\alpha$, etc. Rearranging Eq. 2.48 by factoring $1/cos\beta_k$ out of the bracket, we get:

$$X_E^{(k)} = \frac{M_k}{cos\beta_k}\left[(X_{\rho k}).cos\beta_k - (Y_{\rho k}).sin\beta_k\right]$$
$$Y_E^{(k)} = \frac{M_k}{cos\beta_k}\left[(X_{\rho k}).sin\beta_k + (Y_{\rho k}).cos\beta_k\right] \qquad \text{Eq. 2.49}$$

The magnitude of the time state m_k can be computed by squaring and adding the two equations in Eq. 2.49 as follows:

$$|m_k|^2 = \left(X_E^{(k)}\right)^2 + \left(Y_E^{(k)}\right)^2 \qquad \text{Eq. 2.50}$$

Substituting the expressions for $X_E^{(k)}$ and $Y_E^{(k)}$ from Eq. 2.49, and simplifying, we get:

$$|m_k|^2 = \left(\frac{M_k}{cos\beta_k}\right)^2\left[(X_{\rho k})^2 + (Y_{\rho k})^2\right]$$
$$|m_k|^2 = \left(\frac{M_k}{cos\beta_k}\right)^2(\rho_k)^2 \qquad \text{Eq. 2.51}$$

Thus the magnitude of m_k, is given as:

$$|m_k| = \left|\left(\frac{M_k}{cos\beta_k}\right)\rho_k\right| \qquad \text{Eq. 2.52}$$

Of course the magnitude, M_k, and the direction, β_k, are instantaneously constant

throughout the body while, the radius ρ_k is dependent on the location of point *E* relative to I_k. Thus in general: $m_k \propto \rho_k$.

From Fig. 2.1, The direction of the time state m_k in global frame *{0}*, σ_k, can be described as:

$$\sigma_k = \gamma_k + \beta_k \qquad \text{Eq. 2.53}$$

This is the orientation of m_k in frame $\{0\}$. Note that β_k is instantaneously constant throughout the body, whereas the value of angle γ_k is dependent on the location of point *E* relative to I_k or in other words, the direction of ρ_k.

With this information, the expression for the k^{th} time state of a general point *E* in the rigid body undergoing a planar motion is as follows:.

$$m_k = \left|\frac{M_k}{cos\beta_k}\rho_k\right| e^{i(\gamma_k+\beta_k)}$$

Alternatively, Eq. 2.54

$$m_k = \left(\left|\frac{M_k}{cos\beta_k}\right| e^{i(\beta_k)}\right)\left(|\rho_k| e^{i(\gamma_k)}\right)$$

Eq. 2.54 is a concise and general equation for the magnitude and direction of the k^{th} order time state of a general point *E* on the rigid body. The expression provides the k^{th} order field of the rigid body in motion using the corresponding IC in terms of ρ_k, i.e., the location of any point in the body with respect to the IC, I_k. We can separate out the terms that are constant throughout the rigid body and that are dependent on the location of the particular point w.r.t. the corresponding IC as shown in Eq. 47. An important special case of the general equation occurs when *k=1*, i.e., first order kinematics when $\beta_1 = 90^o$. This is due to the fact that the angle β_k is the tangent of the ratio of two orthogonal components (a component along radius vector ρ_k (denominator) while the other perpendicular to it (numerator)). In case of velocity, there is no component along the

radius vector. Thus the case needs to be handled separately. In general, for k^{th} order motion M_k is the component that is directed along the radius vector. When M_k is zero, $\beta_k = 90^o$. This can be verified for second order kinematics when the angular velocity, ω, of the body is zero while the angular acceleration is non-zero, α. In that case, $\beta_2 = 90^o$ and the Eq. 47 results in a division by zero $(\frac{0}{0})$. This is a special scenario that yields important information of the instantaneous motion state of the body.

Fig. 2.15 illustrates the properties graphically which shows a general k^{th} order motion of a rigid body. E_1, E_2, and E_3 are three distinct points on the body. At a particular point in time, the IC for k^{th} order is located at I_k. For discussion purpose, let the three points be such that the orientations of $\rho_{k(1)}$ and $\rho_{k(2)}$ are instantaneously equal $(\gamma_{k(1)} = \gamma_{k(2)})$. This is true when E_1, E_2, and I_k are collinear. Also let the magnitudes of $\rho_{k(1)}$ and $\rho_{k(3)}$ be equal. This is true when the two points are on a circle with the IC as the origin. The parameters that have constant value for all points in the body are colored red where as the parameters that are dependent on the location of the point are colored green in Fig. 2.15.

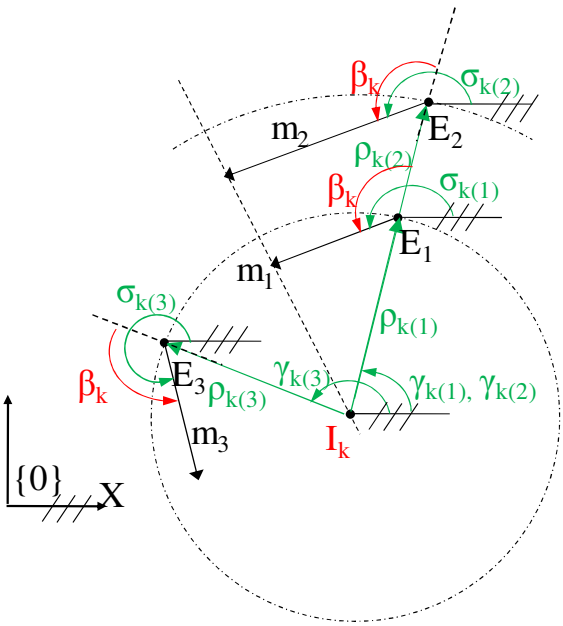

Fig. 2.15: k^{th} Order Kinematics of a General Rigid Body

We can see that m_1 and m_2 are parallel and m_1 and m_3 have the same magnitude. In other words, all points on a radial line will have the same orientation for respective time states and all points at same radial distance will have equal time state magnitudes. This shows the geometric nature of the formulation.

We have presented here an algebraic formulation to represent the k^{th} order kinematic state of a rigid body in terms of the time state of a general point, E, in the body by using the corresponding IC as the reference.

To allow us to understand the formulation, the next section provides a simple example of the first order motion of a general J wheeled mobile platform with powered caster wheels This example is just to familiarize the reader with the formulation. A thorough development of motion synthesis for the mobile platform including the higher order motion synthesis will be dealt with in an ensuing paper.

2.7 Summary and Discussion

This chapter lays out the systematic formulation that enables the kinematic description of a rigid body for up to the fifth order which can be extended to k^{th} order in a straight forward way. Summary of the analytical results is shown in Table 2.1.

The important results of the discussion above are summarized as follows:

1. The mobile platform is a parallel system with a straightforward inverse kinematics. Thus the kinematic formulation using ICs can result in a simpler and yet physically intuitive motion synthesis of mobile platforms

2. The velocity IC is a geometric property for a constrained (1-DOF and 2-DOF) planar general motion. In case of a 3-DOF planar motion, the IC is not based entirely on geometry but depends on the kinematic properties (translational and rotational velocities) of the rigid body motion.

3. In general, the IC of any order follows two properties: directionality and proportionality. That is every time state (such as velocity, acceleration, jerk, etc.) of every point E in the rigid body is at a constant angle β_k to the radius vector ρ_k that joins the point with the corresponding IC I_k. In case of first order (velocity), the angle is 90^o. The magnitude of the time state is proportional to the radius vector, ρ_k.

4. The general equation for k^{th} order motion state of any point in a rigid body under a planar motion can be expressed as follows: $m_k = \left|\frac{M_k}{cos\beta_k}\rho_k\right| e^{i(\gamma_k+\beta_k)}$, where $\left|\frac{M_k}{cos\beta_k}\rho_k\right|$ is the magnitude while $e^{i(\gamma_k+\beta_k)}$ is the direction. Then the proportionality can be analytically described as: $m_k \propto \rho_k$. Also the directionality comes from the fact that the angle between two vectors m_k and ρ_k is β_k.

5. Study of special cases of motion provides valuable physical insight into the motion of the mobile platform.

Table 2.1: Summary of the IC Based Kinematic Formulation for Mobile Platforms

	IC Location	The Orientation Angle	Times States of a General Point 'E'
First Order	$X_{I1} = X_P - \frac{\dot{Y}_P}{\omega}$ $Y_{I1} = Y_P + \frac{\dot{X}_P}{\omega}$	$\beta_1 = 90^o$	$\dot{X}_E = -\omega . Y_{\rho 1}$ $\dot{Y}_E = \omega . X_{\rho 1}$ $m_1 = \rho_1 . \omega,\ \beta_1 = 90^o$
Second Order	$X_{I2} = X_P + \frac{\ddot{X}_P \omega^2 - \ddot{Y}_P \alpha}{\alpha^2 + \omega^4}$ $Y_{I2} = Y_P + \frac{\ddot{X}_P \alpha + \ddot{Y}_P \omega^2}{\alpha^2 + \omega^4}$	$tan\,\beta_2 = -\frac{\alpha}{\omega^2}$	$\ddot{X}_E = -\omega^2 [X_{\rho 2} - Y_{\rho 2} tan\beta_2]$ $\ddot{Y}_E = -\omega^2 [X_{\rho 2} . tan\beta_2 + Y_{\rho 2}]$ $m_2 = \left\| -\frac{\omega^2}{cos\beta_2} \rho_2 \right\| e^{j(\gamma_2 + \beta_2)}$
Third Order	$X_{I3} = X_P + \frac{X_P^{(3)}(3\omega\alpha) - Y_P^{(3)}(\dot{\alpha} - \omega^3)}{(\dot{\alpha} - \omega^3)^2 + (3\omega\alpha)^2}$ $X_{I3} = Y_P + \frac{X_P^{(3)}(\dot{\alpha} - \omega^3) + Y_P^{(3)}(3\omega\alpha)}{(\dot{\alpha} - \omega^3)^2 + (3\omega\alpha)^2}$	$tan\,\beta_3 = -\frac{\dot{\alpha} - \omega^3}{3\omega\alpha}$	$X_E^{(3)} = -3\omega\alpha [X_{\rho 3} - Y_{\rho 2} tan\beta_3]$ $Y_E^{(3)} = -3\omega\alpha [X_{\rho 3} tan\beta_k + Y_{\rho 3}]$ $m_3 = \left\| -\frac{3\omega\alpha}{cos\beta_3} \rho_3 \right\| e^{j(\gamma_3 + \beta_3)}$
Fourth Order	$X_{I4} = X_P + \frac{X_P^{(4)}(4\omega\dot{\alpha} + 3\alpha^2 - \omega^4) - Y_P^{(4)}(\ddot{\alpha} - 6\omega^2\alpha)}{(\ddot{\alpha} - 6\omega^2\alpha)^2 + (4\omega\dot{\alpha} + 3\alpha^2 - \omega^4)^2}$ $Y_{I4} = Y_P + \frac{X_P^{(4)}(\ddot{\alpha} - 6\omega^2\alpha) + Y_P^{(4)}(4\omega\dot{\alpha} + 3\alpha^2 - \omega^4)}{(\ddot{\alpha} - 6\omega^2\alpha)^2 + (4\omega\dot{\alpha} + 3\alpha^2 - \omega^4)^2}$	$tan\,\beta_4 = -\frac{\ddot{\alpha} - 6\omega^2\alpha}{4\omega\dot{\alpha} + 3\alpha^2 - \omega^4}$	$X_E^{(4)} = -(4\omega\dot{\alpha} + 3\alpha^2 - \omega^4) . [X_{\rho 4} - Y_{\rho 4} tan\beta_4]$ $Y_E^{(4)} = -(4\omega\dot{\alpha} + 3\alpha^2 - \omega^4) . [X_{\rho 4} tan\beta_4 + Y_{\rho 4}]$ $m_4 = \left\| -\frac{4\omega\dot{\alpha} + 3\alpha^2 - \omega^4}{cos\beta_4} \rho_4 \right\| e^{j(\gamma_4 + \beta_4)}$
Fifth Order	$X_{I5} = X_P + \frac{X_P^{(5)}(10\alpha\dot{\alpha} + 3\omega\ddot{\alpha} - 10\omega^3\alpha) - Y_P^{(5)}(\alpha^{(3)} - 10\omega^2\dot{\alpha} - 15\omega\alpha^2 + \omega^5)}{(\alpha^{(3)} - 10\omega^2\dot{\alpha} - 15\omega\alpha^2 + \omega^5)^2 + (10\alpha\dot{\alpha} + 3\omega\ddot{\alpha} - 10\omega^3\alpha)^2}$ $Y_{I5} = Y_P + \frac{X_P^{(5)}(\alpha^{(3)} - 10\omega^2\dot{\alpha} - 15\omega\alpha^2 + \omega^5) + Y_P^{(5)}(10\alpha\dot{\alpha} + 3\omega\ddot{\alpha} - 10\omega^3\alpha)}{(\alpha^{(3)} - 10\omega^2\dot{\alpha} - 15\omega\alpha^2 + \omega^5)^2 + (10\alpha\dot{\alpha} + 3\omega\ddot{\alpha} - 10\omega^3\alpha)^2}$	$tan\,\beta_5 = -\frac{\alpha^{(3)} - 10\omega^2\dot{\alpha} - 15\omega\alpha^2 + \omega^5}{10\alpha\dot{\alpha} + 3\omega\ddot{\alpha} - 10\omega^3\alpha}$	$X_E^{(5)} = -(10\alpha\dot{\alpha} + 3\omega\ddot{\alpha} - 10\omega^3\alpha) . [X_{\rho 5} - Y_{\rho 5} tan\beta_5]$ $Y_E^{(5)} = -(10\alpha\dot{\alpha} + 3\omega\ddot{\alpha} - 10\omega^3\alpha) . [X_{\rho 5} tan\beta_5 + Y_{\rho 5}]$ $m_5 = \left\| -\frac{10\alpha\dot{\alpha} + 3\omega\ddot{\alpha} - 10\omega^3\alpha}{cos\beta_5} \rho_5 \right\| e^{j(\gamma_5 + \beta_5)}$

3 KINEMATIC FORMULATION USING INSTANT CENTERS: STUDY OF SPECIAL SCENARIOS

3.1 Introduction

The kinematic formulation proposed here describes a planar 3 Degrees-Of-Freedom (DOF) motion of a general rigid body based on Instant Centers (ICs). A generalized formulation with algebraic representation is developed for up to the fifth order kinematics which is summarized in Table 2.1. This motion theory is being applied to planar wheeled mobile platforms. Though the first order and second order ICs have been previously studied, the higher order kinematics needs further study. Also the expressions for third and higher order motion are highly coupled and more complex than the first and second order motion descriptions. The study of some special case scenarios of planar rigid body motion that involve well documented 1-DOF, 2-DOF motions such as a circle (cylinder /disk/wheel) rolling on a straight line (plane/flat, smooth surface), a circle rolling on a circle, etc., can help us understand the higher order properties further. To this effect, this chapter presents some important special scenarios which helps us understand the physical significance of the formulation using instant centers. Otherwise, numerical specifications for the higher order properties will have little known physical reference as to the meanings of their magnitudes.

This chapter deals with some well represented 1-DOF and 2-DOF motions starting with a circle rolling without slipping on a line. The following sections discuss these scenarios one by one by describing the motion of the system in terms of ICs starting with the first

order IC up to the fourth order IC.

3.2 Case 1: A Circle Rolling on a Straight Line without Slipping

One of the interesting special cases of a 1-DOF planar motion is a cylindrical body undergoing a pure rolling motion on a planar body. The plane containing a circular cross section of the cylinder is considered here. Because of the planar condition, any motion out of the plane is neglected. Due to the pure rolling, the cylindrical body undergoes only 1-DOF planar motion as the linear and rotational motions of the body are coupled. For simplicity, the cylinder is represented as a circle while the plane is represented as a straight line. The following sections discuss the motion properties of a circle rolling on a straight line without slipping. The condition when the circle rolls with some amount of slipping will be discussed later (Sec. 3.4).

3.2.1 Schematic Representation of the System

The general schematic diagram in Fig. 3.1 shows a circle (body 1), with a radius r, rolling on a straight line (body 2). The inertial frame of reference, {0}, is located on the line as shown. The body fixed frame {1} is located at the center of the circle, $P\ [X_P, Y_P]$. Note

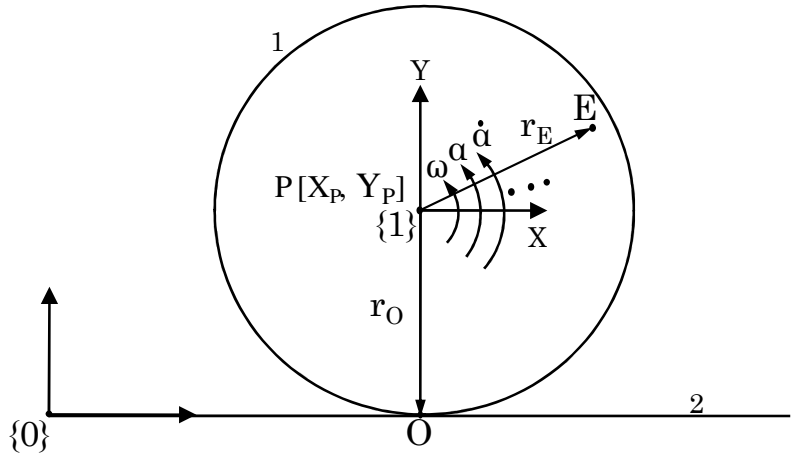

Fig. 3.1: Kinematic State Description of a Circle Rolling on a Straight Line Without Slipping or Skidding

that frames {0} and {1} are always parallel to each other (i.e., Θ is always zero). Point E is a general point in the body located at r_E with respect to frame {1}. The location of point O which is instantaneously located at the point of contact of the circle and the line is r_O *[0, -r]* as expressed in frame {1}.

The following sections detail the kinematics of the system with an emphasis on the ICs starting with the first order formulation. It will be shown that the 1-DOF configuration results in the first order IC that is purely geometric and thus provides valuable information of the physical state of the system. The kinematic formulation will be done using the unity as the radius of the circle 1 (r = 1) as the radius is merely a scaling factor in the description of the motion and does not provide any additional information about the state of the system.

3.2.2 First Order Kinematics for A Circle Rolling on a Straight Line without Slipping

Fig. 3.1 shows the circle rolling at an angular velocity, ω, on the line. In order for a homogeneous circle to roll without slipping, the linear velocity of the circle should be a result of pure rolling only. Then the velocity of the center of the circle, point P, must

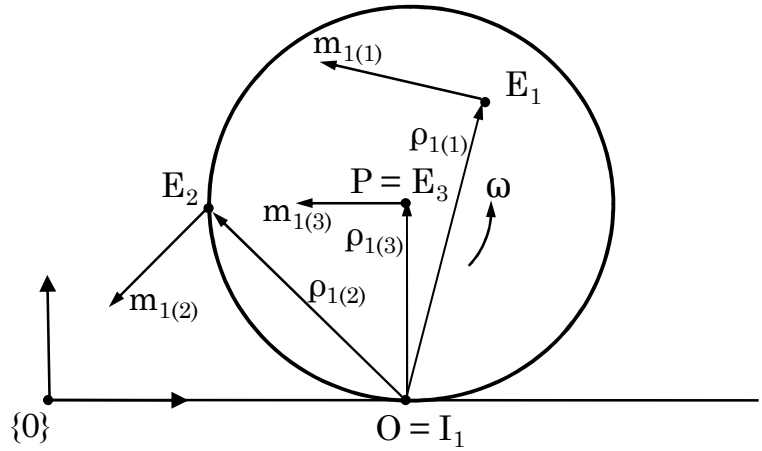

Fig. 3.2: The First Order Motion Description for a Circle Rolling on a Straight Line Without Slipping

meet following condition (Williams, 1995):

$$\dot{X}_P = -\omega r$$
$$\dot{Y}_P = 0 \qquad \text{Eq. 3.1}$$

Using r =1, (unity radius for the circle), we get:

$$\dot{X}_P = -\omega$$
$$\dot{Y}_P = 0 \qquad \text{Eq. 3.2}$$

Now, the location of the velocity IC in frame $\{0\}$ (Eq. 2.5) is computed using Eq. 3.2 as:

$$X_{I1} = X_P$$
$$Y_{I1} = Y_P - 1 \qquad \text{Eq. 3.3}$$

Transforming into the local frame, we get:

$$x_{I1} = 0$$
$$y_{I1} = -1 \qquad \text{Eq. 3.4}$$

This is the location of point O, the point of contact of the circle with the line. Note that location of point O (and thus of the velocity IC) is dependent only on the geometry of the body and is independent of the instantaneous kinematic parameters. In case of a 3-DOF planar motion of a body, the velocity IC also depends on the instantaneous kinematic parameters (such as the linear velocity of the point P as well as angular velocity of the body). The velocities of two general points E_1 and E_2 can then be expressed using the velocity IC as shown in Fig. 3.2.

Next, we study the second order motion properties of the system in terms of the acceleration IC.

3.2.3 SECOND ORDER KINEMATICS FOR A CIRCLE ROLLING ON A STRAIGHT LINE WITHOUT SLIPPING

We get the condition for the circle to roll without slipping for the second order motion by

differentiating Eq. 3.1 with time as follows (Williams, 1995):

$$\ddot{X}_P = -\alpha r$$
$$\ddot{Y}_P = 0 \qquad \text{Eq. 3.5}$$

Using r =1, (unity radius for the circle), we get:

$$\ddot{X}_P = -\alpha$$
$$\ddot{Y}_P = 0 \qquad \text{Eq. 3.6}$$

Since the frames {0} and {1} are parallel, the second order IC location (Eq. 2.18) can be expressed in frame {1} as:

$$x_{I2} = \frac{\ddot{x}_P\,\omega^2 - \ddot{y}_P\alpha}{\alpha^2 + \omega^4}$$
$$y_{I2} = \frac{\ddot{x}_P\,\alpha + \ddot{y}_P\omega^2}{\alpha^2 + \omega^4} \qquad \text{Eq. 3.7}$$

Using Eq. 3.6, Eq. 3.7 can be simplified to give:

$$x_{I2} = \frac{-\alpha\omega^2}{\alpha^2 + \omega^4}$$
$$y_{I2} = \frac{-\alpha^2}{\alpha^2 + \omega^4} \qquad \text{Eq. 3.8}$$

Using the definition of angle β_2 (Eq. 2.20), Eq. 3.8 can be rearranged as:

$$x_{I2} = \frac{tan\beta_2}{1 + tan^2\,\beta_2} = \frac{tan\beta_2}{sec^2\,\beta_2} = sin\,\beta_2 cos\,\beta_2$$
$$y_{I2} = \frac{-tan^2\beta_2}{1 + tan^2\beta_2} = \frac{-tan^2\beta_2}{sec^2\beta_2} = -sin^2\beta_2$$

But,

$$\sin\beta_2\cos\beta_2 = \frac{1}{2}\sin 2\beta_2$$
$$\sin^2\beta_2 = \frac{1-\cos 2\beta_2}{2}$$

Using these trigonometric identities, we can express the location of the acceleration IC in the following form:

$$x_{I2} = 0 + \frac{1}{2}sin\ 2\beta_2$$
$$y_{I2} = -\frac{1}{2} + \frac{1}{2}cos 2\beta_2 \qquad \text{Eq. 3.9}$$

Eq. 3.9 is a parametric equation of a circle with the center at *[0, -$\frac{1}{2}$]* and the radius equal to $\frac{1}{2}$ which shows that the locus of the acceleration IC is a circle. The locus is dependent only on the geometry of the system, as evident from the location of the center and the radius of the locus circle, and independent of the kinematic parameters of the motion. However, the location of the acceleration IC at a particular instant in time depends on the instantaneous value of the angle, β_2, which in turn depends on the values of the angular acceleration α and angular velocity, ω of the circle.

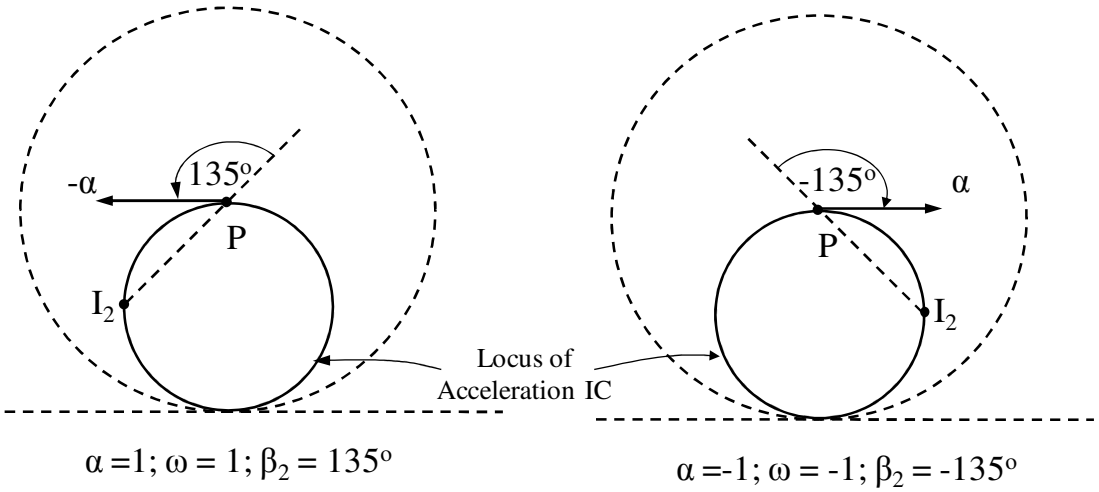

Fig. 3.3: Location of the Acceleration IC based on the Value of Constant Angle β_2 under Two Different Motion Scenarios: a) When Values of both the Angular Acceleration and Angular Velocity of the Circle are Instantaneously 1, and b) When Values of both the Angular Acceleration and Angular Velocity of the Circle are Instantaneously -1

Fig. 3.3 depicts some example scenarios for instantaneous kinematic state of the system. Let us assume that at a particular instant in time, the angular velocity, ω, and angular acceleration, α, of the circle is unity, i.e., α = ω = 1. Using Eq. 2.29, the orientation angle β2 is uniquely computed as 135°. With these values, the location of the acceleration IC is computed from Eq. 3.9 as *[-0.5, -0.5]*. Now when α = ω = -1, β2 is uniquely evaluated as -135°. With -135° for β_2, we compute location for the acceleration IC as *[0.5, -0.5]*. Fig. 3.3 shows the two different scenarios graphically. When α = 1; the acceleration of point P is -1 (Eq. 3.6), thus the acceleration IC location *[-0.5, -0.5]* results in the appropriate value for the constant angle β_2. In the second case as well, the acceleration IC location *[0.5, -0.5]* results in the appropriate value for β_2 as shown.

3.2.3.1 Special Case Scenarios for the Second Order Motion for A Circle Rolling on a Straight Line without Slipping

With regards to the second order motion of the rigid body, there are various interesting special cases that we can discuss.

Case 1: α = 0

When the circle rolls with a constant angular velocity, ω = constant, and no angular

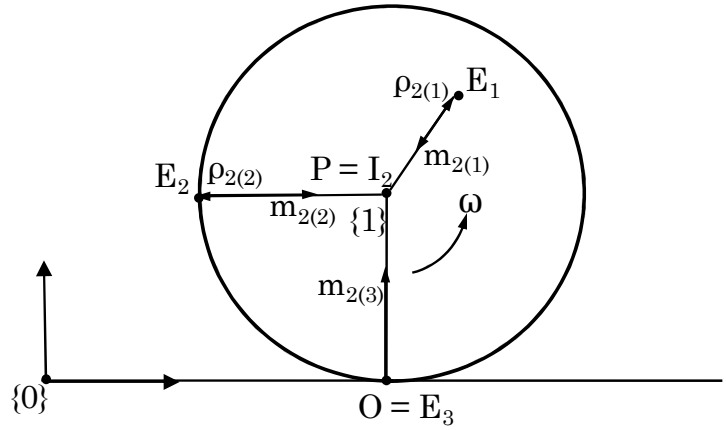

Fig. 3.4: Zero Angular Acceleration: Location of the Acceleration IC is at the Center of the Circle

acceleration, $\alpha = 0$, the acceleration of point P is zero (as per Eq. 3.5) making it the acceleration IC as shown in Fig. 3.4. We can also verify this using the Eq. 3.9. For zero angular acceleration, $\alpha = 0$, and constant, non-zero angular velocity, ω = constant, β_2 is 180^o and thus the Eq. 3.9 results in the acceleration IC location at *[0, 0]*, the location of point P.

Case 2: $\omega = 0$

On the other hand, when the circle starts to move from rest, the circle has finite angular acceleration but zero angular velocity. The instant center for acceleration in this case is at O as shown in Fig. 3.5. Also the angle of the vector orientation, β_2, is -90^o. This can also be verified using Eq. 3.9 which gives the location of acceleration IC location at *[0, -r]* which is point O.

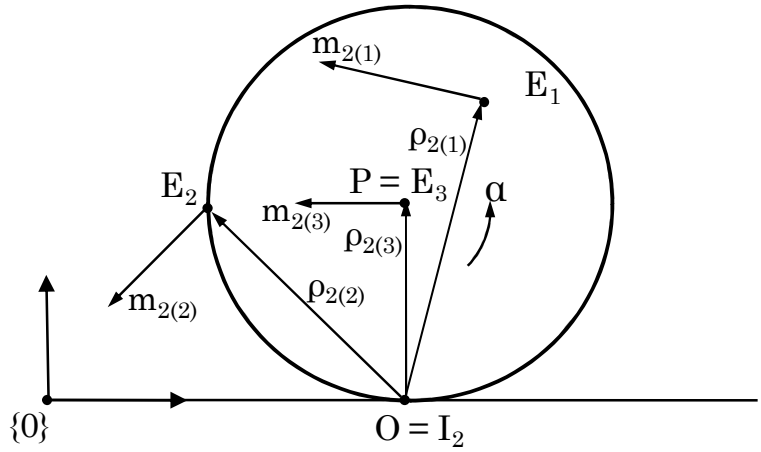

Fig. 3.5: Zero Angular Velocity: The Acceleration Instant Center at the Point of Contact of the Circle and the Straight Line

In general, when both the angular velocity and angular acceleration have non-zero values, the instant center for acceleration is anywhere on the circle as shown by Eq. 3.9. Its location is determined by the value of β_2, which in turn is dependent on the relative magnitude and direction sense (counter-clock-wise positive) of angular velocity and angular acceleration. This is shown in Fig. 3.6.

For a constant value of angular acceleration, if we increase the angular velocity starting from zero, the acceleration IC moves along the circle from O to P. Also with an increase in magnitude of angular acceleration with constant angular velocity the acceleration IC moves towards O. A positive value of acceleration results in I_2 on the left side of the circle while a negative value results it being on the right side. Fig. 3.6 shows this variation graphically. Note that the locus of acceleration IC coincides with the inflection circle for this special case (Vidosic and Tesar, 1967).

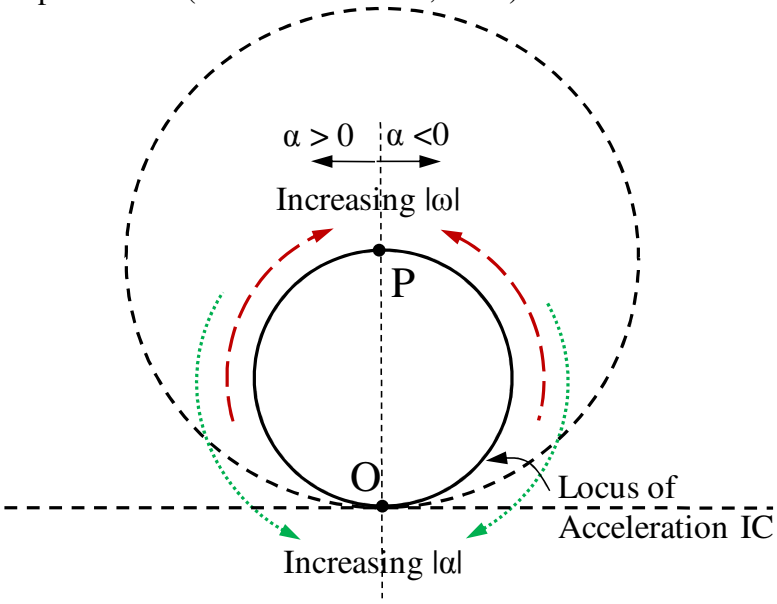

Fig. 3.6: The General Locus of the Acceleration IC for a Circle Rolling on a Straight Line without Slipping is a Circle with Diameter OP

3.2.3.2 Simulation Plot for Second Order Motion of A Circle Rolling on a Straight Line without Slipping

These properties of the acceleration are verified using a simulation plot. In the simulation shown in Fig. 3.7 uses a circle radius of 1 foot rolling without slipping on a line. The circle starts from rest and is subjected to a constant angular acceleration of 1.5 rad/s_2 once and -1.5 rad/s_2 in the next iteration. The resulting locus of instant center is shown Fig. 3.7. Note that initially, the IC is at point O, and as the angular velocity, ω, starts increasing it starts traversing towards the center of the disk, point P. During this

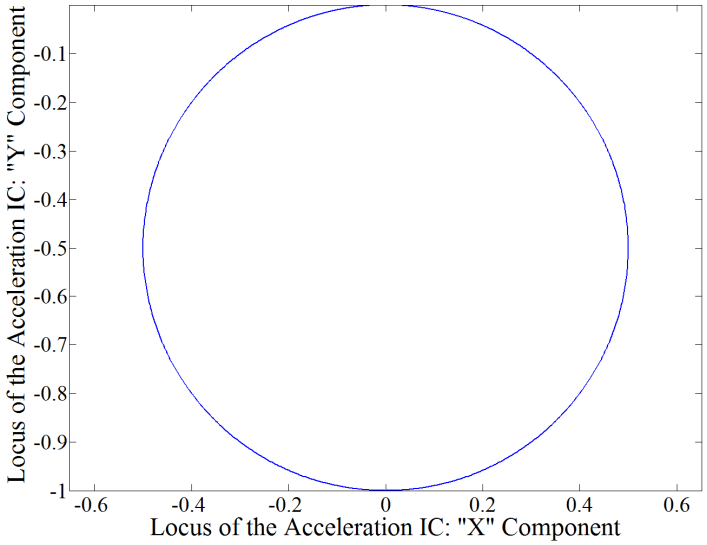

Fig. 3.7: Simulation Plot for the Acceleration IC for a Circle (Radius = 1 ft) Rolling on a Straight Line Without Slipping

simulation it never reaches point P as the angular acceleration, α, is never zero. However as the angular velocity reaches a high value (~25 rad/s), the IC approaches very close to point P as seen in Fig. 3.7.

The second order kinematics formulation for the special case showed us that the use of the acceleration IC, I_2, to describe the acceleration field is insightful since the IC is always located on a circle which is coincident with the inflection circle Vidosic and Tesar (1967). The acceleration field for a general point can be described by a tangential and a normal component of the total acceleration with respect to the radius, ρ_2, of the point from the acceleration IC. The tangential and normal components are proportional to the angular acceleration, α, and angular velocity, ω, respectively. In case of the third order, the tangential and normal components of a general point are proportional to coupled terms involving more than one parameter and thus is more involved than the second order.

The following section discusses the third order motion of the system that we have

considered so far when the circle rolls on the line without slipping. The general equation for third order IC will be used as a starting point for the discussion.

3.2.4 THIRD ORDER KINEMATICS FOR A CIRCLE ROLLING ON A STRAIGHT LINE WITHOUT SLIPPING

Since frames {0} and frame {1} are parallel, the third order IC location (Eq. 2.38) is transformed to frame {1} as follows:

$$x_{I3} = \frac{x_P^{(3)}(3\omega\alpha) - y_P^{(3)}(\dot{\alpha} - \omega^3)}{(\dot{\alpha} - \omega^3)^2 + (3\omega\alpha)^2}$$
$$y_{I3} = \frac{x_P^{(3)}(\dot{\alpha} - \omega^3) + y_P^{(3)}(3\omega\alpha)}{(\dot{\alpha} - \omega^3)^2 + (3\omega\alpha)^2} \qquad \text{Eq. 3.10}$$

The condition for the homogeneous circle to roll without slipping for the third order motion can be computed by differentiating Eq. 3.5 with time as follows:

$$X_P^{(3)} = -r\dot{\alpha}$$
$$Y_P^{(3)} = 0 \qquad \text{Eq. 3.11}$$

Using r = 1, we get:

$$X_P^{(3)} = -\dot{\alpha}$$
$$Y_P^{(3)} = 0 \qquad \text{Eq. 3.12}$$

Using the constraint condition provided by Eq. 3.12, the third order (jerk) IC (Eq. 3.10) for a general motion of the circle can be computed as:

$$x_{I3} = \frac{-\dot{\alpha}(3\omega\alpha)}{(\dot{\alpha} - \omega^3)^2 + (3\omega\alpha)^2}$$
$$y_{I3} = \frac{-\dot{\alpha}(\dot{\alpha} - \omega^3)}{(\dot{\alpha} - \omega^3)^2 + (3\omega\alpha)^2} \qquad \text{Eq. 3.13}$$

The expression can be rearranged by adding an extra term each for the two equations as follows:

$$x_{I3} = \frac{-(\dot{\alpha} - \omega^3)(3\omega\alpha)}{(\dot{\alpha} - \omega^3)^2 + (3\omega\alpha)^2} - \frac{\omega^3(3\omega\alpha)}{(\dot{\alpha} - \omega^3)^2 + (3\omega\alpha)^2}$$
$$y_{I3} = \frac{-(\dot{\alpha} - \omega^3)(\dot{\alpha} - \omega^3)}{(\dot{\alpha} - \omega^3)^2 + (3\omega\alpha)^2} - \frac{\omega^3(\dot{\alpha} - \omega^3)}{(\dot{\alpha} - \omega^3)^2 + (3\omega\alpha)^2} \quad \text{Eq. 3.14}$$

Using the definition of the third order orientation angle, β_3 (Eq. 2.40), Eq. 3.14 can be simplified as:

$$x_{I3} = \frac{1}{2} sin\, 2\beta_3 - \frac{\omega^3(3\omega\alpha)}{(\dot{\alpha} - \omega^3)^2 + (3\omega\alpha)^2}$$
$$y_{I3} = -\frac{1}{2} + \frac{1}{2} cos 2\beta_3 - \frac{\omega^3(\dot{\alpha} - \omega^3)}{(\dot{\alpha} - \omega^3)^2 + (3\omega\alpha)^2} \quad \text{Eq. 3.15}$$

Note that as compared to Eq. 3.9, the two equations in Eq. 3.15 have an extra term each. Thus the locus of third order IC is a circle with the center at *[0, -1/2]* and radius equal to 1/2 superposed by an extra term each for the X and Y component.

3.2.4.1 Simulation Plot of the Third Order Motion of A Circle Rolling on a Straight Line without Slipping

The locus of the third order IC location is plotted using a simulation plot where a circle of radius 1 foot is rolling without slipping on a straight line.

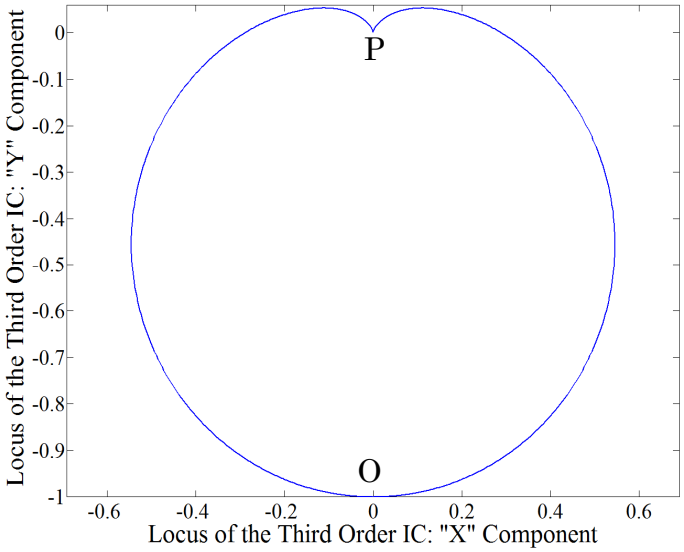

Fig. 3.8: Circle Rolling on a Straight Line without Slipping or Skidding: The Locus of the Third Order IC for a General Motion

Fig. 3.8 shows the result of the simulation. It is found that the locus of the third order IC is dependent only on the geometry and is independent of the kinematic state of the body. The particular location of the third order IC at any instant, however, is dependent on the instantaneous values of the kinematic parameters of the rigid body as the case with second order IC is.

3.2.4.2 Special Case Scenarios for the Third Order Motion of A Circle Rolling on a Straight Line without Slipping

To study the properties of third order IC, study of some special scenarios with regards to the instantaneous kinematic state of the circle is beneficial. To this effect, the following section discusses various special scenarios which are summarized in Table 3.1 following the discussion.

Case 1: $\dot{\alpha} \neq 0, \omega = 0$

When the angular velocity, ω, of the body is zero while the angular jerk, $\dot{\alpha}$, has a nonzero value, regardless of the state of angular acceleration, α, Eq. 3.13 becomes:

$$x_{I3} = 0$$
$$y_{I3} = -1 \qquad \text{Eq. 3.16}$$

This is the location of the point of contact, O. Also with these values of ω, α, and $\dot{\alpha}$, angle β_3 is computed as 90^o. Thus the location of the third order IC in this case is the point of

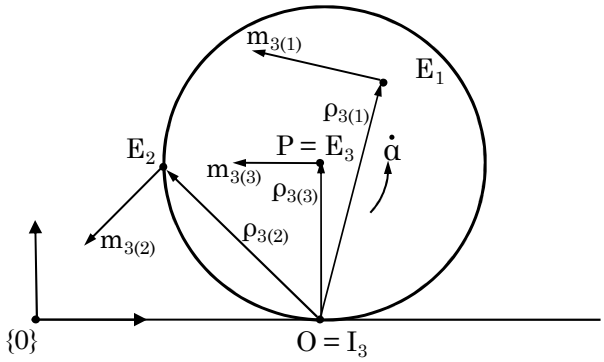

Fig. 3.9: Circle Rolling on a Straight Line without Slipping: The Third Order IC Location when $\dot{\alpha} \neq 0, \omega = 0$

contact, O, of the circle with the line regardless of the value of angular acceleration, α. Every point on the body has third order motion state, m_3, such that its magnitude is proportional to and the direction is orthogonal to the radius, ρ_3. This is shown in Fig. 3.9.

Case 2: $\dot{\alpha} = 0, \omega \neq 0$

When the angular jerk of the circle is instantaneously zero with nonzero angular velocity, ω, the jerk of point P becomes zero (as per Eq. 3.12) regardless of the state of angular acceleration, α. Thus the third order IC lies at point P, instantaneously. The third order orientation angle, β_3 (given by Eq. 2.40) is simplified as:

$$tan\,\beta_3 = -\frac{\omega^3}{3\omega\alpha} \qquad \text{Eq. 3.17}$$

This results into two different scenarios as follows:

Case 2.1: α = 0

The angular acceleration of the body is zero, β_3 becomes 90^o. This is shown in Fig. 3.10.

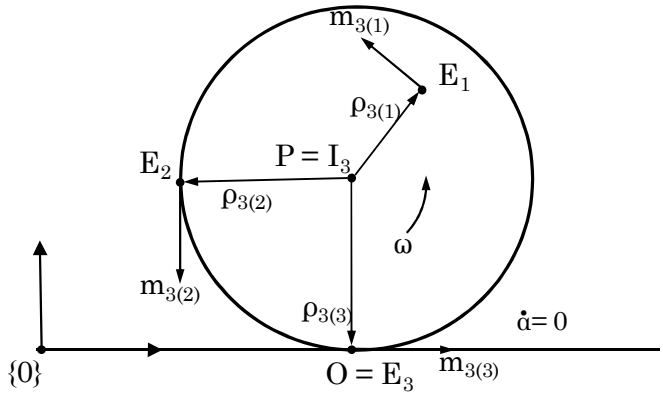

Fig. 3.10: A Circle Rolling on a Straight Line without Slipping: The Third Order IC Location when $\dot{\alpha} = 0, \omega \neq 0, \text{and } \alpha = 0$

Case 2.2: α ≠ 0

The angular acceleration of the body is non-zero. Angle β_3 has a value as computed by Eq. 3.17 rather than 90^o.

Case 3: $\dot{\alpha} \neq 0, \alpha = 0, \omega \neq 0$

When the circle is rolling with nonzero angular velocity, and angular jerk and no angular

acceleration, the location of third order IC (Eq. 3.13) is at:

$$x_{I3} = 0$$
$$y_{I3} = \frac{-\dot{\alpha}}{(\dot{\alpha} - \omega^3)} \qquad \text{Eq. 3.18}$$

Thus, depending on the values of $\dot{\alpha}$ and ω, the location of third order IC is located as shown in Fig. 3.11. Note that when $\dot{\alpha} = \omega^3$, the instant center is located at infinity.

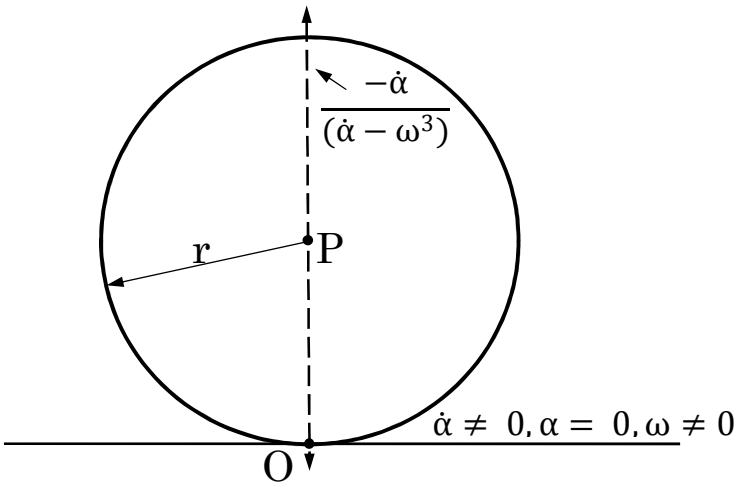

Fig. 3.11: A Circle Rolling on a Straight Line without Slipping: The Third Order IC Location when $\dot{\alpha} \neq 0, \alpha = 0, \omega \neq 0$

3.2.4.3 Summary of the Third Order Motion of A Circle Rolling on a Straight Line without Slipping

Table 3.1 summarizes all special case scenarios for third order motion of a circle rolling on a line. These scenarios identify the location of third order IC for such special cases. Also the resulting value of constant angle β_3 is also shown for each scenario.

Table 3.1: Summary of the Third Order Motion Properties in Special Case Scenarios for a Circle Rolling on a Straight Line

$\dot{\alpha}$	α	ω	IC Location	β_3
0	0	$\neq 0$	*P [0, 0]*	-90^o
0	$\neq 0$	$\neq 0$	*P [0, 0]*	$\tan^{-1}\left(-\frac{\omega^3}{3\omega\alpha}\right)$
0	0	0	∞	90^o
0	$\neq 0$	0	∞	90^o
$\neq 0$	0	0	*O [0, -1]*	90^o
$\neq 0$	$\neq 0$	0	*O [0, -1]*	90^o
$\neq 0$	0	$\neq 0$	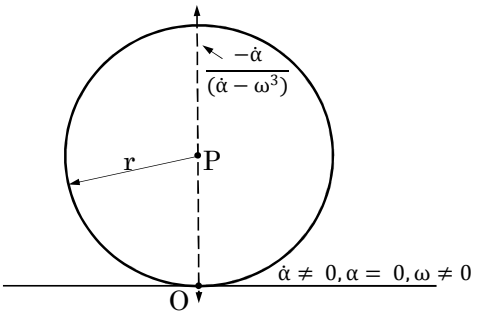	90^o
$\neq 0$	$\neq 0$	$\neq 0$	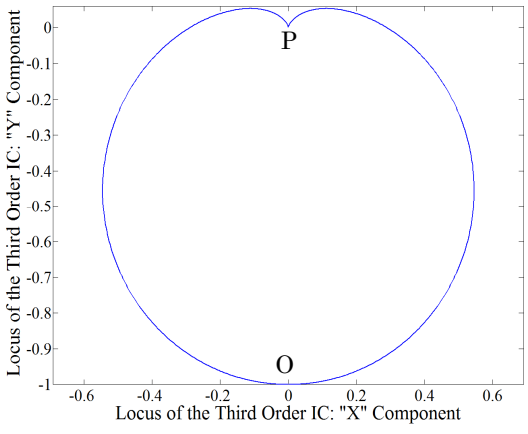	$\tan^{-1}\left(-\frac{\dot{\alpha}-\omega^3}{3\omega\alpha}\right)$

Following section discusses the fourth order motion properties in terms of the fourth order IC for the circle rolling on a line case.

3.2.5 Fourth Order Kinematics of A Circle Rolling on a Straight Line without Slipping

Since frames {0} and frame {1} are parallel, the location of the fourth order IC (Eq. 2.39) in frame {1} at any instant can be computed by following expression:

$$x_{I4} = \frac{x_P^{(4)}(4\omega\dot{\alpha} + 3\alpha^2 - \omega^4) - y_P^{(4)}(\ddot{\alpha} - 6\omega^2\alpha)}{(\ddot{\alpha} - 6\omega^2\alpha)^2 + (4\omega\dot{\alpha} + 3\alpha^2 - \omega^4)^2}$$
$$y_{I4} = \frac{x_P^{(4)}(\ddot{\alpha} - 6\omega^2\alpha) + y_P^{(4)}(4\omega\dot{\alpha} + 3\alpha^2 - \omega^4)}{(\ddot{\alpha} - 6\omega^2\alpha)^2 + (4\omega\dot{\alpha} + 3\alpha^2 - \omega^4)^2} \quad \text{Eq. 3.19}$$

The condition for the homogeneous circle to roll without slipping for the fourth order motion can be computed by differentiating Eq. 3.12 w.r.t. time as follows:

$$X_P^{(4)} = -r\ddot{\alpha}$$
$$Y_P^{(4)} = 0 \quad \text{Eq. 3.20}$$

Using unity for the radius of the circle, we get:

$$X_P^{(4)} = -\ddot{\alpha}$$
$$Y_P^{(4)} = 0 \quad \text{Eq. 3.21}$$

Using the constraint condition provided by Eq. 3.21, the fourth order IC (Eq. 3.19) for a general motion of the circle can be computed as:

$$x_{I4} = \frac{-\ddot{\alpha}(4\omega\dot{\alpha} + 3\alpha^2 - \omega^4)}{(\ddot{\alpha} - 6\omega^2\alpha)^2 + (4\omega\dot{\alpha} + 3\alpha^2 - \omega^4)^2}$$
$$y_{I3} = \frac{-\ddot{\alpha}(\ddot{\alpha} - 6\omega^2\alpha)}{(\ddot{\alpha} - 6\omega^2\alpha)^2 + (4\omega\dot{\alpha} + 3\alpha^2 - \omega^4)^2} \quad \text{Eq. 3.22}$$

The expression can be rearranged by adding an extra term each for the two equations as follows:

$$x_{I4} = \frac{-(\ddot{\alpha} - 6\omega^2\alpha)(4\omega\dot{\alpha} + 3\alpha^2 - \omega^4)}{(\ddot{\alpha} - 6\omega^2\alpha)^2 + (4\omega\dot{\alpha} + 3\alpha^2 - \omega^4)^2} - \frac{6\omega^2\alpha(4\omega\dot{\alpha} + 3\alpha^2 - \omega^4)}{(\ddot{\alpha} - 6\omega^2\alpha)^2 + (4\omega\dot{\alpha} + 3\alpha^2 - \omega^4)^2}$$

$$y_{I4} = \frac{-(\ddot{\alpha} - 6\omega^2\alpha)^2}{(\ddot{\alpha} - 6\omega^2\alpha)^2 + (4\omega\dot{\alpha} + 3\alpha^2 - \omega^4)^2} - \frac{6\omega^2\alpha(\ddot{\alpha} - 6\omega^2\alpha)}{(\ddot{\alpha} - 6\omega^2\alpha)^2 + (4\omega\dot{\alpha} + 3\alpha^2 - \omega^4)^2} \quad \text{Eq. 3.23}$$

Using the definition of angle β_4 (Eq. 2.41) based on the instantaneous kinematic parameters, ω, α, $\dot{\alpha}$, and $\ddot{\alpha}$, we can simplify Eq. 3.23 as:

$$x_{I4} = \frac{1}{2} sin\, 2\beta_4 - \frac{6\omega^2\alpha(4\omega\dot{\alpha} + 3\alpha^2 - \omega^4)}{(\ddot{\alpha} - 6\omega^2\alpha)^2 + (4\omega\dot{\alpha} + 3\alpha^2 - \omega^4)^2}$$

$$y_{I4} = -\frac{1}{2} - \frac{1}{2} cos 2\beta_4 - \frac{6\omega^2\alpha(\ddot{\alpha} - 6\omega^2\alpha)}{(\ddot{\alpha} - 6\omega^2\alpha)^2 + (4\omega\dot{\alpha} + 3\alpha^2 - \omega^4)^2} \quad \text{Eq. 3.24}$$

Note that as compared to Eq. 3.9, the two equations in Eq. 3.24 have an extra term each. Thus the locus of fourth order IC is a circle with the center at *[0, -1/2]* and radius equal to 1/2 superposed by an extra term each for the X and Y component.

3.2.5.1 Simulation Plot for the Fourth Order Motion of A Circle Rolling on a Straight Line without Slipping

The locus of the fourth order IC location is plotted using a simulation plot where a circle of radius 1 foot is rolling without slipping on a straight line. Fig. 3.12 shows the result of the simulation. It is found that the locus of the fourth order IC is dependent only on the geometry and is independent of the kinematic state of the body. The particular location of the fourth order IC at any instant, however, is dependent on the instantaneous values of the kinematic parameters of the rigid body as the case with second order IC is.

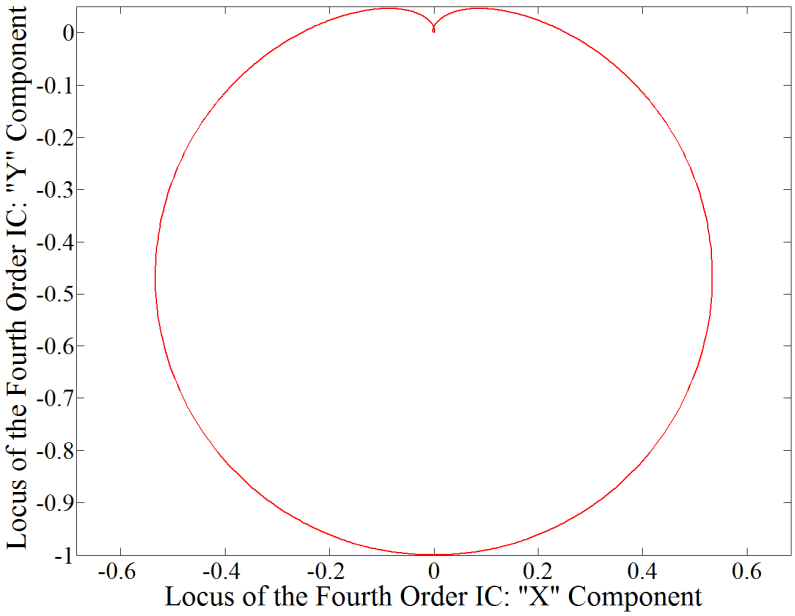

Fig. 3.12: Circle Rolling on a Straight Line without Slipping: The Locus of Fourth Order IC for a General Motion

3.2.5.2 Special Case Scenarios for for the Fourth Order Motion of A Circle Rolling on a Straight Line without Slipping

To study the properties of fourth order IC, study of some special scenarios with regards to the instantaneous kinematic state of the circle is beneficial. To this effect, the following section discusses various special scenarios which are summarized in Table 3.3 following the discussion.

Case 1: $\ddot{\alpha} \neq 0, \alpha = \omega = 0$

When the angular velocity, ω, and angular acceleration, α, of the body are zero while the derivative of angular jerk, ä, has a nonzero value, regardless of the state of angular jerk, ȧ, Eq. 3.13 becomes:

$$x_{I3} = 0$$
$$y_{I3} = -1 \qquad \text{Eq. 3.25}$$

This is the location of the point of contact, O. Also with these values of ω, α, and ȧ, angle

β_3 is computed as 90^o. Thus the location of the fourth order IC in this case is the point of contact, O, of the circle with the line regardless of the value of $\ddot{\alpha}$. Every point on the body has fourth order motion state, m_4, such that its magnitude is proportional to and the direction is orthogonal to the radius, ρ_4. This is shown in Fig. 3.13.

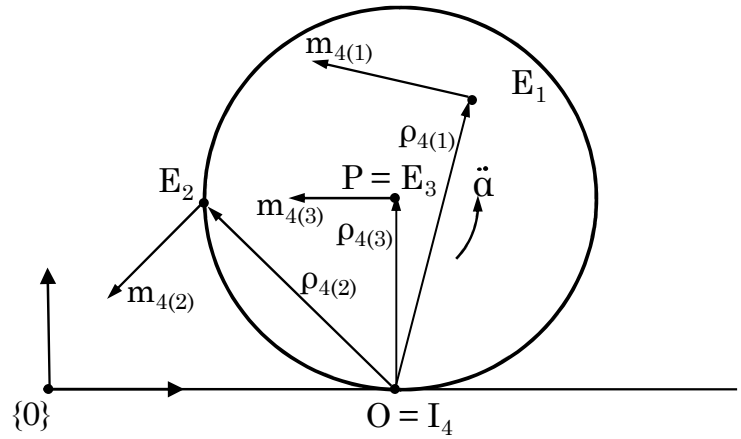

Fig. 3.13: Circle Rolling on a Straight Line without Slipping: The Fourth Order IC Location when $\dot{\alpha} \neq 0, \alpha = \omega = 0$

Case 2: $\ddot{\alpha} = 0$, and $\omega \neq 0$ or $\alpha \neq 0$

When the derivative of the angular jerk, $\ddot{\alpha}$, of the circle is zero and the angular velocity, ω, and/or angular acceleration, α, of the circle are nonzero at a particular instant in time, regardless of the state of angular jerk, $\dot{\alpha}$, the derivative of the jerk of point P is zero (as per Eq. 3.21). Then the fourth order IC lies at point P, instantaneously. The constant angle, β_4 is computed as:

$$tan\,\beta_4 = \frac{6\omega^2\alpha}{4\omega\dot{\alpha} + 3\alpha^2 - \omega^4} \qquad \text{Eq. 3.26}$$

This results into two different scenarios as follows:

Case 2.1: **either $\omega \neq 0$ or $\alpha \neq 0$**

If only one of the two entities (angular acceleration and angular velocity) is nonzero, the numerator of the expression for β_4 becomes zero. Thus if angular acceleration is nonzero,

β_4 is 0^o (atan2 (0, +)), while if angular velocity is zero, β_4 is 180^o (atan2 (0, -)) if angular jerk is zero. If both angular velocity and angular jerk are nonzero then the value of angle β_4 is determined by the sign of the expression $4\omega\dot{\alpha} - \omega^4$. This is summarized in Table 3.2 below.

Table 3.2: Fourth Order Motion for a Circle Rolling on a Straight Line: Special Case Scenario when $\ddot{\alpha} = 0$, and $\omega \neq 0$ or $\alpha \neq 0$. The Fourth Order IC is at point P [0, 0]

$\dot{\alpha}$	α	ω	β_4
Does not affect the outcome	1	0	0^o
0	0	1	180^o
1	0	1	0^o if $(4\omega\dot{\alpha} - \omega^4) > 0$ 180^o if $(4\omega\dot{\alpha} - \omega^4) < 0$

The case when angular velocity, ω, is nonzero is shown in Fig. 3.14. The angle β_4 is 180^o as shown.

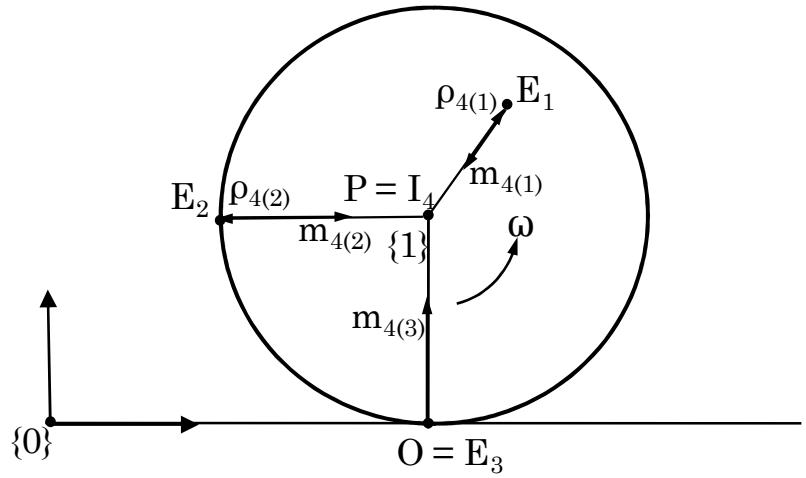

Fig. 3.14: Circle Rolling on a Straight Line without Slipping: The Fourth Order IC Location when $\dot{\alpha} = 0$, and either $\omega \neq 0$ or $\alpha \neq 0$

Case 2.2: When $\alpha \neq 0$ and $\omega \neq 0$

When both ω and α of the circle are nonzero at an instant in time, the angle β_4 is

computed using Eq. 3.26 rather than 0^o or 180^o.

Case 3: $\ddot{\alpha} \neq 0, \alpha \neq 0, \omega = 0$

When the circle is rolling with nonzero angular acceleration, and the derivative angular jerk and no angular velocity, the location of fourth order IC (Eq. 3.13) is at:

$$x_{I4} = \frac{-\ddot{\alpha}\, 3\alpha^2}{(\ddot{\alpha})^2 + (3\alpha^2)^2}$$
$$y_{I3} = \frac{-(\ddot{\alpha})^2}{(\ddot{\alpha})^2 + (3\alpha^2)^2} \qquad \text{Eq. 3.27}$$

And the angle β_4 is computed as:

$$tan\, \beta_4 = -\frac{\ddot{\alpha}}{3\alpha^2} \qquad \text{Eq. 3.28}$$

Using Eq. 3.28, Eq. 3.27 can be simplified as:

$$x_{I4} = \frac{tan\beta_4}{1 + tan^2\, \beta_4} = \frac{tan\beta_4}{sec^2\, \beta_4} = sin\, \beta_4 cos\, \beta_4$$
$$y_{I4} = \frac{-tan^2\beta_4}{1 + tan^2\beta_4} = \frac{-tan^2\beta_4}{sec^2\beta_4} = -sin^2\beta_4$$

We can see using trigonometric identities that:

$$\sin\beta_4 \cos\beta_4 = \frac{1}{2}\sin 2\beta_4$$
$$\sin^2\beta_4 = \frac{1 - \cos 2\beta_4}{2}$$

After further simplification, we can express the location of acceleration IC in the following form:

$$x_{I4} = 0 + \frac{1}{2}\sin 2\beta_2$$
$$y_{I4} = -\frac{1}{2} - \frac{1}{2}\cos 2\beta_2 \qquad \text{Eq. 3.29}$$

Eq. 3.29 is a parametric equation of a circle with center at *[0, -* $\frac{1}{2}$*]* and radius equal to $\frac{1}{2}$. Thus when the circle is rolling with nonzero angular acceleration, α, and the derivative

angular jerk, $\dddot{\alpha}$, and zero angular velocity, ω , the locus of the fourth order IC is a circle as shown in Fig. 3.15. The instantaneous location of acceleration IC depends on value of the angle, β_4, which in turn depends on the values of the angular acceleration α and derivative of angular jerk, $\dddot{\alpha}$, of the circle at the instant in time.

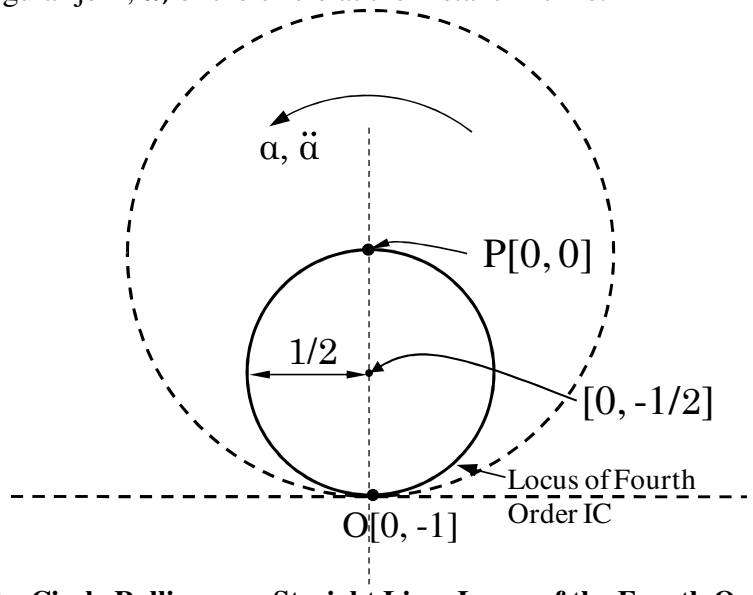

Fig. 3.15: The Circle Rolling on a Straight Line: Locus of the Fourth Order IC when $\ddot{\alpha} \neq 0, \alpha \neq 0, \omega = 0$

Case 4: $\ddot{\alpha} \neq 0, \alpha = 0, \omega \neq 0$

When the circle is rolling with no angular acceleration and nonzero angular velocity, and the derivative angular jerk, the location of fourth order IC (Eq. 3.13) is at:

$$x_{I4} = \frac{-\ddot{\alpha}(4\omega\dot{\alpha} - \omega^4)}{(\ddot{\alpha})^2 + (4\omega\dot{\alpha} - \omega^4)^2}$$
$$y_{I3} = \frac{-(\ddot{\alpha})^2}{(\ddot{\alpha})^2 + (4\omega\dot{\alpha} - \omega^4)^2} \qquad \text{Eq. 3.30}$$

It will be shown that state of angular jerk has no effect on the locus of the fourth order IC in this particular case.

And the angle β_4 is computed as:

$$tan\,\beta_4 = -\frac{\ddot{\alpha}}{4\omega\dot{\alpha} - \omega^4} \qquad \text{Eq. 3.31}$$

Using Eq. 3.31, Eq. 3.30 can be simplified as:

$$x_{I4} = \frac{tan\beta_4}{1 + tan^2\,\beta_4} = \frac{tan\beta_4}{sec^2\,\beta_4} = sin\,\beta_4 cos\,\beta_4$$
$$y_{I4} = \frac{-rtan^2\beta_4}{1 + tan^2\beta_4} = \frac{-rtan^2\beta_4}{sec^2\beta_4} = -sin^2\beta_4$$

We can see using trigonometric identities that:

$$sin\,\beta_4 cos\beta_4 = \frac{1}{2} sin2\beta_4$$
$$sin^2\beta_4 = \frac{1 - cos2\beta_4}{2}$$

After further simplification, we can express the location of acceleration IC in the following form:

$$x_{I4} = 0 + \frac{1}{2} sin\,2\beta_2$$
$$y_{I4} = -\frac{1}{2} + \frac{1}{2} cos2\beta_2 \qquad \text{Eq. 3.32}$$

Eq. 3.29 is a parametric equation of a circle with center at [0, -$\frac{1}{2}$] and radius equal to $\frac{1}{2}$. Thus when the circle is rolling with nonzero angular acceleration, α, and the derivative angular jerk, $\ddot{\alpha}$, and zero angular velocity, ω, the locus of the fourth order IC is a circle as shown in Fig. 3.15. The instantaneous location of acceleration IC depends on value of the angle, β_4, which in turn depends on the values of the angular velocity ω, angular jerk, $\dddot{\alpha}$, and derivative of angular jerk, $\ddot{\alpha}$, of the circle at the instant in time. It can be shown that when the angular jerk is instantaneously zero, the locus of the fourth order IC is still a circle with parametric equation expressed in Eq. 3.33 such that its center is at *[0, -*$\frac{1}{2}$*]* and radius is equal to $\frac{1}{2}$ as follows:

$$x_{I4} = 0 - \frac{1}{2} \sin 2\beta_2$$
$$y_{I4} = -\frac{1}{2} + \frac{1}{2} \cos 2\beta_2 \qquad \text{Eq. 3.33}$$

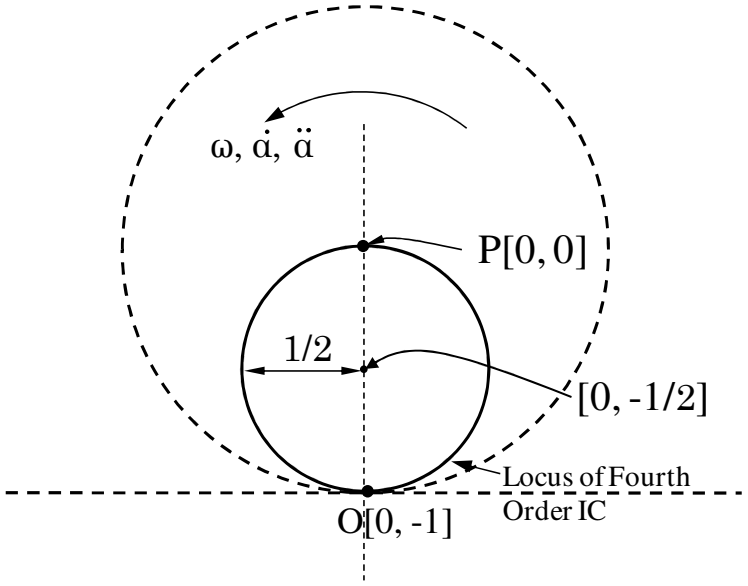

Fig. 3.16: Circle Rolling on a Straight Line: The Locus of the Fourth Order IC when $\ddot{\alpha} \neq 0, \alpha = 0, \omega \neq 0$

3.2.5.3 Summary of the Fourth Order Motion of A Circle Rolling on a Straight Line without Slipping

Table 3.3 summarizes all special case scenarios for fourth order motion of a circle rolling on a line. These scenarios identify the location of fourth order IC for such special cases. Also the resulting value of constant angle β_4 is also shown for each scenario.

Table 3.3: Summary of the Fourth Order Motion Properties in Special Case Scenarios for a Circle Rolling on a Straight Line

$\ddot{\alpha}$	$\dot{\alpha}$	α	ω	*IC Location*	β_4
0	No Effect	0	0	∞	90^o
0	0	0	$\neq 0$	*P [0, 0]*	0^o
0	No Effect	$\neq 0$	0	*P [0, 0]*	180^o
0	No Effect	$\neq 0$	$\neq 0$	*P [0, 0]*	$\tan^{-1}\left(\frac{6\omega^2\alpha}{4\omega\dot{\alpha}+3\alpha^2-\omega^4}\right)$
0	$\neq 0$	0	$\neq 0$	*P [0, 0]*	0^o or 180^o
$\neq 0$	No Effect	0	0	*O [0, -r]*	90^o
$\neq 0$	0 or nonzero	0	$\neq 0$	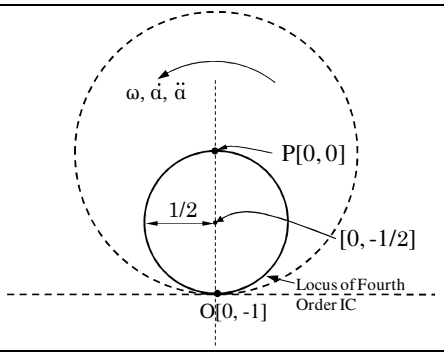	$\dot{\alpha} \neq 0$: $\tan^{-1}\left(-\frac{\ddot{\alpha}}{4\omega\dot{\alpha}-\omega^4}\right)$ $\dot{\alpha} = 0$: $\tan^{-1}\left(\frac{\ddot{\alpha}}{\omega^4}\right)$
$\neq 0$	No Effect	$\neq 0$	0	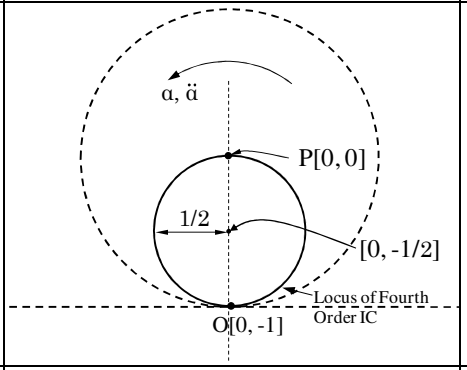	$\tan^{-1}\left(-\frac{\ddot{\alpha}}{3\alpha^2}\right)$
$\neq 0$	$\neq 0$	$\neq 0$	$\neq 0$	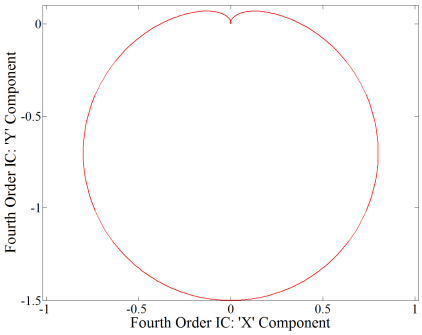	$\tan^{-1}\left(\frac{-(\ddot{\alpha}-6\omega^2\alpha)}{4\omega\dot{\alpha}+3\alpha^2-\omega^4}\right)$

3.3 Case 2: A Circle Rolling on another Circle

Another interesting special motion involving a rolling cylinder involves a cylinder rolling on the inside or outside of another cylinder (a hollow cylinder when rolling inside). Due to the pure rolling, this is also a 1-DOF motion. For representational simplicity, the cylinders have been considered as circles for the following formulation. The following sections discuss the motion of the circle starting with the first order motion up to the fourth order motion.

3.3.1 KINEMATIC DESCRIPTION OF THE SYSTEM

In case of a circle rolling on another circle, there are two scenarios as depicted in Fig. 3.17. In Fig. 3.17-a), a schematic diagram of a homogeneous circle of radius r (circle 1) rolling without slipping on the inside (the concave side) of a circle of radius r_2 (circle 2) is shown. Fig. 3.17 b) shows a homogeneous circle of radius r (circle 1) rolling without slipping on the outside (the convex side) a circle of radius r_2 (circle 2). In either case,

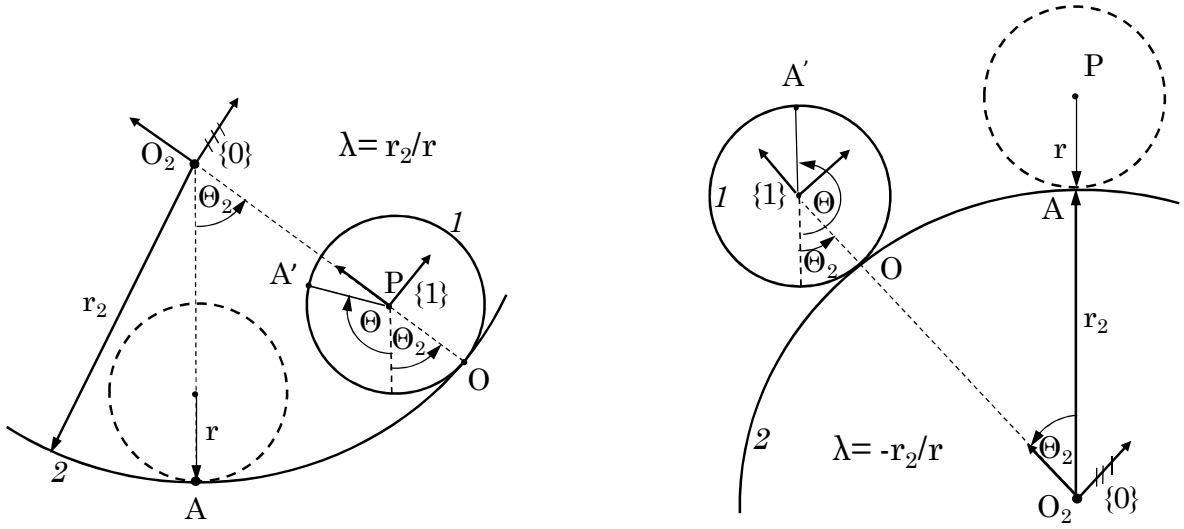

Fig. 3.17: Kinematic Description of a Circle Rolling on another Circle without Slipping a) Circle 1 Rolls the Inside of Circle 2; b) Circle 1 Rolls on the Outside of Circle 2

circle 2 is fixed in space with center at O_2 where the global frame {0} is located such that its Y axis is instantaneously oriented parallel to the line joining O_2 and the point of contact of the two circles. Frame {1} is a moving frame attached to circle 1 at its center, P such that its Y axis always points towards O_2. Thus frames {0} and {1} are always parallel. Let the circle 1 roll inside circle 2 so as to make an angle Θ_2 ($<AO_2O = \Theta_2$). In Fig. 3.17, the dotted circle represents the initial position while the bold circle represents the final position of the circle 1. Point A (which is fixed in the circle 1) is the initial point of contact of circles 1 and 2 which moves to A' during the prescribed motion. Let us assume that the circle 1 has rotated by an angle Θ during the motion.

Let us define a dimensionless term λ that defines the ratio of the radii of the circles in either case. For case a), when the circle 1 rolls inside circle 2, the two radius vectors are in the same direction at the point contact of the two circles, thus $\lambda = r_2/r$ while, for case b), the two radius vectors are in opposite direction, hence $\lambda = -r_2/r$. It will be shown that the choice of this dimensionless number helps us use same analytical formulation for both the cases. The positive value of λ is limited by the fact that the radius of circle 1 must be less than the circle 2. When $\lambda = 1$, no rolling of circle 1 is possible without slipping. The only relative motion between the two circles when $\lambda = 1$ is that due to slipping. However no such condition exists for the negative value of since a larger circle can roll on a smaller circle as long as both the radii are nonzero. Thus the condition on the value of λ is as follows:

$$0 > \lambda > 1 \qquad \text{Eq. 3.34}$$

For circle 1 to roll on circle 2 without slipping in both the cases, the length of arcs AO and OA' must be equal. Note that for case a), Θ and Θ_2 are in opposite direction while for case b), Θ and Θ_2 are in same direction. Thus the necessary condition for rolling without slipping for case a) is (Cowie, 1961):

$$r_2\Theta_2 = r(\Theta_2 - \Theta) \quad \text{Eq. 3.35}$$

and for case b) is (Cowie, 1961):

$$r_2\Theta_2 = r(\Theta - \Theta_2) \quad \text{Eq. 3.36}$$

Rearranging the terms, we get for case a):

$$(r_2 - r)\Theta_2 = -r\Theta \quad \text{Eq. 3.37}$$

And for case b):

$$(r_2 + r)\Theta_2 = r\Theta \quad \text{Eq. 3.38}$$

Using the definition of λ, we can reduce both Eq. 3.37 and Eq. 3.38 into one formulation as:

$$(\lambda - 1)\Theta_2 = -\Theta \quad \text{Eq. 3.39}$$

Rearranging Eq. 3.39, we get:

$$\Theta_2 = -\frac{\Theta}{(\lambda - 1)} \quad \text{Eq. 3.40}$$

Differentiating Eq. 3.40 with respect to time repetitively, we get:

$$\begin{aligned} \omega_2 &= -\frac{\omega}{(\lambda - 1)} \\ \alpha_2 &= -\frac{\alpha}{(\lambda - 1)} \\ \dot{\alpha}_2 &= -\frac{\dot{\alpha}}{(\lambda - 1)} \end{aligned} \quad \text{Eq. 3.41}$$

With this kinematic description, we define the motion of the circle in both cases starting with first order motion as follows. In order to have unified results, we will normalize formulation by using the radius of circle 1 as the unity, i.e., r = 1. Note that the radius of circle 1, r, is merely a scaling factor and its inclusion in the formulation keeps user from focusing the most important geometric parameter of the system, viz., λ.

3.3.2 First Order Kinematics of A Circle Rolling on another Circle

From Fig. 3.17-a), we can see that the velocity of the center (point P), of circle 1 for case

a) can be expressed in terms of parameter Θ_2 as:

$$V_P = (r_2 - r)\omega_2 \qquad \text{Eq. 3.42}$$

Similarly for case b):

$$V_P = -(r_2 + r)\omega_2 \qquad \text{Eq. 3.43}$$

Using the definition of λ for case a) and b), we can reduce Eq. 3.42 and Eq. 3.43 to:

$$V_P = r(\lambda - 1)\omega_2 \qquad \text{Eq. 3.44}$$

Putting radius of circle 1 as the unity, r = 1, in Eq. 3.44, we get:

$$V_P = (\lambda - 1)\omega_2 \qquad \text{Eq. 3.45}$$

Now, using Eq. 3.41, we can express the Eq. 3.45 in terms of parameter Θ as:

$$V_P = -\omega \qquad \text{Eq. 3.46}$$

But in frame {1},

$$\dot{x}_P = V_P = -\omega$$
$$\dot{y}_P = 0 \qquad \text{Eq. 3.47}$$

The velocity IC is computed in frame {1} as:

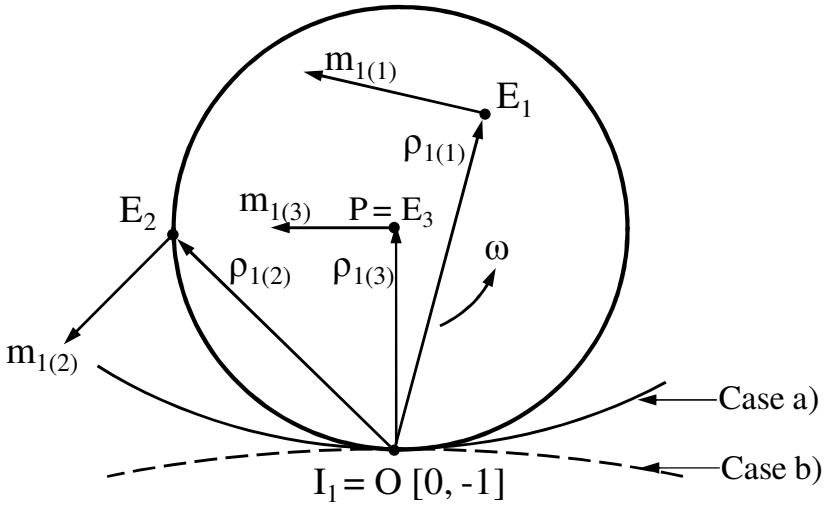

Fig. 3.18: The Locus of Velocity IC for the general Motion of a Circle Rolling on another Circle: Case a) Circle 1 Rolls on the Inside of Circle 2, and Case b) Circle 1 Rolls on the Outside of Circle 2

$$x_{I1} = -\frac{{}^0\dot{Y}_P}{\omega}$$
$$y_{I1} = \frac{{}^0\dot{X}_P}{\omega} \qquad \text{Eq. 3.48}$$

Using Eq. 3.47, we get:

$$x_{I1} = 0$$
$$y_{I1} = -1 \qquad \text{Eq. 3.49}$$

This is the location of the instantaneous point of contact of circle 1 with circle 2 which is independent of kinematic parameters of motion in both the cases, namely, when the circle 1 rolls inside circle 2 as well as when circle 1 rolls on the outside of circle 2 . Thus the velocity IC, in this case, is a purely geometric property and is located at the point of contact of the two circles. Fig. 3.18 shows the location of the velocity IC for both the cases as well as velocities of various points in the body in terms of the velocity IC.

3.3.3 SECOND ORDER KINEMATICS OF A CIRCLE ROLLING ON ANOTHER CIRCLE

The total acceleration of the center (point P) of circle 1 undergoing an angular acceleration α_2 and angular velocity ω_2 for case a) is computed as (Cowie, 1961):

$$\mathrm{A_P} = (\mathrm{r_2} - \mathrm{r})\alpha_2 + (\mathrm{r_2} - \mathrm{r})(\omega_2)^2 \qquad \text{Eq. 3.50}$$

Similarly the total acceleration of the center of circle 1 for case b) is:

$$\mathrm{A_P} = -(\mathrm{r_2} + \mathrm{r})\alpha_2 - (\mathrm{r_2} + \mathrm{r})(\omega_2)^2 \qquad \text{Eq. 3.51}$$

Using definition of λ for case a) and b), and r = 1, we can reduce Eq. 3.50 and Eq. 3.51 in terms of the angular velocity, ω, and the angular acceleration, α, of circle 1 as follows:

$$A_P = -\alpha + \frac{1}{(\lambda - 1)}\omega^2 \qquad \text{Eq. 3.52}$$

The two components of the total acceleration expressed in frame {1} are:

$$\ddot{x}_P = -\alpha \qquad \text{Eq. 3.53}$$

$$\ddot{y}_P = \frac{1}{(\lambda - 1)}\omega^2$$

In order to compute the location of acceleration IC using Eq. 3.53, Eq. 3.7 can be expanded as follows:

$$x_{I2} = \frac{-\alpha\,\omega^2 - \frac{1}{(\lambda-1)}\omega^2\alpha}{\alpha^2 + \omega^4}$$
$$y_{I2} = \frac{-\alpha^2 + \frac{1}{(\lambda-1)}\omega^4}{\alpha^2 + \omega^4} \qquad \text{Eq. 3.54}$$

Consider the expression for x_{I2} in Eq. 3.54:

$$x_{I2} = \frac{-\alpha\,\omega^2 - \frac{1}{(\lambda-1)}\omega^2\alpha}{\alpha^2 + \omega^4} = \frac{-\lambda\alpha\,\omega^2}{(\lambda-1)(\alpha^2+\omega^4)} \qquad \text{Eq. 3.55}$$

Using the definition of angle β_2 (Eq. 2.20), we can rearrange Eq. 3.55 as follows:

$$x_{I2} = \frac{\lambda}{(\lambda-1)}\frac{tan\beta_2}{1+tan^2\,\beta_2} = \frac{\lambda}{(\lambda-1)}\frac{tan\,\beta_2}{sec^2\,\beta_2} = \frac{\lambda}{(\lambda-1)}sin\,\beta_2 cos\,\beta_2$$

But $\sin\beta_2\cos\beta_2 = \frac{1}{2}\sin(2\beta_2)$. Thus after further simplification, we get:

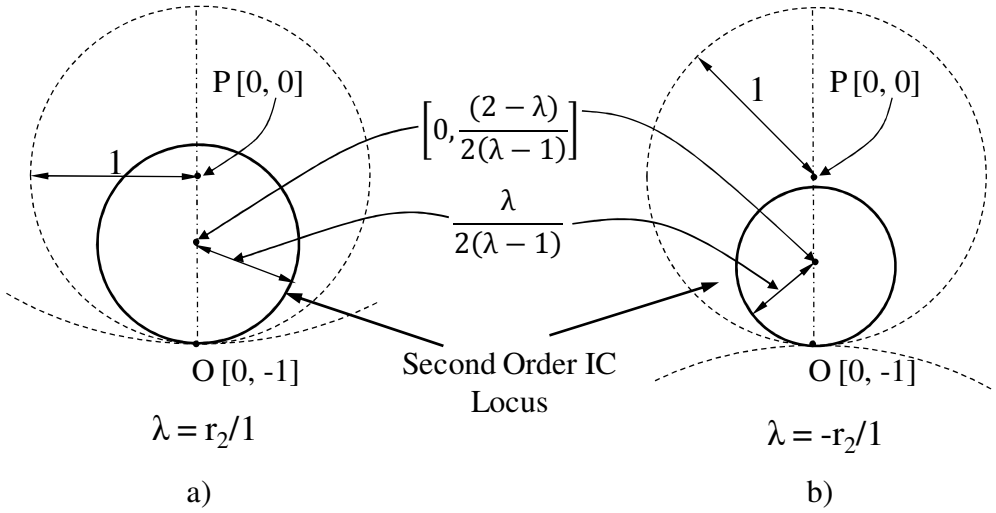

Fig. 3.19: The Locus of Acceleration IC for the General Motion of a Circle Rolling on Another Circle: Case a) Circle 1 Rolls on the Inside of Circle 2, and Case b) Circle 1 Rolls on the Outside of Circle 2

$$x_{I2} = \frac{\lambda}{2(\lambda-1)}\, sin(2\beta_2) \qquad \text{Eq. 3.56}$$

Similarly, consider the expression for y_{I2} in Eq. 3.54:

$$y_{I2} = \frac{-\alpha^2 + \frac{1}{(\lambda-1)}\omega^4}{\alpha^2+\omega^4} = \frac{-\lambda\,\alpha^2 + \alpha^2 + \omega^4}{(\lambda-1)(\alpha^2+\omega^4)} = \frac{1}{(\lambda-1)} - \frac{\lambda\,\alpha^2}{(\lambda-1)(\alpha^2+\omega^4)}$$

Again using the definition of angle β_2 (Eq. 2.20), we can rearrange the expression for ${}^1I_{2y}$ as:

$$y_{I2} = \frac{1}{(\lambda-1)} - \frac{\lambda}{(\lambda-1)}\frac{tan^2\,\beta_2}{(1+tan^2\,\beta_2)} = \frac{1}{(\lambda-1)} - \frac{\lambda}{(\lambda-1)}sin^2\,\beta_2$$

But $\sin^2\beta_2 = \left(\frac{1-\cos(2\beta_2)}{2}\right)$. Thus the expression for y_{I2} can be simplified as following:

$$y_{I2} = \frac{(2-\lambda)}{2(\lambda-1)} + \frac{\lambda}{2(\lambda-1)}cos(2\beta_2) \qquad \text{Eq. 3.57}$$

Restating the equations for the locus of acceleration IC in case of a circle rolling inside another circle we get:

$$\begin{aligned} x_{I2} &= 0 + \frac{\lambda}{2(\lambda-1)}\, sin\,2\beta_2 \\ y_{I2} &= \frac{(2-\lambda)}{2(\lambda-1)} + \frac{\lambda}{2(\lambda-1)}cos(2\beta_2) \end{aligned} \qquad \text{Eq. 3.58}$$

Note that this is a parametric equation of a circle with the center at $\left[0, \frac{(2-\lambda)}{2(\lambda-1)}\right]$, and the radius equal to $\frac{\lambda}{2(\lambda-1)}$. This locus circle shown in Fig. 3.19 is also the inflection circle for this special case (Vidosic and Tesar, 1967). The radius of the locus circle is dependent only on the geometric parameter, λ, and independent of the kinematic parameters. Thus the second order IC is a geometric entity for this particular special case.

3.3.3.1 On the Radius of the Acceleration IC Locus Circle

We can make several observations about the influence of the value of radii ratio, λ, on the radius of the acceleration IC circle from, Eq. 3.58, and Fig. 3.19 as follows:

1. When the value of λ is positive (case a), the radius of the acceleration IC locus

$\left(\frac{\lambda}{2(\lambda-1)}\right)$ will be greater than half of the radius of circle 1 ($\frac{1}{2}$ since in this case, r = 1) for a finite value of λ because when λ is positive, the term $\frac{\lambda}{(\lambda-1)}$ will always be greater than 1. Thus the diameter of the acceleration IC locus circle in case of a circle rolling on the inside of another circle will always be greater than the radius of the rolling circle (circle 1). When the radii ratio λ increases, the radius of the acceleration IC locus circle decreases as we can see from the expression for the radius, $\frac{\lambda}{2(\lambda-1)}$. Note that the positive value of λ must always be greater than 1 (i.e., $r_2 > r$).

2. On the other hand, when the value of λ is negative (case b), There are two scenarios:

   2.1. $|\lambda| \geq 1$: When $r_2 \geq r$, the radius of the acceleration IC locus $\left(\frac{\lambda}{2(\lambda-1)}\right)$ will be smaller than half the radius of circle 1 for finite value of λ. This is because, for negative values of λ, the magnitude of the term $\frac{\lambda}{(\lambda-1)}$ will be smaller than 1. Thus the diameter of acceleration IC locus in case of a circle rolling on the inside of another circle will always be smaller than the radius of the rolling circle (circle 1) for this case. When the magnitude of the radii ratio, λ, increases the radius of the acceleration IC locus circle increases as we can see from the expression for the radius, $\frac{\lambda}{2(\lambda-1)}$. When λ is infinity, the acceleration IC radius approaches the radius of the circle 1. This is because when $|\lambda| \gg 1, (\lambda - 1) \cong \lambda$, and the term $\frac{\lambda}{2(\lambda-1)}$ approaches $\frac{1}{2}$.

   2.2. $|\lambda| < 1$. When the radius of circle 1 is larger than the radius of circle 2, the radius of the acceleration IC locus $\left(\frac{\lambda}{2(\lambda-1)}\right)$ will be smaller than half the radius of circle 2 for finite value of λ. When the radius of circle 2 is much smaller than that of circle 1, i.e., when $|\lambda| \gg 1$, the radius of the acceleration IC approaches $\frac{\lambda}{2}$. Note that when r =1, $|\lambda| = r_2$.

In other words, the radius of the acceleration IC locus for the case of a circle rolling on the outside of another circle is smaller than (or equal to) half of the smaller of the two radii (radius of rolling and fixed circle). When the rolling cylinder radius is ∞ i.e., r = ∞, the condition is a straight line rolling on a circle, while when the fixed cylinder radius is infinity, i.e., $r_2 = \infty$, the condition becomes a circle rolling on a line. These conditions are shown in Fig. 3.20.

3. In the limiting case when $\lambda = \infty$, we can simplify the expression for the acceleration IC (Eq. 3.54) as:

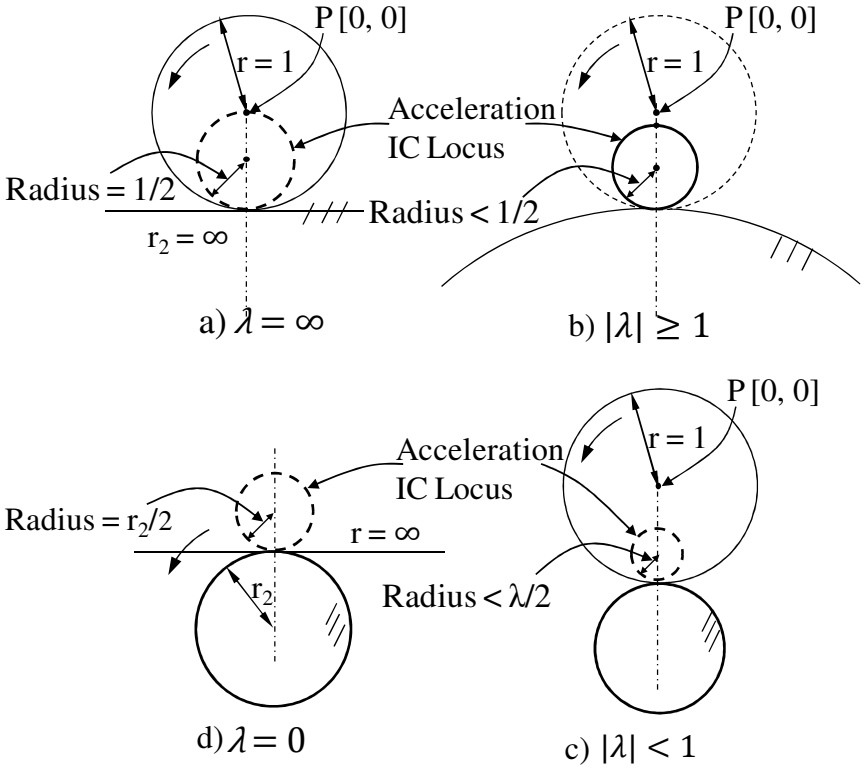

Fig. 3.20: General Locus of the Acceleration IC for Circle Rolling on the Outside of another Circle (Negative λ) for Different Scenarios: a) Circle 2 (the Fixed Circle) is a Straight Line (r2 = ∞, thus λ = ∞) (Sec. 3.2), b) Circle 2 is Larger than or Equal to Circle 1 ($|\lambda| \geq 1$), c) Circle 2 is Smaller than Circle 1 (|λ| < 1), and d) Circle 1 (the Rolling Circle) is a Straight Line (r = ∞, thus λ = 0)

$$x_{I2} = \left.\frac{-\alpha\,\omega^2 - \frac{1}{(\lambda-1)}\omega^2}{\alpha^2+\omega^4}\right|_{\lambda=\infty} = \frac{-\alpha\,\omega^2}{\alpha^2+\omega^4}$$

$$y_{I2} = \left.\frac{-\alpha^2 + \frac{1}{(\lambda-1)}\omega^4}{\alpha^2+\omega^4}\right|_{\lambda=\infty} = \frac{-\alpha^2}{\alpha^2+\omega^4} \qquad \text{Eq. 3.59}$$

Comparing this equation with the locus of acceleration IC when a circle rolls on a straight line without slipping (Eq. 3.8), we see that they are identical. Thus we see that the second order motion of a circle rolling on a straight line is a special case of the second order motion of the circle on a circle when $\lambda = \infty$.

A simulation plot shown in Fig. 3.21 depicts these properties graphically. The simulation shows that as the magnitude of λ increases for both the positive and negative values of λ, the radius of acceleration IC locus circle starts approaches the corresponding radius in

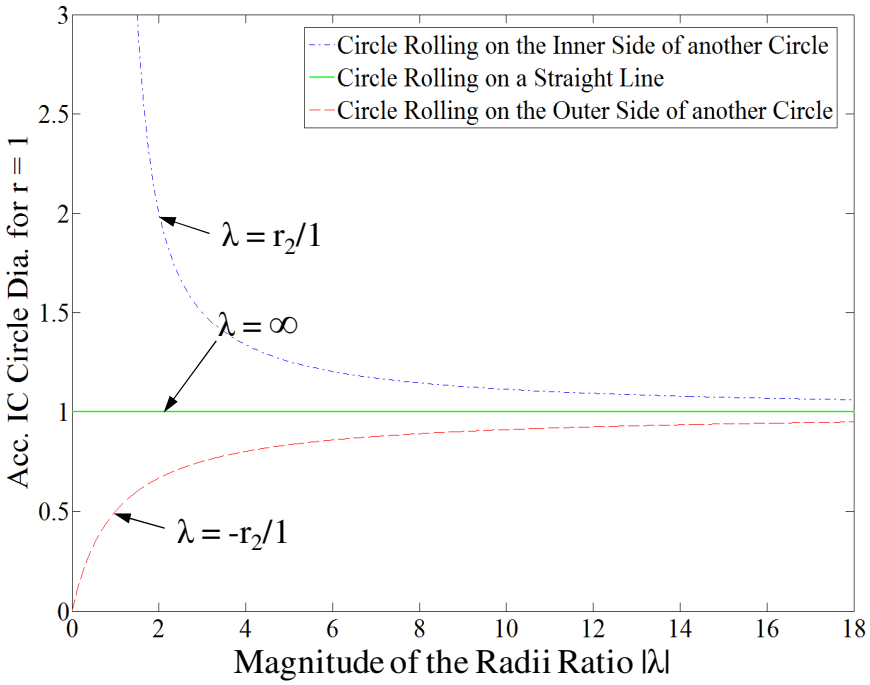

Fig. 3.21: The Acceleration IC Locus Radius for Rolling Circles, Three Special Cases: 1) Circle Rolling on a Straight Line, 2) Circle Rolling on the Inner Side of another Circle, and 3) Circle Rolling on the Outer Side of another Circle

case of the circle rolling on a straight line.

3.3.3.2 Special Case Scenarios for Second Order Motion of A Circle Rolling on another Circle

We have established that the shape of the locus of the acceleration IC is a circle dependent on the geometric parameter, λ for the particular system in the 1 DOF motion. The particular location of acceleration IC, I_2, is dependent on instantaneous kinematic parameters, α, and ω. We will now study some interesting special case scenarios for the values of the kinematic parameters.

Case 1: $\alpha \neq 0; \text{and } \omega = 0$

When the angular acceleration, α, of the body is nonzero while the angular velocity, ω, is zero, the acceleration IC given by Eq. 3.54 is located at:

$$x_{I2} = 0$$
$$y_{I2} = -1 \qquad \text{Eq. 3.60}$$

One of the scenarios in which this happens is when the body is starting its motion from rest. With $\alpha \neq 0; \text{and } \omega = 0$, the value of second order orientation angle β_2 (Eq. 2.20) is computed as 90^o. The location of the acceleration IC given by Eq. 3.60 can also

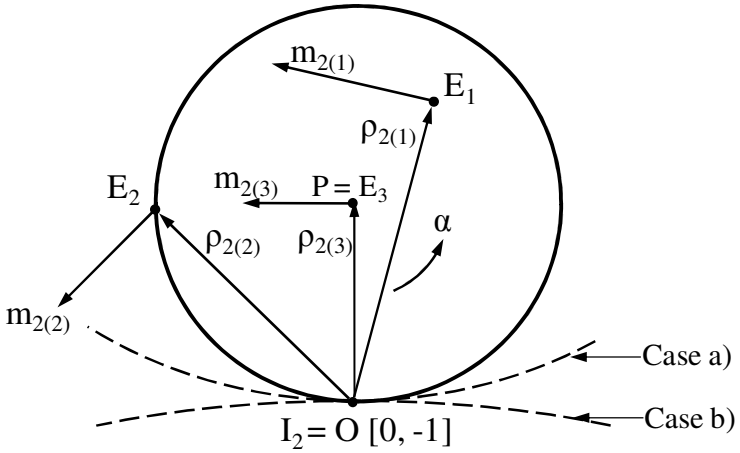

Fig. 3.22: A Circle Rolling on another Circle: The Acceleration IC Location when $\alpha \neq 0, \omega = 0$: Case a) Circle 1 Rolls on the Inside of Circle 2, and Case b) Circle 1 Rolls on the Outside of Circle 2

be verified using Eq. 3.58 when β_2 is 90°. This is the location of the point of contact of the two circles as shown in Fig. 3.22.

Case 2: $\alpha = 0$; and $\omega \neq 0$

When the body is moving with constant angular velocity, ω, the angular acceleration, α, is zero. The acceleration IC given by Eq. 3.54 is then located at:

$$x_{I2} = 0$$
$$y_{I2} = \left[0, \frac{1}{(\lambda - 1)}\right] \qquad \text{Eq. 3.61}$$

The value of angle β_2 is 180°. The location of the acceleration IC given by Eq. 3.61 is dependent on the value of λ. As shown in Fig. 3.23, if λ is positive (it is always greater than 1), the location of the IC is above the center of circle 1, i.e., point P, while if λ is negative, the location of the IC is below the center of circle 1, i.e., point P. When λ is infinity, the IC is located at point P which is the acceleration IC for the circle rolling on a

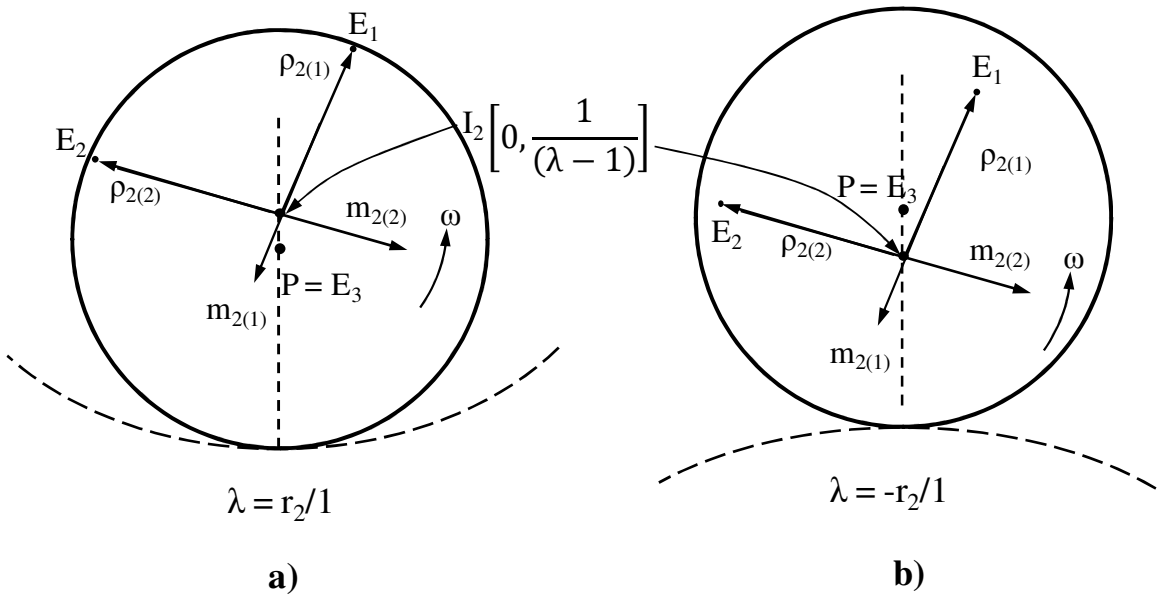

Fig. 3.23: The Acceleration IC Location when $\alpha = 0, \omega \neq 0$ for a Circle Rolling on another Circle: Case a) Circle 1 Rolls on the Inside of Circle 2, and Case b) Circle 1 Rolls on the Outside of Circle 2

straight line when ω is constant (Fig. 3.4).

Case 3: $\alpha \neq 0$; and $\omega \neq 0$

In general, when $\alpha \neq 0$, and $\omega \neq 0$, the acceleration IC is located on the locus circle as shown in Fig. 3.19. Its exact location is dependent on the instantaneous value of angle β_2 which in turn is dependent on the instantaneous values of kinematic parameters of the rolling circle, namely, ω, and α. In Sec. 3.2.3, we discussed some example scenarios the acceleration IC location for a circle rolling on a straight line (Fig. 3.3).

In the following Section, we will discuss the third order motion properties of the system.

3.3.4 THIRD ORDER KINEMATICS OF A CIRCLE ROLLING ON ANOTHER CIRCLE

The condition for the homogeneous circle to roll on the inside of another circle without slipping for the third order motion for case a) is computed as (Cowie, 1961):

$$J_P = (r_2 - r)(\dot{\alpha}_2 - \omega_2^3) + (r_2 - r)3\omega_2\alpha_2 \qquad \text{Eq. 3.62}$$

Similarly the total acceleration of the center of circle 1 for case b) is:

$$J_P = -(r_2 + r)(\dot{\alpha}_2 - \omega_2^3) - (r_2 + r)3\omega_2\alpha_2 \qquad \text{Eq. 3.63}$$

Using definition of λ for case a) and b), we can reduce Eq. 3.62 and Eq. 3.63 in terms of the angular velocity, ω, and the angular acceleration, α, of circle 1 as follows:

$$J_P = -r\dot{\alpha} + \frac{r}{(\lambda-1)^2}\omega^3 + \frac{r}{(\lambda-1)}3\omega\alpha$$

Using r = 1, we get:

$$J_P = -\dot{\alpha} + \frac{1}{(\lambda-1)^2}\omega^3 + \frac{1}{(\lambda-1)}3\omega\alpha$$

Thus the X and Y component of the jerk for point P owing to the third order motion of circle 1 without skidding on circle 2 is given by:

$$X_P^{(3)} = -\dot{\alpha} + \frac{1}{(\lambda-1)^2}\omega^3$$
$$Y_P^{(3)} = \frac{1}{(\lambda-1)}3\omega\alpha \qquad \text{Eq. 3.64}$$

Using the constraint condition provided by Eq. 3.64, the third order (jerk) IC (Eq. 3.10) for a general third order motion of the circle can be computed as:

$$x_{I3} = \frac{\left(-\dot{\alpha} + \frac{1}{(\lambda-1)^2}\omega^3\right)(3\omega\alpha) - \frac{1}{(\lambda-1)}3\omega\alpha(\dot{\alpha}-\omega^3)}{(\dot{\alpha}-\omega^3)^2 + (3\omega\alpha)^2}$$

$$y_{I3} = \frac{\left(-\dot{\alpha} + \frac{1}{(\lambda-1)^2}\omega^3\right)(\dot{\alpha}-\omega^3) + \frac{1}{(\lambda-1)}(3\omega\alpha)^2}{(\dot{\alpha}-\omega^3)^2 + (3\omega\alpha)^2} \qquad \text{Eq. 3.65}$$

3.3.4.1 Simulation Plot for the Fourth Order Motion of A Circle Rolling on another Circle

The locus of the third order IC location is plotted using a simulation plot where a circle of radius 1 foot is rolling without slipping on another circle. For case a, parameter λ was varied as shown in Fig. 3.24 from 3 to ∞. On the negative side (case b), λ is varied from -0.5 to -∞. It is found that the locus is dependent only on the geometric parameter, λ and is independent of the kinematic state of the body. The particular location of the third order

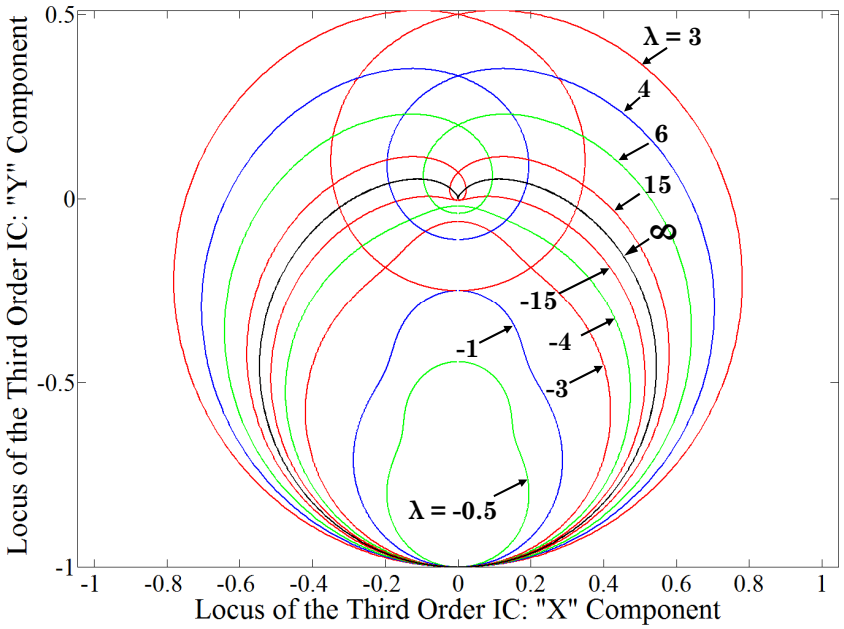

Fig. 3.24: The Locus of the Third Order IC for the General Motion of a Circle Rolling on Another Circle when a) (λ>0) Circle 1 Rolls on the Inside of Circle 2, and b) (λ<0) Circle 1 Rolls on the Outside of Circle 2

IC at any instant, however, is dependent on the instantaneous values of the kinematic parameters of the rigid body. As the value of parameter, λ, becomes larger, the locus of the IC starts approaching the shape of the locus of third order IC (Fig. 3.24) in the special case discussed earlier when the circle rolled on a straight line. Thus the locus is bounded by the locus of the acceleration IC in the case of a circle rolling on a straight line for both the cases. We can show this analytically by evaluating Eq. 3.65 for the case when λ=∞ as follows:

$$x_{I3} = \left.\frac{\left(-\dot{\alpha} + \frac{1}{(\lambda-1)^2}\omega^3\right)(3\omega\alpha) - \frac{1}{(\lambda-1)}3\omega\alpha(\dot{\alpha}-\omega^3)}{(\dot{\alpha}-\omega^3)^2 + (3\omega\alpha)^2}\right|_{\lambda=\infty}$$

$$= \frac{(-\dot{\alpha})(3\omega\alpha)}{(\dot{\alpha}-\omega^3)^2 + (3\omega\alpha)^2}$$

Eq. 3.66

$$y_{I3} = \left.\frac{\left(-\dot{\alpha} + \frac{1}{(\lambda-1)^2}\omega^3\right)(\dot{\alpha}-\omega^3) + \frac{1}{(\lambda-1)}(3\omega\alpha)^2}{(\dot{\alpha}-\omega^3)^2 + (3\omega\alpha)^2}\right|_{\lambda=\infty}$$

$$= \frac{(-\dot{\alpha})(\dot{\alpha}-\omega^3)}{(\dot{\alpha}-\omega^3)^2 + (3\omega\alpha)^2}$$

Comparing, with Eq. 3.13, we see that the equation Eq. 3.66 becomes identical to Eq. 3.13 when λ=∞.

3.3.4.2 Special Case Scenarios for the Third Order Motion of A Circle Rolling on another Circle

Next, we will discuss some special case scenarios that exist in the third order motion of the circle.

Case 1: $\dot{\alpha} \neq 0, \omega = 0$

When the angular velocity, ω, of the body is zero while the angular jerk, α̇, has a nonzero value. The location of the third order IC, regardless of the state of the angular acceleration, α, becomes:

$$x_{I3} = 0$$
$$y_{I3} = -1 \qquad \text{Eq. 3.67}$$

This is the location of the point of contact, O. Also with these values of ω, α, and $\dot{\alpha}$, angle β_3 is computed as -90°. Thus the location of the third order IC in this case is the point of contact, O, of the circle with the line regardless of the value of angular acceleration, α. Every point on the body has third order motion state, m_3, such that its magnitude is proportional to and direction is orthogonal to the radius, ρ_3. This is shown in Fig. 3.25.

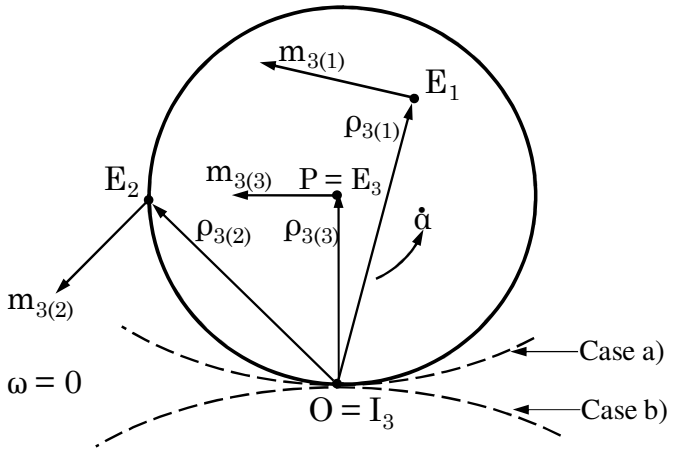

Fig. 3.25: The Third Order IC Location when $\dot{\alpha} \neq 0, \omega = 0$ for a Circle Rolling on another Circle: Case a) Circle 1 Rolls on the Inside of Circle 2, and Case b) Circle 1 Rolls on the Outside of Circle 2

Case 2: $\dot{\alpha} = 0, \alpha = 0$, **and** $\omega \neq 0$

When the angular jerk and the angular acceleration of the circle are instantaneously zero with nonzero angular velocity, ω, the location of the instant center is at:

$$x_{I3} = 0$$
$$y_{I3} = -\frac{1}{(\lambda - 1)^2} \qquad \textit{Eq. 3.68}$$

This is a fixed location independent of the magnitude of the instantaneous angular velocity, also the constant angle β_3 becomes -90°. As shown in Fig. 3.26, if λ is positive

(it is always greater than 1), the location of the IC is below the center of circle 1, i.e., point P, while if λ is negative, the location of the IC is above the center of circle 1, i.e., point P. When λ is infinity, the IC is located at point P which is the acceleration IC for the circle rolling on a straight line when ω is constant (Fig. 3.10).

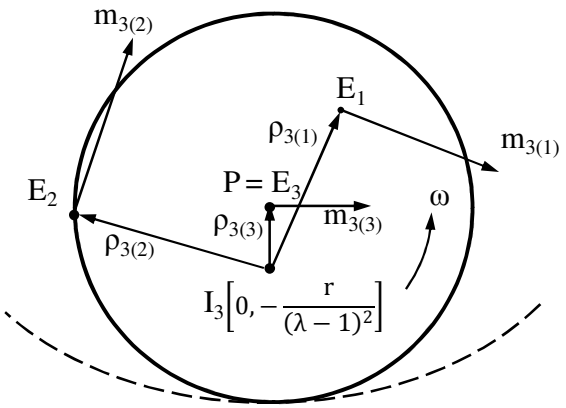

Fig. 3.26: The Third Order IC Location when $\dot{\alpha} = 0, \alpha = 0$, and $\omega \neq 0$ for A Circle Rolling on another Circle: Shown Here is the Case when Circle 1 Rolls on the Inside of Circle 2

Case 3: $\dot{\alpha} = 0, \alpha \neq 0$, and $\omega \neq 0$

When only the angular jerk of the circle is zero, the location of third order IC is computed as:

$$x_{I3} = \frac{\frac{1}{(\lambda-1)^2}\omega^3 3\omega\alpha + \frac{1}{(\lambda-1)}\omega^3 3\omega\alpha}{(\omega^3)^2 + (3\omega\alpha)^2}$$
$$y_{I3} = \frac{-\frac{1}{(\lambda-1)^2}(\omega^3)^2 + \frac{1}{(\lambda-1)}(3\omega\alpha)^2}{(\omega^3)^2 + (3\omega\alpha)^2} \qquad \text{Eq. 3.69}$$

Consider the expression for x_{I3}:

$$x_{I3} = \frac{\frac{1}{(\lambda-1)^2}\omega^3 3\omega\alpha - \frac{1}{(\lambda-1)}\omega^3 3\omega\alpha}{(\omega^3)^2 + (3\omega\alpha)^2} = \frac{\lambda}{(\lambda-1)^2}\frac{\omega^3 3\omega\alpha}{(\omega^3)^2 + (3\omega\alpha)^2}$$

Using the definition of angle β_3, we get:

$$x_{I3} = \frac{\lambda}{(\lambda-1)^2}\frac{tan\beta_3}{1+tan^2\,\beta_3} = \frac{\lambda}{(\lambda-1)^2}sin\,\beta_3 cos\,\beta_3 = \frac{\lambda}{2(\lambda-1)^2}sin2\beta_3$$

Now, rearranging the terms in the expression for y_{I3}, we get:

$$y_{I3} = \frac{-\frac{1}{(\lambda-1)^2}(\omega^3)^2 + \frac{1}{(\lambda-1)}(3\omega\alpha)^2}{(\omega^3)^2+(3\omega\alpha)^2} = -\frac{1}{(\lambda-1)^2} + \frac{\lambda}{(\lambda-1)^2}\frac{(3\omega\alpha)^2}{(\omega^3)^2+(3\omega\alpha)^2}$$

Using the definition of angle β_3, we get:

$$y_{I3} = -\frac{1}{(\lambda-1)^2} + \frac{\lambda}{(\lambda-1)^2}\frac{tan^2\,\beta_3}{(1+tan^2\,\beta_3)} = -\frac{(2-\lambda)}{2(\lambda-1)^2} + \frac{\lambda}{2(\lambda-1)^2}cos2\beta_3$$

Restating the third order IC location, we get:

$$x_{I3} = 0 + \frac{\lambda}{2(\lambda-1)^2}sin2\beta_3$$
$$y_{I3} = --\frac{(2-\lambda)}{2(\lambda-1)^2} + \frac{\lambda}{2(\lambda-1)^2}cos2\beta_3 \qquad \text{Eq. 3.70}$$

Thus we can see that the locus of third order IC for the motion of the circle when the angular jerk, $\dot{\alpha}$, is zero is a circle with radius of $\frac{\lambda}{2(\lambda-1)^2}$, and center at $\left[0, -\frac{(2-\lambda)}{2(\lambda-1)^2}\right]$. Thus

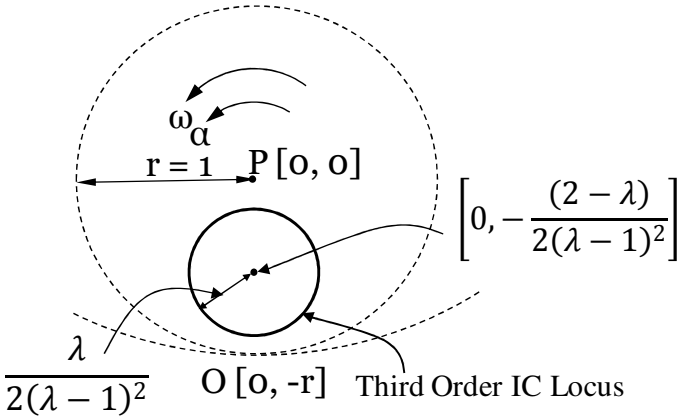

Fig. 3.27: The Locus of Third Order IC for $\dot{\alpha} = 0, \alpha \neq 0, \omega \neq 0$ for A Circle Rolling on another Circle: Shown Here is the Case when Circle 1 Rolls on the Inside of Circle 2

when the larger circle has radius twice the radius of the rolling circle, the radius of the third order IC locus becomes zero, which is verified using a simulation plot. Fig. 3.27 shows a graphical representation of this special case when $\lambda = 3$.

Case 3: $\dot{\alpha} \neq 0, \alpha = 0, \omega \neq 0$

When the circle is rolling with nonzero angular velocity, and angular jerk and no angular acceleration, the location of third order IC (Eq. 3.13) is at:

$$x_{I3} = 0$$
$$y_{I3} = \frac{-\dot{\alpha} + \frac{1}{(\lambda-1)^2}\omega^3}{(\dot{\alpha} - \omega^3)} \qquad \text{Eq. 3.71}$$

Thus, depending on the values of $\dot{\alpha}$ and ω, the location of third order IC is located as shown in Fig. 3.28. Note that when $\dot{\alpha} = \omega^3$, the instant center is located at infinity.

Summary

Table 3.4 summarizes all special case scenarios for the third order motion of a circle rolling inside another circle. These scenarios identify the location of third order IC for such special cases. Also the resulting value of constant angle β_3 is also shown for each scenario.

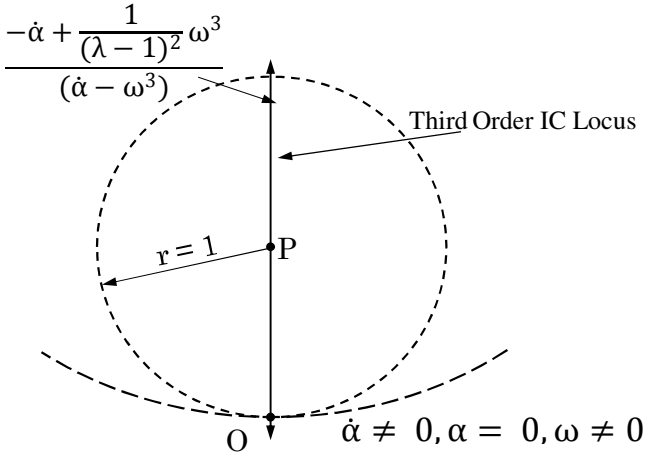

Fig. 3.28: A Circle Rolling on another Circle: The Third Order IC Location when $\dot{\alpha} \neq 0, \alpha = 0, \omega \neq 0$

Table 3.4: Third Order Motion for a Circle Rolling Inside another Circle: Summary of Special Cases

$\dot{\alpha}$	α	ω	IC Location	β_3
0	0	$\neq 0$	*P [0, 0]*	-90^o
0	$\neq 0$	$\neq 0$	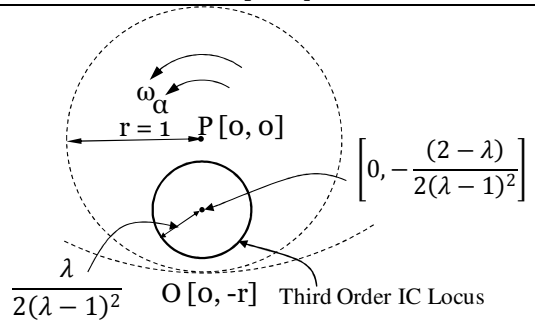	$\tan^{-1}\left(-\frac{\omega^3}{3\omega\alpha}\right)$
0	No Effect	0	∞	90^o
$\neq 0$	No Effect	0	*O [0, -r]*	90^o
$\neq 0$	0	$\neq 0$	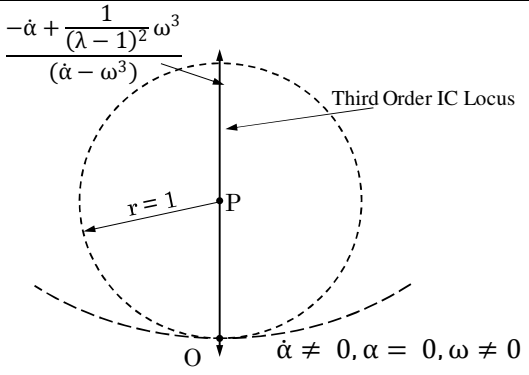	90^o or -90^o
$\neq 0$	$\neq 0$	$\neq 0$	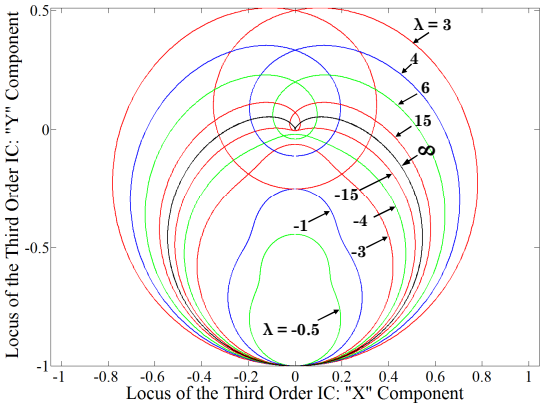	$\tan^{-1}\left(-\frac{\dot{\alpha}-\omega^3}{3\omega\alpha}\right)$

3.3.5 FOURTH ORDER MOTION OF A CIRCLE ROLLING ON ANOTHER CIRCLE

The condition for the homogeneous circle to roll inside another circle (case a) without slipping for the fourth order motion can be computed in terms of parameter Θ_2 as follows (Cowie, 1961):

$$\dot{\mathrm{J}}_{\mathrm{P}} = (\mathrm{r}_2 - \mathrm{r})\left(\ddot{\alpha}_2 - 6\omega_2{}^2\alpha_2\right) + (\mathrm{r}_2 - \mathrm{r})(4\omega_2\dot{\alpha}_2 + 3\alpha_2{}^2 - \omega_2{}^4) \qquad \text{Eq. 3.72}$$

For the circle to roll on the outside of another circle (case b), the condition is:

$$\dot{\mathrm{J}}_{\mathrm{P}} = -(\mathrm{r}_2 + \mathrm{r})\left(\ddot{\alpha}_2 - 6\omega_2{}^2\alpha_2\right) - (\mathrm{r}_2 + \mathrm{r})(4\omega_2\dot{\alpha}_2 + 3\alpha_2{}^2 - \omega_2{}^4) \qquad \text{Eq. 3.73}$$

Using definition of λ for case a) and b), we can reduce Eq. 3.72 and Eq. 3.73 as follows:

$$\dot{\mathrm{J}}_{\mathrm{P}} = \mathrm{r}(\lambda - 1)\left(\ddot{\alpha}_2 - 6\omega_2{}^2\alpha_2\right) + \mathrm{r}(\lambda - 1)(4\omega_2\dot{\alpha}_2 + 3\alpha_2{}^2 - \omega_2{}^4) \qquad \text{Eq. 3.74}$$

Using Eq. 3.41, and r = 1, we can express Eq. 3.74 in terms of parameter Θ as follows:

$$\dot{\mathrm{J}}_{\mathrm{P}} = -\ddot{\alpha} + \frac{1}{(\lambda-1)^2}6\omega^2\alpha + \frac{1}{(\lambda-1)}4\omega\dot{\alpha} + \frac{1}{(\lambda-1)}3\alpha^2 - \frac{1}{(\lambda-1)^3}\omega^4$$

Thus the X and Y component of the jerk for point P owing to the fourth order motion of circle 1 without skidding on circle 2 in both the cases, namely, positive and negative values of λ, is given by:

$$\mathrm{X}_{\mathrm{P}}^{(4)} = -\ddot{\alpha} + \frac{1}{(\lambda-1)^2}6\omega^2\alpha$$
$$\mathrm{Y}_{\mathrm{P}}^{(4)} = \frac{1}{(\lambda-1)}4\omega\dot{\alpha} + \frac{1}{(\lambda-1)}3\alpha^2 - \frac{1}{(\lambda-1)^3}\omega^4 \qquad \text{Eq. 3.75}$$

Using the constraint condition provided by Eq. 3.75, the fourth order (jerk) IC (Eq. 2.39) for a general fourth order motion of the circle can be computed as:

$$x_{I4} = \frac{\left(-\mathrm{r}\ddot{\alpha} + \frac{\mathrm{r}}{(\lambda-1)^2}6\omega^2\alpha\right)(4\omega\dot{\alpha} + 3\alpha^2 - \omega^4) - \left(\frac{\mathrm{r}}{(\lambda-1)}4\omega\dot{\alpha} + \frac{\mathrm{r}}{(\lambda-1)}3\alpha^2 - \frac{\mathrm{r}}{(\lambda-1)^3}\omega^4\right)(\ddot{\alpha} - 6\omega^2\alpha)}{(\ddot{\alpha} - 6\omega^2\alpha)^2 + (4\omega\dot{\alpha} + 3\alpha^2 - \omega^4)^2} \qquad \text{Eq. 3.76}$$

$$y_{I4} = \frac{\left(-\mathrm{r}\ddot{\alpha} + \frac{\mathrm{r}}{(\lambda-1)^2}6\omega^2\alpha\right)(\ddot{\alpha} - 6\omega^2\alpha) + \left(\frac{\mathrm{r}}{(\lambda-1)}4\omega\dot{\alpha} + \frac{\mathrm{r}}{(\lambda-1)}3\alpha^2 - \frac{\mathrm{r}}{(\lambda-1)^3}\omega^4\right)(4\omega\dot{\alpha} + 3\alpha^2 - \omega^4)}{(\ddot{\alpha} - 6\omega^2\alpha)^2 + (4\omega\dot{\alpha} + 3\alpha^2 - \omega^4)^2}$$

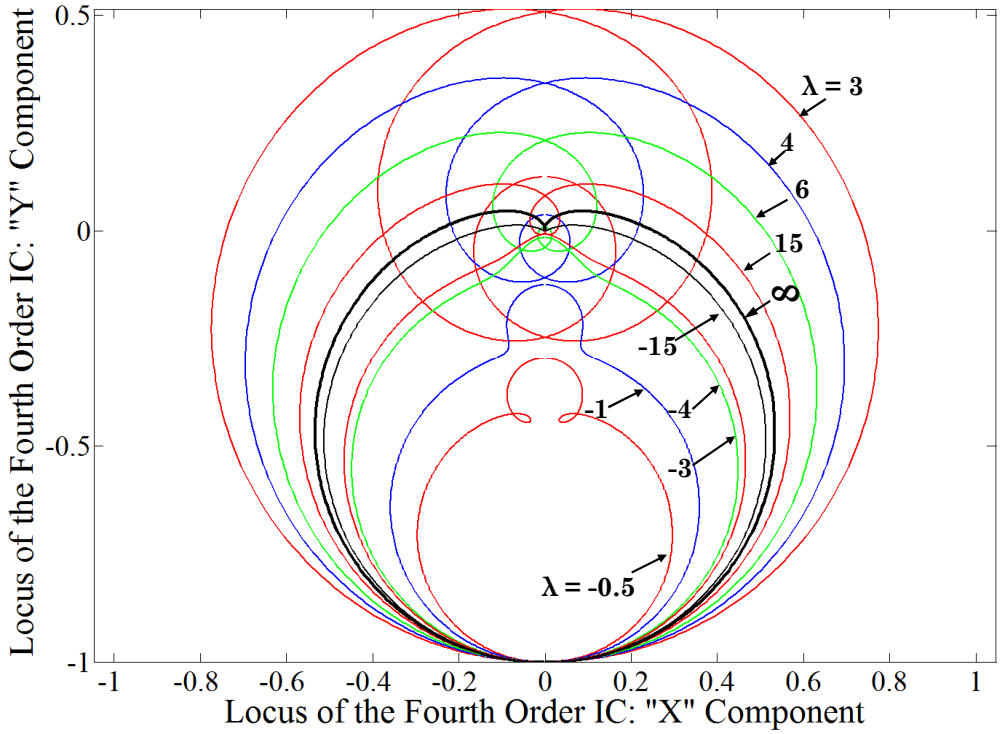

Fig. 3.29: A Circle Rolling on another Circle: The Locus of the Fourth Order IC Location for General Motion

Eq. 3.76 is the locus equation for the fourth order IC for both the cases discussed above. In order to study the general shape of the locus, a simulation plot was programmed which will be discussed next.

3.3.5.1 Simulation Plot for Fourth Order Motion of A Circle Rolling on another Circle

The locus of the fourth order IC location is plotted using a simulation plot where a circle of radius 1 foot is rolling without slipping on another circle. For case a, parameter λ was varied as shown in Fig. 3.29 from 3 to ∞. On the negative side (case b), λ is varied from -0.5 to -∞. It is found that the locus is dependent only on the geometric parameter, λ and is independent of the kinematic state of the body. The particular location of the third order IC at any instant, however, is dependent on the instantaneous values of the kinematic parameters of the rigid body. As the value of parameter, λ, becomes larger, the locus of

the IC starts approaching the shape of the locus of the fourth order IC (Fig. 3.12) in the special case discussed earlier when the circle rolled on a straight line. Thus the locus is bounded by the locus of the acceleration IC in the case of a circle rolling on a straight line for both the cases. We can show this analytically by evaluating Eq. 3.76 for the case when λ=∞ as follows:

$$x_{I4} = \left.\frac{\left(-\ddot{\alpha}+\frac{1}{(\lambda-1)^2}6\omega^2\alpha\right)(4\omega\dot{\alpha}+3\alpha^2-\omega^4)-\left(\frac{1}{(\lambda-1)}4\omega\dot{\alpha}+\frac{1}{(\lambda-1)}3\alpha^2-\frac{1}{(\lambda-1)^3}\omega^4\right)(\ddot{\alpha}-6\omega^2\alpha)}{(\ddot{\alpha}-6\omega^2\alpha)^2+(4\omega\dot{\alpha}+3\alpha^2-\omega^4)^2}\right|_{\lambda=\infty}$$

$$= \frac{(-\ddot{\alpha})(4\omega\dot{\alpha}+3\alpha^2-\omega^4)}{(\ddot{\alpha}-6\omega^2\alpha)^2+(4\omega\dot{\alpha}+3\alpha^2-\omega^4)^2} \qquad \text{Eq. 3.77}$$

$$y_{I4} = \left.\frac{\left(-\ddot{\alpha}+\frac{1}{(\lambda-1)^2}6\omega^2\alpha\right)(\ddot{\alpha}-6\omega^2\alpha)+\left(\frac{1}{(\lambda-1)}4\omega\dot{\alpha}+\frac{1}{(\lambda-1)}3\alpha^2-\frac{1}{(\lambda-1)^3}\omega^4\right)(4\omega\dot{\alpha}+3\alpha^2-\omega^4)}{(\ddot{\alpha}-6\omega^2\alpha)^2+(4\omega\dot{\alpha}+3\alpha^2-\omega^4)^2}\right|_{\lambda=\infty}$$

$$= \frac{(-\ddot{\alpha})(\ddot{\alpha}-6\omega^2\alpha)}{(\ddot{\alpha}-6\omega^2\alpha)^2+(4\omega\dot{\alpha}+3\alpha^2-\omega^4)^2}$$

Eq. 3.77 is identical to Eq. 3.22 which is the equation of the locus of the fourth order IC for a circle rolling on a straight line.

3.3.5.1 Special Case Scenarios for Fourth Order Motion of A Circle Rolling on another Circle

The following section discusses various scenarios for instantaneous kinematics for the fourth order motion of a circle on another circle. The scenarios are summarized in Table 3.5 following the discussion.

Case 1: $\ddot{\alpha} \neq 0, \alpha = \omega = 0$

When the angular velocity, ω, and the angular acceleration, α, of the body are zero while the derivative of angular jerk, ä, has a nonzero value, regardless of the state of angular jerk, α̇, Eq. 3.76 becomes:

$$x_{I4} = 0$$
$$y_{I4} = -\mathrm{r} \qquad \text{Eq. 3.78}$$

This is the location of the point of contact, O. Also with these values of ω, α, α̇, and α̈, angle β_4 is computed as 90^o. Thus the location of the fourth order IC in this case is the point of contact, O, of the circle with the line regardless of the value of α̈. Every point on the body has fourth order motion state, m_4, such that its magnitude is proportional to and the direction is orthogonal to the radius, ρ_4. This is shown in Fig. 3.30.

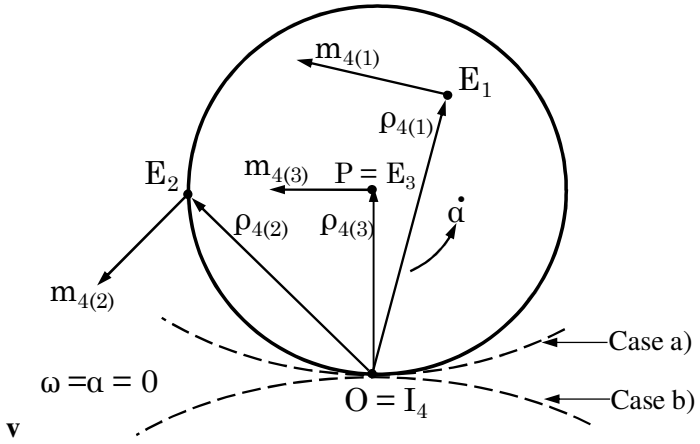

Fig. 3.30: The Fourth Order IC Location when $\ddot{\alpha} \neq 0, \dot{\alpha} = \alpha = \omega = 0$ for a Circle Rolling on another Circle: Case a) Circle 1 Rolls on the Inside of Circle 2, and Case b) Circle 1 Rolls on the Outside of Circle 2

Case 2: $\ddot{\alpha} = \dot{\alpha} = \alpha = 0, \omega \neq 0$

When the circle is rolling with a constant angular velocity at a particular instant in time, the derivative of the angular jerk, $\ddot{\alpha}$, the angular jerk, $\dot{\alpha}$, and the angular acceleration, α, of the circle are all zero. The fourth order IC is located at:

$$x_{I4} = 0$$
$$y_{I4} = \frac{1}{(\lambda - 1)^3} \qquad \text{Eq. 3.79}$$

The constant angle, β_4 (Eq. 2.41) is computed as:

$$\beta_4 = 0°$$

Note that for a positive value of λ (case a), the fourth order IC, I_4, is located above the center of circle, point P, as shown in Fig. 3.31. While for a negative value of λ (case b), I_4 is located below the center of circle, point P. Fig. 3.31 shows only case when λ is positive.

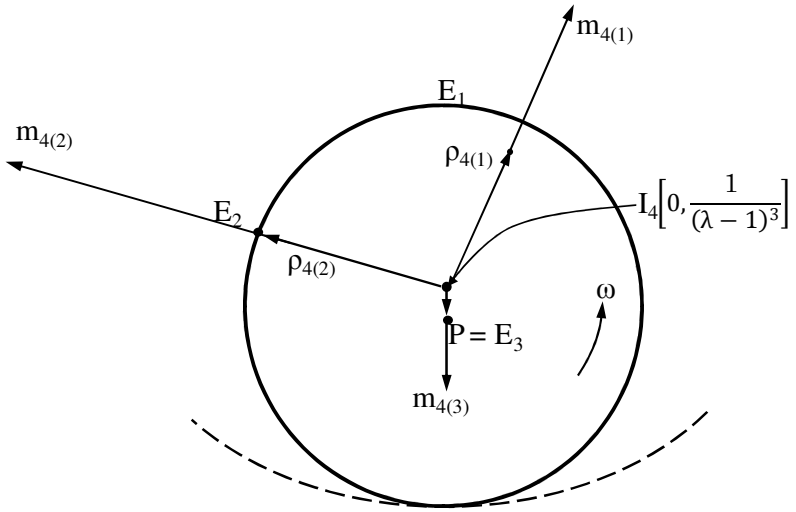

Fig. 3.31: The Fourth Order IC Location when $\omega \neq 0, \ddot{\alpha} = \dot{\alpha} = \alpha = 0$ for A Circle Rolling on another Circle: Shown Here is the Case when Circle 1 Rolls on the Inside of Circle 2

Case 3: $\ddot{\alpha} = \alpha = 0, \omega \neq 0; \dot{\alpha} \neq 0$

When the derivative of the angular jerk, $\ddot{\alpha}$, and the angular acceleration, α, of the circle are zero and the angular velocity, ω, and the angular jerk, $\dot{\alpha}$, of the circle are nonzero at a particular instant in time, the fourth order IC is located at:

$$x_{I4} = 0$$

$$y_{I4} = \frac{\left(\frac{1}{(\lambda-1)} 4\omega\dot{\alpha} - \frac{1}{(\lambda-1)^3}\omega^4\right)(4\omega\dot{\alpha} - \omega^4)}{(4\omega\dot{\alpha} - \omega^4)^2} \qquad \text{Eq. 3.80}$$

The constant angle, β_4, is either 0 or 180° depending on whether the term $(4\omega\dot{\alpha} - \omega^4)$ is positive or negative at the particular instant. This is shown in Fig. 3.32 which shows a particular instant for a circle rolling inside another circle (case a) when β_4 is 180°.

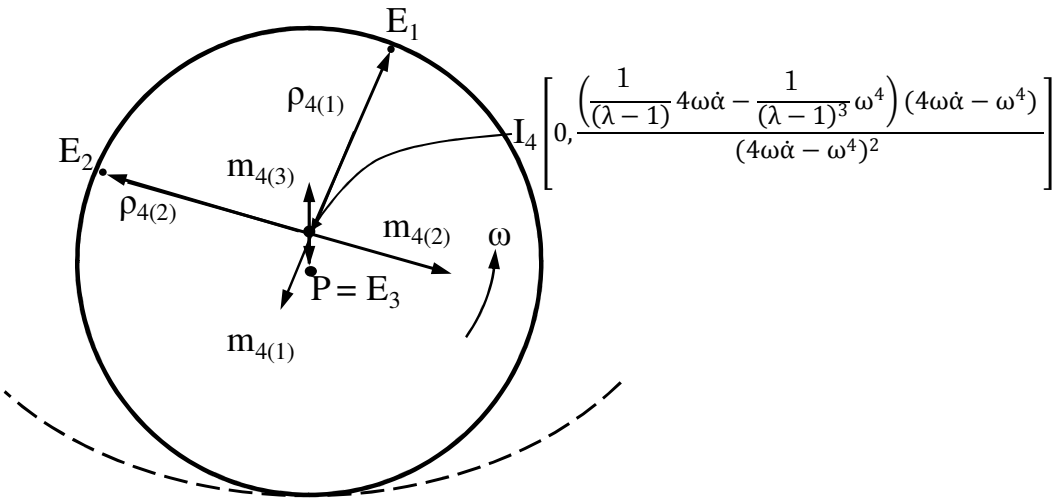

Fig. 3.32: The Fourth Order IC Location when $\omega \neq 0, \dot{\alpha} \neq 0, \ddot{\alpha} = \alpha = 0$ for A Circle Rolling on another Circle: Shown Here is the Case when Circle 1 Rolls on the Inside of Circle 2

Case 4: $\ddot{\alpha} = \dot{\alpha} = \omega = 0, \alpha \neq 0$

When the derivative of the angular jerk, $\ddot{\alpha}$, the angular jerk, $\dot{\alpha}$, and the angular velocity, ω, of the circle are zero and the angular acceleration, α, of the circle is nonzero at a particular instant in time, the fourth order IC is located at:

$$x_{I4} = 0$$
$$y_{I4} = \frac{\mathrm{r}}{(\lambda - 1)} \qquad \text{Eq. 3.81}$$

The constant angle, β_4 is computed as:

$$\beta_4 = 180°$$

Note that for a positive value of λ (case a), the fourth order IC, I_4, is located above the center of circle, point P, as shown in Fig. 3.33. While for a negative value of λ (case b), I_4 is located below the center of circle, point P. Fig. 3.33 shows only case when λ is positive.

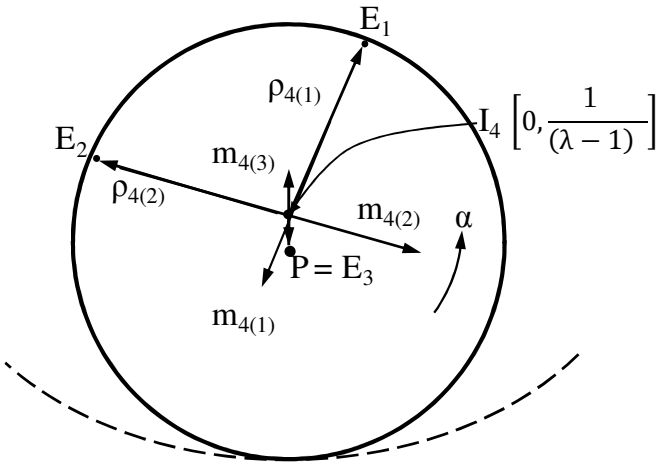

Fig. 3.33: The Fourth Order IC Location when $\omega \neq 0, \dot{\alpha} \neq 0, \ddot{\alpha} = \alpha = 0$ for a Circle Rolling on another Circle: Shown Here is the Case when Circle 1 Rolls on the Inside of Circle 2

Case 5: $\boldsymbol{\ddot{\alpha} \neq 0; \omega \neq 0, \alpha = \dot{\alpha} = 0}$

When the angular acceleration, α, and the angular jerk, $\dot{\alpha}$, of the circle are zero while the derivative of the angular jerk, $\ddot{\alpha}$, and the angular velocity, ω, of the circle are nonzero at a particular instant in time, the fourth order IC is located at:

$$x_{I4} = \frac{(\ddot{\alpha}\omega^4) + \left(\frac{1}{(\lambda-1)^3}\right)(\ddot{\alpha}\omega^4)}{(\ddot{\alpha})^2 + (-\omega^4)^2}$$
$$y_{I4} = \frac{(-\ddot{\alpha})(\ddot{\alpha}) + \left(\frac{1}{(\lambda-1)^3}\omega^4\right)(\omega^4)}{(\ddot{\alpha})^2 + (-\omega^4)^2} \qquad \text{Eq. 3.82}$$

Consider the X component:

$$x_{I4} = \frac{(\ddot{\alpha}\omega^4) + \left(\frac{1}{(\lambda-1)^3}\right)(\ddot{\alpha}\omega^4)}{(\ddot{\alpha})^2 + (\omega^4)^2} = \frac{\left(\frac{(1+(\lambda-1)^3)}{(\lambda-1)^3}\right)(\ddot{\alpha}\omega^4)}{(\ddot{\alpha})^2 + (\omega^4)^2}$$

Simplifying using the definition of angle β_4 we get:

$$x_{I4} = \frac{\left(\frac{(1+(\lambda-1)^3)}{(\lambda-1)^3}\right)tan\beta_4}{1 + tan^2\,\beta_4} = \frac{\left(\frac{(1+(\lambda-1)^3)}{(\lambda-1)^3}\right)tan\beta_4}{sec^2\,\beta_4}$$
$$= \left(\frac{(1+(\lambda-1)^3)}{(\lambda-1)^3}\right)sin\,\beta_4 cos\,\beta_4 = \left(\frac{(1+(\lambda-1)^3)}{2(\lambda-1)^3}\right)\sin 2\beta_4$$

Consider the Y component:

$$y_{I4} = \frac{(-\ddot{\alpha})(\ddot{\alpha}) + \left(\frac{1}{(\lambda-1)^3}\omega^4\right)(\omega^4)}{(\ddot{\alpha})^2 + (\omega^4)^2} = \frac{-((\ddot{\alpha})^2 + (\omega^4)^2) + \left(\frac{(1+(\lambda-1)^3}{(\lambda-1)^3}\right)(\omega^4)^2}{(\ddot{\alpha})^2 + (\omega^4)^2}$$

$$= -1 + \frac{\left(\frac{(1+(\lambda-1)^3}{(\lambda-1)^3}\right)(\omega^4)^2}{(\ddot{\alpha})^2 + (\omega^4)^2}$$

Using the definition of angle $\beta_4 = tan^{-1}\left(\frac{\ddot{\alpha}}{\omega^4}\right)$, we get:

$$y_{I3} = -1 + \left(\frac{(1+(\lambda-1)^3)}{(\lambda-1)^3}\right)\frac{tan^2\,\beta_4}{(1+tan^2\,\beta_4)} = -\frac{1}{2(\lambda-1)^3} + \frac{(1+(\lambda-1)^3)}{2(\lambda-1)^3}cos2\beta_4$$

Thus the fourth order IC location parametric equation is:

$$x_{I4} = 0 + \left(\frac{(1+(\lambda-1)^3)}{2(\lambda-1)^3}\right)\sin 2\beta_4$$

$$y_{I4} = -\frac{((\lambda-1)^3-1)}{2(\lambda-1)^3} + \frac{(1+(\lambda-1)^3)}{2(\lambda-1)^3}cos2\beta_4 \qquad \text{Eq. 3.83}$$

This is a parametric equation of a circle with the radius of $\frac{(1+(\lambda-1)^3)}{2(\lambda-1)^3}$ and center at $\left[0, -\frac{((\lambda-1)^3-1)}{2(\lambda-1)^3}\right]$. Fig. 3.34 shows a case when λ = 3.

Case 6: $\ddot{\boldsymbol{\alpha}} \neq \mathbf{0}; \boldsymbol{\alpha} \neq \mathbf{0}, \dot{\boldsymbol{\alpha}} = \boldsymbol{\omega} = \mathbf{0}$

When the angular velocity, ω, and the angular jerk, $\dot{\alpha}$, of the circle are zero while the angular acceleration, α, and the derivative of the angular jerk, $\ddot{\alpha}$, of the circle are nonzero

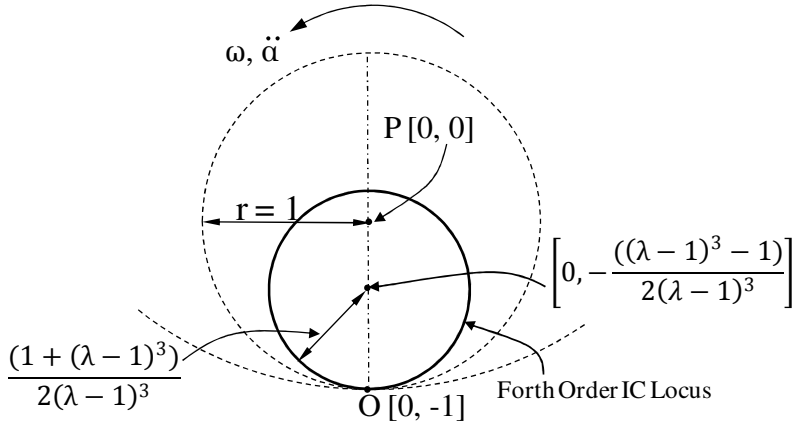

Fig. 3.34: The Fourth Order IC Location when $\boldsymbol{\omega} \neq \mathbf{0}, \ddot{\boldsymbol{\alpha}} \neq \mathbf{0}, \dot{\boldsymbol{\alpha}} = \boldsymbol{\alpha} = \mathbf{0}$ for a Circle Rolling on another Circle: Shown Here is the Case when Circle 1 Rolls on the Inside of Circle 2

at a particular instant in time, the fourth order IC is located at:

$$x_{I4} = \frac{-(3\alpha^2\ddot{\alpha}) - \left(\frac{1}{(\lambda-1)}\right)(3\alpha^2\ddot{\alpha})}{(\ddot{\alpha})^2 + (3\alpha^2)^2}$$
$$y_{I4} = \frac{(-\ddot{\alpha})(\ddot{\alpha}) + \left(\frac{1}{(\lambda-1)}3\alpha^2\right)(3\alpha^2)}{(\ddot{\alpha})^2 + (3\alpha^2)^2} \qquad \text{Eq. 3.84}$$

Consider the X component:

$$x_{I4} = \frac{-(3\alpha^2\ddot{\alpha}) - \left(\frac{1}{(\lambda-1)}\right)(3\alpha^2\ddot{\alpha})}{(\ddot{\alpha})^2 + (3\alpha^2)^2} = \frac{-\frac{\lambda}{(\lambda-1)}(3\alpha^2\ddot{\alpha})}{(\ddot{\alpha})^2 + (3\alpha^2)^2}$$

Simplifying using the definition of angle $\beta_4 = tan^{-1}\left(\frac{\ddot{\alpha}}{3\alpha^2}\right)$ we get:

$$x_{I4} = \frac{-\frac{\lambda}{(\lambda-1)}tan\beta_4}{1 + tan^2\beta_4} = \frac{-\frac{\lambda}{(\lambda-1)}tan\beta_4}{sec^2\beta_4} = -\frac{\lambda}{(\lambda-1)}sin\,\beta_4 cos\,\beta_4$$
$$= -\frac{\lambda}{(\lambda-1)}\sin 2\beta_4$$

Consider the Y component:

$$y_{I4} = \frac{(-\ddot{\alpha})(\ddot{\alpha}) + \left(\frac{1}{(\lambda-1)}3\alpha^2\right)(3\alpha^2)}{(\ddot{\alpha})^2 + (3\alpha^2)^2} = \frac{-((\ddot{\alpha})^2 + (\omega^4)^2) + \frac{\lambda}{(\lambda-1)}(\omega^4)^2}{(\ddot{\alpha})^2 + (\omega^4)^2}$$
$$= -1 + \frac{\frac{\lambda}{(\lambda-1)}(\omega^4)^2}{(\ddot{\alpha})^2 + (\omega^4)^2}$$

Using the definition of angle β_4, we get:

$$y_{I3} = -1 + \frac{\lambda}{(\lambda-1)}\frac{tan^2\beta_4}{(1 + tan^2\beta_4)} = -\frac{(2-\lambda)}{2(\lambda-1)} + \frac{\lambda}{2(\lambda-1)}cos2\beta_4$$

Thus the fourth order IC location parametric equation is:

$$x_{I4} = 0 - \frac{\lambda}{2(\lambda-1)}\sin 2\beta_4$$
$$y_{I4} = -\frac{(2-\lambda)}{2(\lambda-1)} + \frac{\lambda}{2(\lambda-1)}cos2\beta_4 \qquad \text{Eq. 3.85}$$

This is a parametric equation of a circle with the radius of $\frac{\lambda}{2(\lambda-1)}$ and center at $\left[0, -\frac{(2-\lambda)}{2(\lambda-1)}\right]$. Fig. 3.35 shows the locus for $\lambda = 3$.

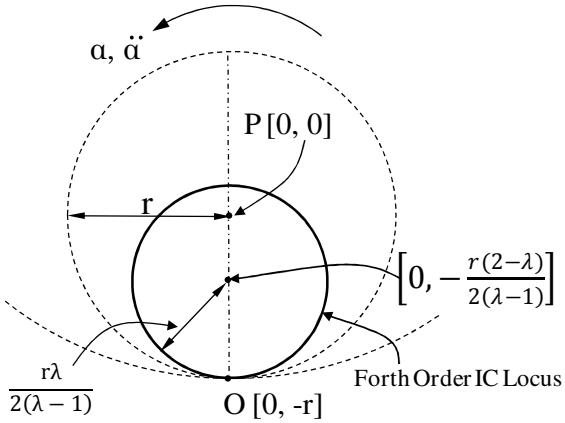

Fig. 3.35: The Fourth Order IC Location when $\alpha \neq 0, \ddot{\alpha} \neq 0, \dot{\alpha} = \omega = 0$ for a Circle Rolling on another Circle: Shown Here is the Case when Circle 1 Rolls on the Inside of Circle 2

3.3.5.2 Summary of Fourth Order Motion of A Circle Rolling on another Circle

Table 3.5 summarizes all special case scenarios for fourth order motion of a circle rolling on a line. These scenarios identify the location of fourth order IC for such special cases. Also the resulting value of constant angle β_4 is also shown for each scenario.

Table 3.5: Summary of the Fourth Order Motion Properties for Special Case Scenarios for a Circle Rolling inside another Circle

$\ddot{\alpha}$	$\dot{\alpha}$	α	ω	*IC Location*	$tan(\beta_4)$
0	No Effect	0	0	∞	90^o
0	0	0	$\neq 0$	$\left[0, \frac{r}{(\lambda-1)^3}\right]$	180^o
0	No Effect	$\neq 0$	0	$\left[0, \frac{r}{(\lambda-1)}\right]$	0^o
0	No Effect	$\neq 0$	$\neq 0$	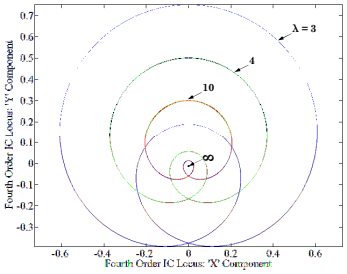	$\tan^{-1}\left(\frac{6\omega^2\alpha}{4\omega\dot{\alpha}+3\alpha^2-\omega^4}\right)$
0	$\neq 0$	0	$\neq 0$	$\left[0, \frac{\left(\frac{r}{(\lambda-1)}4\omega\dot{\alpha} - \frac{r}{(\lambda-1)^3}\omega^4\right)(4\omega\dot{\alpha}-\omega^4)}{(4\omega\dot{\alpha}-\omega^4)^2}\right]$	0^o or 180^o
$\neq 0$	No Effect	0	0	*O [0, -r]*	90^o
$\neq 0$	0	0	$\neq 0$	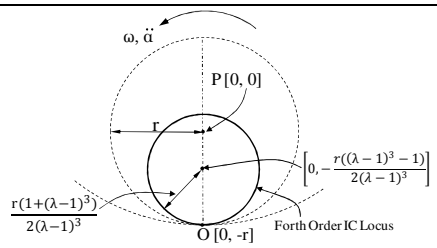	$\dot{\alpha} \neq 0$: $\tan^{-1}\left(-\frac{\ddot{\alpha}}{4\omega\dot{\alpha}-\omega^4}\right)$ $\dot{\alpha} = 0$: $\tan^{-1}\left(\frac{\ddot{\alpha}}{\omega^4}\right)$
$\neq 0$	No Effect	$\neq 0$	0	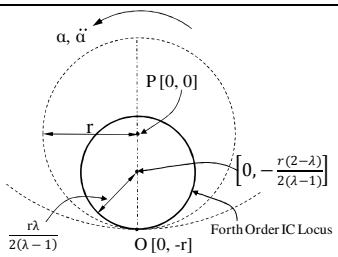	$\tan^{-1}\left(-\frac{\ddot{\alpha}}{3\alpha^2}\right)$
$\neq 0$	$\neq 0$	$\neq 0$	$\neq 0$	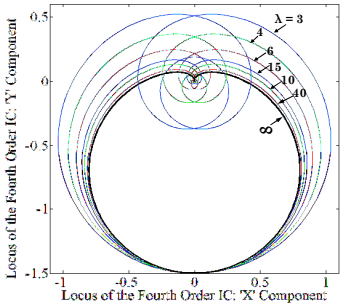	$\tan^{-1}\left(\frac{-(\ddot{\alpha}-6\omega^2\alpha)}{4\omega\dot{\alpha}+3\alpha^2-\omega^4}\right)$

Another interesting special motion involving a rolling circle occurs when the circle rolls on another larger circle. Due to the pure rolling, this is also a 1-DOF motion. Following section discusses the motion of the circle starting with the first order motion up to the fourth order motion.

3.4 Case 3: Circle Rolling with Slipping on a Straight Line

In Sec. 3.2, we studied a special case where a circle rolls on a straight line without slipping. The section discussed the motion of the circle up to the fourth order with an emphasis on corresponding ICs. A fixed, non-orientable wheel (such as a wheel of a skid-steered platform) rolling on a smooth and flat ground is an obvious example of the special case motion. Though the study of circle rolling without slipping provides the reader with some valuable information, we know that wheels do slip/slide. Thus study of the scenario where a circle (representing a wheel/cylinder/disk) rolls on a straight line (representing a surface/ground/plane) with some amount of slippage is important. The following section discusses this case in some detail. This is a planar case study, hence the slipping/sliding in the rolling direction only is considered and any out plane slipping (skidding) is neglected for the scope of this chapter. Following section discusses the typical types of slipping that a wheel encounters from kinematic point of view.

3.4.1 WHEEL SLIPPING AND SLIDING

Slipping, skidding and sliding are all different terms each with special meanings in the literature for wheel modeling (Campion et al., 1996; Wong, 2001; Jazar, 2008). Here we describe the meaning and scope of each term.

3.4.1.1 Definition of Slipping

Slipping occurs during a sudden acceleration of an automobile on a slippery surface. This results in a higher rotational velocity, ω, of a wheel without a commensurate increase in the linear velocity of the wheel in rolling direction. Fig. 3.36 shows the slipping of a wheel graphically. The wheel of radius r rolls with an angular velocity of ω on the surface and has a linear velocity V_P.

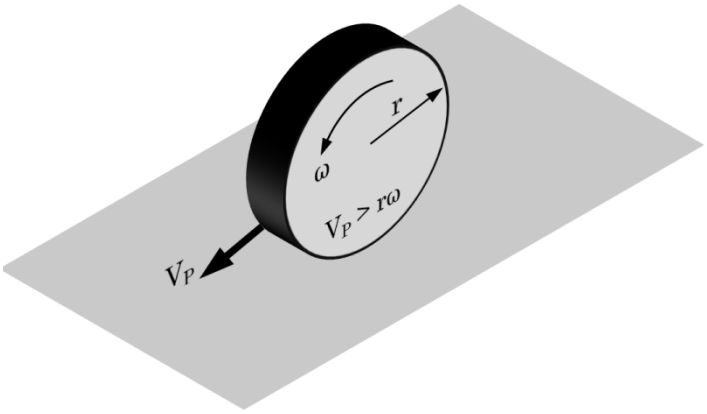

Fig. 3.36: A Schematic Diagram Depicting Slipping of a Wheel

Thus the constraint condition for slipping is:

$$|V_P| = \left|\dot{X}_P\right| < |r\omega| \qquad \text{Eq. 3.86}$$

3.4.1.2 Definition of Skidding

Wang and Low (2006) define skidding as the phenomenon that occurs during cornering of a wheel. Due to lateral inertial forces, the wheel tends to move out of plane as shown in Fig. 3.37.

Kinematically, skidding is represented as follows:

$$\dot{Z}_P \neq 0 \qquad \text{Eq. 3.87}$$

As we are studying the motion of the wheel in the plane containing the rolling, we do not study the properties of skidding in this section

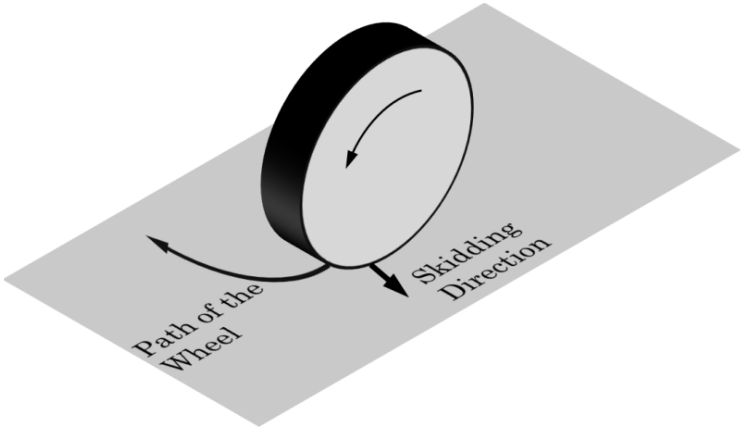

Fig. 3.37: The Schematic Representation of Wheel Skidding

3.4.1.3 Definition of Sliding

Sliding here is defined as the phenomenon that occurs during a sudden deceleration (braking) of an automobile on a slippery surface. This results in a reduced rotational velocity of a wheel without commensurate reduction in the linear velocity in the rolling direction.

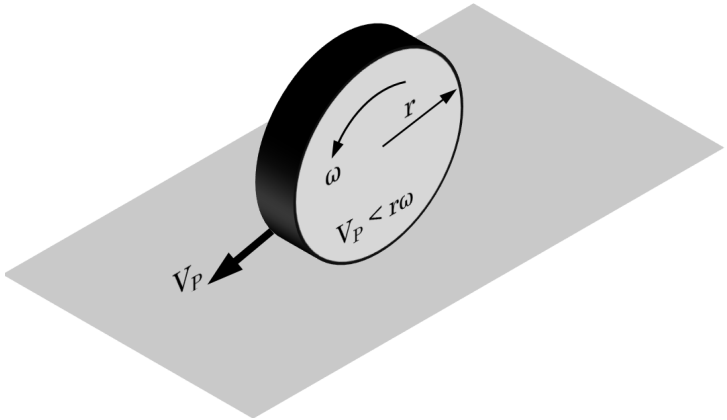

Fig. 3.38: The Schematic Representation of Wheel Sliding

Thus

$$|V_P| = |\dot{X}_P| > |r\omega| \qquad \text{Eq. 3.88}$$

3.4.2 THE SLIPPAGE FACTOR

Due to the longitudinal slipping/sliding, the motion becomes a 2-DOF motion. Let us define the slippage factor, ε, such that:

$$V_P = -(1-\varepsilon)r\omega$$
$$\varepsilon = 1 - \frac{V_P}{r\omega} \qquad \text{Eq. 3.89}$$

Wong (2001) defined this term as longitudinal slip as follows:

$$\varepsilon = \left(1 - \frac{V_P}{r\omega}\right) \times 100\% \qquad \text{Eq. 3.90}$$

The value of slippage, ε, can be both positive and negative $\{\varepsilon \in [-\infty, 1]\}$. The positive value of slippage means that the wheel is slipping ($\varepsilon > 0$). Thus the linear velocity of the wheel is less than the case with pure rolling as can be verified from Eq. 3.89. When the wheel is spinning in place, the slippage factor is 1 as the wheel rolling results in no linear velocity. On the contrary, the negative value of slippage means that the wheel is sliding ($\varepsilon < 0$). The linear velocity of the wheel in this case is more than the case with pure rolling as the wheel continues to slide even after reduction in rolling (angular) velocity. When the wheel is locked due to braking and still continues to slide, the slippage factor goes to negative infinity linear velocity is finite even with zero angular velocity. Thus the range for the value of the slippage factor is:

$$slipping: \varepsilon \in (0, 1]$$
$$sliding: \varepsilon \in (0, -\infty] \qquad \text{Eq. 3.91}$$

With this definition we can analyze the motion of the wheel rolling on a smooth and flat ground. As we consider only the planar motion, we will use a circle to represent the wheel

and a line to represent the surface in the formulation. In the next section we discuss the first order motion of the system. The formulation will be normalized by using unity radius for the circle as the radius of the circle serves merely as a scaling factor.

3.4.3 First Order Motion of Circle Rolling with Slipping on a Straight Line

For circle rolling with slipping/sliding on a straight line, the constraint equation is given by following expression:

$$\dot{X}_P = -(1-\varepsilon)r\omega$$
$$\dot{Y}_P = 0 \qquad \text{Eq. 3.92}$$

Using unity radius, i.e., r = 1, we get:

$$\dot{X}_P = -(1-\varepsilon)\omega$$
$$\dot{Y}_P = 0 \qquad \text{Eq. 3.93}$$

Using the equation for the first order IC (Eq. 2.5) and the constraint equation for the circle given by Eq. 3.95, the location of velocity IC can then be computed as:

$$x_{I1} = 0$$
$$y_{I1} = -(1-\varepsilon) \qquad \text{Eq. 3.94}$$

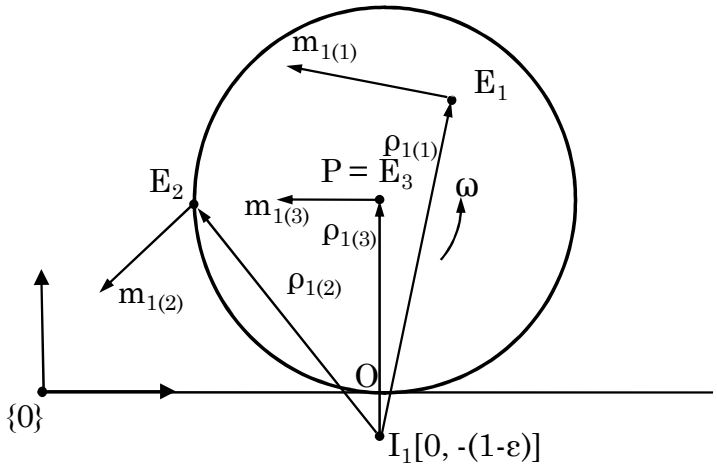

Fig. 3.39: A Circle Rolling with Slipping on a Straight Line: First Order IC Location for a General Motion of the Circle

Fig. 3.39 illustrates the velocity IC location and the resulting velocities of various points in the circle. Note that based on the value of the ε, the location of the velocity IC could be above or below point O. In Fig. 3.39, the value of slippage factor is negative there by pushing the velocity IC further away from the center of the circle. This can be verified by the fact that in general, larger the linear velocity component for the instantaneous kinematics for a particular angular velocity component, further away the instant center is from the point of interest, P. on the contrary, when the slippage factor is positive the velocity IC shifts towards the center of the circle.

3.4.4 SECOND ORDER MOTION OF CIRCLE ROLLING WITH SLIPPING ON A STRAIGHT LINE

Differentiating Eq. 3.92, we get the acceleration for the center of the circle, P, as:

$$\ddot{X}_P = -(1-\varepsilon)r\alpha$$
$$\ddot{Y}_P = 0 \qquad \text{Eq. 3.95}$$

Using r = 1, we get:

$$\ddot{X}_P = -(1-\varepsilon)\alpha$$
$$\ddot{Y}_P = 0 \qquad \text{Eq. 3.96}$$

Using the constraint condition given by Eq. **3.96**, the location of the second order IC (Eq. 2.18) can be computed as:

$$x_{I2} = \frac{-(1-\varepsilon)\alpha\omega^2}{\alpha^2+\omega^4}$$
$$y_{I2} = \frac{-(1-\varepsilon)\alpha^2}{\alpha^2+\omega^4} \qquad \text{Eq. 3.97}$$

Using the second order orientation angle, β_2 (Eq. 2.20), Eq. 3.97 can be rearranged as:

$$x_{I2} = \frac{(1-\varepsilon)tan\beta_2}{1+tan^2\,\beta_2} = \frac{(1-\varepsilon)tan\beta_2}{sec^2\,\beta_2} = (1-\varepsilon)sin\,\beta_2 cos\,\beta_2$$
$$y_{I2} = \frac{-(1-\varepsilon)tan^2\beta_2}{1+tan^2\beta_2} = \frac{-(1-\varepsilon)tan^2\beta_2}{sec^2\beta_2} = -(1-\varepsilon)sin^2\beta_2$$

After further simplification, we can express the location of acceleration IC in the following form:

$$x_{I2} = 0 + \frac{(1+\varepsilon)}{2} sin2\beta_2$$
$$y_{I2} = -\frac{(1+\varepsilon)}{2} + \frac{(1+\varepsilon)}{2} cos2\beta_2 \qquad \text{Eq. 3.98}$$

Eq. 3.98 is a parametric equation of a circle with center at $\left[0, -\frac{(1-\varepsilon)}{2}\right]$ and radius equal to $\frac{(1-\varepsilon)}{2}$ which shows that the locus of the acceleration IC is a circle. The instantaneous location of acceleration IC depends on value of the angle, β_2, which in turn depends on the values of the angular acceleration α and angular velocity, ω, of the circle.

Thus due to the slippage, the second order IC locus (circle) diameter reduces (increases for negative value) by the slippage factor.

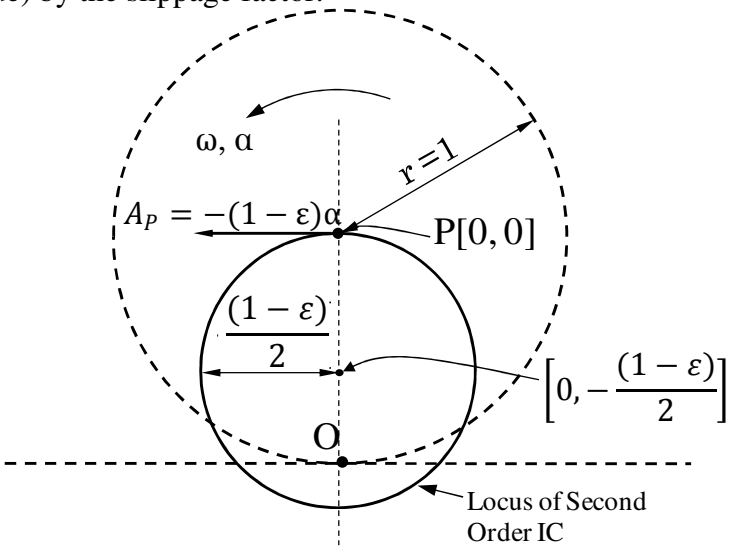

Fig. 3.40: Circle Rolling on a Straight Line with Slipping or Skidding: The General Locus of the Second Order IC

3.4.4.1 Special Case Scenarios for the Second Order Motion of Circle Rolling with Slipping on a Straight Line

With regards to the second order motion of the rigid body, there are various interesting special cases that we can discuss.

Case 1: $\alpha = 0$

When the circle rolls with a constant angular velocity, ω = constant, and no angular acceleration, $\alpha = 0$, the acceleration of point P is zero (as per Eq. 3.96) making it the acceleration IC as shown in Fig. 3.41. We can also verify this using the Eq. 3.98. For zero angular acceleration, $\alpha = 0$, and constant, non-zero angular velocity, ω = constant, β_2 is 180^{o} and thus the Eq. 3.98 results in the acceleration IC location at *[0, 0]*, the location of point P.

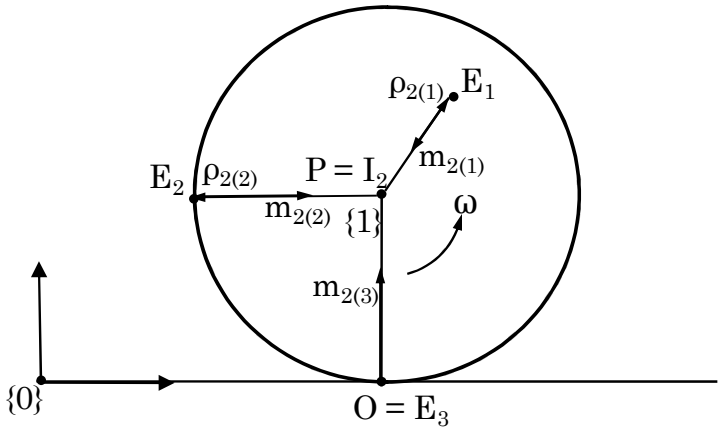

Fig. 3.41: Location of the Acceleration IC for a Circle Rolling on a Straight Line with Slipping when $\alpha = 0$

Case 2: $\omega = 0$

On the other hand, when the circle starts to move from rest, the circle has finite angular acceleration but zero angular velocity. The instant center for acceleration in this case is at *[0, - (1-ε)]* as shown in Fig. 3.42. Also the angle of the vector orientation, β_2, is -90^{o}.

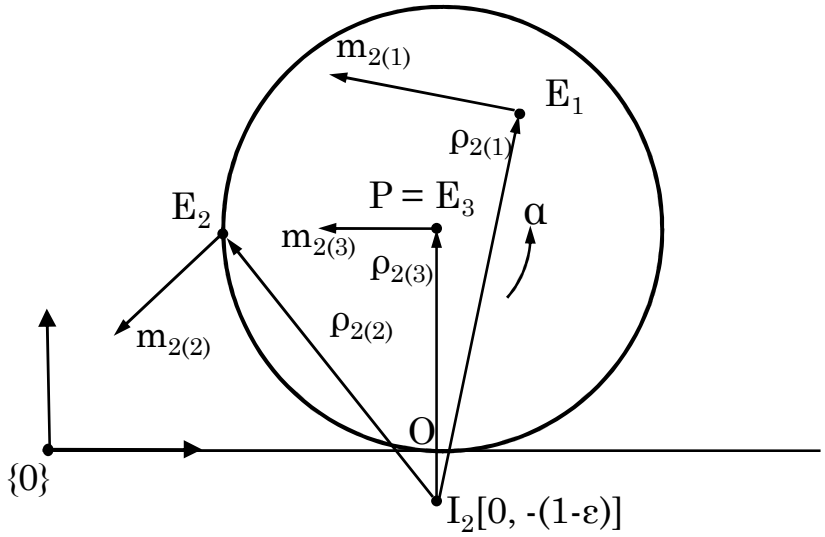

Fig. 3.42: Location of the Acceleration IC for a Circle Rolling on a Straight Line with Slipping when $\omega = 0$

3.4.4.2 Simulation Plot

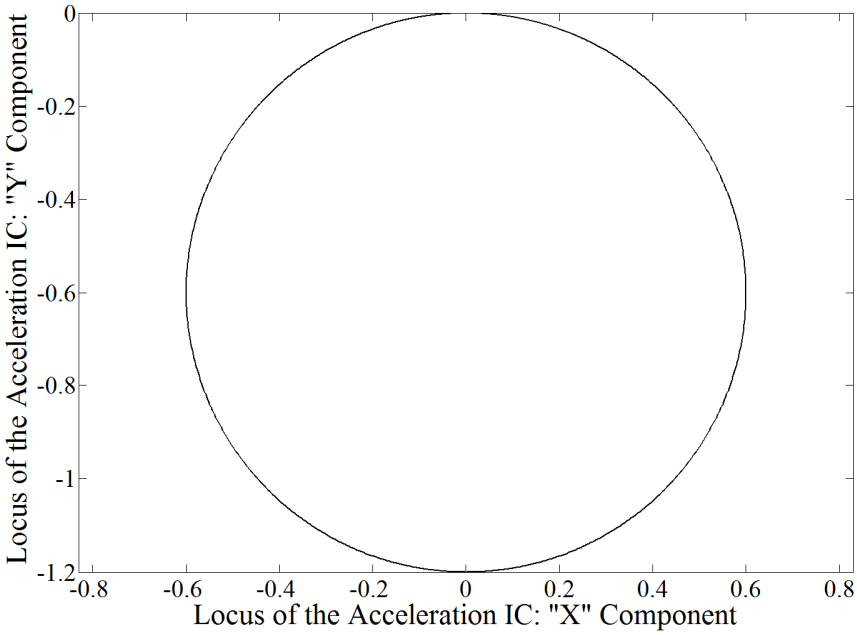

Fig. 3.43: Simulation Plot showing the General Locus of the Acceleration IC for a Circle Rolling on a Straight Line with Slipping/Skidding

A simulation plot was run to verify these results. In the simulation a circle with radius 1 foot is rolling with a slippage of -0.2 (skidding). During the time based simulation, the instantaneous acceleration was varied from -2.5 rad/s^2 to 2.5 rad/s^2 with corresponding

value of angular velocity for each time step. The resulting locus for the second order IC is plotted and is shown in Fig. 3.43. Notice that with the slippage factor of -0.2, the diameter of the acceleration IC locus is 1.2 foot.

3.4.5 THIRD ORDER MOTION OF CIRCLE ROLLING WITH SLIPPING ON A STRAIGHT LINE

Differentiating Eq. 3.95, we get the jerk of the center point, P, of the circle as:

$$X_P^{(3)} = -(1-\varepsilon)\mathrm{r}\dddot{\alpha}$$
$$Y_P^{(3)} = 0 \qquad \text{Eq. 3.99}$$

Using r = 1, we get:

$$X_P^{(3)} = -(1-\varepsilon)\dddot{\alpha}$$
$$Y_P^{(3)} = 0 \qquad \text{Eq. 3.100}$$

Using the constraint condition provided by Eq. 3.100, the third order (jerk) IC (Eq. 2.40) for a general motion of the circle can be computed as:

$$x_{I3} = \frac{-(1-\varepsilon)\dddot{\alpha}(3\omega\alpha)}{(\dddot{\alpha}-\omega^3)^2+(3\omega\alpha)^2}$$
$$y_{I3} = \frac{-(1-\varepsilon)\,\dddot{\alpha}(\dddot{\alpha}-\omega^3)}{(\dddot{\alpha}-\omega^3)^2+(3\omega\alpha)^2} \qquad \text{Eq. 3.101}$$

Eq. 3.101 is a parametric equation for the locus of the third order IC for general third order motion.

3.4.5.1 Simulation Plot for the Third Order Motion of Circle Rolling with Slipping on a Straight Line

The locus of the third order IC for a circle of 1 foot rolling on a straight line with slipping (ε = -0.2) is plotted using a simulation plot shown in Fig. 3.44. It is found that the locus of the third order IC is dependent only on the geometric parameter, r, and is independent of the kinematic state of the body. The particular location of the third order IC at any instant, however, is dependent on the instantaneous values of the kinematic parameters of

the rigid body as the case with second order IC is.

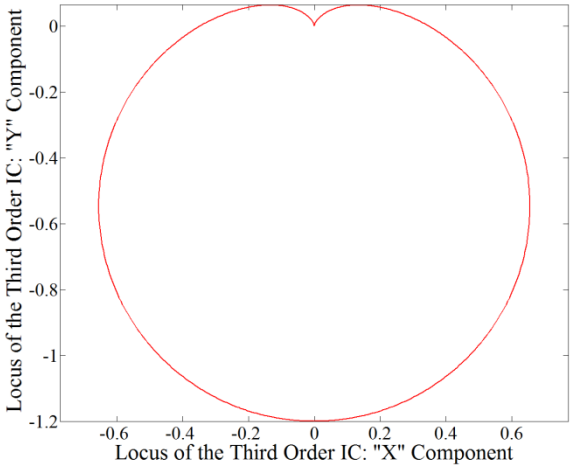

Fig. 3.44: Simulation Plot Showing the Locus of the Third Order IC for a Circle (r = 1ft) Rolling on a Straight Line with Skidding (ε = -0.2)

3.4.5.2 Special Case Scenarios for Third Order Motion of Circle Rolling with Slipping on a Straight Line

The instantaneous state of kinematic parameters give rise to many interesting special case scenarios much as when the circle is rolling on the straight line without slipping/skidding. The analysis of these special cases is on the same line as Case 1 (Sec. 3.2). Table 3.6 summarizes the special cases with an emphasis on the third order IC, I_3, location and value of the third order orientation angle, β_3 for each case.

Table 3.6: Summary of the Third Order Motion Properties in Special Case Scenarios for a Circle Rolling on a Straight Line with Slipping/Skidding

$\dot{\alpha}$	α	ω	IC Location	β_3
0	0	$\neq 0$	*P [0, 0]*	-90^o
0	$\neq 0$	$\neq 0$	*P [0, 0]*	$\tan^{-1}\left(-\frac{\omega^3}{3\omega\alpha}\right)$
0	0	0	∞	90^o
0	$\neq 0$	0	∞	90^o
$\neq 0$	0	0	*O [0, -(1-ε)]*	90^o
$\neq 0$	$\neq 0$	0	*O [0, -(1-ε)]*	90^o
$\neq 0$	0	$\neq 0$	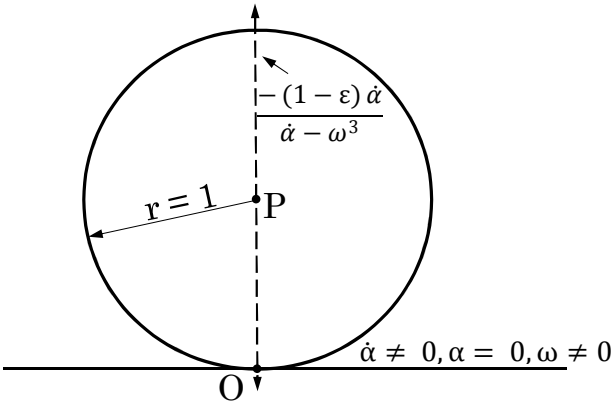	90^o
$\neq 0$	$\neq 0$	$\neq 0$	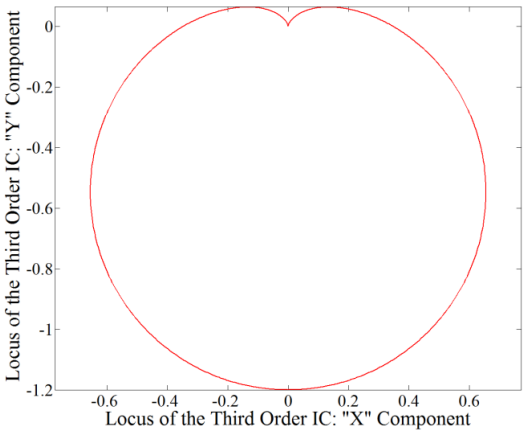	$\tan^{-1}\left(-\frac{\dot{\alpha}-\omega^3}{3\omega\alpha}\right)$

3.4.6 FOURTH ORDER MOTION OF CIRCLE ROLLING WITH SLIPPING ON A STRAIGHT LINE

Differentiating Eq. 3.99, we get the derivative of the jerk of the center point, P, of the circle as:

$$X_P^{(4)} = -(1-\varepsilon)\mathrm{r}\dddot{\alpha}$$
$$Y_P^{(4)} = 0 \qquad \text{Eq. 3.102}$$

Using r = 1, we get:

$$X_P^{(4)} = -(1-\varepsilon)\dddot{\alpha}$$
$$Y_P^{(4)} = 0 \qquad \text{Eq. 3.103}$$

Using the constraint condition provided by Eq. 3.103, the fourth order (jerk) IC (Eq. 2.39) for a general motion of the circle can be computed as:

$$x_{I4} = \frac{-(1-\varepsilon)\,\dddot{\alpha}(4\omega\dot{\alpha} + 3\alpha^2 - \omega^4)}{(\dddot{\alpha} - 6\omega^2\alpha)^2 + (4\omega\dot{\alpha} + 3\alpha^2 - \omega^4)^2}$$
$$y_{I3} = \frac{-(1-\varepsilon)\ddot{\alpha}(\dddot{\alpha} - 6\omega^2\alpha)}{(\dddot{\alpha} - 6\omega^2\alpha)^2 + (4\omega\dot{\alpha} + 3\alpha^2 - \omega^4)^2} \qquad \text{Eq. 3.104}$$

This is a equation for locus of the fourth order IC in case of a general motion of the circle rolling on a straight with slipping where the slippage factor is ε.

3.4.6.1 Simulation Plot of Fourth Order Motion of Circle Rolling with Slipping on a Straight Line

In order to study the shape of the locus of the fourth order IC, a simulation plot was generated for a circle of 1 foot rolling on a straight line with slipping (ε = -0.2). Fig. 3.45 shows the resulting plot of the simulation. It is found that the locus of the third order IC is dependent only on the geometric parameter, r, and is independent of the kinematic state of the body. The particular location of the third order IC at any instant, however, is dependent on the instantaneous values of the kinematic parameters of the rigid body as the case with second order IC is.

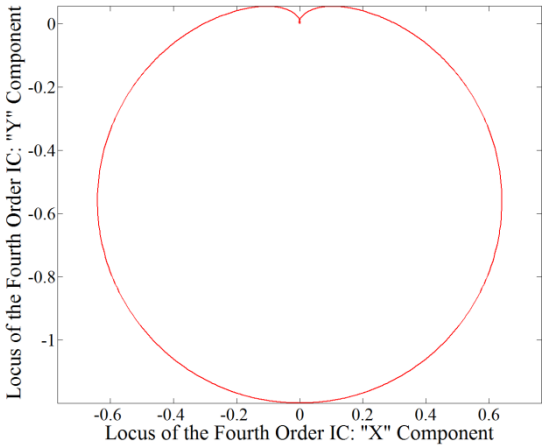

Fig. 3.45: Simulation Plot Showing the Locus of the Forth Order IC for a Circle (*r = 1ft*) Rolling on a Straight Line with Skidding (*ε = -0.2*)

3.4.6.2 Special Case Scenarios for Fourth Order Motion of Circle Rolling with Slipping on a Straight Line

The instantaneous state of kinematic parameters give rise to many interesting special case scenarios much as when the circle is rolling on the straight line without slipping/skidding. The analysis of these special cases is on the same line as Case 1 (Sec. 3.2). Table 3.7 summarizes the special cases with an emphasis on the fourth order IC, I_4, location and value of the third order orientation angle, β_4 for each case.

Table 3.7: Summary of the Fourth Order Motion Properties in Special Case Scenarios for a Circle Rolling on a Straight Line

$\ddot{\alpha}$	$\dot{\alpha}$	α	ω	*IC Location*	β_4
0	No Effect	0	0	∞	90^o
0	0	0	$\neq 0$	*P [0, 0]*	0^o
0	No Effect	$\neq 0$	0	*P [0, 0]*	180^o
0	No Effect	$\neq 0$	$\neq 0$	*P [0, 0]*	$\tan^{-1}\left(\frac{6\omega^2\alpha}{4\omega\dot{\alpha}+3\alpha^2-\omega^4}\right)$
0	$\neq 0$	0	$\neq 0$	*P [0, 0]*	0^o or 180^o
$\neq 0$	No Effect	0	0	*O [0, -(1-ε)]*	90^o
$\neq 0$	0 or nonzero	0	$\neq 0$	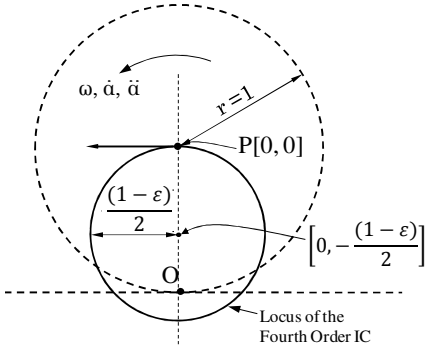	$\dot{\alpha} \neq 0$: $\tan^{-1}\left(-\frac{\ddot{\alpha}}{4\omega\dot{\alpha}-\omega^4}\right)$ $\dot{\alpha} = 0$: $\tan^{-1}\left(\frac{\ddot{\alpha}}{\omega^4}\right)$
$\neq 0$	No Effect	$\neq 0$	0	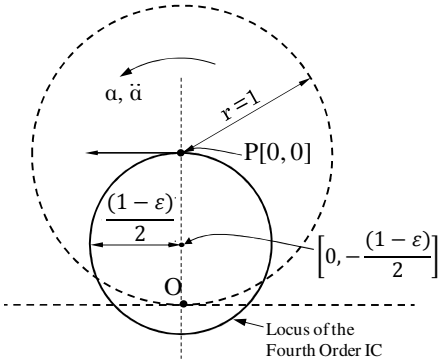	$\tan^{-1}\left(-\frac{\ddot{\alpha}}{3\alpha^2}\right)$
$\neq 0$	$\neq 0$	$\neq 0$	$\neq 0$	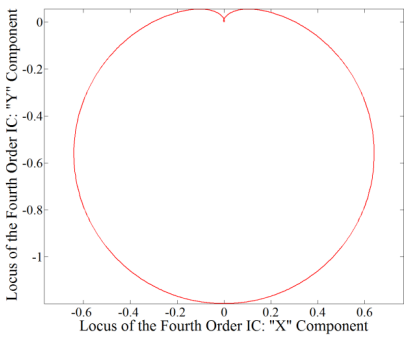	$\tan^{-1}\left(\frac{-(\ddot{\alpha}-6\omega^2\alpha)}{4\omega\dot{\alpha}+3\alpha^2-\omega^4}\right)$

Next, we investigate a special scenario where a line is rolling on a fixed circle without

rolling.

3.5 Case 4: A Line Rolling without Slipping on a Circle

One of the interesting special cases of 1-DOF motion is the motion of a straight line that is rolling on a circle without slipping. This case is the inverse of a circle rolling on a line. We discussed this scenario in Sec. 3.2 at length. Note that the relative motion between these two scenarios should be same as this is a motion between two same bodies. However, the absolute motion of the moving body is different for either body. The following sections discuss various instantaneous motion properties of this system from the first order to the fourth order.

3.5.1 SCHEMATIC REPRESENTATION OF THE SYSTEM

Fig. 3.46 shows a straight line of infinite length (body 1) rolling on a circle of radius r (body 2) without slipping or skidding. Frame {0} is a global frame located at the center O of the circle as shown. Frame {1} is a body fixed frame initially located at P such that frames {0} and {1} are parallel. During the finite motion, let the point P moves to P' in frame {0} such that the final position of the line makes an angle Θ with the initial

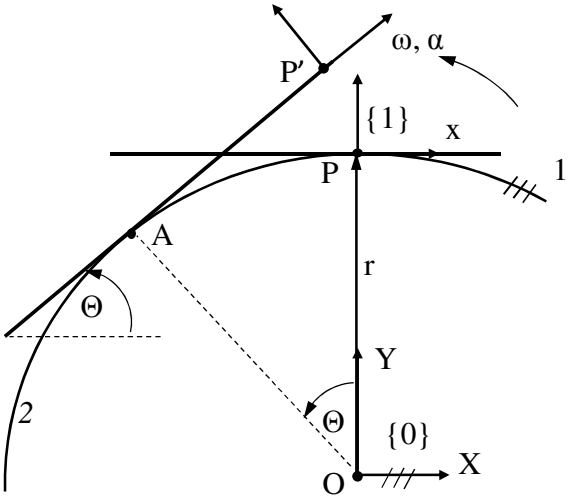

Fig. 3.46: Kinematic State Description of a Straight Line Rolling on a Circle Without Slipping or Skidding

position.

We know that, the locus of a fixed point on the line, P, rolling on a circle is an involute curve. The parametric equation for the particular frame assignment in frame {0} is:

$$X_P = r(-sin(\Theta) + \Theta\, cos(\Theta))$$
$$Y_P = r(cos\,\Theta + \Theta\, sin\,\Theta) \qquad \text{Eq. 3.105}$$

The following section details the first order motion of the line in terms of the motion of point O. The system would be normalized by using unity as the radius of the circle as the radius is merely a scaling factor and does not provide any extra physical information.

3.5.2 First Order Motion of A Line Rolling without Slipping on a Circle

The velocity of point P in frame {0} can be computed by differentiating Eq. 3.105 with time as follows:

$$\dot{X}_P = r\left(-\dot{\Theta}\, cos(\Theta) + \dot{\Theta}\, cos(\Theta) - \Theta\dot{\Theta}\, sin\,\Theta\right) = -r\Theta\omega\, sin\,\Theta$$
$$\dot{Y}_P = r\left(-\dot{\Theta}\, sin(\Theta) + \dot{\Theta}\, sin(\Theta) + \Theta\dot{\Theta}\, cos\,\Theta\right) = r\Theta\omega\, cos\,\Theta \qquad \text{Eq. 3.106}$$

Using the unity radius for the circle 1, we get:

$$\dot{X}_P = -\Theta\omega\, sin\,\Theta$$
$$\dot{Y}_P = \Theta\omega\, cos\,\Theta \qquad \text{Eq. 3.107}$$

Since the linear velocity is a free vector, the location of origin is irrelevant; we can transform the velocity of point P from frame {0} to frame {1} by a rotation matrix alone as follows:

$$\begin{bmatrix}\dot{x}_P\\ \dot{y}_P\end{bmatrix} = \begin{bmatrix}cos\Theta & sin\Theta\\ -sin\Theta & cos\Theta\end{bmatrix}\begin{bmatrix}\dot{X}_P\\ \dot{Y}_P\end{bmatrix} \qquad \text{Eq. 3.108}$$

Then, the velocity of point P is in frame {1} as follows:

$$\dot{x}_P = -\Theta\omega\, sin\Theta\, cos\Theta + \Theta\omega\, sin\Theta\, cos\Theta = 0$$
$$\dot{y}_P = \Theta\omega\, cos^2\Theta + \Theta\omega\, sin^2\Theta = \Theta\omega \qquad \text{Eq. 3.109}$$

The velocity IC (Eq. 2.5) for the line 1 can then computed using Eq. 3.109 as follows:

$$x_{I1} = -\frac{\dot{y}_P}{\omega} = -\Theta$$
$$y_{I1} = \frac{\dot{x}_P}{\omega} = 0 \qquad \text{Eq. 3.110}$$

Thus us the location of the velocity IC is $I_1\,[-\Theta,\ 0]$. Note that for the line to roll on circle 1 (r=1) without slipping, the length of line segment AP' must be equal to the arc length between P and A which is equal to Θ. Thus the location of the velocity IC is coincident with the point of contact, A, of the line with the circle.

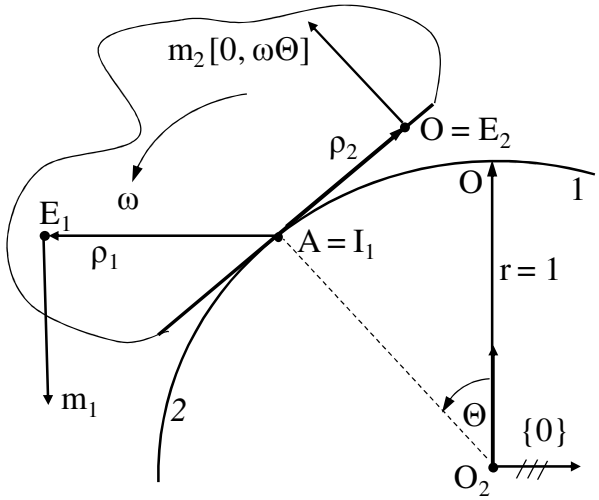

Fig. 3.47: Location of the First Order IC for a Straight Line Rolling on a Circle Without Slipping or Skidding

Fig. 3.47 shows the location of the velocity IC, I_1, and the velocities of the general points in the line. Note that E_1, a general point is a point in the extended body of the line 1. Thus, in general, the velocity IC for a line rolling on a circle is located at the point of contact of the line and the circle at all times.

Next, we discuss the second order motion of the line.

3.5.3 SECOND ORDER KINEMATICS OF A LINE ROLLING WITHOUT SLIPPING ON A CIRCLE

The acceleration of point P in frame {0} can be computed by differentiating Eq. 3.106 with time as follows:

$$\ddot{X}_P = \frac{d}{dt}\left(-r\Theta\dot{\Theta}\,sin\,\Theta\right) = -r(\dot{\Theta}^2 sin\Theta + \Theta\ddot{\Theta}sin\Theta + \Theta\dot{\Theta}^2 cos\Theta)$$
$$\ddot{Y}_P = \frac{d}{dt}\left(r\Theta\dot{\Theta}\,cos\,\Theta\right) = r(\dot{\Theta}^2 cos\Theta + \Theta\ddot{\Theta}cos\Theta - \Theta\dot{\Theta}^2 sin\Theta) \quad \text{Eq. 3.111}$$

Using the unity radius for the circle 1 (r = 1), we get:

$$\ddot{X}_P = -(\omega^2 sin\Theta + \Theta\alpha sin\Theta + \Theta\omega^2 cos\Theta)$$
$$\ddot{Y}_P = \omega^2 cos\Theta + \Theta\alpha cos\Theta - \Theta\omega^2 sin\Theta \quad \text{Eq. 3.112}$$

Eq. 3.112 is the equation of the acceleration of point P in frame {0}. Similar to the velocity, we can transform the acceleration point P from frame {0} to frame {1} as follows:

$$\begin{bmatrix}\ddot{x}_P \\ \ddot{y}_P\end{bmatrix} = \begin{bmatrix} cos\Theta & sin\Theta \\ -sin\Theta & cos\Theta\end{bmatrix}\begin{bmatrix}\ddot{X}_P \\ \ddot{Y}_P\end{bmatrix} \quad \text{Eq. 3.113}$$

Thus Eq. 3.112 can be transformed in frame {1} to get the acceleration of point P in frame {1} as follows:

$$\ddot{x}_P = -\Theta\omega^2$$
$$\ddot{y}_P = \omega^2 + \Theta\alpha \quad \text{Eq. 3.114}$$

The acceleration IC (Eq. 2.18) for the line 1 can then computed using Eq. 2.18 in frame {1} as follows:

$$x_{I2} = \frac{-\Theta\omega^4 - (\omega^2 + \Theta\alpha)\alpha}{\alpha^2 + \omega^4} = -\Theta + \frac{-\omega^2\alpha}{\alpha^2 + \omega^4}$$
$$y_{I2} = \frac{-\Theta\omega^2\,\alpha + (\omega^2 + \Theta\alpha)\omega^2}{\alpha^2 + \omega^4} = \frac{\omega^4}{\alpha^2 + \omega^4} \quad \text{Eq. 3.115}$$

Using the definition of the orientation angle, β_2, and trigonometric identities, Eq. 3.115 can be represented as:

$$x_{I2} = -\Theta + \frac{tan\beta_2}{1 + tan^2\,\beta_2} = -\Theta + sin\,\beta_2 cos\,\beta_2$$
$$y_{I2} = \frac{1}{1 + tan^2\beta_2} = \frac{1}{sec^2\beta_2} = cos^2\beta_2$$

But from trigonometric identities, we get:

$$sin\,\beta_2 cos\,\beta_2 = \frac{1}{2} sin\,2\beta_2$$
$$cos^2\beta_2 = \frac{1 + cos\,2\beta_2}{2}$$

Thus the parametric equation for the locus of the second order IC of a line rolling on a circle without slipping is as follows:

$$x_{I2} = -\Theta + \frac{1}{2}\sin 2\beta_2$$
$$y_{I2} = \frac{1}{2} + \frac{1}{2}\cos 2\beta_2 \qquad \text{Eq. 3.116}$$

Notice that this is a parametric equation for a circle with the center at *[-Θ, 1/2]* and the radius equal to 1/2. Fig. 3.48 shows the locus of the acceleration IC, I_2, for general motion of the line on the circle with no slipping. The instantaneous special case scenarios such as zero angular acceleration and zero angular velocity can be studied similar to the inverse case of a circle rolling on a line (Sec. 3.2).

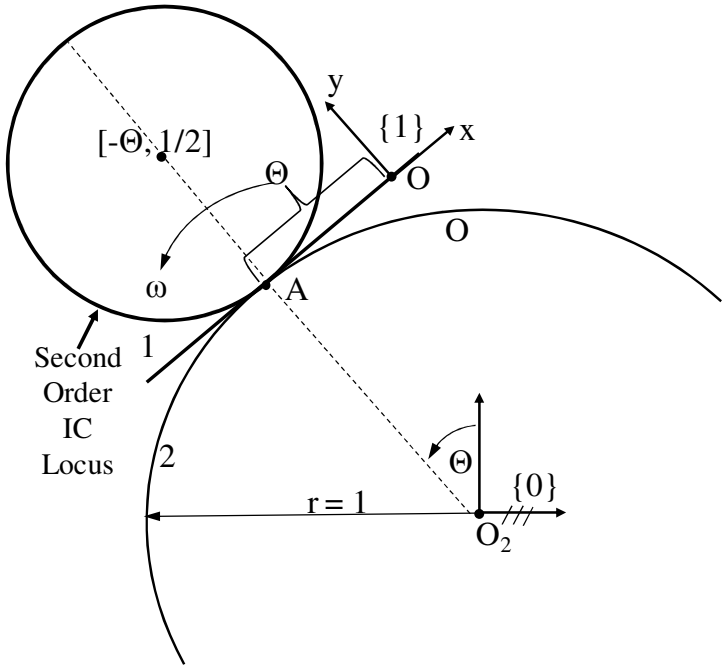

Fig. 3.48: Locus of the Second Order IC for a Straight Line Rolling on a Circle Without Slipping or Skidding is a Circle

By differentiating the acceleration of point P given by Eq. 3.111, we get the description of the third order motion of the point P. This description can be used to discuss the locus of the third order motion as discussed in the following section.

3.5.4 THIRD ORDER KINEMATICS OF A LINE ROLLING WITHOUT SLIPPING ON A CIRCLE

The jerk of point O in frame {0} can be computed by differentiating Eq. 3.111 with time as follows:

$$X_P^{(3)} = \frac{d}{dt}\left(-r(\dot{\Theta}^2 sin\Theta + \Theta\ddot{\Theta}sin\Theta + \Theta\dot{\Theta}^2 cos\Theta)\right)$$

$$= r(-2\omega\alpha sin\Theta - \omega^3 cos\Theta - \omega\alpha sin\Theta - \Theta\dot{\alpha}sin\Theta - \Theta\omega\alpha cos\Theta - \omega^3 cos\Theta$$

$$- 2\Theta\omega\alpha cos\Theta + \Theta\omega^3 sin\Theta)$$

$$Y_P^{(3)} = \frac{d}{dt}\left(r(\dot{\Theta}^2 cos\Theta + \Theta\ddot{\Theta}cos\Theta - \Theta\dot{\Theta}^2 sin\Theta)\right) \qquad \text{Eq. 3.117}$$

$$= r(2\omega\alpha cos\Theta - \omega^3 sin\Theta + \omega\alpha cos\Theta + \Theta\dot{\alpha}cos\Theta - \Theta\omega\alpha sin\Theta - \omega^3 sin\Theta$$

$$- 2\Theta\omega\alpha sin\Theta - \Theta\omega^3 cos\Theta)$$

Using the unity radius for the circle 1, we get:

$$X_P^{(3)} = -2\omega\alpha sin\Theta - \omega^3 cos\Theta - \omega\alpha sin\Theta - \Theta\dot{\alpha} sin\Theta - \Theta\omega\alpha cos\Theta - \omega^3 cos\Theta - 2\Theta\omega\alpha cos\Theta + \Theta\omega^3 sin\Theta$$

$$Y_P^{(3)} = 2\omega\alpha cos\Theta - \omega^3 sin\Theta + \omega\alpha cos\Theta + \Theta\dot{\alpha} cos\Theta - \Theta\omega\alpha sin\Theta - \omega^3 sin\Theta - 2\Theta\omega\alpha sin\Theta - \Theta\omega^3 cos\Theta \quad \text{Eq. 3.118}$$

We can transform the velocity point O from frame {0} to frame {1} as follows:

$$\begin{bmatrix} x_P^{(3)} \\ y_P^{(3)} \end{bmatrix} = \begin{bmatrix} cos\Theta & sin\Theta \\ -sin\Theta & cos\Theta \end{bmatrix} \begin{bmatrix} X_P^{(3)} \\ Y_P^{(3)} \end{bmatrix} \quad \text{Eq. 3.119}$$

Thus Eq. 3.112 can be transformed in frame {1} to get the velocity of point P in frame {1} as follows:

$$x_P^{(3)} = -2\omega^2 - 3\Theta\omega\alpha$$
$$y_P^{(3)} = 3\omega\alpha + \Theta\dot{\alpha} - \Theta\omega^3 \quad \text{Eq. 3.120}$$

The acceleration IC (Eq. 2.18) for the line 1 can then computed using Eq. 3.109 as follows:

$$x_{I3} = \frac{(-2\omega^2 - 3\Theta\omega\alpha)3\omega\alpha - (3\omega\alpha + \Theta\dot{\alpha} - \Theta\omega^3)(\dot{\alpha} - \omega^3)}{(\dot{\alpha} - \omega^3)^2 + (3\omega\alpha)^2}$$
$$y_{I3} = \frac{(-2\omega^2 - 3\Theta\omega\alpha)(\dot{\alpha} - \omega^3) + (3\omega\alpha + \Theta\dot{\alpha} - \Theta\omega^3)3\omega\alpha}{(\dot{\alpha} - \omega^3)^2 + (3\omega\alpha)^2} \quad \text{Eq. 3.121}$$

Using this parametric equation, the third order IC is plotted as shown in Fig. 3.49 which shows the locus of the third order IC, I_3, for a general motion of a line on a circle of unity radius with no slipping. The special case motion scenarios (such as when the angular velocity ω is zero or angular acceleration α is zero) for second and third order can be formulated similarly to the earlier studied sections (Sections 3.1 through 3.4). The study of the fourth order motion can be similarly performed.

3.6 Summary and Discussion

In this chapter we studied some well represented special case motions in the light of the instantaneous invariants theory that was developed in Chapter 2. This was done because the higher order motion properties pertaining to a general 3DOF planar motion

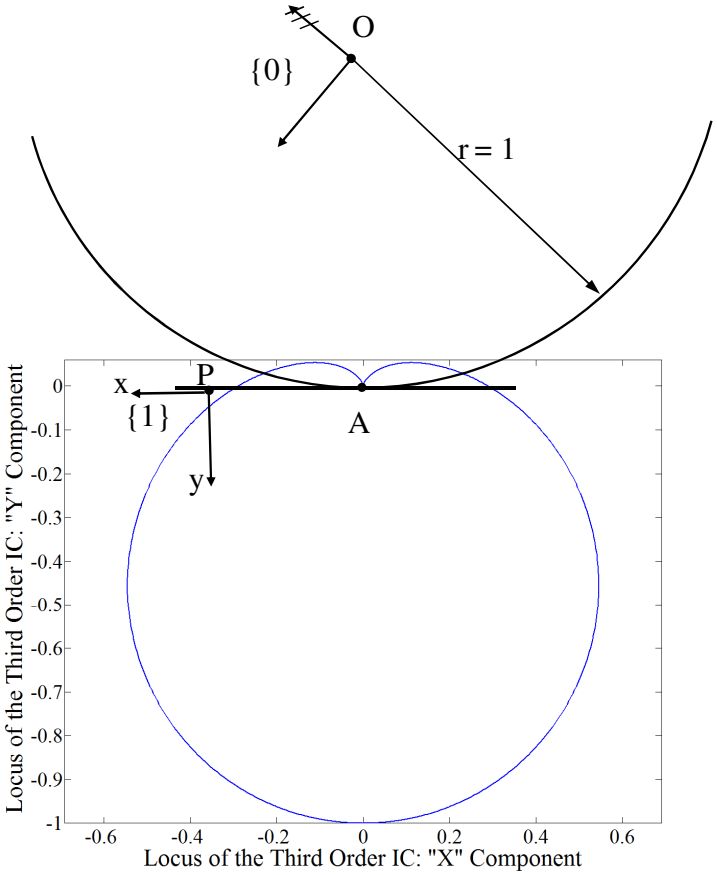

Fig. 3.49: Locus of the Third Order IC for a Straight Line Rolling on a Circle Without Slipping or Skidding is a Circle

contained highly coupled kinematic terms leading to nonlinearity. By studying a set of 1DOF motions, we showed that the loci of the second, third and fourth order ICs for a general motion in each case are purely geometric. The instantaneous locations of the ICS are however dependent on the kinematic states (angular velocity ω, angular acceleration α, etc.) of the rigid body.

Following are some of the observations pertaining to various ICs:

1. The velocity IC for the 1-DOF motions studied is always located at the point of contact of the two bodies rolling without slip.
2. In case of rolling with slip, the velocity IC shifts by the slippage factor as defined in Sec. 3.4 (Eq. 3.94).
3. The locus of the acceleration IC in case of the 1DOF motions (rolling without slip) is a circle coincident with the corresponding inflection circle (Fig. 3.20).
4. When the bodies rolled with slip (2-DOF motion), the diameter of the circle changes by the slippage factor (Fig. 3.40).
5. The third and fourth order ICs for 1-DOF motions are purely geometric in nature. The study of special cases of instantaneous kinematic states resulted in certain analytical shapes such as a straight line or a circle which are shown in Table 3.1-Table 3.5.
6. For the 2-DOF case with slip, the loci of the third or fourth order ICs were scaled by the slippage factors similarly to the second order IC locus (Fig. 3.44).

Table 3.8 summarizes the loci for the first four orders of IC in case of a circle (representing the cylindrical rigid bodies such as a wheel) of unity radius rolling on a straight line (representing the planar rigid bodies such as a flat and smooth ground) in case of the rolling without slipping and rolling with slipping conditions.

Table 3.8: Summary of the IC Loci for a Circle Rolling on a Straight Line

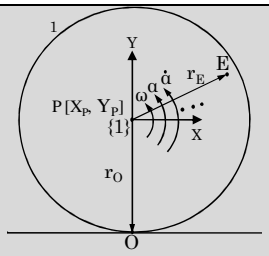	**Rolling Without Slip** **1-DOF Motion**	**Rolling With Slip (ε)** **2-DOF Motion**
First Order IC Location, I_1	Point *O [0, -r]*	*[0, -r(1-ε)]*
Locus of Second Order IC, I_2	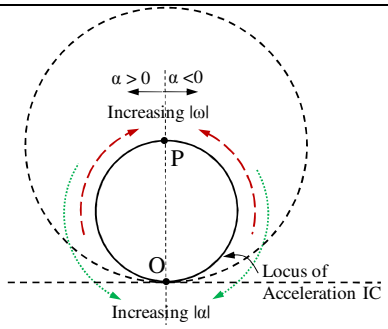	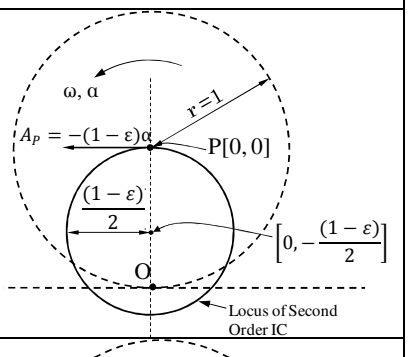
Locus of the Third Order IC	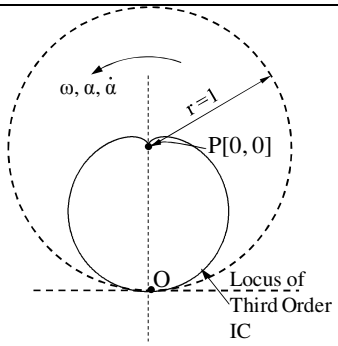	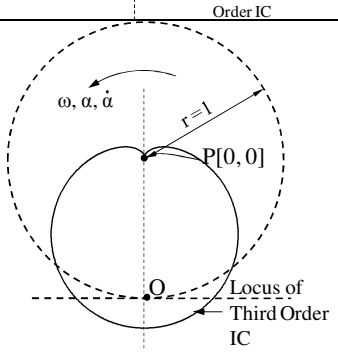
Locus of the Fourth Order IC	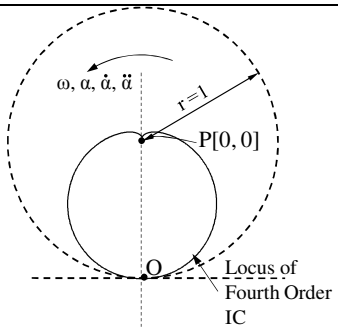	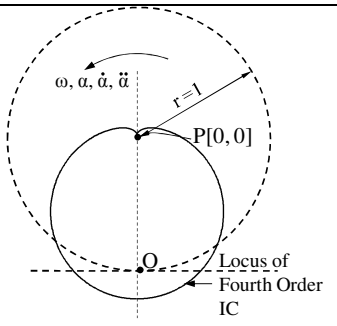

4 MOBILE PLATFORM CONFIGURATIONS

In this chapter, we discuss various kinematic configurations for planar mobile platforms. The chapter is organized such that the platforms that fall under the same kinematic category are discussed together. The motion synthesis for all platforms under the same category is discussed in the following section. The operational space motion description for the class of mobile platforms is followed by specific motion synthesis methodology for each individual kinematic configuration. For ex., the skid-steer platforms, tricycle like platforms, and Ackerman steered platforms fall under the category of platforms that have fixed wheels on either side of the platform. Thus the kinematic configuration of each platform is discussed one by one followed by a common motion synthesis section for that class of platforms.

4.1 Platforms with Fixed Wheels Mounted on a Common Rolling Axis on Either Side

When a mobile platform has fixed (non-orientable) wheels, the motion of the platform is restricted because of the pure rolling constraint (i.e., the kinematic constraint on the wheel that does not allow a lateral motion) (Campion et al., 1996; Alexander and Maddocks, 1989; Muir and Newman, 1987). When one or more fixed wheels (or tracks) are mounted on either side of the platform in pairs such that each pair has a common rolling axis, the mobile platform can move only in the forward and reverse direction and rotate about a point on the common rolling axis. It cannot move along the common center line axis (i.e., in the lateral direction) without slipping or skidding, making the platform a 2-DOF configuration. This is true regardless of whether the fixed wheels are actively driven or passively trailing/leading. The common kinematic formulation for all platforms

that have such a set of fixed wheels/tracks stems from the fact that, at any instant, a 2-DOF motion of the platform can be simplified as a rotation about a selected point (i.e., instant center of velocity) that lies on the wheel rolling axis. These mobile platforms are always oriented in the direction of travel, thanks to the motion constraint. The different platforms falling under this category are:

- Skid-Steer Platforms
- Tricycle Like Platforms
- Ackerman-Steer Platforms.

The following sections discuss the architectures of these platforms.

4.1.1 SKID-STEER PLATFORMS

Skid-steer platforms are some of the simplest configurations of mobile platforms and involve one or more fixed and powered wheels or tracks arranged on either side of the platform. The two sides are independently driven and coordinated such that the rotational motion is achieved by differencing the velocities on each side, hence they are alternatively known as differentially driven platforms (Papadopoulos and Poulakakis, 2000). Fig. 4.1 shows some example skid-steer platforms.

As the four wheeled and six wheeled platforms contain all fixed wheels, it is possible to provide suspensions for the wheels making the configurations suitable for outdoor conditions. However, due to the skid-steer orientation control, the platform motions involve slippage and thus are inaccurate in responding to motion commands. The following section enumerates the various kinematic configurations for the mobile platforms that fall under this category.

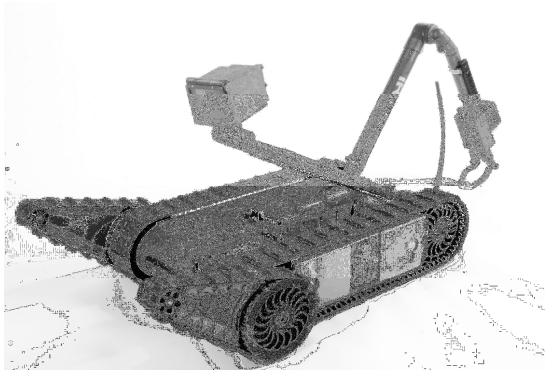

(a)

(b)

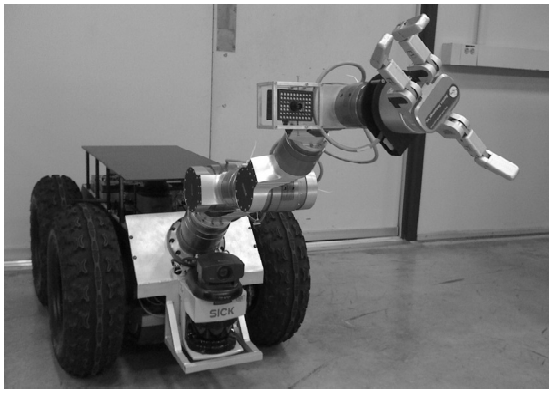

(c)

(d)

Fig. 4.1: Different Kinematic Configurations of Skid-Steer Platforms. (a) A Platform with Tracks (PackBot EOD from iRobot Corporation, Picture Reproduced from www.irobot.com), (b) a Two Wheeled Statically Unstable Platform (RMP200 from Segway Inc., Picture Reproduced from www.segway.com), (c) a Four Wheeled, Skid-Steer Platform (RMP400 from Segway Inc., Picture shows the Mobile Manipulation System at RRG), and (d) a Six Wheeled, Skid-Steer Platform (Crusher from NREC, CMU, Picture Reproduced from : http://www.rec.ri.cmu.edu/projects/crusher/photos/index.htm)

4.1.1.1 Two Wheeled Platforms

As shown in Fig. 4.2, this configuration has only one powered wheel on each side of the platform and is a statically unstable design (as shown in Fig. 4.1-a). However if there are one or more passive caster wheels attached to the platform, this configuration can be gravity force stabilized. This configuration is suitable for indoor/on-road conditions. As there is no skidding required for rotational motion, this configuration is less noisy than a four or six wheeled configuration.

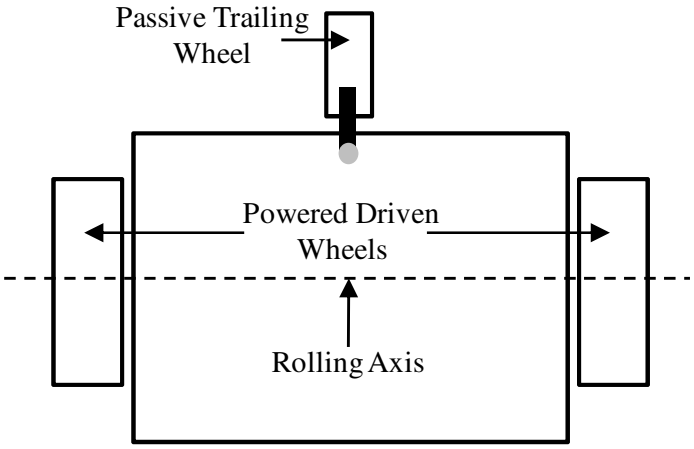

Fig. 4.2: Different Wheel Configurations for Skid-Steer Platforms: Two Wheeled Platform with Passive Caster Wheels

4.1.1.2 Four Wheeled Platform

Shown in Fig. 4.3, a four wheeled platform is a statically stable configuration. The operation of the platform lacks motion command accuracy since there is more skidding during turning than the two wheeled platform design. A straight line motion is efficient and fast. This configuration is frequently used for off-road conditions because of its simplicity, stability, ruggedness and compactness. Fig. 4.1-c shows an example of such a platform.

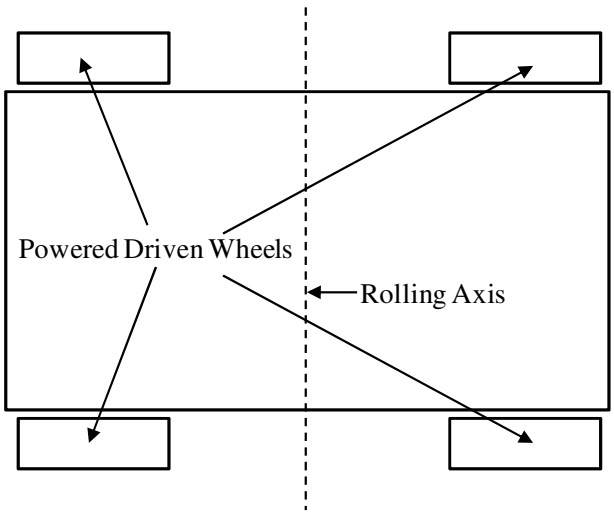

Fig. 4.3: Different Wheel Configurations for Skid-Steer Platforms: Four Wheeled Platform

4.1.1.3 Six Wheeled Platform

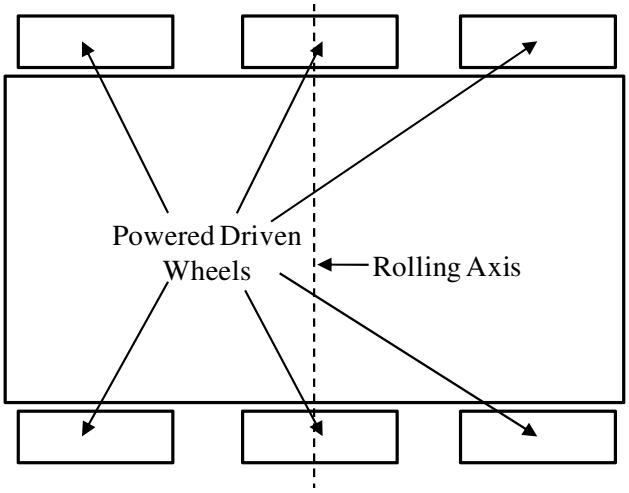

Fig. 4.4: Different Wheel Configurations for Skid-Steer Platforms: Six Wheeled Platform

The platform with three wheels on each side (Fig. 4.4) is a stable configuration and provides good payload carrying capacity. A compliant suspension is necessary in order for all of the wheels to maintain ground contact as shown in Fig. 4.1-d. This configuration is used for off-road conditions because of its stability and ruggedness. However it has limited dexterity due to its fixed wheel configuration. It is inefficient and lacks directional accuracy since there is significant skidding during turning. The six wheels reduce soil pressure when carrying heavy loads.

4.1.1.4 Tracked Platform

This configuration is also known as tank-steer as it uses independently driven tracks on either side of the platforms like an armored tank. Due to the tracks, it has very good traction, stability and load carrying capacity (low ground pressure) required because of the armor's weight. Thus it is particularly suitable for off-road conditions. A schematic representation of such a platform is shown in Fig. 4.5.

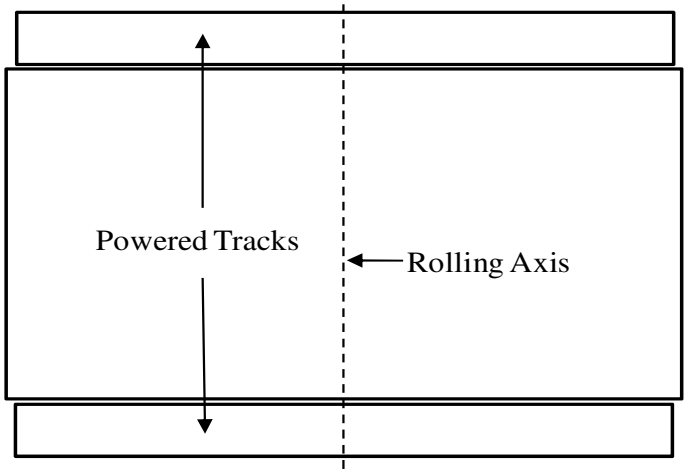

Fig. 4.5: Different Wheel Configurations for Skid-Steer Platforms: Platform with Tracks

4.1.2 TRICYCLE PLATFORMS

One version of tricycle mobile platform has a 2DOF front wheel that is powered for driving and steering as shown in Fig. 4.6. The two trailing wheels are passive and are non-orientable (fixed). This system has good dexterity and is good for medium speed operations. The wheels can be suspended using passive or active suspension systems making the platform suitable for outdoor operations.

Due to the arrangement of the fixed passive wheels, the velocity IC is constrained along

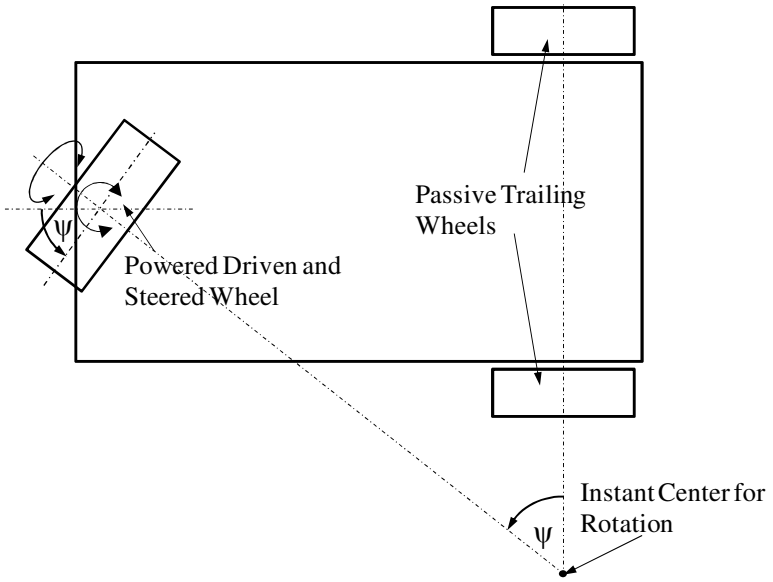

Fig. 4.6: A Tricycle like Mobile Platform (Actively Steered and Driven front Wheel with Two Trailing Passive Fixed Wheels)

the wheel axis just as the case with the skid-steer platform. However, the difference in the kinematic configuration is the input DOF. In the case of a skid-steer platform, the fixed wheels are independently driven. Thus the linear motion is the average of the two wheel motions (or the coordinated motions on the two sides of platform) and the rotational motion is due to the differencing of the two wheel motions. In the case of a tricycle, the rotational motion is due to the steering angle ψ while the linear motion is due to the wheel rolling.

The procedure for finding the ICs based on corresponding motion requirements (refer Sec. 4.1.4.1) is identical to the skid steer platform. What differs is the possible motion synthesis based on the location of ICs for the instantaneous motion.

4.1.3 ACKERMAN STEER PLATFORMS

This platform configuration has a car like placement of wheels, i.e., two front wheels that are used for steering using an Ackerman steering differential mechanism (Wong, 2001) and two trailing wheels. It could have either front wheels driven or rear wheels driven. From the kinematics point of view, this configuration can be modeled as a tricycle as it also has a driving and a steering input. Thus for motion synthesis, we will use a tricycle model to compute the input DOF requirements. Note that a tricycle like platform can rotate the powered wheel by 90^{o} so that the platform can turn in place about an IC in the rear axis center point. Ackerman-steer platforms are incapable of turning in place.

4.1.3.1 Ackerman-Steer Front Wheels with Two Passive Trailing Wheels

As shown in Fig. 4.7, this configuration has two trailing wheels. With only two passive wheels, there is no skidding required for turning from the kinematic stand point (skidding may occur due to inaccurate motions, insufficient traction or large lateral forces). This configuration is similar to a passenger car. The differential mechanism is

designed so that all axes always intersect at the velocity IC on the passive wheel axle center line.

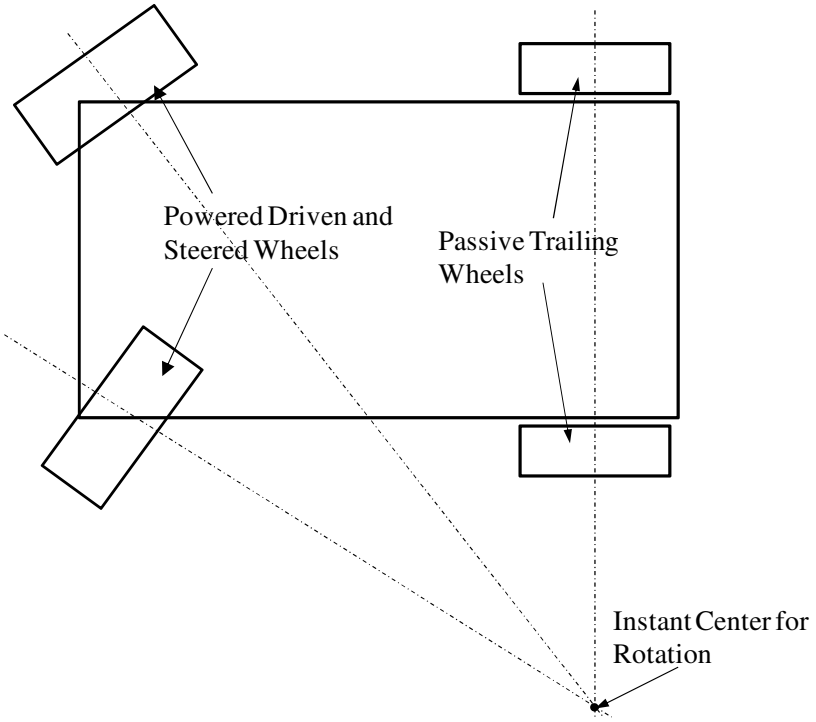

Fig. 4.7: Ackerman Steered Platform Schematic Diagram (A 2DOF Active Input System with Coordinated Steering and Driving for Front Two Wheels and Passive Trailing Fixed Wheels)

4.1.3.2 Ackerman Steered Front Wheels with Four Passive Trailing Wheels

With four passive wheels, this has higher payload carrying capacity and can carry more volume. Fig. 4.8 shows a schematic representation of a six wheeled platform with Ackerman-steer.

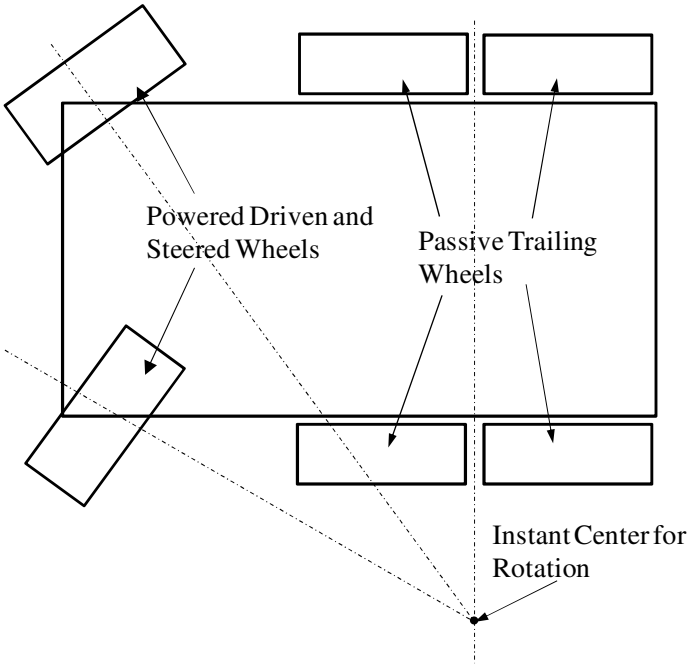

Fig. 4.8: Ackerman Steered Platform Schematic Diagram (A 2DOF Active Input System with Coordinated Steering and Driving for Front Two Wheels and Four Passive Trailing Fixed Wheels)

4.1.3.3 Ackerman Steered Front Wheels with Passive /Active Trailing Tracks

The platform has tracks instead of fixed wheels as shown in Fig. 4.9. The tracks can be active or passive. When the tracks are powered the platform configuration is like a half track as shown in Fig. 4.10. Due to the tracks it has very good traction, stability and load carrying capacity (low ground pressure). This makes the configuration suitable on soft, off road surfaces such as battlefields or construction sites.

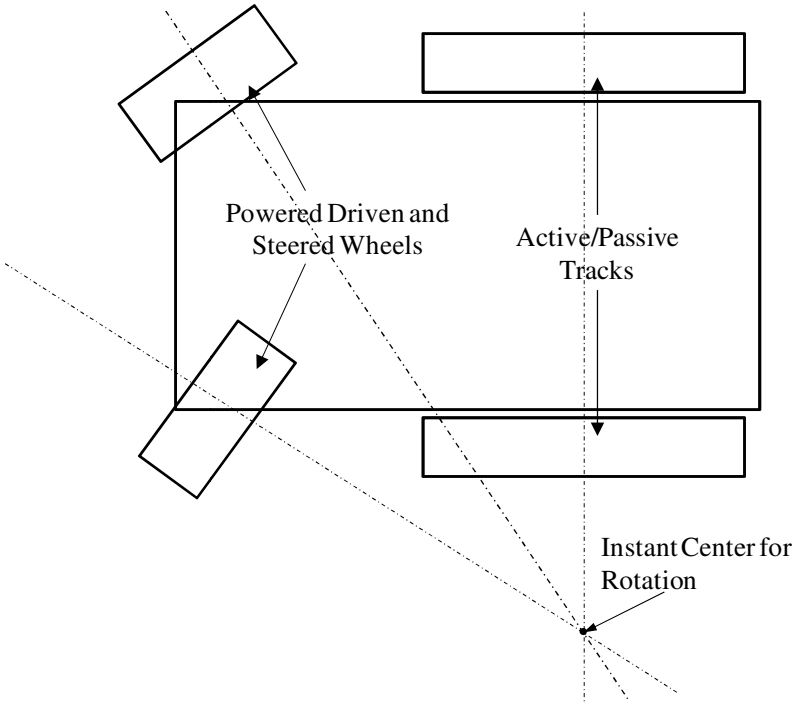

Fig. 4.9: Ackerman Steer Platform with Trailing Active/Passive Tracks

Note that the description of operational space motion requirement for any of the above platform configurations is done in terms of the linear motion specification (velocity, acceleration, and jerk etc.) of the POI and the angular motion specification of the platform rigid body. Based on the motion requirements, we then identify the location of corresponding IC. Because of the constraint due to the fixed wheels, the motion specification is identical to all aforementioned platform configurations (Fig. 4.11). The

Fig. 4.10: An Example of Halftrack Vehicle [Wikimedia]

difference is in the motion synthesis (inverse kinematics) for each individual platform configuration due to the difference in the active (input) DOFs. The following section discusses the overall motion synthesis of the mobile platforms for the first three orders of motion.

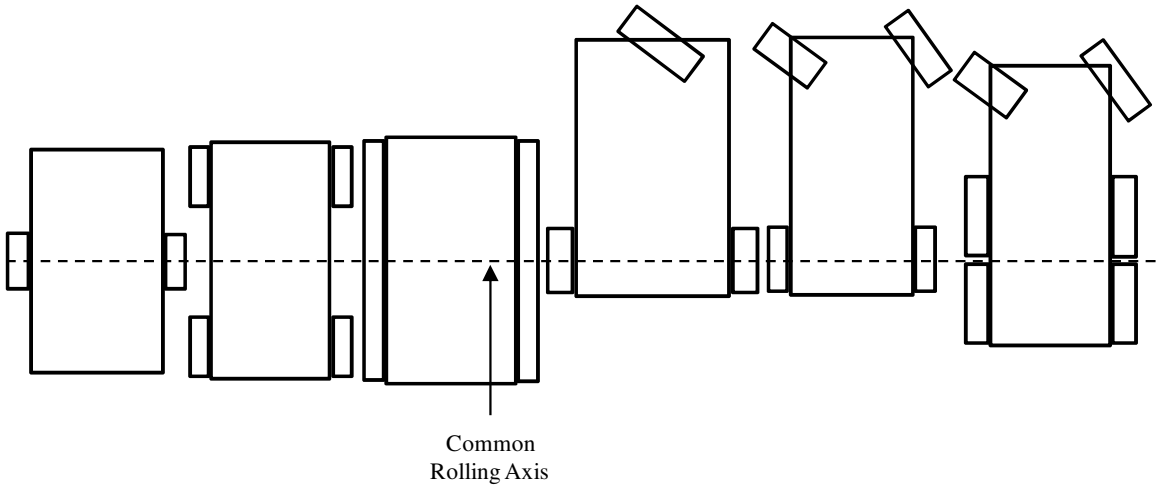

Fig. 4.11: Common Rolling Axis for the Class of Mobile Platforms with Fixed Wheels on Both Sides

4.1.4 KINEMATIC FORMULATION FOR THE PLATFORMS WITH FIXED WHEELS

Fig. 4.12 shows a mobile platform with a wheel on each side, a representative of the aforementioned class of mobile platforms that have one or more fixed wheels on either side of the platform. The diameter of the wheels is d and the distance between the two wheels is *2b*. For discussions purpose, let us select the midpoint between the two wheel attachment points to be the Point of Interest (POI). The body fixed frame {1} and an inertial reference frame {0} are both instantaneously located at P. Thus, the operational space motion is specified in terms of motion of point P and the rotational motion of the platform body. Note that by choosing a point of interest that is offset from the wheel axis, we can define a motion in the Y direction as well (Papadopoulos and Poulakakis, 2000). We will also discuss the case when we choose this more general location of a point on the body as the POI. Using this model, the following section discusses the kinematic

formulation of the class of mobile platforms for up to the third order as follows.

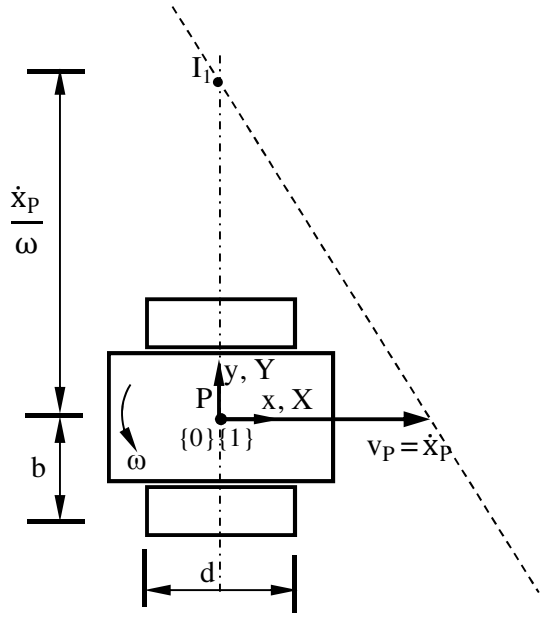

Fig. 4.12: Kinematic Description for the Class of Mobile Platforms with Fixed Wheels on Either Side of the Platform, the First Order IC is Constrained on the Wheel Rolling Axis

Papadopoulos and Poulakakis (2000) presented a Jacobian based kinematic model for a skid-steer mobile platform. The Jacobian becomes singular when the point of interest is placed along the wheel axis. Hence their choice of point of interest was constrained to be offset from the wheel axis. However we will show that the IC based formulation can synthesize the first order motion of the mobile platform for cases when the point of interest is both on and off the wheel axis. The following sections discuss the motion synthesis of the platform starting with the first order motion. The motion state of various points in the body was represented in Chapter 2 by generic notation $m_{k(j)}$ where $k = 1, 2, 3, \ldots,$ is the order of motion and $j = 1, 2, 3, \ldots,$ iterates through the wheel subsystems. For the mobile platform motion synthesis, we will use more physical symbols to represent the kinematic properties such as v_j for velocity, a_j for acceleration and $\dot{a}_j$ for jerk of point E_j.

4.1.4.1 The First Order Motion Synthesis for the Platforms with Fixed Wheels

Due to the 2-DOF motion of the platform, the linear motion of point P is constrained to move only in the *X* direction (the wheel rolling direction). Thus the mobile platform always faces the direction of motion. Any motion in the direction of wheel axis (Y direction) happens only due to skidding and slipping if any. For kinematic synthesis, we assume no slipping and skidding of the platform. This constraint can be expressed mathematically in terms of velocity of point P, v_P, as follows:

$$\dot{X}_P = v_P$$
$$\dot{Y}_P = 0 \qquad \text{Eq. 4.1}$$

The location of the instant center depending on the motion requirement in terms of linear velocity, v_P of point P and angular velocity, ω, of the rigid body is computed as:

$$X_{I1} = 0$$
$$Y_{I1} = \frac{\dot{X}_P}{\omega} \qquad \text{Eq. 4.2}$$

Thus the locus of the velocity IC is coincident with the wheel axis and its instantaneous location is determined by the linear and angular velocity requirements of the platform motion.

When the point of interest is offset from the wheel axis, motion along the *y* axis is possible (Papadopoulos and Poulakakis, 2000) as shown in Fig. 4.13 where the point P is at an offset distance *c* from the wheel axis. The mobile platform is a *2*-DOF configuration, thus the motion is described in terms of the *X* and Y components ($\dot{X}_P$ and $\dot{Y}_P$) of v_P at any instant. Note that since the velocity IC is constrained along the wheel axis, we have:

$$X_{I1} = -c \qquad \text{Eq. 4.3}$$

Thus, we can compute the angular velocity required for this motion using Eq. 2.5 as:

$$\omega = \frac{\dot{Y}_P}{c} \qquad \text{Eq. 4.4}$$

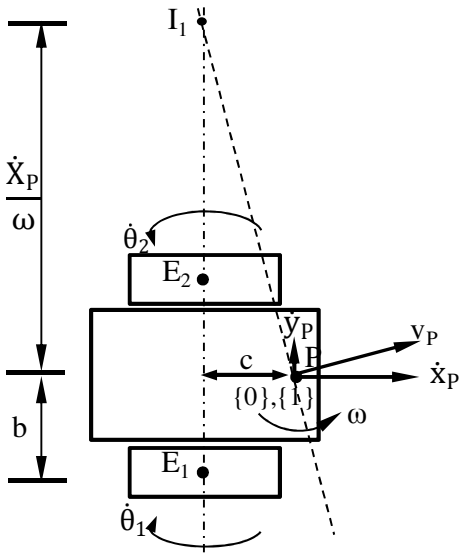

Fig. 4.13: Motion Description of Operational Space in Terms of an End-Effector that is Offset from the Wheel Rolling Axis

Then the location of the velocity IC is given as:

$$X_{I1} = -c$$
$$Y_{I1} = \frac{\dot{X}_P}{\omega} \qquad \text{Eq. 4.5}$$

First Order Motion Synthesis: Skid-Steer Platform

The two inputs for the motion synthesis for a skid-steer platforms are the wheel velocities on the two sides of the platform, $\dot{\theta}_1$ and $\dot{\theta}_2$. The locations of wheels in frame {1} are, respectively, *E1* [*0, -b*], and *E2* [*0, b*]. The radius of the wheel subsystems with respect to the velocity IC can be computed as follows:

$$X_{\rho 1(1)} = 0$$
$$Y_{\rho 1(1)} = -b - \frac{\dot{X}_P}{\omega}$$
$$X_{\rho 1(2)} = 0 \qquad \text{Eq. 4.6}$$
$$Y_{\rho 1(2)} = b - \frac{\dot{X}_P}{\omega}$$

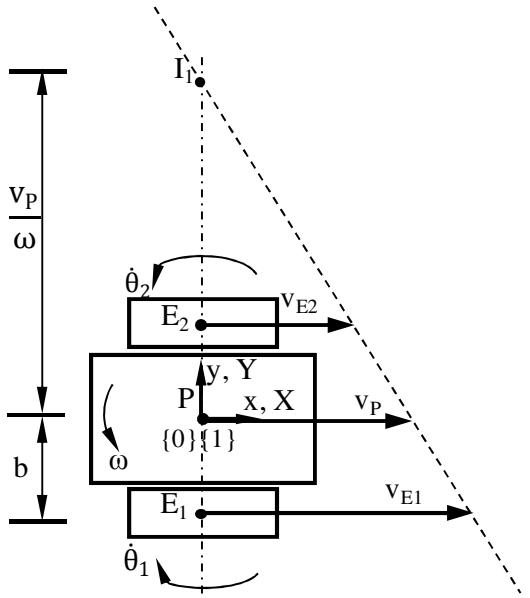

Fig. 4.14: The First Order Motion Synthesis for a Skid-Steer Mobile Platform Based on the First Order IC Location

Based on the velocity IC location, we compute the wheel velocities for a skid steer platform as follows (Eq. 2.8):

$$\begin{aligned} \dot{X}_{E1} &= -Y_{\rho 1(1)}\omega = \dot{X}_P + b\omega \\ \dot{Y}_{E1} &= X_{\rho 1(1)}\omega = 0 \\ \dot{X}_{E2} &= -Y_{\rho 1(2)}\omega = \dot{X}_P - b\omega \\ \dot{Y}_{E2} &= X_{\rho 1(2)}\omega = 0 \end{aligned} \qquad \text{Eq. 4.7}$$

The required wheel inputs in terms of wheel angular velocities are:

$$\begin{aligned} \dot{\theta}_1 &= \frac{\dot{X}_{E1}}{d/2} \\ \dot{\theta}_2 &= \frac{\dot{X}_{E2}}{d/2} \end{aligned} \qquad \text{Eq. 4.8}$$

Thus based on the instantaneous first order motion requirement of the operational space (linear velocity v_p of P and angular velocity ω of the platform), we can independently compute the wheel input (wheel velocities) motion requirement as shown in Fig. 4.14.

First Order Motion Synthesis: Tricycle and Ackerman-Steer Platforms

Fig. 4.15 shows a general schematic of a tricycle/Ackerman-steer platform. The active 2DOF wheel is at a distance *s* from the wheel axis of the two passive, trailing wheels. The distance between the two trailing wheels is *2b*. For the motion synthesis, the choice of point of interest is dictated by the application of the mobile platform. For discussion purpose, the point of interest (shown as point P) is chosen as a point midway between the two fixed trailing wheels on the wheel axis. The motion plan of the platform is then specified in terms of the linear motion of point P and the angular motion of the platform. The following section discusses the first order motion synthesis.

The 2DOF active wheel has two inputs, one for driving and the other for steering. Low and Leow (2005) state that the steering input is used for position control while the driving input for velocity control. Thus we compute the orientation angle which is the input for steering actuator as follows:

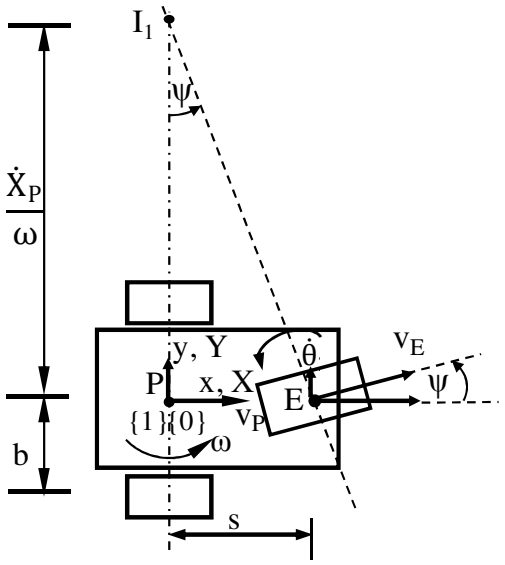

Fig. 4.15: The First Order Motion Synthesis for a Tricycle Like/Ackerman-Steer Mobile Platform Based on the First Order IC Location

$$\psi = \tan^{-1}\left(\frac{X_E - X_{I1}}{Y_E - Y_{I1}}\right) = \tan^{-1}\left(\frac{s}{-\dot{X}_P/\omega}\right) \qquad \text{Eq. 4.9}$$

This is the steering angle with respect to its zero position. The driving input is computed as follows:

$$v_E = \rho_1 \omega$$
$$\dot{\theta} = \frac{v_E}{d/2} = \frac{2\rho_1 \omega}{d}$$
$$where, \rho_1 = \sqrt{{X_{\rho 1}}^2 + {Y_{\rho 1}}^2} \qquad \text{Eq. 4.10}$$
$$X_{\rho 1} = s;\ Y_{\rho 1} = -\frac{\dot{X}_P}{\omega},$$

and d = active wheel diameter

Thus, based on the location of the velocity IC, we can compute the input motion that is required at any instant in time.

We can synthesize the second order motion of the platform in a much similar way, which will be discussed in the next section.

4.1.4.2 The Second Order Motion Synthesis for the Platforms with Fixed Wheels

Before we discuss the second order IC properties of this class of mobile platforms, let us consider a general second order motion of point P as shown in Fig. 4.16. The total

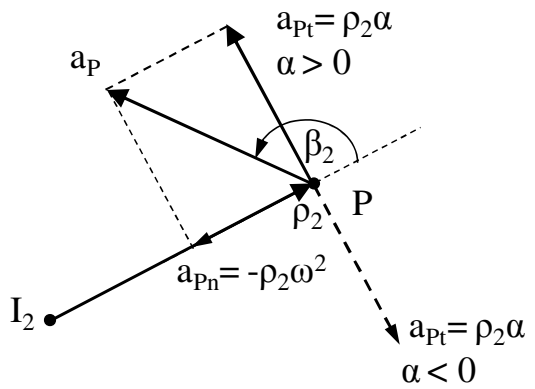

Fig. 4.16: Tangential and Normal Components of the Acceleration of a General Point with respect to the Acceleration IC

acceleration of point P a_P can be separated into two orthogonal components, namely, the tangential component a_{Pt} and the normal component a_{Pn} with respect to the radius ρ_2 from the acceleration IC I_2. The magnitude (and direction) of the tangential component a_{Pt} is dependent on the values of angular acceleration, α, of the rigid body, and the radius ρ_2 as shown in Fig. 4.16. Obviously, tangential component a_{Pt} is orthogonal to the radius ρ_2.

Due to the constrained motion of the class of mobile platforms with fixed wheels on either side, the tangential component of the total acceleration of the Point of Interest P is constrained to be along the rolling direction only. As a result, the second order IC is constrained along the rolling axis. Thus, based on the linear acceleration a_P of point P and the angular velocity ω and angular acceleration α of the platform, we compute the location of the second order IC as follows:

$$X_{I2} = 0$$
$$Y_{I2} = \rho_2 = \frac{\ddot{X}_P}{\alpha} = \frac{\ddot{Y}_P}{\omega^2} \qquad \text{Eq. 4.11}$$

Notice that the location of the second order IC is fixed by choice of the acceleration a_P of point P and either the angular velocity ω or the angular acceleration α of the platform.

Second Order Motion Synthesis: Skid-Steer Platform

With the location of the second order IC known, we can compute the acceleration requirements for the wheel attachment points E_1 and E_2 as follows. The radii of the wheel attachment points from the acceleration IC can be computed as:

$$X_{\rho 2} = X_E - X_{I2}$$
$$Y_{\rho 2} = Y_E - Y_{I2} \qquad \text{Eq. 4.12}$$

Thus,

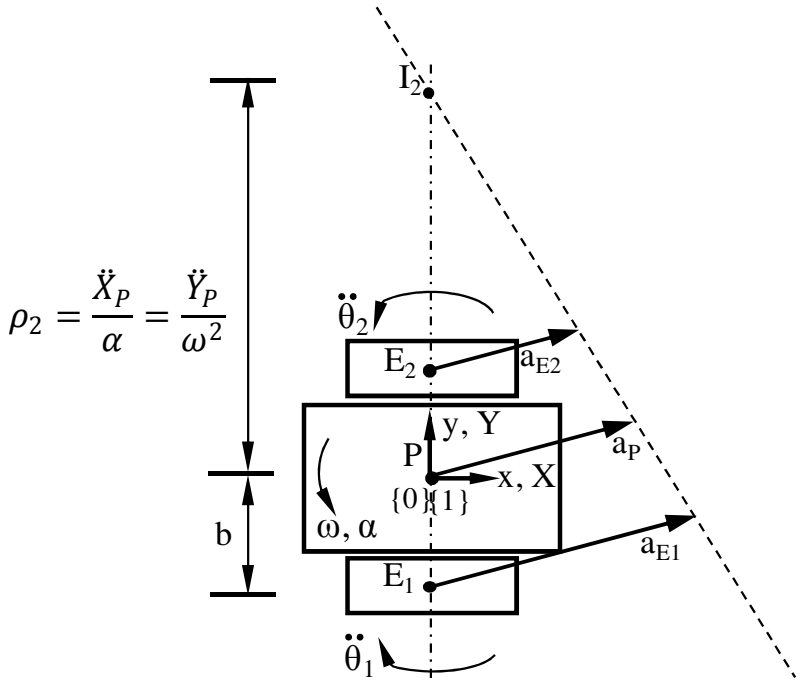

Fig. 4.17: The Second Order Motion Synthesis for a Skid-Steer Mobile Platform Based on the Second Order IC Location

$$X_{\rho 2(1)} = 0$$
$$Y_{\rho 2(1)} = -b - \rho_2$$
$$X_{\rho 2(2)} = 0$$
$$Y_{\rho 2(2)} = b - \rho_2 \qquad \text{Eq. 4.13}$$

The acceleration of the two wheel subsystems may be computed using Eq. 2.22 as:

$$\ddot{X}_{E1} = X_{\rho 2(1)}\omega^2 - Y_{\rho 2(1)}\alpha = (\rho_2 + b)\alpha = \frac{\ddot{\theta}_1 d}{2}$$
$$\ddot{Y}_{E1} = X_{\rho 2(1)}\alpha + Y_{\rho 2(1)}\omega^2 = -(\rho_2 + b)\omega^2$$
$$\ddot{X}_{E2} = X_{\rho 2(2)}\omega^2 - Y_{\rho 2(2)}\alpha = (\rho_2 - b)\alpha = \frac{\ddot{\theta}_2 d}{2}$$
$$\ddot{Y}_{E2} = X_{\rho 2(2)}\alpha + Y_{\rho 2(2)}\omega^2 = -(\rho_2 - b)\omega^2 \qquad \text{Eq. 4.14}$$

In Sec. 3.2, we studied the motion scenario of a circle rolling on a straight line. We showed that the second order motion of the circle without slipping is governed by

following constraint (Eq. 3.5):

$$\ddot{X}_E = -\alpha r = -\frac{\ddot{\theta} d}{2} \qquad \text{Eq. 4.15}$$

In case of the wheel rolling on the ground, the *X* component of the acceleration is $\ddot{X}_{E1}$. Thus the second order wheel inputs in terms of the angular accelerations are computed using Eq. 4.14 and Eq. 4.15 as:

$$\ddot{\theta}_1 = -2\frac{\ddot{X}_{E1}}{d}$$
$$\ddot{\theta}_2 = -2\frac{\ddot{X}_{E2}}{d} \qquad \text{Eq. 4.16}$$

Fig. 4.17 shows an example motion synthesis at an instant in time.

Second Order Motion Synthesis: Tricycle, Ackerman-Steer Platforms

The tricycle input motion synthesis for second order can be computed as follows. The total acceleration a_E of the wheel subsystem has two components, tangential component a_{Et} and normal component a_{En}. The tangential acceleration is orthogonal to radius ρ_2 as

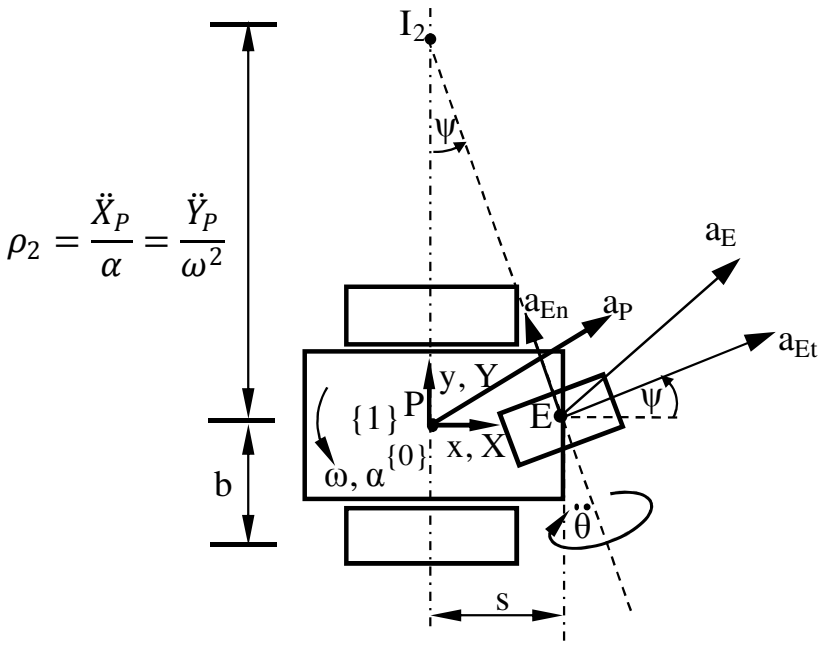

Fig. 4.18: The Second Order Motion Synthesis for a Tricycle Like/Ackerman-Steer Mobile Platform Based on the Second Order IC Location

shown. The centripetal acceleration is a result of first order rotation alone. We can command the required acceleration input from the active wheel only when the wheel is aligned in the direction of tangential acceleration. Thus with the known location for the second order IC, we can compute the steering angle as follows:

$$\psi = tan^{-1}\left(\frac{s}{-\rho_2}\right) \qquad \text{Eq. 4.17}$$

The required second order input from the wheel is then computed as:

$$a_{Et} = \rho_2 \alpha = \frac{\ddot{\theta} d}{2}$$
$$where, X_{\rho 2} = s;\ Y_{\rho 2} = \frac{\ddot{X}_P}{\alpha} \qquad \text{Eq.4.18}$$

The second order wheel inputs in terms of the angular accelerations are then computed as:

$$\ddot{\theta} = 2\frac{a_{Et}}{d} \qquad \text{Eq. 4.19}$$

Fig. 4.18 shows a typical scenario during the motion synthesis of a tricycle like platform at a particular instant in time. Note that Ackerman steer platforms also have identical two DOF systems. Thus the same motion synthesis applies to Ackerman-steer platforms.

4.1.4.3 Third Order Motion Synthesis for the Platforms with Fixed Wheels

The third order motion of the class of mobile platforms with fixed wheels on either side is constrained in the way similar to the second order motion. Thus, the tangential component of the total jerk of the Point of Interest *P* is constrained to be along the rolling direction only. As a result, the third order IC is constrained along the rolling axis. Thus, based on the linear jerk $\dot{a}_P$ of point *P,* and the angular velocity ω, the angular acceleration α, and the angular jerk $\dot{\alpha}$ of the platform, we compute the location of the third order IC as follows:

$$X_{I3} = 0$$
$$Y_{I3} = \rho_3 = \frac{X_P^{(3)}}{\dot{\alpha} - \omega^3} = \frac{Y_P^{(3)}}{3\omega\alpha} \qquad \text{Eq. 4.20}$$

Notice that the location of the third order IC is fixed by choice of the jerk a_P of point P and combination either the angular velocity ω and the angular jerk $\dot{\alpha}$ or the angular velocity ω and the angular acceleration α of the platform.

Third Order Motion Synthesis: Skid-Steer Platform

With the location of the third order IC known, we can compute the jerk requirements from the wheel attachment points E_1 and E_2 as follows. The radius $\rho_{3(j)}$ of the wheel subsystem *j* with respect to the third order IC can be computed as:

$$X_{\rho 3} = X_E - X_{I3}$$
$$Y_{\rho 3} = Y_E - Y_{I3} \qquad \text{Eq. 4.21}$$

Thus,

$$X_{\rho 3(1)} = 0$$
$$Y_{\rho 3(1)} = -b - \rho_3$$
$$X_{\rho 3(2)} = 0 \qquad \text{Eq. 4.22}$$
$$Y_{\rho 3(2)} = b - \rho_3$$

The acceleration of the two wheel subsystems may be computed using Eq. 2.22 as:

$$X_{E1}^{(3)} = X_{\rho 3(1)} 3\omega\alpha - Y_{\rho 3(1)}(\dot{\alpha} - \omega^3) = (\rho_3 + b)(\dot{\alpha} - \omega^3)$$
$$Y_{E1}^{(3)} = X_{\rho 3(1)}(\dot{\alpha} - \omega^3) + Y_{\rho 3(1)} 3\omega\alpha = -(\rho_3 + b)3\omega\alpha$$
$$X_{E2}^{(3)} = X_{\rho 3(2)}\omega^2 - Y_{\rho 3(2)}\alpha = (\rho_3 - b)\alpha \qquad \text{Eq. 4.23}$$
$$Y_{E2}^{(3)} = X_{\rho 3(2)}\alpha + Y_{\rho 3(2)}\omega^2 = -(\rho_3 - b)\omega^2$$

In Sec. 3.2, we studied the motion scenario of a circle rolling on a straight line. We showed that the third order motion of the circle without slipping is governed by the following constraint (Eq. 3.11):

$$X_E^{(3)} = -\dot{\alpha} r = -\frac{\theta^{(3)} d}{2} \qquad \text{Eq. 4.24}$$

In case of the wheel rolling on the ground, the *X* component of the jerk is $X_E^{(3)}$. Thus the third order wheel inputs in terms of the angular jerks are computed using Eq. 4.23 and Eq. 4.24 as:

$$\theta_1^{(3)} = -2\frac{X_{E1}^{(3)}}{d}$$
$$\theta_2^{(3)} = -2\frac{X_{E2}^{(3)}}{d} \qquad \text{Eq. 4.25}$$

Fig. 4.19 shows an example motion synthesis for a skid-steer mobile platform at an instant in time.

Third Order Motion Synthesis: Tricycle, Ackerman-Steer Platforms

The tricycle input motion synthesis for the third order can be computed as follows.

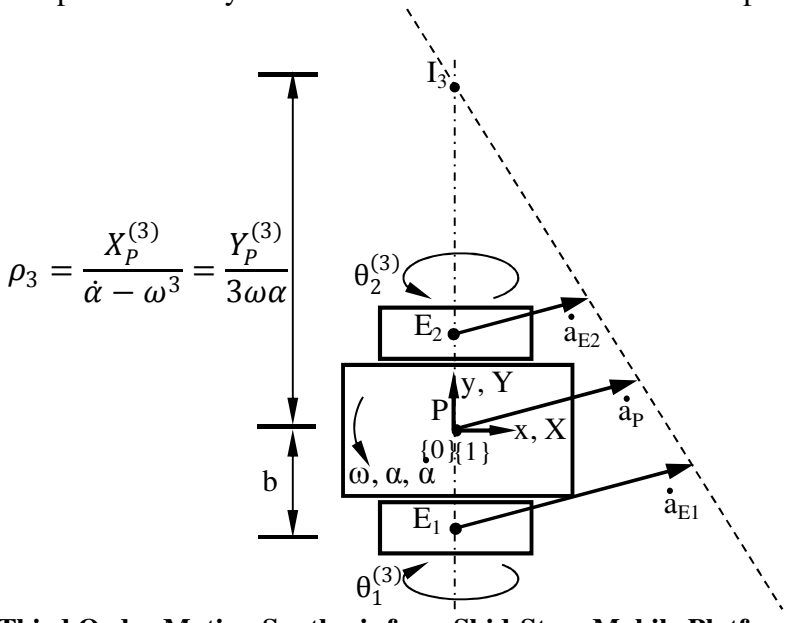

Fig. 4.19: The Third Order Motion Synthesis for a Skid-Steer Mobile Platform Based on the Second Order IC Location

The total jerk $\dot{a}_P$ of the wheel subsystem has two components, tangential component $\dot{a}_{Pt}$ and normal component $\dot{a}_{Pn}$. We can command the required jerk input from the active wheel in the form of the tangential jerk only by first aligning wheel in the directon of tangential jerk. Thus with the known location for the third order IC, we can compute the steering angle as follows:

$$\psi = tan^{-1}\left(\frac{s}{-\rho_3}\right) \qquad \text{Eq. 4.26}$$

The required third order input from the wheel is then computed as:

$$\dot{a}_t = \rho_3(\dot{\alpha} - \omega^3) = \frac{\theta^{(3)} d}{2}$$
$$\rho_3 = \sqrt{{X_{\rho 2}}^2 + {Y_{\rho 2}}^2} \qquad \text{Eq. 4.27}$$
$$where, X_{\rho 3} = s;\ Y_{\rho 3} = \frac{X_P^{(3)}}{(\dot{\alpha} - \omega^3)}$$

The third order wheel inputs in terms of the angular jerks are computed using Eq. 4.23 and Eq. 4.27 as:

$$\theta^{(3)} = -2\frac{X_E^{(3)}}{d} \qquad \text{Eq. 4.28}$$

Fig. 4.20 shows a typical scenario during the motion synthesis of a tricycle like platform at a particular instant in time.

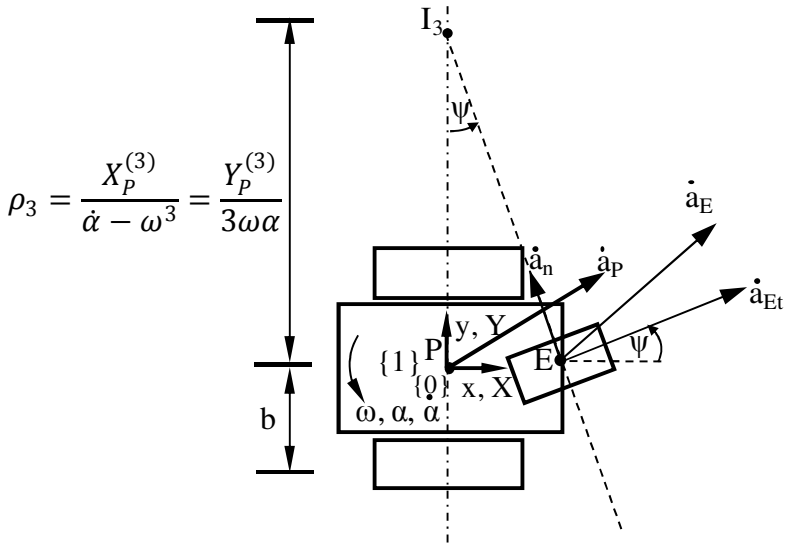

Fig. 4.20: The Third Order Motion Synthesis for a Tricycle Like/Ackerman-Steer Mobile Platform Based on the Third Order IC Location

4.1.5 SUMMARY

We discussed the motion synthesis of a class of mobile platforms that have one or more fixed (both active/passive) wheels/tracks on either side of the platform body for the three orders of motion (velocity, acceleration, and jerk). The motion synthesis for further higher orders is possible along the same lines. We showed that the description of operational space motions is identical across the various configurations of the platforms. We also discussed the effect of choice of the location of the point of interest on the motion description and overall motion synthesis. We observed that due to the 2-DOF constrained motion capabilities of the platforms, the instant centers for first, second and third order lie on the common rolling axis at all times as shown in Fig. 4.21. This constraint restricts the operator's choices in terms of dexterous motions. With a dexterous platform such as an omnidirectional platform we can choose the locations of various ICs for better/smoother motion synthesis.

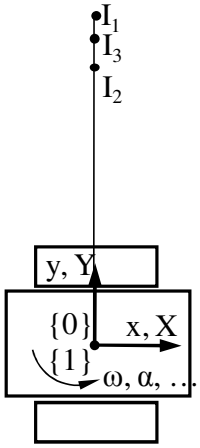

Fig. 4.21: The Location of Various ICs for the Class of Mobile Platforms with Fixed Wheels on Either Side

We will study a simple scenario that can help elaborate the motion synthesis process that now becomes effective in platform operations. Consider a general mobile platform traversing a trajectory that changes from concave to convex at point C as shown in Fig. 4.22. Point P is the Point Of Interest on the platform. When the mobile platform is the one from the class of mobile platforms discussed above, it is oriented so that it always faces the direction of travel (i.e., the orientation of the platform is always equal to angle subscribed by the robot on the circular arc). It can be shown that the ICs for velocity, acceleration, jerk, etc., are located at the center of the curvature (i.e., center of the circle). Thus the normal components of acceleration, jerk of point *P* are directed towards the center of the circle as shown in Fig. 4.22. When the mobile platform crosses point C, and the normal acceleration, jerk etc. instantaneously switch to the opposite direction resulting in large higher order properties and thus causing a shock and uncertainty.

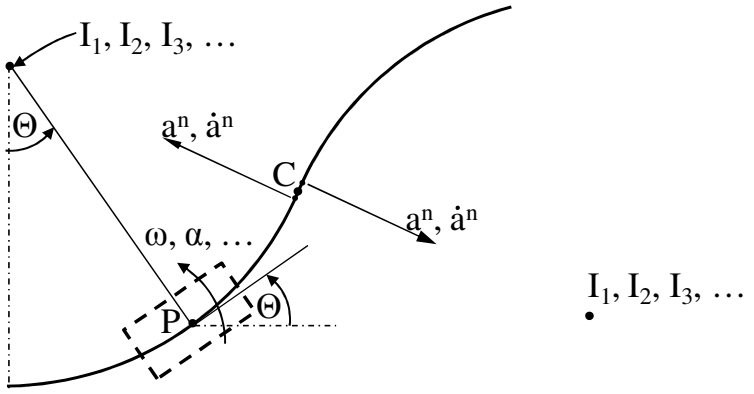

Fig. 4.22: Mobile Platform Traversing Circular Trajectory

With a more dexterous platform, we can eliminate the shock and uncertainty as follows. To prevent the shock, we can put a restriction on the motion properties of a point of interest P on the platform such that the normal acceleration and jerk of point P at point C on the curve vanish, whereby point *C* becomes a stationary inflection point (i.e., the curvature at point C is zero and it is stationary at this value). To accomplish this, we select the IC locations, the instantaneous motion states of point P, and the mobile platform such that the velocity, acceleration and the jerk of point P are instantaneously

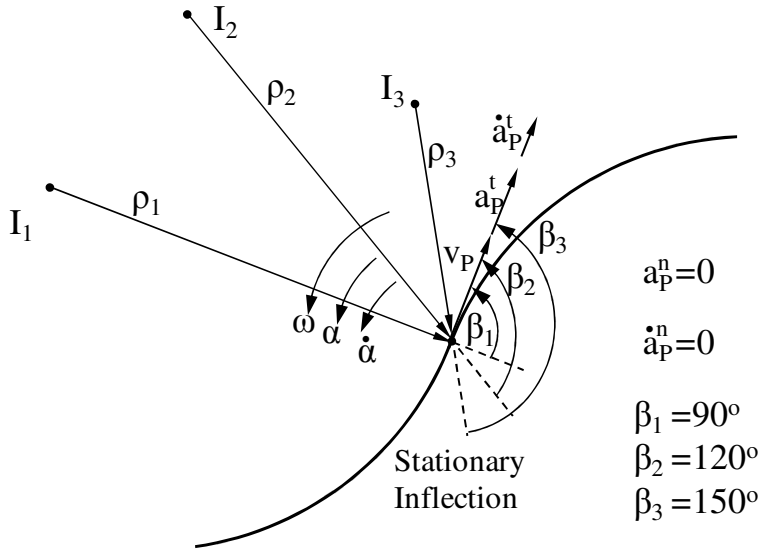

Fig. 4.23: Higher Order Properties for a Mobile Platform Traversing a Trajectory

parallel to each other and tangential to the trajectory at point C as shown in Fig. 4.23. This high quality motion planning is possible with a mobile platform that is omnidirectional. The following section discusses such a class of omnidirectional mobile platforms with active caster wheels.

4.2 Omnidirectional Platforms with Active Offset (Caster) Wheels

A powered caster wheel is an off-centered orientable and driven wheel; i.e., it has two actuators, one for driving and the other for steering as shown in Fig. 4.25. A platform with a minimum of two powered caster wheels has an omnidirectional (3-DOF planar motion) capability with a singularity free work space (Campion et al., 1996; Oetomo and Ang, 2008; Yi and Kim, 2002). The omnidirectional capability allows the platform to move instantaneously in any direction with any desired orientation, a highly desirable capability for indoor and cluttered settings. The following sections detail the motion synthesis of wheeled mobile platforms with active caster wheels. We will discuss the configuration details of this class of mobile platforms starting with a two active wheeled mobile platform up to a general J ($j = 1, 2, 3, \ldots, J$) wheeled mobile platform. The motion synthesis will be done for the generalized case of a J wheeled platform.

Fig. 4.24: An Example of the Mobile Platform with Active Caster Wheels (Picture Reproduced from Low and Leow [2006a])

A platform with J powered caster wheels has $2J$ active input joints. It has, however, only three degrees of freedom in the operational space because of its planar motion. Thus the configuration becomes redundantly actuated for even a two wheeled platform. Yi et al (2002) proposed a kinematic formulation for such a platform in which the forward kinematics of each wheel subsystem is computed in terms of three degrees of freedom input space (they used a passive DOF as shown in Fig. 4.25) and three degrees of freedom operational space. The redundancy of the excess input space was then resolved using a higher order loop constraint method by first choosing three independent and active input degrees of freedom. The IC based formulation proposed in this paper uses a more direct and physically intuitive approach to the inverse kinematics problem in contrast to the method proposed in (Yi and Kim, 2002). The formulation also provides a straight forward extension of the method to higher order formulations as will be studied in the following sections.

Campion et al. (1996) and Oetomo and Ang (2008) state that for singularity free

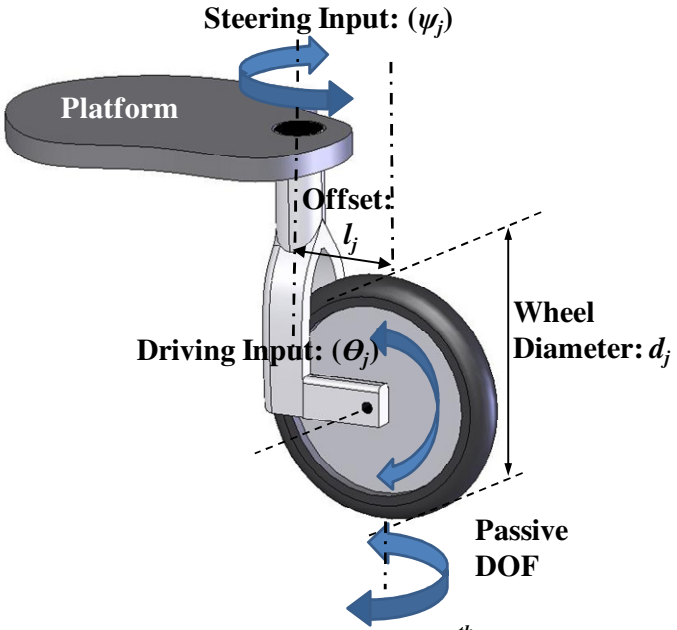

Fig. 4.25: A Schematic Representation of the general j^{th} Wheel Subsystem with an Active Caster Wheel

workspace, the omnidirectional mobile platform with powered caster wheels should have a minimum of two wheels with full actuation (i.e. both steering and driving actuation). However having more than two active wheels presents more choice of actuation which can be exploited to get a better control solution. Note that for a serial manipulator, the actuation redundancy results in more than one set of joint positions to achieve the desired point of interest position. Similarly, for parallel mechanisms such as a mobile platform there are multiple input force/torque solutions for a desired operational space force/torque requirement. Thus the redundancy in case of serial mechanisms is in the position domain; while in case of parallel mechanisms, the redundant actuation yields redundancy in the force domain (Yi and Freeman, 1993). Hence, redundantly actuated mobile platforms are beneficial.

4.2.1 KINEMATIC CONFIGURATIONS FOR MOBILE PLATFORMS WITH ACTIVE CASTER WHEELS

The following sections discuss various configurations of mobile platforms with active caster wheels starting with a *2* wheeled platform up to a general *J* wheeled platform. Subsequently, the motion synthesis for the first three orders of output motion will be discussed for a general platform in terms of the j^{th} wheel subsystem.

4.2.1.1 Platform with Two Active caster Wheels

This is the mobile platform with a minimum number of actuators required as a sufficient number of independent inputs to provide adequate control of the platform motion for singular free kinematics. However with only two wheels, it is not a stable configuration unless there are passive wheels for support. Fig. 4.26 shows one such configuration that has a rectangular platform with two active caster wheels placed laterally in the center with four passive casters across corners for support. Note that the

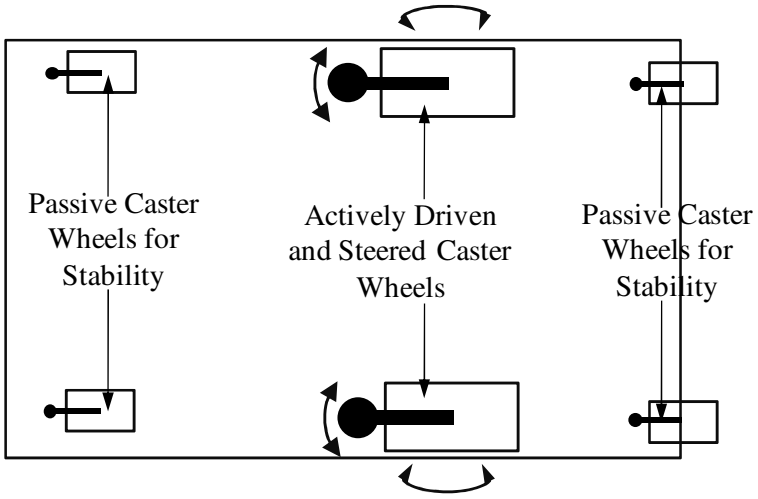

Fig. 4.26: Mobile Platform with Two Laterally Arranged, Independently Driven and Steered Caster Wheels with Passive Caster Wheels

four passive caster wheels are just for support. The configuration could be stabilized with just one passive wheel. When the length of the platform is much larger than the width (a common case for robot gurneys in hospitals (www.conmedisys.com), a small differential error in the input for the active wheels may be magnified as significant output motion errors. This effect can be reduced by placing the active wheels longitudinally instead of laterally. Fig. 4.27 shows a rectangular platform with two active caster wheels longitudinally placed in the center with four passive casters across corners for support. Notice that by spacing the active casters further apart we get a controllable and stable design.

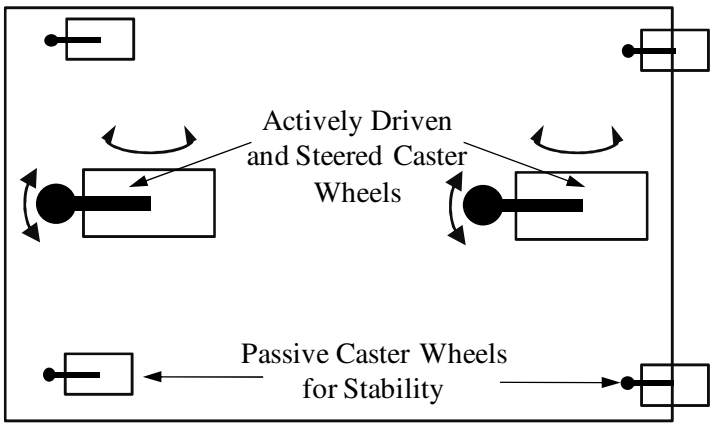

Fig. 4.27: Mobile Platform with Two Independently Driven and Steered Caster Wheels with Passive Caster Wheels

4.2.1.2 Platform with Three Active Caster Wheels

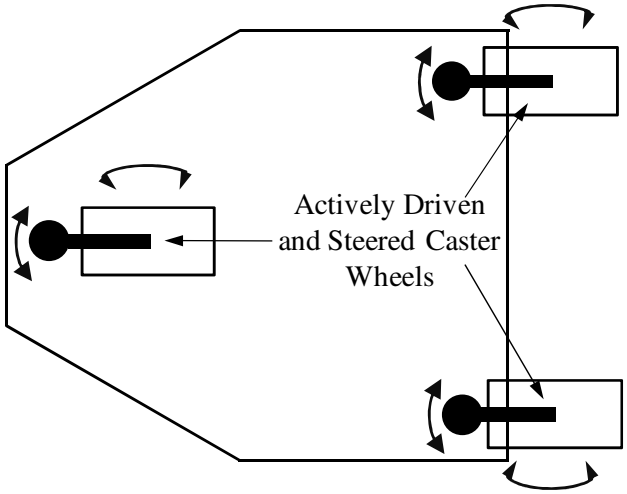

Fig. 4.28: Mobile Platform with Three Independently Driven and Steered Caster Wheels

With addition of one more active wheel, we reduce the need for passive support wheels. Typically, the arrangement of wheels is such that it looks like a tricycle as shown in Fig. 4.28. Because there are only three driven points of contact of the platform with the ground, all the wheels maintain contact with the ground at all times. However, this configuration may have a tendency to tip over in case of an unbalanced load (especially when arranged closer to the two rear wheels). A more stable configuration such as a four wheeled rectangular platform is discussed next.

4.2.1.3 Platform with Four Active caster Wheels

With addition of one more active wheel, we get a stable design in a rectangular (or square) platform. Also with one extra active wheel, the platform has a higher payload carrying capacity. Conversely, for the same payload capacity as a three wheeled platform, smaller size actuators could be used. However all four wheels may not maintain ground

contact on uneven surfaces if they are rigidly attached to the frame. A compliant suspension in this case would help the wheels maintain the contact.

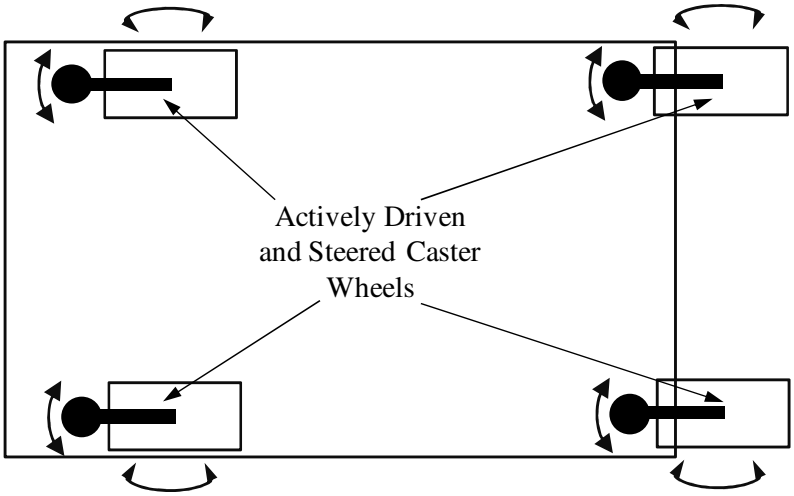

Fig. 4.29: Mobile Platform with Four Independently Driven and Steered Caster Wheels

It is possible to add more than four wheels for added payload and stability. We will discuss the scenario for a general J wheeled platform that will lead us to a generalized kinematic formulation for this general class of mobile platform.

4.2.1.4 A General Mobile Platform with *J* Active caster Wheels

Fig. 4.30 shows a schematic diagram of a general J wheeled mobile platform of a general wheel arrangement. The following section details the formulation for the mobile platform with *J* caster wheels in terms of a general wheel subsystem *j (j=1, 2, 3, …, J)*. Various platform geometry parameters of the platform are shown in Fig. 4.30 and described here.

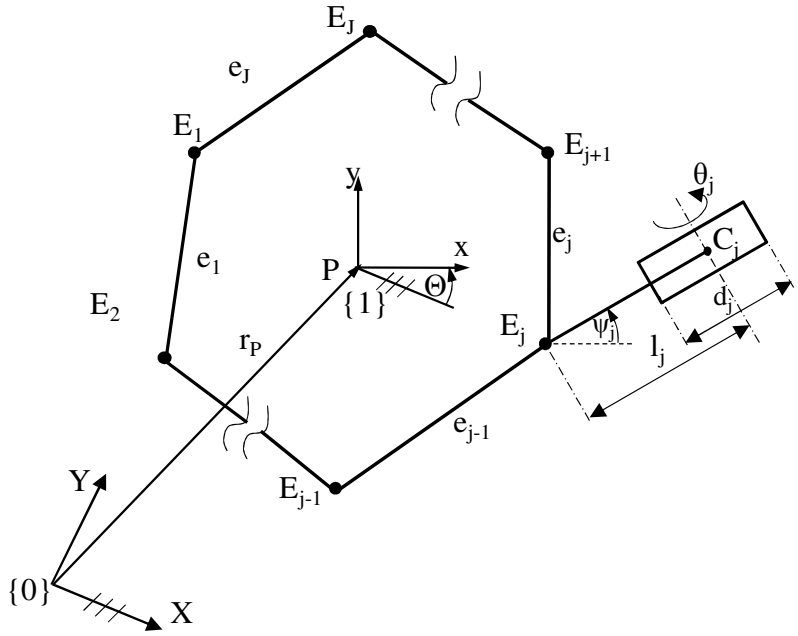

Fig. 4.30: Geometric Description of a *J* Wheeled Mobile Platform with Caster Wheels

In Fig. 4.30,

{0}: A global fixed reference frame, (*OXY*),

r_P: The location of the Point of Interest (POI or *P*) on the platform with respect to frame *{0}*, (*Pxy*)

{1}: A frame fixed to the platform body with origin at *P*,

Θ: The angle frame *{1}* makes with frame *{0}*,

l_j: The length of steering link for wheel *j.* The length may or may not be equal for all wheel subsystems,

E_j: The point of attachment of steering link *j* to the platform (wheel subsystem attachment point),

e_j: The length between E_j and E_{j-1}, values for e_j*'s* may or may not be equal for all wheel subsystems,

θ_j: The rotation of each wheel *j* about its rolling axis. Anticlockwise rotation as seen from E_{j+1} is positive.

ψ_j: The steering angle, angle made by steering link with the X axis of Frame *{1}*. In other words, the rotation of each wheel j about its vertical axis at E_j. Anticlockwise rotation is positive.

d_j: The diameter of drive wheel j,

C_j: The location of center of wheel j.

4.2.2 KINEMATIC FORMULATION FOR A GENERAL WHEELED MOBILE PLATFORM WITH *J* CASTER WHEELS

For planar motions of the platform, the velocity of body fixed point *Ej* is dependent on the driving and steering inputs $\dot{\theta}_J$ and $\dot{\psi}_J$ as shown in Fig. 4.31. The motion state of various points in the body was represented in Chapter 2 by generic notation $m_{k(j)}$ where $k = 1, 2, 3, \ldots,$ is the order of motion and $j = 1, 2, 3, \ldots,$ iterates through the wheel subsystems. For the mobile platform motion synthesis, we will use more physical symbols to represent the kinematic properties such as v_j for velocity, a_j for acceleration and $\dot{a}_j$ for jerk of point E_j. Thus the component v_{js} of the velocity v_j of a general point *Ej* is the velocity component due to steering and v_{jd} is the velocity component due to driving. These contributions due to steering (v_{js}) and driving (v_{jd}) are calculated as follows:

$$v_{js} = \dot{\psi}_J l_j$$
$$v_{jd} = \dot{\theta}_J \frac{d_j}{2} \qquad \text{Eq. 4.29}$$

Based on the required output in terms of the velocity of point *P* as well as the angular velocity of the platform, we locate the velocity IC using Eq. 2.5. Using the IC to describe the motion state of point *Ej* helps separate the kinematic and geometric information of the motion (as evident from Eq. 2.49). Studying the IC location relative to the body as well as the location of various points of interests in the body relative to the IC provides valuable information about kinematic requirements from the platform. Using IC as a

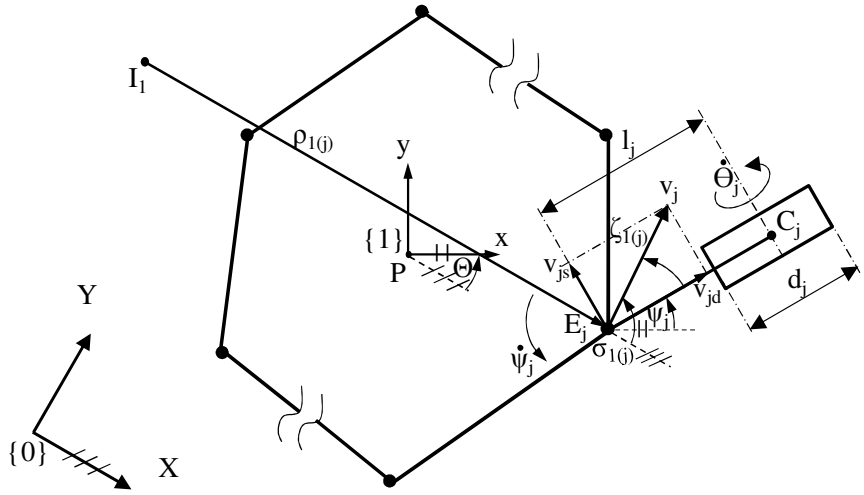

Fig. 4.31: Velocity of Wheel Attachment Point, E_j, Expressed in Terms of the First Order IC.

foundation also generalizes the formulation for higher order motion since we can compute the k^{th} order time state of any point on the body in the same way. Therefore, we compute the velocity of the wheel attachment points E_j using Eq. 2.8 for $\dot{X}_{Ej}$ and $\dot{Y}_{Ej}$ (which can also be computed using Eq. 2.2). This is the total velocity, v_j, required for wheel subsystem *j*. As discussed in Chapter 2, angle $\sigma_{1(j)}$ is the angle the total velocity of a point makes with the global frame {0}. The subscript *1* in the symbol is for the first order of motion and the subscript *j* in the bracket is for the j^{th} wheel subsystem.

We know the location of wheel attachment point E_j in the body fixed frame *{1}* which can be used to compute the location of E_j in frame *{0}* using Eq. 2.1. Also we know the direction, $\sigma_{1(j)}$, of the velocity, v_j, in global frame {0}. With the current steering angle ψ_j, we can compute the angle between the total velocity v_j and the steering link. Let's denote this angle as $\zeta_{1(j)}$ which can be computed as:

$$\zeta_{1(j)} = \sigma_{1(j)} - \Theta - \psi_j \qquad \text{Eq. 4.30}$$

Then the required steering and driving velocity input can be computed as:

$$v_{jd} = v_j \cos(\zeta_{1(j)})$$
$$v_{js} = v_j \sin(\zeta_{1(j)}) \qquad \text{Eq. 4.31}$$

This is the velocity of the j^{th} wheel subsystem. The velocity of all the other subsystems can be similarly computed and commanded. Note that by choosing the driving and steering input in terms of $\dot{\theta}_j$ and $\dot{\psi}_j$, we can command the velocity of E_j in any arbitrary direction as the two inputs are mutually orthogonal. The desired magnitude of v_j is limited by the dynamic capabilities of the wheel actuators and also by the allowable traction at the wheel-ground contact. This means that the velocities v_j for all points E_j can always be met by these two independent wheel inputs.

4.2.3 THE SECOND ORDER MOTION SYNTHESIS FOR THE PLATFORMS WITH ACTIVE CASTER WHEELS

In a way similar to the first order motion, the motion requirement of the platform can be described in terms of the linear motion of POI and the angular motion of the platform. Since this is a 3-DOF configuration, we can specify a combination of an arbitrary linear acceleration and angular acceleration at any instant of time. Let $\ddot{X}_P$and $\ddot{Y}_P$ be the acceleration for point P, and ω and α be the angular velocity and acceleration of the platform required at an instant in time. Let $a_P = \sqrt{\ddot{X}_P^2 + \ddot{Y}_P^2}$ be the total acceleration of point P. We can specify an instantaneous inertial frame $\{2\}$ for XY such that its X axis is aligned with the direction of a_P as shown in Fig. 4.32. Thus in frame $\{2\}$ we have:

$$\begin{aligned} \ddot{X}_P &= a_P \\ \ddot{Y}_P &= 0 \end{aligned} \qquad \text{Eq. 4.32}$$

With this motion requirement, the second order IC (given by Eq. 2.18) is located in frame $\{2\}$ at:

$$\begin{aligned} X_{I2} &= \frac{a_P\,\omega^2}{\alpha^2 + \omega^4} \\ Y_{I2} &= \frac{a_P\,\alpha}{\alpha^2 + \omega^4} \end{aligned} \qquad \text{Eq. 4.33}$$

Let us define a temporary variable d_2 such that:

$$d_2 = \frac{a_P}{\alpha} \qquad \text{Eq. 4.34}$$

Notice that based on the signs of the linear and angular accelerations (a_P and α) at an instant, the value of d_2 can be either negative or positive.

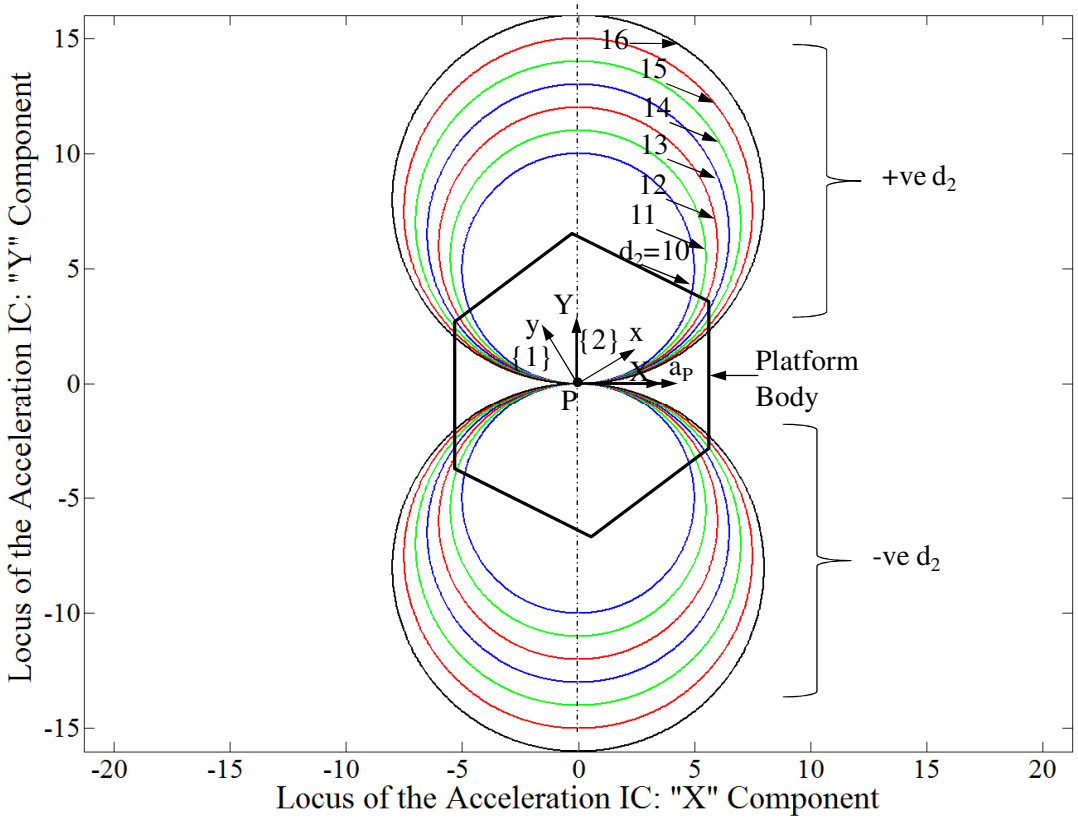

Fig. 4.32: The Loci of the Second Order IC for a General *J* Wheeled Mobile Platforms

Thus the second order IC location is computed as:

$$X_{I2} = \frac{d_2 \alpha \omega^2}{\alpha^2 + \omega^4}$$
$$Y_{I2} = \frac{d_2 \alpha^2}{\alpha^2 + \omega^4} \qquad \text{Eq. 4.35}$$

In Chapter 2, we defined angle β_2 (Eq. 2.20) as follows:

$$tan(\beta_2) = -\frac{\alpha}{\omega^2} \qquad \text{Eq. 4.36}$$

Using the definition of angle β_2, Eq. 4.35 can be rearranged to get:

$$X_{I2} = \frac{d_2 tan\beta_2}{1 + tan^2\,\beta_2} = -d_2 sin\,\beta_2 cos\,\beta_2$$
$$Y_{I2} = \frac{d_2 tan^2\beta_2}{1 + tan^2\beta_2} = d_2 sin^2\beta_2$$

After further simplification, the locus of the second order IC is given by following expression:

$$X_{I2} = 0 - \frac{d_2}{2} sin\,2\beta_2$$
$$Y_{I2} = \frac{d_2}{2} - \frac{d_2}{2} cos2\beta_2 \qquad \text{Eq. 4.37}$$

Eq. 4.37 is a parametric equation of a circle with center at *[0,* $\frac{d_2}{2}$*]* and radius equal to $\frac{d_2}{2}$ which shows that the locus of the acceleration IC is a circle. Reviewing the parametric equation in Eq. 4.37, we see that the diameter of the circle is a ratio of the instantaneous linear acceleration of point P, a_P, and the angular acceleration, α, of the platform body. The instantaneous location of acceleration IC depends on value of the angle, β_2 (Eq. 2.20), which in turn depends on the values of the angular acceleration α and angular velocity, ω of the platform. A simulation plot in Fig. 4.32 shows the loci of the second order IC for both positive and negative values of d_2.

Let us look at a couple of numerical examples that look at specific scenarios.

1. At a particular time, let the linear acceleration of point P be $-2.5\frac{\text{ft}}{\text{s}^2}$, approximately *1/13th* of gravitational constant (*32.2 ft/s*^{2}). Let the angular velocity ω of the platform at the instant be *0.5* $\frac{\text{rad}}{\text{s}}$, and the angular acceleration α be *0.25* $\frac{rad}{s^2}$. With these motion parameters, the instantaneous value of the parameter, d_2 given by Eq. 4.34 is computed as 10. This is the diameter of the second order IC circle for the particular values of a_P and α. With the numerical value of α and ω, the value of the second order orientation angle β_2 (Eq. 2.20) is computed as *135*^{o}. With this information, we can locate the instant center as

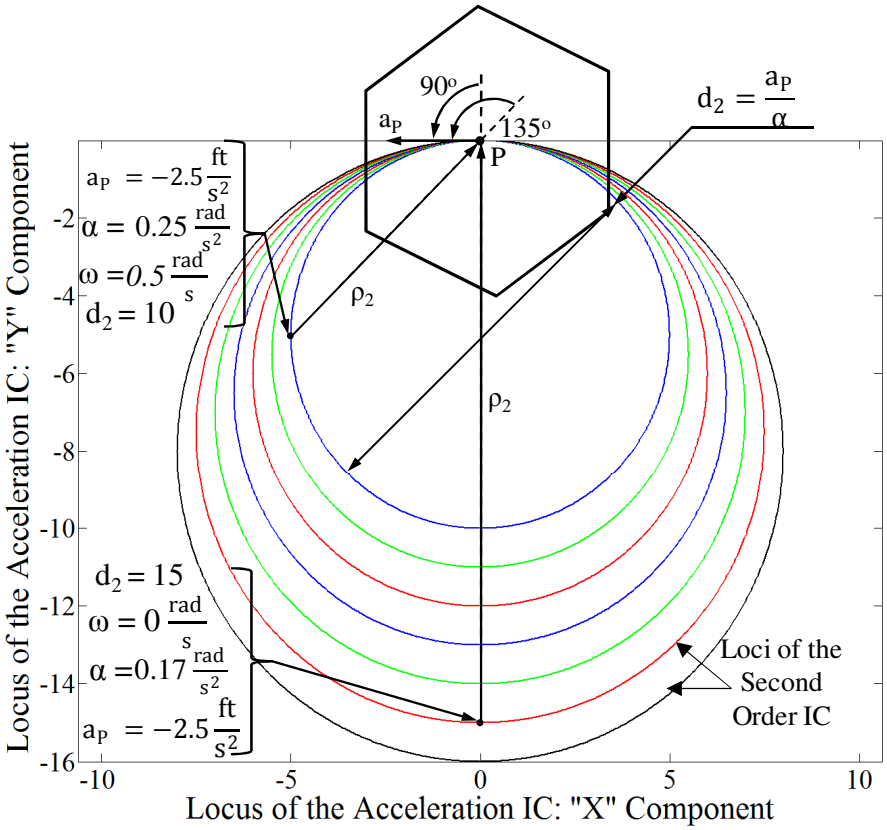

Fig. 4.33: Example Locations of the Second Order IC for Mobile Platforms with *J* Active Caster Wheels

shown in Fig. 4.33. The location of the IC is verified using Eq. 4.37 as [*-5, -5*] which is the same location as computed above.

2. In another instant, with the same linear acceleration requirement, ($a_P = -2.5\frac{ft}{s^2}$), let the platform angular motion requirement is such that, the angular velocity ω be $0\ \frac{rad}{s}$ and the angular acceleration α be $0.17\ \frac{rad}{s^2}$. With this information, the value of parameter d_2 is computed as 15 and the second order orientation angle β_2 is 90°. This is shown in Fig. 4.33 as well.

Each circle in the simulation represents a ratio $d_2 = a_P/\alpha$ of linear and angular acceleration while the specific location of IC is dependent on the orientation angle β_2, ($\beta_2 = tan^{-1}(\alpha/\omega^2)$) tangent of the ratio of the angular acceleration and the angular velocity squared. Note that this set of loci is independent of platform geometry and size and could

be used across platforms for visualization/operation. Using this formulation, operator can specify the platform motion in the following different ways:

1. Choose a_p, ω and α; determine I_2 (could be determined by choosing radius ρ_2 of point P with I_2) and β_2.
2. Choose a_P, I_2 and β_2; determine ω and α.
3. Choose I_2, β_2 and ω or α; determine $a_{P,}$ α or ω.

Following are some guidelines for choosing numerical values for various parameters:

1. For a value of a_P, smaller α increases the diameter of the IC circle.
2. Larger values of ω for a particular value of α shift the second order IC across the circle towards point P.
3. Higher ρ_2 results in lower α for a particular value of a_P.

With the known location of the second order IC in frame {0}, the second order motion requirement of the j^{th} wheel subsystem can be computed as follows. We compute the acceleration of the wheel attachment points E_j using Eq. 2.22 for $\ddot{X}_{Ej}$ and $\ddot{Y}_{Ej}$ as follows:

$$\ddot{X}_E = -\omega^2\left[X_{\rho 2} - Y_{\rho 2} tan\, \beta_2\right]$$
$$\ddot{Y}_E = -\omega^2\left[X_{\rho 2} tan\beta_2 + Y_{\rho 2}\right] \qquad \text{Eq. 4.38}$$

This is the total acceleration, a_j, required for wheel subsystem j. We know the location of wheel attachment point E_j in the body fixed frame *{1}* which can be used to compute the location of E_j in frame *{0}* using Eq. 2.1. Also we know the direction, $\sigma_{2(j)}$, of the acceleration, a_j, in global frame {0}. With the current steering angle ψ_j, we can compute the angle between the total acceleration a_j and the steering link. Let's denote this angle as $\zeta_{2(j)}$ which can be computed as:

$$\zeta_{2(j)} = \sigma_{2(j)} - \Theta - \psi_j \qquad \text{Eq. 4.39}$$

Then the required steering and driving input can be computed as:

$$a_{jd} = a_j \cos(\zeta_{2(j)})$$
$$a_{js} = a_j \sin(\zeta_{2(j)}) \qquad \text{Eq. 4.40}$$

This is the acceleration of the j^{th} wheel subsystem. The acceleration of all the other subsystems can be similarly computed and commanded.

4.2.3.1 Computation of Wheel Input Accelerations

The total acceleration required from wheel subsystem *j* is composed in acceleration in wheel rolling direction a_{jd} and in orthogonal direction to rolling a_{js} as expressed in Eq. 4.40. To compute the steering and driving input accelerations $\ddot{\theta}$ and $\ddot{\psi}$ respectively, consider a representative 2-DOF wheel subsystem as shown in Fig. 4.34 where the body fixed frame *xy* and inertial reference frame *XY* are coincident and parallel at the instant. Angle ψ is the steering input and angle θ is the driving input of the system.

Due to the steering and driving inputs, the linear acceleration of *E* has the following components:

1. The tangential acceleration due to the acceleration of steering input $\ddot{\psi}$:

The linear acceleration of point *E* due to the angular acceleration of the steering input is

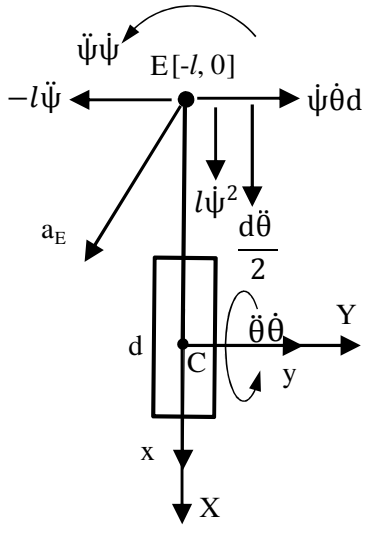

Fig. 4.34: The Linear Acceleration of a Wheel Subsystem

computed as follows:

$$a_{Etangential} = -l\ddot{\psi} \qquad \text{Eq. 4.41}$$

The direction of the tangential acceleration of point E is in the –*Y* direction as shown in Fig. 4.34.

2. Centripetal acceleration of point E due to the angular velocity $\dot{\psi}$ of steering input:

The centripetal acceleration of E due to the steering angular velocity is computed as following:

$$a_{Ecentripetal} = l\dot{\psi}^2 \qquad \text{Eq. 4.42}$$

The direction of the centripetal acceleration is in the *X* direction shown in Fig. 4.34.

3. The linear acceleration of point E due to the driving $\ddot{\theta}$

We studied in Sec 3.2 that when a circle is rolling on a straight line, the relationship between the angular acceleration $\ddot{\theta}$ of the rolling circle and the linear acceleration of the wheel center C is given by (Eq. 3.5):

$$a_{Crelative} = a_{El} = \frac{\ddot{\theta} d}{2} \qquad \text{Eq. 4.43}$$

Note that the total rigid body of the wheel subsystem including the point E has same linear acceleration in the said direction. The direction of the component of acceleration is in the *X* direction as shown in Fig. 4.34.

4. Coriolis acceleration:

The combination of the linear velocity due to the driving $\frac{d\dot{\theta}}{2}$ and steering angular velocity $\dot{\psi}$ results in the Coriolis acceleration which is computed as:

$$a_{Ecoriolis} = 2\dot{\psi}\frac{\dot{\theta}d}{2} = \dot{\psi}\dot{\theta}d \qquad \text{Eq. 4.44}$$

The direction of the Coriolis component of acceleration is in the Y direction as shown in Fig. 4.34.

The total acceleration of point E is the sum of all the components as follows:

$$\ddot{X}_E = l\dot{\psi}^2 + \frac{\ddot{\theta}d}{2}$$
$$\ddot{Y}_E = -l\ddot{\psi} + \dot{\psi}\dot{\theta}d \qquad \text{Eq. 4.45}$$

Using Eq. 4.40 and Eq. 4.45, the driving and steering inputs are computed as follows:

$$\ddot{\theta}_j = 2\frac{a_{jd} - l_j\dot{\psi}_j^2}{d}$$
$$\ddot{\psi}_j = \frac{-a_{js} + \dot{\psi}_j\dot{\theta}_j d_j}{l_j} \qquad \text{Eq. 4.46}$$

4.2.3.2 Third Order Motion Synthesis for the Platforms with Active Caster Wheels

As with the second order, we can specify an instantaneous frame {2} such that its x axis is aligned with the total jerk $\dot{a}_P$ of point P. Then we have:

$$X_P{}^{(3)} = \dot{a}_P$$
$$Y_P{}^{(3)} = 0 \qquad \text{Eq. 4.47}$$

Thus the third order IC for the general *J* wheeled platform is computed as:

$$X_{I3} = \frac{\dot{a}_P(3\omega\alpha)}{(\dot{\alpha} - \omega^3)^2 + (3\omega\alpha)^2}$$
$$Y_{I3} = \frac{\dot{a}_P(\dot{\alpha} - \omega^3)}{(\dot{\alpha} - \omega^3)^2 + (3\omega\alpha)^2} \qquad \text{Eq. 4.48}$$

Let us define a temporary parameter d_3 such that:

$$d_3 = \frac{\dot{a}_P}{\dot{\alpha}} \qquad \text{Eq. 4.49}$$

Using the definition of d_3, we can rearrange Eq. 4.48 as follows:

$$X_{I3} = \frac{\dot{\alpha} d_3 (3\omega\alpha)}{(\dot{\alpha} - \omega^3)^2 + (3\omega\alpha)^2}$$
$$Y_{I3} = \frac{\dot{\alpha} d_3 (\dot{\alpha} - \omega^3)}{(\dot{\alpha} - \omega^3)^2 + (3\omega\alpha)^2} \qquad \text{Eq. 4.50}$$

Note that as with the second order, the third order scalar coefficient d_3 can also have negative and positive values. A simulation plot in Fig. 4.35 shows the loci of third order IC for a set of different values of the scalar coefficient d_3.

As shown, each curve represents a particular numerical value of the scalar parameter d_3. As for the specific location of the third order IC at a particular instant in time, it is dependent on the value of the third order orientation angle β_3 defined in Chapter 2 which is computed as follows:

$$\beta_3 = tan^{-1}\left(-\frac{\dot{\alpha} - \omega^3}{3\omega\alpha}\right) \qquad \text{Eq. 4.51}$$

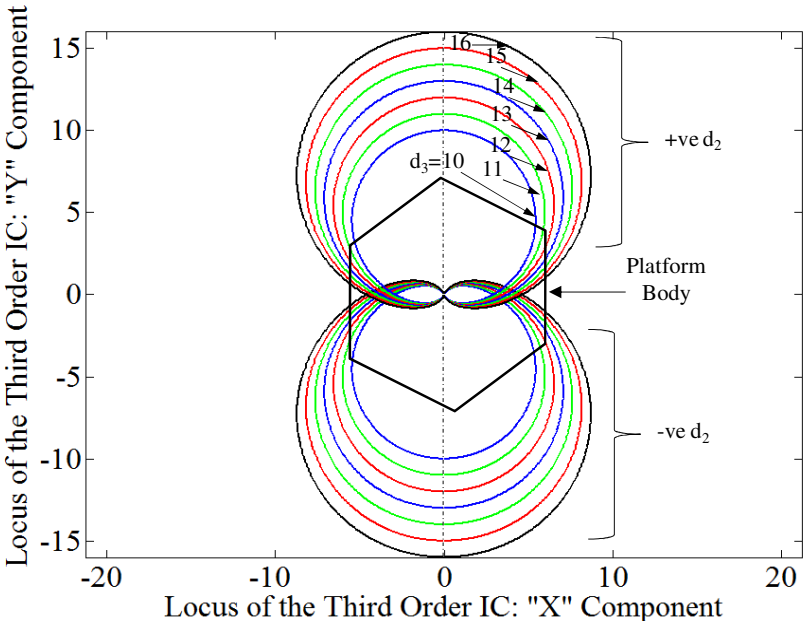

Fig. 4.35: The Loci of the Third Order IC for a General *J* Wheeled Platform with *J* Active Caster Wheels

We will use a numerical example that will elaborate a specific case. At a particular time, let the linear jerk of point P $\dot{a}_P$ be *3.2* $\frac{ft}{s^3}$. Let the angular velocity ω of the platform at the instant be *0.4* $\frac{rad}{s}$, and the angular acceleration α be *0.2* $\frac{rad}{s^2}$ and the angular jerk $\dot{\alpha}$ be *0.2* $\frac{rad}{s^3}$. With these motion parameters, the instantaneous value of the parameter, d_3 given by Eq. 4.49 is computed as 16. With the numerical value of $\dot{\alpha}$, α and ω, the value of the third order orientation angle β_3 (Eq. 2.20) is computed as 150°. With this information, we can locate the instant center as shown in Fig. 4.36. The location of the IC is verified using Eq. 4.50 as *[6.3, 3.57]* which is the same location as computed above.

Each curve in the simulation represents a particular ratio d_3 of linear and angular jerk, $\dot{a}_P$ and $\dot{\alpha}$, respectively. Using this formulation, the operator can choose the operational parameters in the following different ways:

1. Choose $\dot{a}_P$, ω, α and $\dot{\alpha}$; determine I_3 (could be determined by choosing radius ρ_3 of point P from I_3) and β_3.

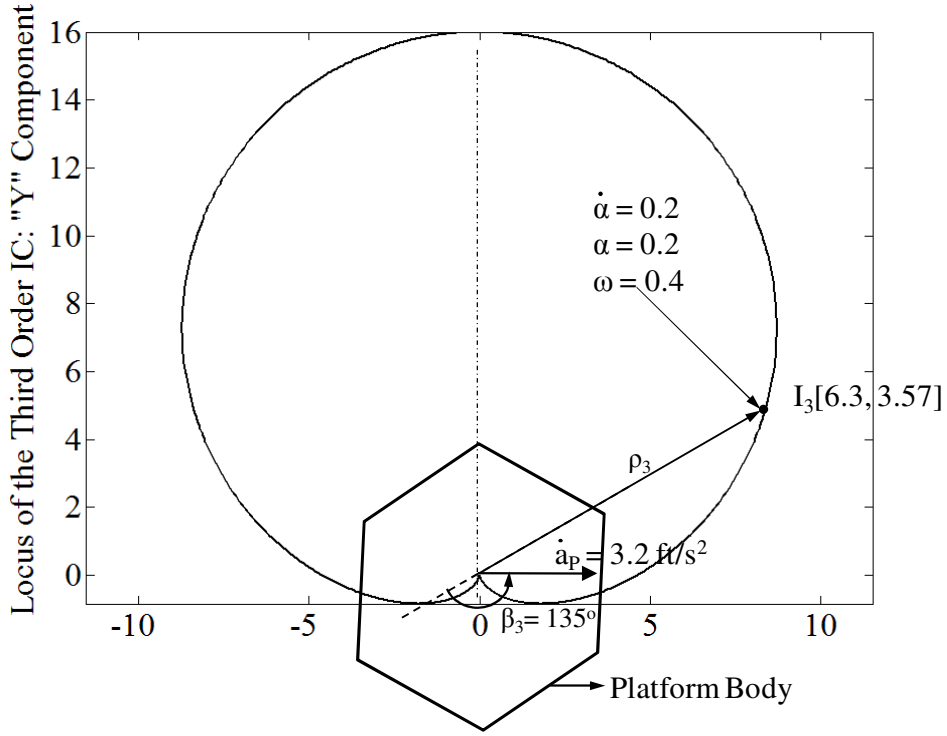

Fig. 4.36: A Numerical Example for the Third Order IC Location

2. Choose $\dot{a}_P$, I_3 and β_3; determine ω, α and $\dot{\alpha}$.

3. Choose I_3, β_3 and ω and α or $\dot{\alpha}$; determine $\dot{a}_P$.and $\dot{\alpha}$ or α.

Following are some guidelines for choosing numerical values for various parameters:

1. For a value of $\dot{a}_P$, smaller $\dot{\alpha}$ increases the scale of the IC locus.

2. Larger values of ω for a particular value of $\dot{\alpha}$ shift the third order IC across the locus circle towards point P.

3. Higher ρ_3 results in lower $\dot{\alpha}$ for a particular value of $\dot{a}_P$ and vice versa.

4. Choosing a small β_3 (between $\frac{\pi}{2}$ and π) (Eq. 4.51) reduces size of α but increases $\dot{\alpha}$. Notice that the magnitude of β_3 can vary between 0 and π. For a particular value of β_3, a large ω decreases $\dot{\alpha}$ by the cube.

5. Choosing a small β_3 (between $\frac{\pi}{2}$ and π) (Eq. 4.51) increases (Fig. 4.36) size of ρ_3 and vice versa.

With the known location of the third order IC in frame $\{0\}$, the third order motion requirement of the j^{th} wheel subsystem can be computed as follows. We compute the jerk of the wheel attachment points E_j using Eq. 2.44 as follows:

$$X_j^{(3)} = -3\omega\alpha\left[\left(X_{\rho 3}\right) - \left(Y_{\rho 3}\right)tan\beta_3\right]$$
$$Y_j^{(3)} = -3\omega\alpha\left[\left(X_{\rho 3}\right)tan\beta_3 + \left(Y_{\rho 3}\right)\right] \qquad \text{Eq. 4.52}$$

This is the total jerk, $\dot{a}_j = \sqrt{\left(X_j^{(3)}\right)^2 + \left(Y_j^{(3)}\right)^2}$, required for wheel subsystem j. We know the location of wheel attachment point E_j in the body fixed frame *{1}* which can be used to compute the location of E_j in frame *{0}* using Eq. 1. Also we know the direction, $\sigma_{3(j)}$, of the jerk, $\dot{a}_j$, in global frame $\{0\}$. With the current steering angle ψ_j, we can compute the angle between the total jerk $\dot{a}_j$ and the steering link. Let's denote this angle as $\zeta_{3(j)}$ which can be computed as:

$$\zeta_{3(j)} = \sigma_{3(j)} - \Theta - \psi_j \qquad \text{Eq. 4.53}$$

Then the required steering and driving input can be computed as:

$$\dot{a}_{jd} = \dot{a}_j \cos(\zeta_{3(j)})$$
$$\dot{a}_{js} = \dot{a}_j \sin(\zeta_{3(j)}) \qquad \text{Eq. 4.54}$$

This is the jerk of the j^{th} wheel subsystem. The jerk of all the other subsystems can be similarly computed and commanded.

4.3 Platforms with Centered Wheels

Fig. 4.37: An Example of Centered Wheel Omnidirectional Robot (Seekur from Mobile Robots Inc., Picture Reproduced from http://robotika.cz/competitions/fieldrobot2009/cs). A Mobile Platform with Four Active Centered Wheels

In the preceding section, we studied the class of mobile platforms that have active caster wheels. A special case of caster wheel is an actively driven and steered wheel that has no offset ($l_j = 0$). As shown by Eq. 4.31, the steering input results in a linear motion of the wheel attachment point orthogonal to the rolling direction because of the location of the steering actuator offset to the vertical wheel axis. The combination of the two orthogonal inputs (steering and driving) results in a linear motion in any direction arbitrarily. In the absence of an offset, the centered wheel lacks this ability (Campion et al., 1996). However, for a motion in a desired direction, the wheel can be steered into the direction using the steering input first and then driven using the driving input. In

summary, the steering input is used as a linear motion input in case of a caster wheel and as a position input in case of a centered wheel. This means that the steering angle ψ_j provides for the velocity vector direction of the powered wheel. Thus a mobile platform composed of multiple 2-DOF centered wheels has an ability to go in any direction by first steering the wheel into that direction, not instantaneously. In absence of an offset, a centered wheel is compact, rugged, and has low passive forces acting due to absence of a moment arm. A centered wheel does not allow passive steering and thus is not fault tolerant to the steering actuator failure. There are two different designs for the centered steered and driven wheels. The traditional design has an actuator for steering and the other for driving similar to the caster wheel design discussed in Sec. 4.2. The alternative designed proposed in (Low and Leow, 2005) is called a dual wheel where two actuators are arranged across rolling axis and drive two adjacent wheels. The steering is achieved by differencing of the two actuator inputs just as a differentially driven platform only at the wheel subsystem level. The advantage of the dual wheel over the prior design is that the two actuators are of the same size and capacity.

4.3.1 DIFFERENT CONFIGURATIONS FOR THE PLATFORMS WITH ACTIVE CENTERED WHEELS

The simplest configuration involving active 2-DOF centered wheel is a tricycle platform with an active centered wheel and two passive fixed trailing wheels. We discussed the configuration in Sec. 4.1.2 under the class of mobile platforms with fixed wheels on either side of the platform body (Sec. 4.1). The following sections discuss various configurations mobile platforms that use two or more active centered wheels. We start with a 2 wheeled configuration

4.3.1.1 Platform with Two Active Centered Wheels

A mobile platform with two active wheels is statically instable and needs passively driven caster wheels for physical support. In case of a rectangular platform, there are two different configurations possible.

Two Laterally Placed Active Centered Wheels

In this case, the active wheels are placed at the center laterally as shown in Fig. 4.38. The translations along any directions can be achieved by steering the active wheels in the direction in a coordinated manner. For rotational motion, either differencing of wheel velocities (when they are oriented parallel to each other) can be used or the two wheels can be oriented so as to cause a rotational motion about the desired instant center. This placement allows turn in place motion. The small distance between the two wheels can result in the magnification of an error in input command.

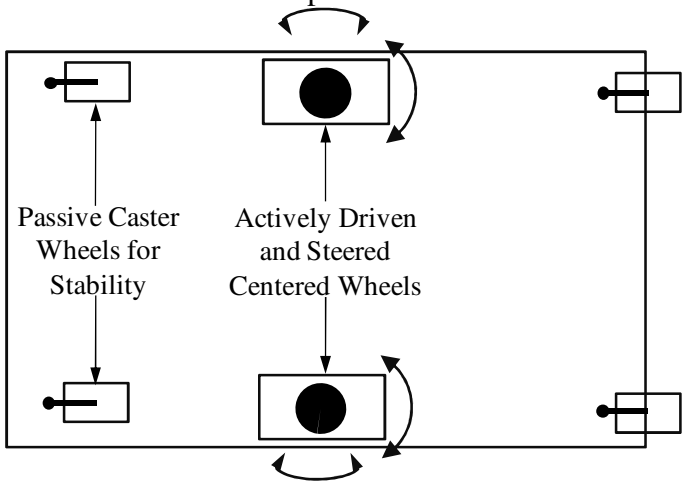

Fig. 4.38: A Mobile Platform with Two Active Centered Wheels Placed Laterally

Two Longitudinally Placed Active Centered Wheels

A longitudinal placement of wheels results in a greater distance between the wheels. This reduces the effect of input error on the overall platform position error. The longitudinal placement also results in better payload distribution across the two active wheels. The translation and orientation control can be achieved by orienting the wheels. Turning in

place can be achieved by rotating the wheels by 90 degrees (to be perpendicular to the platform axis) and then differencing the wheel velocities. As the configuration does not need differential speeds for usual turning it should have a less noisy operation than the former configuration (Fig. 4.39).

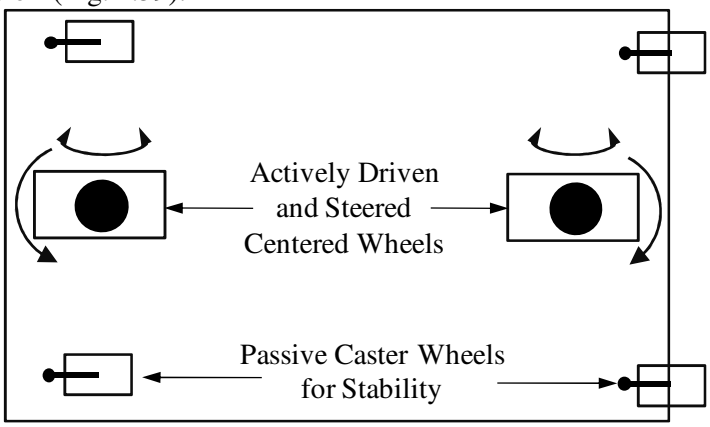

Fig. 4.39: A Mobile Platform with Two Independently Driven and Steered Wheels with Centered Steering

4.3.1.2 Platforms with Three Active Centered Wheels

The platform with three active centered wheels does not need passive wheels for static stability. With only three contact points, the platform makes contact with the ground with all three wheels at all times. As discussed for platforms with Caster wheels, the three wheeled platform may have a tendency to tip over due to an uneven load. A typical configuration for a three wheeled platform is shown in Fig. 4.40.

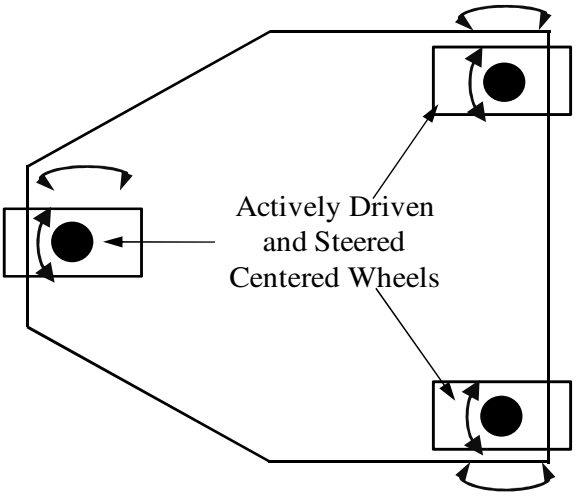

Fig. 4.40: A Mobile Platform with Three Independently Driven and Steered Wheels with Centered Steering

4.3.1.3 Platforms with Four Active Centered Wheels

A platform with four active centered wheels is a balanced configuration and provides stability for tip-over. However, a compliant suspension is needed for all four wheels to maintain contact with the ground. Fig. 4.41 shows a four active centered wheeled platform.

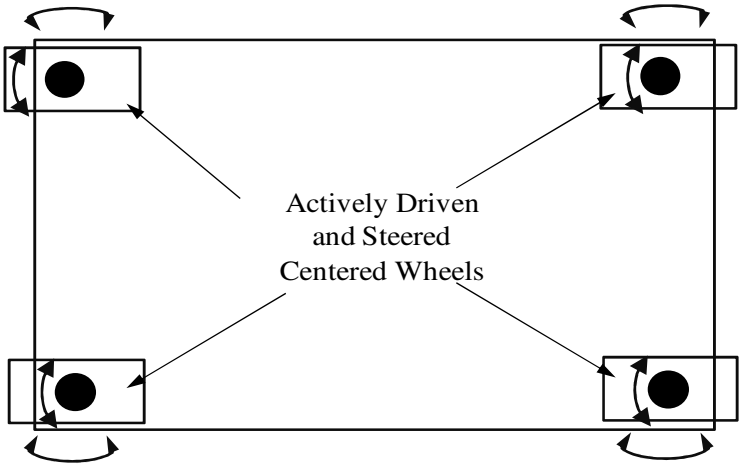

Fig. 4.41: A Mobile Platform with Four Independently Driven and Steered Wheels with Centered Steering

As with the platform with Caster wheels, more than four active centered wheels could be added to support higher payload and to allow for a polygonal (or circular) geometry of

the platform body. The IC based formulation can be generalized so that motion of all the configurations discussed above can be an analyzed and synthesized. The following sections discuss the kinematic formulation for a general J wheeled platform for motion up to the third order.

4.3.2 KINEMATIC DESCRIPTION FOR THE PLATFORMS WITH ACTIVE CENTERED WHEELS

Various geometric parameters of the platform are shown in Fig. 4.42 and described here.

In Fig. 4.42,

{0}: A global fixed reference frame (*OXY*),

${}^{o}r_{P}$: The location of a Point of Interest (POI or *P*) on the platform with respect to frame *{0}*,

{1}: Frame fixed to the platform body (*Pxy*),

Θ*:* The angle frame *{1}* makes with frame *{0}*,

E_j*:* The point of intersection of the vertical axis of wheel *j* with the platform,

e_j*:* The length between E_j and E_{j-1}, values for e_j*'s* may or may not be equal for all wheel subsystems,

θ_j: The rotation of each wheel *j* about its rolling axis. Anticlockwise rotation as seen from E_{j+1} is positive.

ψ_j: The steering angle, angle made by wheel rolling direction with the X axis of Frame *{1}*. In other words, the rotation of each wheel *j* about vertical axis at E_j. Anticlockwise rotation is positive.

d_j: The diameter of wheel *j*, values for d_j*'s* may or may not be equal for all wheel subsystems

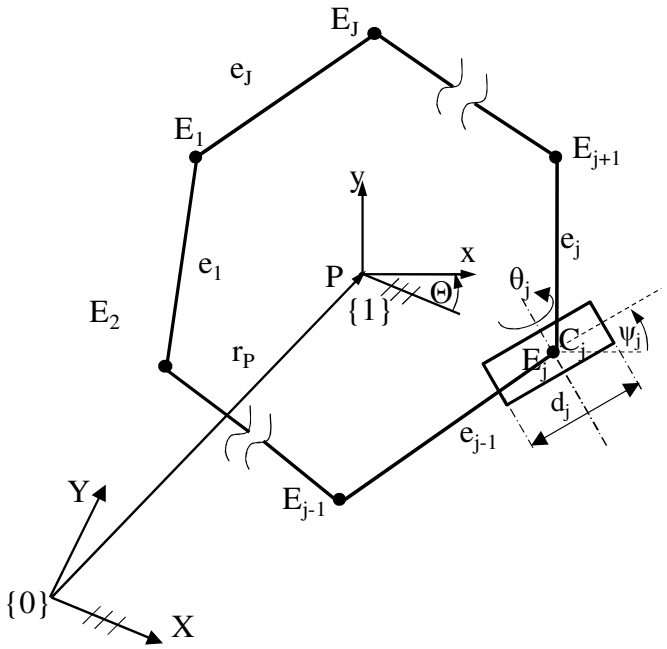

Fig. 4.42: Schematic Representation of a Mobile Platform with *J* Active Centered Wheels

Next, we discuss the first order motion synthesis for the j^{th} wheel subsystems.

4.3.2.1 First Order Motion Synthesis for the Platforms with Active Centered Wheels

The first order motion of the platform at any instant in time is expressed in terms of the linear velocity v_P (in terms of x and y components) of the Point of Interest *P* and the angular velocity ω of the platform body. Based on the required output we locate the velocity IC using Eq. 2.5 as follows:

$$X_{I1} = X_P - \frac{\dot{Y}_P}{\omega}$$
$$Y_{I1} = Y_P + \frac{\dot{X}_P}{\omega} \qquad \text{Eq. 4.55}$$

Using the IC to describe the motion state of point *Ej* helps separate the kinematic and geometric information of the motion. Studying the IC location relative to the body as well as the location of various points of interests in the body relative to the IC provides valuable information about kinematic requirements from the platform. Therefore, we

compute the velocity of the wheel attachment points E_j using Eq. 2.8 for $\dot{X}_{Ej}$ and $\dot{Y}_{Ej}$ as follows:

$$\dot{X}_E = -Y_{\rho 1}\omega$$
$$\dot{Y}_E = X_{\rho 1}\omega \qquad \text{Eq. 4.56}$$

This is the total velocity v_j required for wheel subsystem *j*. We know the location of wheel attachment point E_j in the body fixed frame *{1}* which can be used to compute the location of E_j in frame *{0}* using Eq. 2.1. Also we know the direction, $\sigma_{1(j)}$, of the velocity, v_j, in global frame {0}. With the current steering angle ψ_j, we can compute the angle between the total velocity v_j and the current direction of the wheel. Let's denote this angle as $\zeta_{1(j)}$ which can be computed as:

$$\zeta_{1(j)} = \sigma_{1(j)} - \Theta - \psi_j \qquad \text{Eq. 4.57}$$

This is the position input to the steering actuator. The driving input is computed as:

$$v_j = \dot{\theta}_J \frac{d_j}{2}$$
$$\therefore \dot{\theta}_J = v_j \frac{2}{d_j} \qquad \text{Eq. 4.58}$$

Angle $\zeta_{1(j)}$ and the angular velocity $\dot{\theta}_J$ are the steering and driving input requirements, respectively, for the j^{th} wheel subsystem. We can compute these input requirements for each wheel subsystem similarly. I.e., they may be treated as independent inputs.

4.3.2.2 The Second Order Motion Synthesis for the Platforms with Active Centered Wheels

Similar to the way in which the first order motion is described, the second order motion requirement of the platform can be described in terms of the linear acceleration a_P of the Point of Interest and the angular acceleration α of the platform. Since this is a 3-DOF configuration, we can specify a combination of an arbitrary linear acceleration a_P and angular acceleration α at any instant of time. Let $\ddot{X}_P$ and $\ddot{Y}_P$ be the acceleration for

point P, and ω and α be the angular velocity and acceleration of the platform required at an instant in time. Let a_P be the total acceleration of point P. We can specify an instantaneous inertial reference frame {2} such that its *X* axis is aligned with the direction of a_P as shown in Fig. 4.43. Thus in frame {2} we have:

$$\ddot{X}_P = a_P$$
$$\ddot{Y}_P = 0 \qquad \text{Eq. 4.59}$$

With this motion requirement, the second order IC (given by Eq. 2.18) is located in frame {2} at:

$$X_{I2} = \frac{a_P\,\omega^2}{\alpha^2 + \omega^4}$$
$$Y_{I2} = \frac{a_P\,\alpha}{\alpha^2 + \omega^4} \qquad \text{Eq. 4.60}$$

Let us define a temporary variable d_2 such that:

$$d_2 = \frac{a_P}{\alpha} \qquad \text{Eq. 4.61}$$

Notice that based on the signs of the linear and angular accelerations (a_P and α) at an instant, the value of the scalar coefficient d_2 can be either negative or positive.

Thus the second order IC location is computed as:

$$x_{I2} = \frac{d_2\alpha\omega^2}{\alpha^2 + \omega^4}$$
$$y_{I2} = \frac{d_2\alpha^2}{\alpha^2 + \omega^4} \qquad \text{Eq. 4.62}$$

Using the definition of angle β_2 (Eq. 4.36), Eq. 4.62 can be rearranged as:

$$x_{I2} = \frac{d_2 tan\beta_2}{1 + tan^2\,\beta_2} = -d_2 sin\,\beta_2 cos\,\beta_2$$
$$y_{I2} = \frac{d_2 tan^2\beta_2}{1 + tan^2\beta_2} = d_2 sin^2\beta_2$$

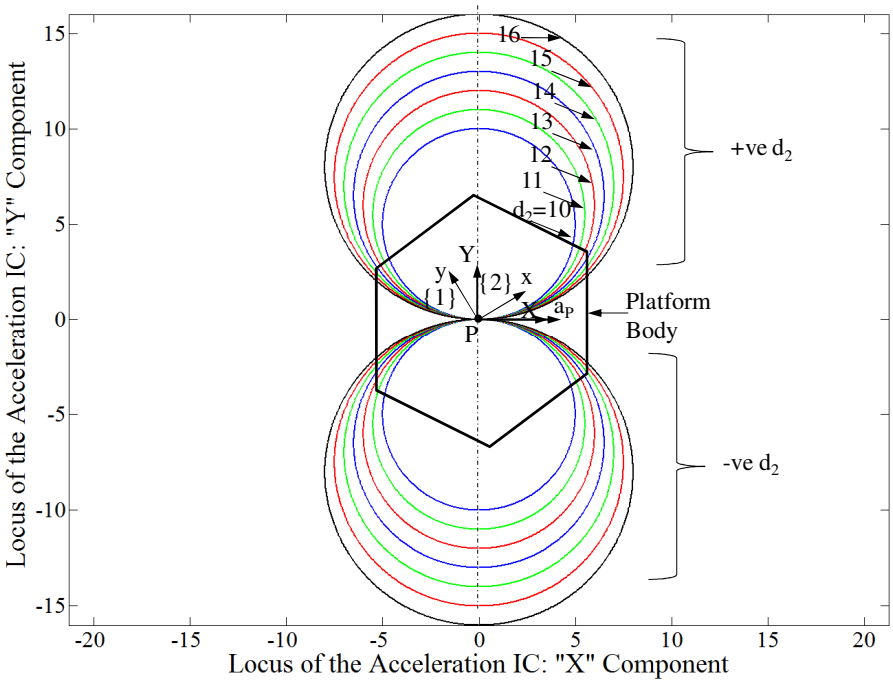

Fig. 4.43: The Loci of the Second Order IC for a General *J* Wheeled Mobile Platforms

After further simplification, the locus of the second order IC is given by following expression:

$$x_{I2} = 0 - \frac{d_2}{2} sin\, 2\beta_2$$
$$y_{I2} = \frac{d_2}{2} - \frac{d_2}{2} cos 2\beta_2 \qquad \text{Eq. 4.63}$$

Eq. 4.63 is a parametric equation of a circle with center at *[0,* $^{d_2}/_2$*]* and radius equal to $^{d_2}/_2$ which shows that the locus of the acceleration IC is a circle of diameter $d_2 = a_P/\alpha$.

Reviewing the parametric equation in Eq. 4.63, we see that the diameter of the circle is a ratio of the instantaneous linear acceleration of point P, a_P, and the angular acceleration, α, of the platform body. The instantaneous location of acceleration IC depends on value of the angle, β_2 (Eq. 4.36), which in turn depends on the values of the angular acceleration α and angular velocity, ω of the circle. A simulation plot in Fig. 4.43 shows the loci of the second order IC for both positive and negative values of d_2.

Let us look at a couple of numerical examples that look at specific scenarios.

3. At a particular time, let the linear acceleration of point P be $-2.5\frac{\text{ft}}{\text{s}^2}$, approximately *1/13th* of gravitational constant (*32.2 ft/s²*). Let the angular velocity ω of the platform at the instant be *0.5* $\frac{\text{rad}}{\text{s}}$, and the angular acceleration α be *0.25* $\frac{rad}{s^2}$. With these motion parameters, the instantaneous value of the parameter, d_2 given by Eq. 4.61 is computed as 10. This is the diameter of the second order IC circle for the particular values of a_P and α. With the numerical value of α and ω, the value of the second order orientation angle β_2 (Eq. 4.36) is computed as 135^o. With this information, we can locate the instant center as shown in Fig. 4.44. The location of the IC is verified using Eq. 4.63 as *[-5, -5]* which is the same location as computed above.

4. In another instant, with the same linear acceleration requirement, ($a_P = -2.5\frac{ft}{s^2}$), let the platform angular motion requirement is such that, the angular velocity ω be *0* $\frac{rad}{s}$ and

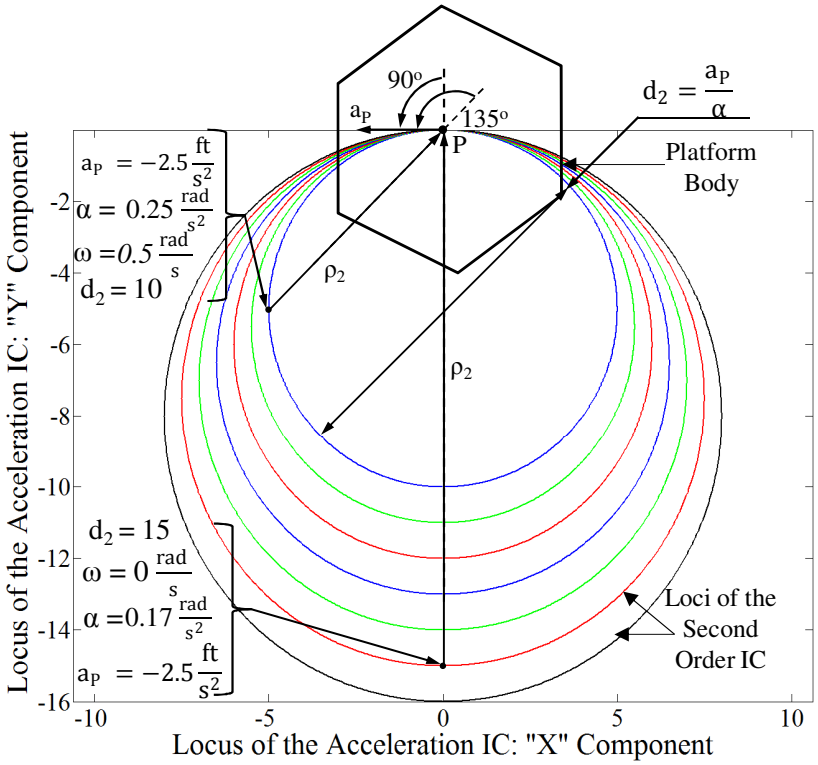

Fig. 4.44: Example Locations of the Second Order IC for Mobile Platforms with *J* Active Centered Wheels

the angular acceleration α be $0.17\frac{rad}{s^2}$. With this information, the value of parameter d_2 is computed as 15 and the second order orientation angle is 90^o. This is shown in Fig. 4.44 as well.

Each circle in the simulation represents a ratio of linear and angular acceleration. Note that this set of loci is independent of platform geometry and size and could be used across platforms for visualization/operation. Using this formulation, operator can choose the operational ways in following different ways:

4. Choose a_p, ω and α; determine I_2 (could be determined by choosing radius ρ_2 of point P with I_2) and β_2.
5. Choose a_P, I_2 and β_2; determine ω and α.
6. Choose I_2, β_2 and ω or α; determine a_P and α or ω.

Following are some guidelines for choosing numerical values for various parameters:

1. For a value of a_P, smaller α increases the diameter of the IC circle.
2. Larger values of ω for a particular value of α shift the second order IC across the circle towards point P.
3. Higher ρ_2 results in lower α for a particular value of a_P.

With the known location of the second order IC in frame $\{0\}$, the second order motion requirement of the j^{th} wheel subsystem can be computed as follows. We compute the acceleration of the wheel attachment points E_j using Eq. 2.20 for $\ddot{X}_{Ej}$ and $\ddot{Y}_{Ej}$. This is the total acceleration, a_j, required for wheel subsystem j. We know the location of wheel attachment point E_j in the body fixed frame *{1}* which can be used to compute the location of E_j in frame *{0}* using Eq. 2.1. Also we know the direction, $\sigma_{2(j)}$, of the acceleration, a_j, in global frame $\{0\}$. With the current steering angle ψ_j, we can compute the angle between the total acceleration a_j and the current direction of the wheel. Let's denote this angle as $\zeta_{2(j)}$ which can be computed as:

$$\zeta_{2(j)} = \sigma_{2(j)} - \Theta - \psi_j \qquad \text{Eq. 4.64}$$

Angle $\zeta_{2(j)}$ is the position input for the steering actuator. The required input for the driving actuator is the linear acceleration a_j.

The following section discusses the third order motion properties of the general mobile platform.

4.3.2.3 Third Order Motion Synthesis for the Platforms with Active Centered Wheels

As with the second order, we can specify an instantaneous inertial reference frame {2} such that its *X* axis is aligned with the total jerk $\dot{a}_P$ of point P. Then we have:

$$X_P{}^{(3)} = \dot{a}_P$$
$$Y^{(3)} = 0 \qquad \text{Eq. 4.65}$$

The location of the third order IC based on the linear jerk of point *P* and the angular motion of the platform is computed as (Eq. 2.38):

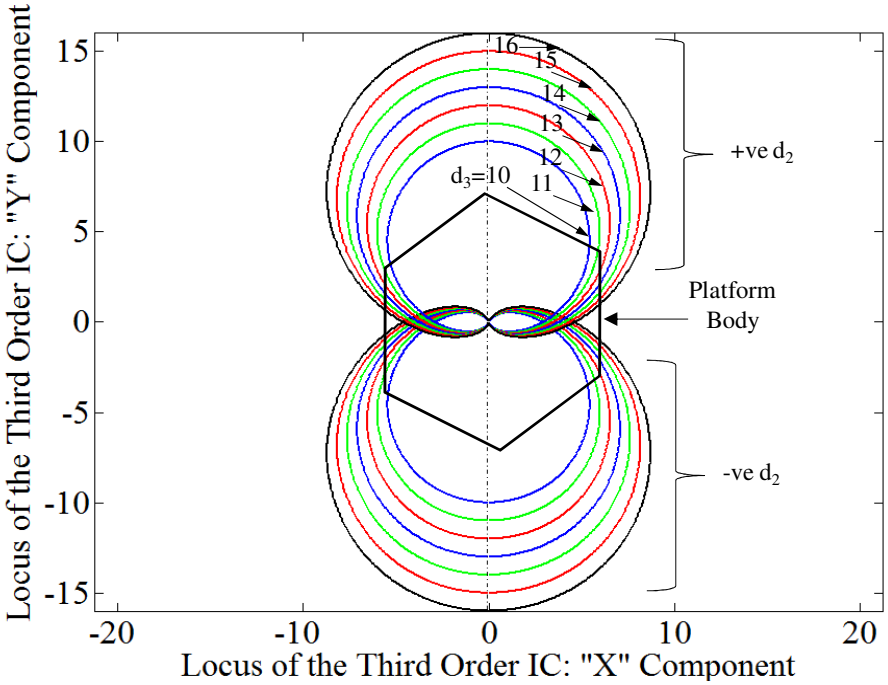

Fig. 4.45: Locus of the Third Order IC for a General Mobile Platform with *J* Centered Wheels

$$X_{I3} = X_P + \frac{X_P^{(3)}(3\omega\alpha) - Y_P^{(3)}(\dot{\alpha} - \omega^3)}{(\dot{\alpha} - \omega^3)^2 + (3\omega\alpha)^2}$$
$$Y_{I3} = Y_P + \frac{X_P^{(3)}(\dot{\alpha} - \omega^3) + Y_P^{(3)}(3\omega\alpha)}{(\dot{\alpha} - \omega^3)^2 + (3\omega\alpha)^2} \quad \text{Eq. 4.66}$$

Using Eq. 4.66, the third order IC for the general *J* wheeled platform is computed as:

$$X_{I3} = \frac{\dot{a}_P(3\omega\alpha)}{(\dot{\alpha} - \omega^3)^2 + (3\omega\alpha)^2}$$
$$Y_{I3} = \frac{\dot{a}_P(\dot{\alpha} - \omega^3)}{(\dot{\alpha} - \omega^3)^2 + (3\omega\alpha)^2} \quad \text{Eq. 4.67}$$

Let us define a temporary parameter d_3 such that:

$$d_3 = \frac{\dot{a}_P}{\dot{\alpha}} \quad \text{Eq. 4.68}$$

Using the definition of the scalar coefficient d_3, we can rearrange Eq. 4.67 as follows:

$$x_{I3} = \frac{\dot{\alpha} d_3(3\omega\alpha)}{(\dot{\alpha} - \omega^3)^2 + (3\omega\alpha)^2}$$
$$y_{I3} = \frac{\dot{\alpha} d_3(\dot{\alpha} - \omega^3)}{(\dot{\alpha} - \omega^3)^2 + (3\omega\alpha)^2} \quad \text{Eq. 4.69}$$

Note that as with the second order, the third order scalar coefficient d_3 also has negative and positive value. A simulation plot in Fig. 4.45 shows the loci of third order IC for a set of different values of the scalar coefficient d_3.

As shown, each curve represents a particular numerical value of the scalar coefficient d_3. As for the specific location of the third order IC at a particular instant in time, it is dependent on the value of the third order orientation angle β_3 ($\beta_3 = tan^{-1}\left(-\frac{\dot{\alpha}-\omega^3}{3\omega\alpha}\right)$). We will use a numerical example that will elaborate a specific case.

At a particular time, let the linear jerk of point P $\dot{a}_P$ be *3.2* $\frac{ft}{s^3}$. Let the angular velocity ω of the platform at the instant be *0.4* $\frac{rad}{s}$, and the angular acceleration α be *0.2* $\frac{rad}{s^2}$ and the angular jerk $\dot{\alpha}$ be *0.2* $\frac{rad}{s^3}$. With these motion parameters, the instantaneous value of

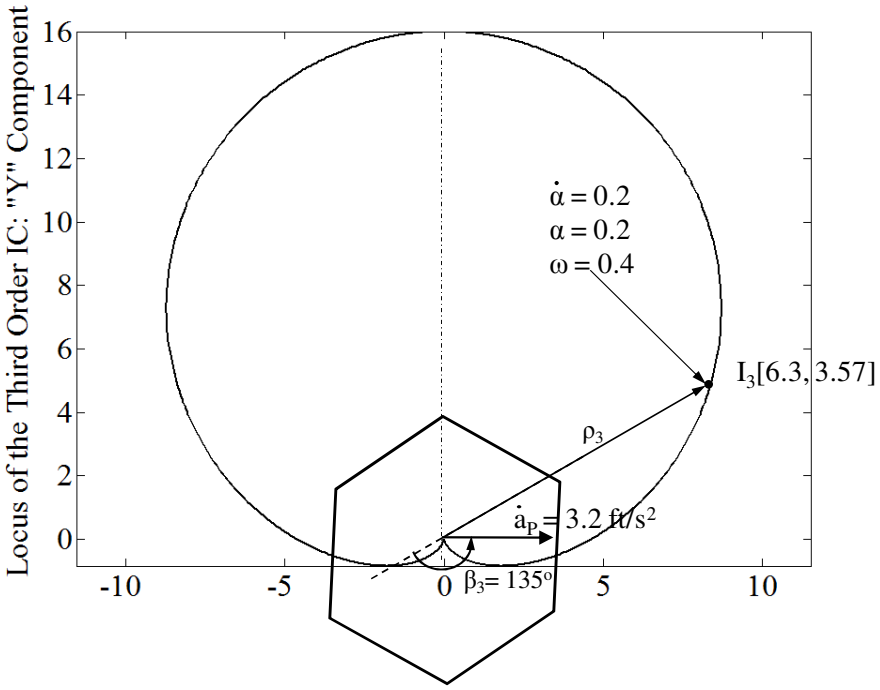

Fig. 4.46: A Numerical Example for the Third Order IC Location

the parameter, d_3 given by Eq. 4.68 is computed as 16. With the numerical value of $\dot{\alpha}$, α and ω, the value of the third order orientation angle β_3 (Eq. 2.20) is computed as 150^o. With this information, we can locate the instant center as shown in Fig. 4.46. The location of the IC is verified using Eq. 4.69 as *[6.3, 3.57]* which is the same location as computed above.

Based on the location of the third order IC, the requirements of the j^{th} wheel subsystem can be computed as follows. We compute the jerk of the wheel attachment points E_j using Eq. 4.52 as follows. This is the total jerk, $\dot{a}_j$, required for wheel subsystem *j*. We know the location of wheel attachment point E_j in the body fixed frame *{1}* which can be used to compute the location of E_j in frame *{0}* using Eq. 2.1. Also we know the direction, $\sigma_{3(j)}$, of the jerk, $\dot{a}_j$, in global frame {0}. With the current steering angle ψ_j, we can compute the angle between the total jerk $\dot{a}_j$ and the steering link. Let's denote this angle as $\zeta_{3(j)}$ which can be computed as:

$$\zeta_{3(j)} = \sigma_{3(j)} - \Theta - \psi_j \qquad \text{Eq. 4.70}$$

Angle $\zeta_{3(j)}$ is the position input for the steering actuator. The required input for the driving actuator is the linear jerk $\dot{a}_j$.

4.4 Platforms with Omnidirectional Wheels

Thus far, we have studied the mobile platforms that use various configurations of conventional wheels. In this section, we will discuss the mobile platforms that employ a class of wheels that are specially designed for omnidirectional capability. A typical design of an omnidirectional wheel has the ability to actively move in rotational direction while it is unconstrained in the direction normal to the plane of the wheel. These designs are sought after because they are intuitive, require minimum actuation and thus may be easy to control (Ferriere et al., 1996).

There are various designs proposed in literature (Pin and Mori, 1994; Borenstein and Evans, 1997; West and Asada, 1992). One of the most widely used designs is called a Mecanum wheel. This wheel was invented in 1973 by Bengt Ilon from Mecanum AB, a Swedish company (Byun and Song, 2003). It has a circular wheel with rollers placed at an angle circumferentially as shown in Fig. 4.47. A special case of this design when the rollers are placed at 90^o (such that the passive direction of the wheel is along the wheel axis) is popularly known as Omni-wheels.

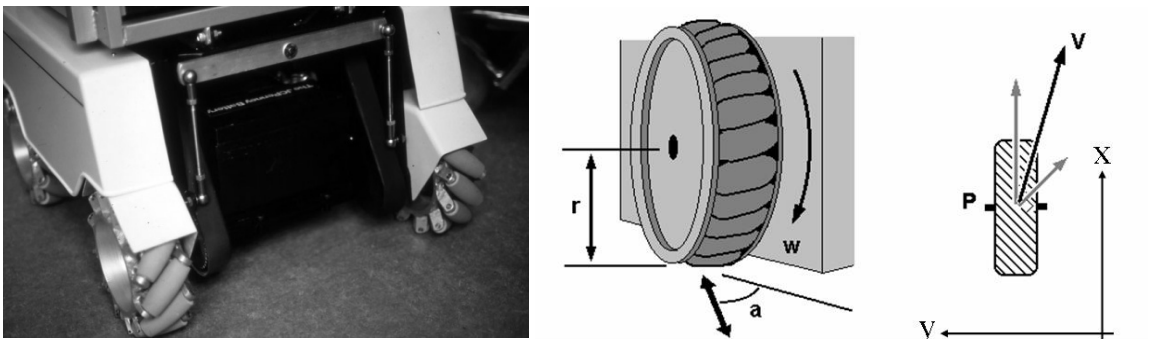

Fig. 4.47: An Illustrative Mecanum Wheel (Picture Reproduced from Wikimedia Commons: http://en.wikipedia.org/wiki/File:IlonWheelchair.jpg)

Fig. 4.48: An Omni-wheel Design (Picture Reproduced from Wikimedia Commons: http://upload.wikimedia.org/wikipedia/commons/d/d9/Yhst-33833170891817_1977_3727729.jpg)

Typically, the rollers are passively driven and transmit a portion of the force applied in the rotational direction to the normal direction of wheel's forward travel. The combination of the forces from all the wheels results in a direction of force which moves the platform in that direction. The initial designs had problems such as having a gap in the two successive rollers which caused noise and vibration, inability to negotiate uneven surfaces, inefficiency due to the fact that the rollers transmit a portion of force in normal direction, all of which have been alleviated to some extent by subsequent efforts (Byun and Song, 2003; Diegel et al., 2002). Some of the other omnidirectional wheel designs are discussed in (Pin and Mori, 1994; Borenstein and Evans, 1997; West and Asada, 1992).

For a 3-DOF unconstrained motion of the platform, we would need a minimum of 3 active inputs. Thus the minimum set of wheels required by a platform with Omni wheels is three. The following section discusses some typical mobile platform configurations that employ Omni-wheels.

4.4.1 DIFFERENT CONFIGURATIONS FOR THE MOBILE PLATFORMS WITH OMNI-WHEELS

4.4.1.1 Mobile Platform with Three Omni-wheels

A three wheeled mobile as shown in Fig. 4.49 has three independently driven wheels arranged symmetrically around the platform. Because of the passive direction, with a three wheel design, there are inherent losses during motion. This is because during motion in any direction, there is at least one wheel bleeding energy because it is not aligned with the direction of motion. However all three wheels always maintain contact with the ground.

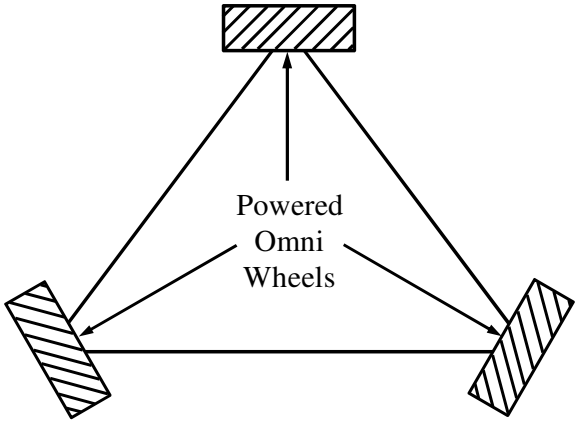

Fig. 4.49: A Mobile platform with Omni Wheels

4.4.1.2 Mobile Platform Configurations with Four Omni wheels

With four wheels it is possible to arrange wheels such that only two wheels are actuated to move in a principle direction, while the other two wheels remain idle. However the configuration needs compliant suspension for all the wheels to maintain contact with ground at all times.

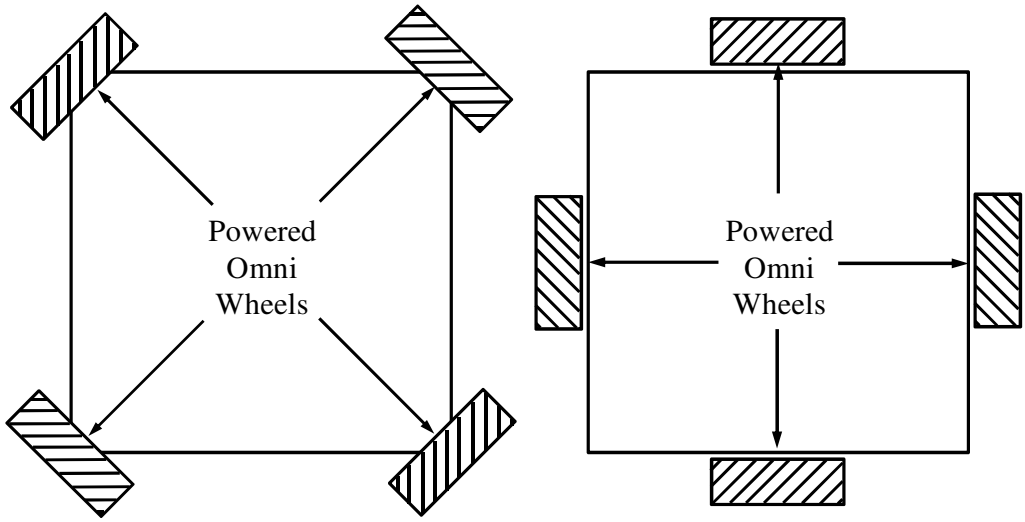

Fig. 4.50: A Mobile Platform with Four Omni Wheels: a) Obliquely Arranged Wheels, b) Wheels Arranged in Principal Directions

An arrangement with more than four wheels is possible in a similar fashion. Note that, in general a fourth wheel configuration is more efficient than a third wheeled configuration, a six wheeled configuration is more efficient than a five wheeled platform and so on because a pair of wheels aligned in a direction can be engaged for motion in that direction keeping other wheels inactive. It can be seen that the payload capacity of the platform is lesser when compared to a similar configuration involving a conventional wheel because of the energy loss and the fact that not all the wheels contribute to the motion at all times.

4.4.2 KINEMATIC DESCRIPTION FOR A GENERAL PLATFORM WITH *J* OMNI WHEELS

The kinematic formulation is done for a general *J* wheeled platform. Various platform geometry parameters of the platform are shown in Fig. 4.51 and described here.

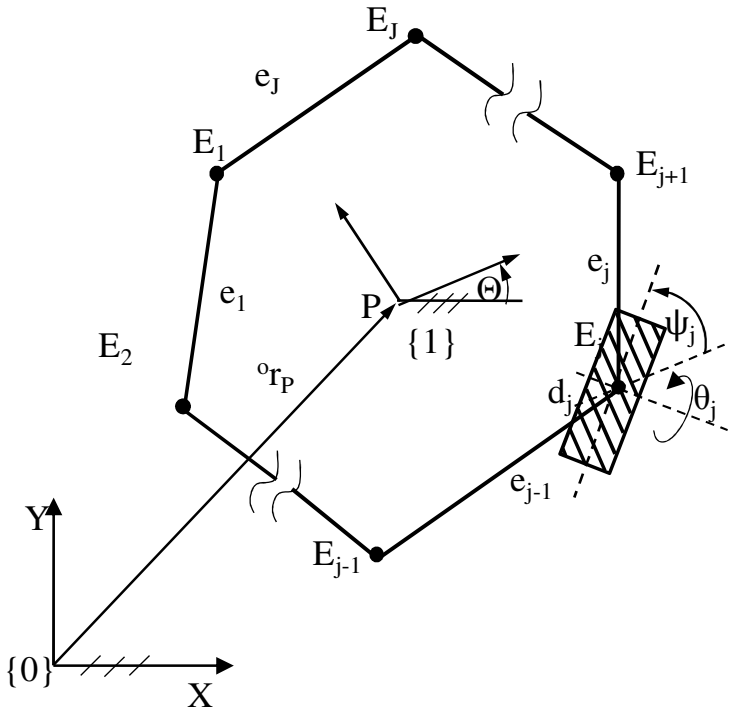

Fig. 4.51: The Schematic Representation of a General Mobile Platform with *J* Omni Wheels

In Fig. 4.51,

{0}: A global fixed frame,

r_P: The location of a point of interest on the platform with respect to frame *{0}*,

{1}: Frame fixed to the platform body,

Θ: The angle frame *{1}* makes with frame *{0}*,

E_j*:* The point of intersection of the vertical axis of wheel *j* with the platform,

e_j*:* The length between E_j and E_{j-1}, values for e_j*'s* may or may not be equal for all wheel subsystems,

θ_j: The rotation of each wheel *j* about its axis. Anticlockwise rotation as seen from E_{j+1} is positive.

ψ_j: The steering angle, angle made by wheel rolling direction with the X axis of Frame *{1}*. Notice that this is a fixed angle for Omni wheels. Anticlockwise rotation is positive. Note that ψ_j is negative in the configuration shown.

d_j: The diameter of wheel j,

Using this notation, the motion synthesis for a general mobile platform with Omni wheels is done as follows.

4.4.2.1 First Order Motion Synthesis for the Mobile Platform with Omni Wheels

The following are the steps to follow for motion synthesis.

- The output space requirements for the mobile platform is expressed in terms of the velocity v_P of point P ($\dot{X}_P$ and $\dot{Y}_P$) and angular velocity ω of the mobile platform.
- Based on the required output, we locate the velocity IC using Eq. 2.5.
- We compute the velocity of the wheel attachment points E_j using Eq. 2.8 for $\dot{X}_{Ej}$ and $\dot{Y}_{Ej}$ (which can also be computed using Eq. 2.2). This is the total velocity, v_j, required for wheel subsystem j.
- We know the location of wheel attachment point E_j in the body fixed frame *{1}* which can be used to compute the location of E_j in frame *{0}* using Eq. 2.1.

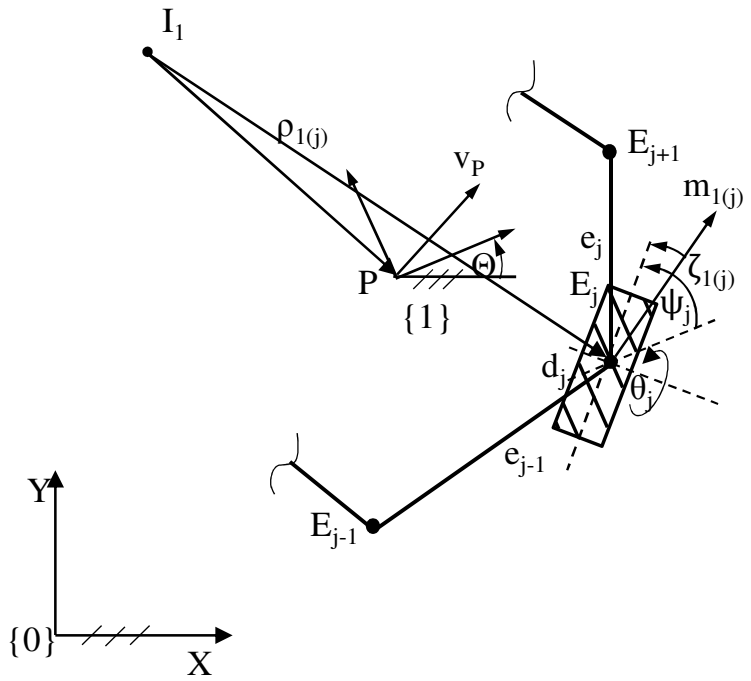

Fig. 4.52: Motion Synthesis for j^{th} Wheel

- Also we know the direction, $\sigma_{1(j)}$, of the velocity, v_j, in global frame {0}. With the steering angle ψ_j, we can compute the angle between the total velocity v_j and the wheel rolling direction. Let's denote this angle as $\zeta_{1(j)}$ as shown in which can be computed as:

$$\zeta_{1(j)} = \sigma_{1(j)} - \Theta - \psi_j \qquad \text{Eq. 4.71}$$

- Then the required driving velocity input for j^{th} wheel can be computed as:

$$v_{jd} = \dot{\theta}_j \frac{d_j}{2} = v_j \cos \zeta_{1(j)} \qquad \text{Eq. 4.72}$$

This is the velocity of the j^{th} wheel subsystem.

A Numerical Example to Demonstrate the First Order Motion Synthesis of Mobile Platform with Omni Wheels:

Consider the four wheeled platform shown in Fig. 4.53. At the particular instant in time, the platform (frame {1}) is oriented at 45° with frame {0}. Let the required operational

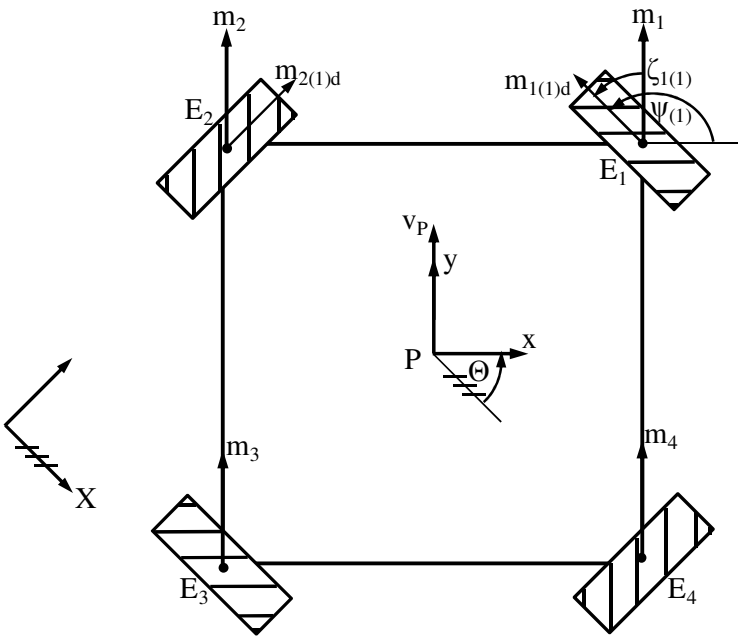

Fig. 4.53: The First Order Motion Synthesis for a Mobile Platform with Four Omni Wheels

space velocity be $\dot{X}_P = -1ft/s, \dot{Y}_P = \frac{1ft}{s} (v_P = 1.414ft/s)$, ω = 0 rad/s. With this, the input velocity for wheel 1 is computed as follows. For wheel 1, the steering angle $\psi_{(1)}$ is 270°. The input velocity $v_{(1)}$ is equal to v_P Thus the value of $\zeta_{1(1)}$ is computed as 45°. Also $v_{(1)}$ = 1.414 ft/s since this is a pure translational motion. The angle $\sigma_{1(1)}$ is computed as 270°. Angle $\zeta_{1(j)}$ is then computed using Eq. 4.71 as 45°. Thus the driving input for wheel 1 is computed using Eq. 4.72 as $2ft/s$. Similarly, the driving wheel input for wheel 2 is also computed as $2ft/s$. The two inputs combine to move the platform by the required point of interest velocity, v_P = 1.414 ft/s (as expressed in frame {1}).

4.4.2.2 The Second Order Motion Synthesis for the Mobile Platform with Omni Wheels

Similar to the way in which the first order motion is described, the second order motion requirement of the platform can be described in terms of the linear acceleration a_P of the Point of Interest and the angular acceleration α of the platform. Since this is a 3-DOF configuration, we can specify a combination of an arbitrary linear acceleration a_P and angular acceleration α at any instant of time. Let $\ddot{X}_P$and $\ddot{Y}_P$be the acceleration for point P, and ω and α be the angular velocity and acceleration of the platform required at an instant in time. Let a_P be the total acceleration of point P. We can specify an instantaneous inertial reference frame {2} such that its *X* axis is aligned with the direction of a_P as shown in Fig. 4.43. Thus in frame {2} we have:

$$\ddot{X}_P = a_P$$
$$\ddot{Y}_P = 0 \qquad \text{Eq. 4.73}$$

With this motion requirement, the second order IC (given by Eq. 2.18) is located in frame {2} at:

$$X_{I2} = \frac{a_P\,\omega^2}{\alpha^2 + \omega^4}$$
$$Y_{I2} = \frac{a_P\,\alpha}{\alpha^2 + \omega^4} \qquad \text{Eq. 4.74}$$

Let us define a temporary variable d_2 such that:

$$d_2 = \frac{a_P}{\alpha} \qquad \text{Eq. 4.75}$$

Notice that based on the signs of the linear and angular accelerations (a_P and α) at an instant, the value of the scalar coefficient d_2 can be either negative or positive.

Thus the second order IC location is computed as:

$$x_{I2} = \frac{d_2\alpha\omega^2}{\alpha^2 + \omega^4}$$
$$y_{I2} = \frac{d_2\alpha^2}{\alpha^2 + \omega^4} \qquad \text{Eq. 4.76}$$

Using the definition of angle β_2 (Eq. 4.36), Eq. 4.62 can be rearranged as:

$$x_{I2} = \frac{d_2 tan\beta_2}{1 + tan^2\,\beta_2} = -d_2 sin\,\beta_2 cos\,\beta_2$$
$$y_{I2} = \frac{d_2 tan^2\beta_2}{1 + tan^2\beta_2} = d_2 sin^2\beta_2$$

After further simplification, the locus of the second order IC is given by following expression:

$$x_{I2} = 0 - \frac{d_2}{2} sin\,2\beta_2$$
$$y_{I2} = \frac{d_2}{2} - \frac{d_2}{2} cos2\beta_2 \qquad \text{Eq. 4.77}$$

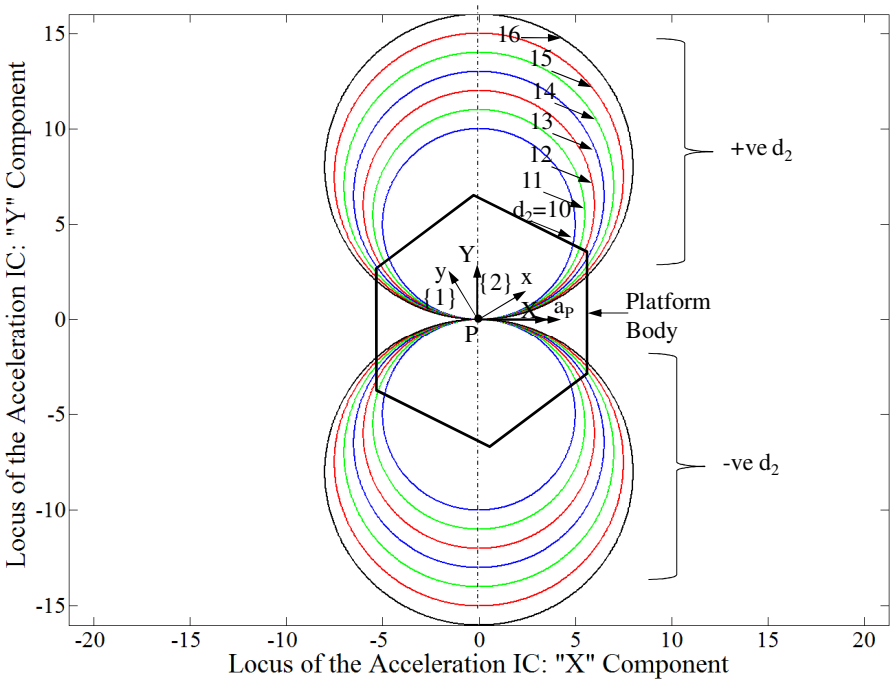

Fig. 4.54: The Loci of the Second Order IC for a General *J* Wheeled Mobile Platforms

Eq. 4.63 is a parametric equation of a circle with center at $[0, {}^{d_2}/_2]$ and radius equal to ${}^{d_2}/_2$ which shows that the locus of the acceleration IC is a circle of diameter $d_2=a_P/\alpha$.

Reviewing the parametric equation in Eq. 4.63, we see that the diameter of the circle is a ratio of the instantaneous linear acceleration of point P, a_P, and the angular acceleration, α, of the platform body. The instantaneous location of acceleration IC depends on value of the angle, β_2 (Eq. 4.36), which in turn depends on the values of the angular acceleration α and angular velocity, ω of the circle. A simulation plot in Fig. 4.43 shows the loci of the second order IC for both positive and negative values of d_2.

Let us look at a couple of numerical examples that look at specific scenarios.

1. At a particular time, let the linear acceleration of point P be $-2.5\frac{\text{ft}}{\text{s}^2}$, approximately *1/13th* of gravitational constant (*32.2 ft/s²*). Let the angular velocity ω of the platform at the instant be *0.5* $\frac{\text{rad}}{\text{s}}$, and the angular acceleration α be *0.25* $\frac{rad}{s^2}$. With these motion parameters, the instantaneous value of the parameter, d_2 given by Eq. 4.61 is computed as 10. This is the diameter of the second order IC circle for the particular values of a_P and α. With the numerical value of α and ω, the value of the second order orientation angle β_2 (Eq. 4.36) is computed as 135^o. With this information, we can locate the instant center as shown in Fig. 4.44. The location of the IC is verified using Eq. 4.63 as *[-5, -5]* which is the same location as computed above.

2. In another instant, with the same linear acceleration requirement, ($a_P = -2.5\frac{ft}{s^2}$), let the platform angular motion requirement is such that, the angular velocity ω be *0* $\frac{rad}{s}$ and

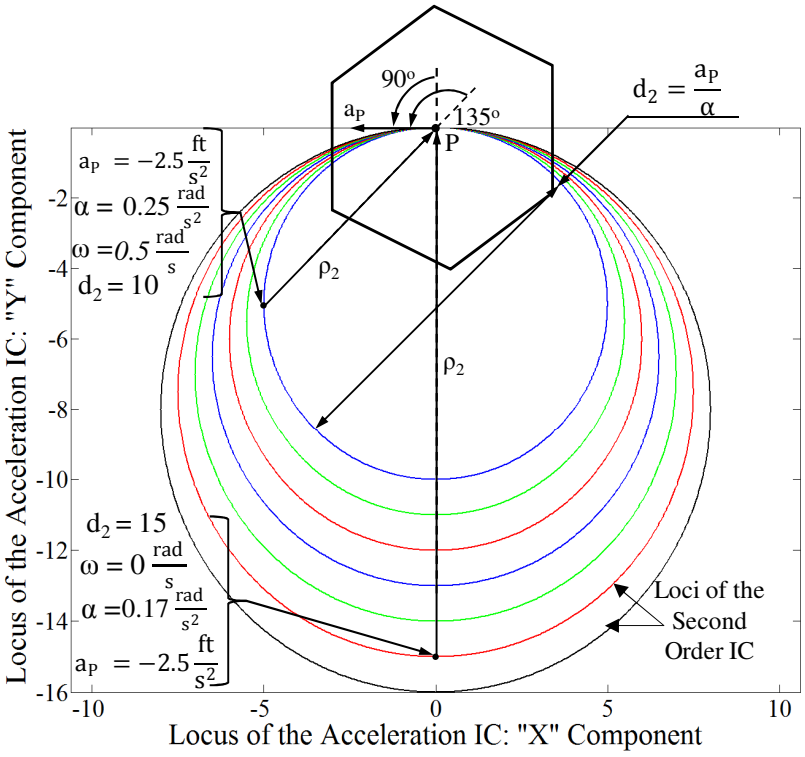

Fig. 4.55: Example Locations of the Second Order IC for Mobile Platforms with *J* Active Centered Wheels

the angular acceleration α be $0.17\frac{rad}{s^2}$. With this information, the value of parameter d_2 is computed as 15 and the second order orientation angle is 90^o. This is shown in Fig. 4.44 as well.

Each circle in the simulation represents a ratio of linear and angular acceleration. Note that this set of loci is independent of platform geometry and size and could be used across platforms for visualization/operation. Using this formulation, operator can choose the operational ways in following different ways:

1. Choose a_p, ω and α; determine I_2 (could be determined by choosing radius ρ_2 of point P with I_2) and β_2.
2. Choose a_P, I_2 and β_2; determine ω and α.
3. Choose I_2, β_2 and ω or α; determine a_P and α or ω.

Following are some guidelines for choosing numerical values for various parameters:

1. For a value of a_P, smaller α increases the diameter of the IC circle.
2. Larger values of ω for a particular value of α shift the second order IC across the circle towards point P.
3. Higher ρ_2 results in lower α for a particular value of a_P.

With the known location of the second order IC in frame $\{0\}$, the second order motion requirement of the j^{th} wheel subsystem can be computed as follows. We compute the acceleration of the wheel attachment points E_j using Eq. 2.20 for $\ddot{X}_{Ej}$ and $\ddot{Y}_{Ej}$. This is the total acceleration, a_j, required for wheel subsystem j. We know the location of wheel attachment point E_j in the body fixed frame *{1}* which can be used to compute the location of E_j in frame *{0}* using Eq. 2.1. Also we know the direction, $\sigma_{2(j)}$, of the acceleration, a_j, in global frame $\{0\}$. With the current steering angle ψ_j, we can compute the angle between the total acceleration a_j and the current direction of the wheel. Let's denote this angle as $\zeta_{2(j)}$ which can be computed as:

$$\zeta_{2(j)} = \sigma_{2(j)} - \Theta - \psi_j \qquad \text{Eq. 4.78}$$

Angle $\zeta_{2(j)}$ is the position input for the steering actuator. The required input for the driving actuator is the linear acceleration a_j.

The following section discusses the third order motion properties of the general mobile platform.

4.4.2.3 Third Order Motion Synthesis for the Mobile Platform with Omni Wheels

As with the second order, we can specify an instantaneous inertial reference frame {2} such that its *X* axis is aligned with the total jerk $\dot{a}_P$ of point P. Then we have:

$$X_P{}^{(3)} = \dot{a}_P$$
$$Y^{(3)} = 0 \qquad \text{Eq. 4.79}$$

The location of the third order IC based on the linear jerk of point *P* and the angular motion of the platform is computed as (Eq. 2.38):

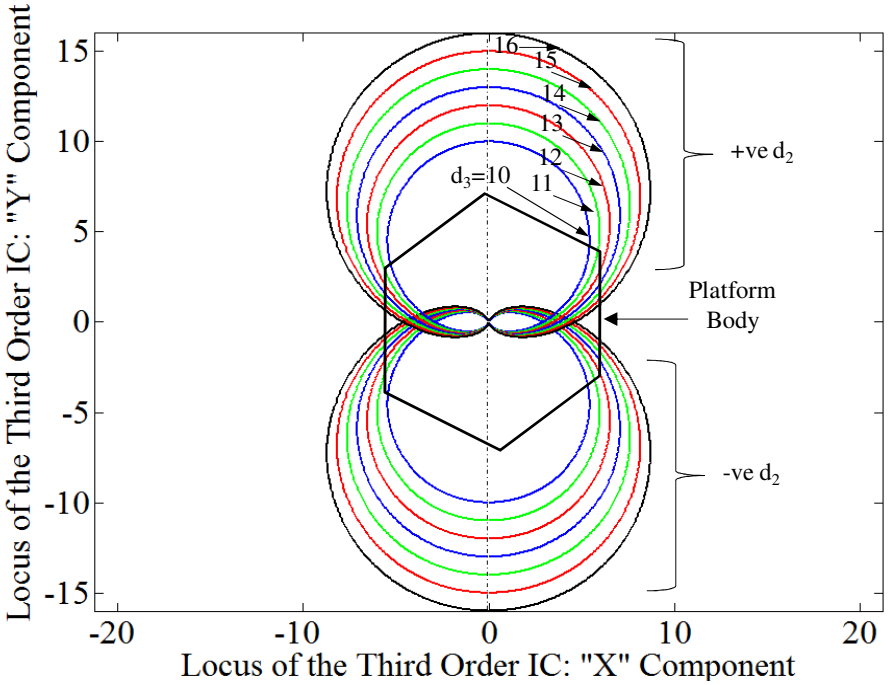

Fig. 4.56: Locus of the Third Order IC for a General Mobile Platform with *J* Centered Wheels

$$X_{I3} = X_P + \frac{X_P^{(3)}(3\omega\alpha) - Y_P^{(3)}(\dot{\alpha} - \omega^3)}{(\dot{\alpha} - \omega^3)^2 + (3\omega\alpha)^2}$$
$$Y_{I3} = Y_P + \frac{X_P^{(3)}(\dot{\alpha} - \omega^3) + Y_P^{(3)}(3\omega\alpha)}{(\dot{\alpha} - \omega^3)^2 + (3\omega\alpha)^2} \quad \text{Eq. 4.80}$$

Using Eq. 4.66, the third order IC for the general *J* wheeled platform is computed as:

$$X_{I3} = \frac{\dot{a}_P(3\omega\alpha)}{(\dot{\alpha} - \omega^3)^2 + (3\omega\alpha)^2}$$
$$Y_{I3} = \frac{\dot{a}_P(\dot{\alpha} - \omega^3)}{(\dot{\alpha} - \omega^3)^2 + (3\omega\alpha)^2} \quad \text{Eq. 4.81}$$

Let us define a temporary parameter d_3 such that:

$$d_3 = \frac{\dot{a}_P}{\dot{\alpha}} \quad \text{Eq. 4.82}$$

Using the definition of the scalar coefficient d_3, we can rearrange Eq. 4.67 as follows:

$$x_{I3} = \frac{\dot{\alpha} d_3(3\omega\alpha)}{(\dot{\alpha} - \omega^3)^2 + (3\omega\alpha)^2}$$
$$y_{I3} = \frac{\dot{\alpha} d_3(\dot{\alpha} - \omega^3)}{(\dot{\alpha} - \omega^3)^2 + (3\omega\alpha)^2} \quad \text{Eq. 4.83}$$

Note that as with the second order, the third order scalar coefficient d_3 also has negative and positive value. A simulation plot in Fig. 4.45 shows the loci of third order IC for a set of different values of the scalar coefficient d_3.

As shown, each curve represents a particular numerical value of the scalar coefficient d_3. As for the specific location of the third order IC at a particular instant in time, it is dependent on the value of the third order orientation angle β_3 ($\beta_3 = tan^{-1}\left(-\frac{\dot{\alpha}-\omega^3}{3\omega\alpha}\right)$). We will use a numerical example that will elaborate a specific case.

At a particular time, let the linear jerk of point P $\dot{a}_P$ be *3.2* $\frac{ft}{s^3}$. Let the angular velocity ω of the platform at the instant be *0.4* $\frac{rad}{s}$, and the angular acceleration α be *0.2* $\frac{rad}{s^2}$ and the angular jerk $\dot{\alpha}$ be *0.2* $\frac{rad}{s^3}$. With these motion parameters, the instantaneous value of

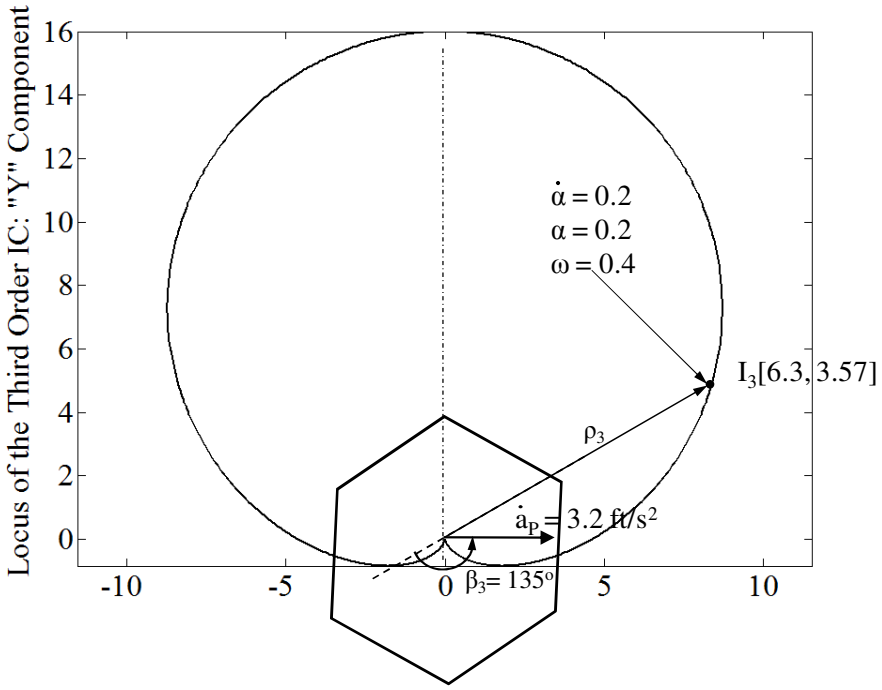

Fig. 4.57: A Numerical Example for the Third Order IC Location

the parameter, d_3 given by Eq. 4.68 is computed as 16. With the numerical value of $\dot{\alpha}$, α and ω, the value of the third order orientation angle β_3 (Eq. 2.20) is computed as 150^o. With this information, we can locate the instant center as shown in Fig. 4.46. The location of the IC is verified using Eq. 4.69 as *[6.3, 3.57]* which is the same location as computed above.

Based on the location of the third order IC, the requirements of the j^{th} wheel subsystem can be computed as follows. We compute the jerk of the wheel attachment points E_j using Eq. 4.52 as follows. This is the total jerk, $\dot{a}_j$, required for wheel subsystem *j*. We know the location of wheel attachment point E_j in the body fixed frame *{1}* which can be used to compute the location of E_j in frame *{0}* using Eq. 2.1. Also we know the direction, $\sigma_{3(j)}$, of the jerk, $\dot{a}_j$, in global frame {0}. With the current steering angle ψ_j, we can compute the angle between the total jerk $\dot{a}_j$ and the steering link. Let's denote this angle as $\zeta_{3(j)}$ which can be computed as:

$$\zeta_{3(j)} = \sigma_{3(j)} - \Theta - \psi_j \qquad \text{Eq. 4.84}$$

Angle $\zeta_{3(j)}$ is the position input for the steering actuator. The required input for the driving actuator is the linear jerk $\dot{a}_j$.

4.5 Summary and Discussions

This chapter studied various mobile platform configurations that are limited to planar motions. We categorized the mobile platform into four distinct categories:

1. Platforms that have one or more fixed wheels (or tracks) on both sides,
2. Platforms with two or more active 2-DOF caster wheels,
3. Platforms with two or more active 2-DOF centered wheels, and
4. Platforms with specially designed omnidirectional wheels.

We showed that the platforms with fixed wheels on both sides are capable of motions that require the platforms to face the direction of travel at all times. We also showed that for these platforms, all the ICs are constrained to lie on the common rolling axis at all times.

The platforms with active caster wheels are truly omnidirectional; i.e., they have ability to move in any direction instantaneously. This allows for all ICs to be arbitrarily placed providing the user with wide range of choices as shown in the demonstrative example (Sec. 4.1.5). Both the steering and driving inputs in this case are used as rate inputs.

The platforms with active centered wheels are also omnidirectional; however before traveling in a direction, the wheels must be steered into the direction of travel first. This is because the steering input is used as a position input here. Again due to omnidirectional capability, locations of all ICs can be arbitrarily chosen giving user wide range of choices.

The platforms with omnidirectional wheels are also truly omnidirectional for more than three wheels. However as shown in Appendix A, they are complex, have low load

capacity, low maintainability, and lack standardization. Table 4.1 compares the four categories of platforms on a qualitative basis.

Table 4.1: Qualitative Comparison of the Four Categories of Planar Mobile Platforms

Platform Configs / *Attributes*	**Fixed Wheels on Both Sides**	**Active Caster Wheels**	**Active Centered Wheels**	**Omnidirectional Wheels**
Dexterity	Low Dexterity	High Dexterity	Good Dexterity	High Dexterity
Ruggedness	High Ruggedness	Moderate Ruggedness	Good Ruggedness	Low Ruggedness
Efficiency	Low Efficiency	High Efficiency	High Efficiency	Least Efficient
Sensitivity to Ground Quality	Least Sensitive	Sensitive	Moderately Sensitive	Most Sensitive
Fault Tolerance	Low Fault Tolerance	High Fault Tolerance	No Fault Tolerance (when Steering Actuator Fails)	Low Fault Tolerance (Zero Fault Tolerance up to the Four Wheeled Configurations)
Number of Actuators per wheel	1	2	2	1

5 DEMONSTRATIVE EXAMPLES OF THE MOTION SYNTHESIS FOR PLATFORMS WITH CONVENTIONAL WHEELS

The goal of this chapter is to investigate the dexterity of the mobile platforms with conventional wheels by presenting a set of motion plan examples. Thus far, we have studied various platform configurations involving conventional wheels. They were categorized into three distinct classes based on their kinematic capabilities as follows:

1. Platforms with active/passive fixed wheels on both sides,
2. Platforms with all active 2-DOF caster (independently driven and offcenter-steered) wheels,
3. Platforms with all active 2-DOF centered (independently driven and center-steered) wheels.

Note that classes 2 and 3 represent all similar platforms with 3 or more active driven 2DOF wheels. This chapter presents a few examples to discuss the dexterity of the class of platforms. For the discussions, we choose the 3 representative platforms as shown in Fig. 5.1, one each from the aforementioned classes as follows:

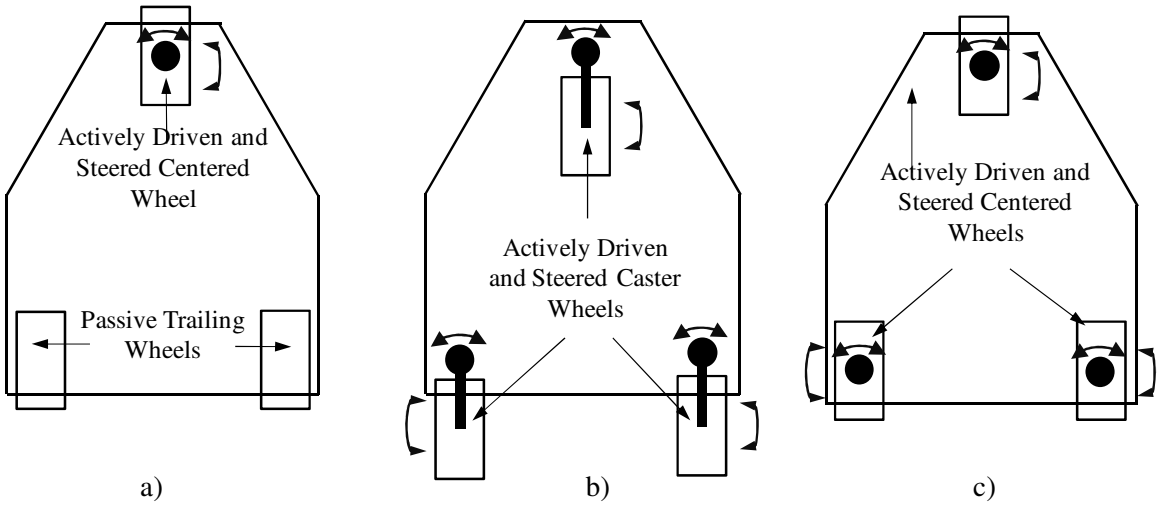

Fig. 5.1: Platform Configurations with Conventional Wheels: a) A Tricycle Platform with a 2-DOF Front Wheel and Two Passive, Trailing, Fixed Wheels; b) A Tricycle Platform with 3 Active (2-DOF) Caster Wheels, and c) A Tricycle Platform with 3 Active (2-DOF) Centerd Wheels

1. A tricycle platform: A platform with a 2-DOF active front wheel and two passive, trailing, fixed wheels,
2. An omnidirectional platform with 3 active (2-DOF) caster wheels,
3. An omnidirectional platform with 3 Active (2-DOF) centered wheels.

For discussion purposes, we choose the three platforms with identical size and shape. Fig. 5.2 shows the geometric parameters for the platforms which are common to all the platforms. The distance between the two rear wheels is *2b* while the distance between the line joining two rear wheels and the front wheels is *3b*. Let the Point of Interest *P* be at the geometric center of the line segment joining the two rear wheel attachment points E_2, and E_3. A body fixed frame {*1*} is attached to the platform with *P* as the origin. The locations of the three wheel attachment points in frame {*1*} are E_1 *[0, 3b]*, E_2 *[-b, 0]*, and E_3 *[b, 0]*. Let the diameter of all the wheels in the platforms be *d*. For caster wheels, let the offset distance of the wheel vertical axis from the wheel attachment point be *l*. Let θ_j be the driving input variable and ψ_j be the steering input variable for the j^{th} wheel as shown in Fig. 5.2.

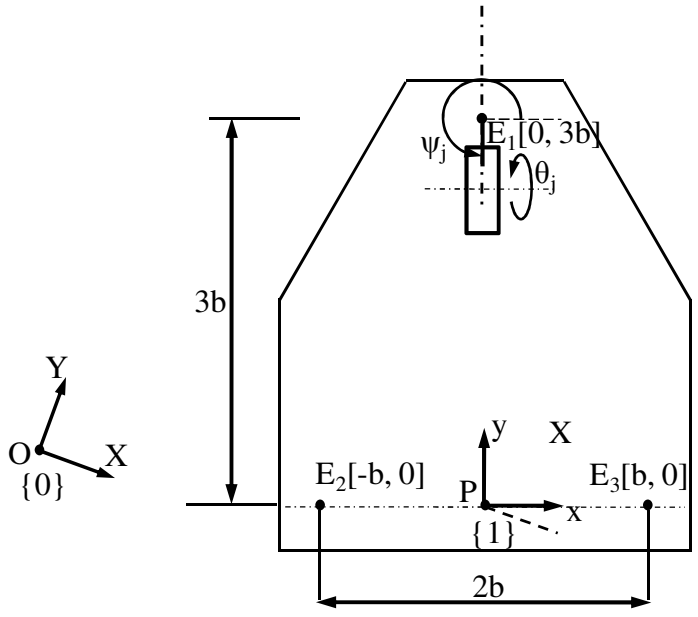

Fig. 5.2: Common Geometric Description of Three Wheeled Platforms

With the geometric description the platforms, we discuss a few scenarios that show the commonalities and differences of the platforms as follows. Note that all dynamic issues (forces, torques, slipping, skidding, etc.) are considered after the motion plan has been developed.

5.1 Straight Line Motion of the Mobile Platforms

In this section we will discuss a scenario when the platforms travel in a straight line motion. There are two ways in which the platforms can travel on a straight line path; namely, when the platforms always face the direction of travel and when the platforms have some angular orientation control along with the straight line motion.

5.1.1 Straight Line Motion without Orientation Change

The simplest motion of the platforms is a motion that involves a straight line motion of the platform in the direction of the platform heading (orientation) as shown in Fig. 5.3.

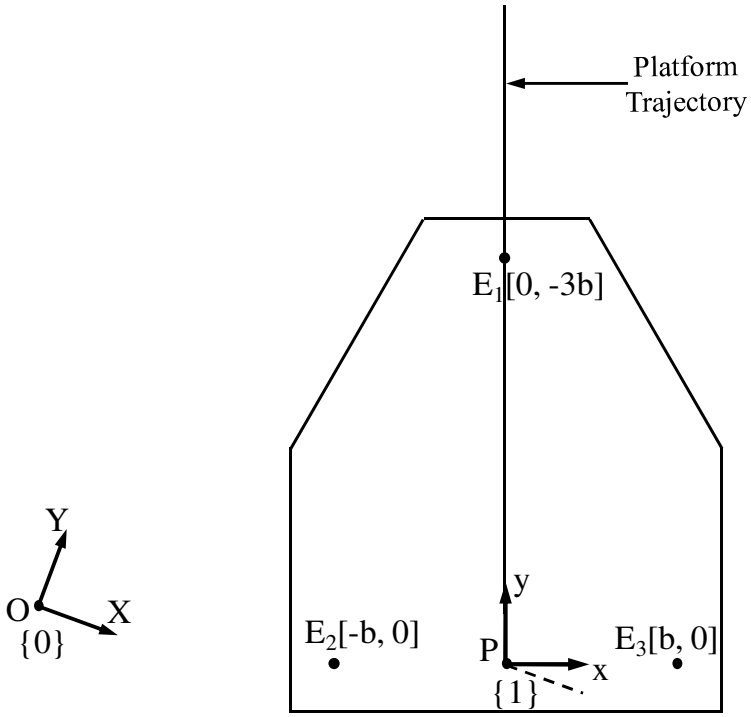

Fig. 5.3: A Straight Line Motion of the Platforms

All the three platforms can accomplish this motion by commanding the driving actuator alone (provided the wheels are initially aligned in the direction of travel) as follows:

$$\dot{\theta}_j = \frac{v_P}{d/2} = 2\frac{v_P}{d}$$

$$\dot{\psi}_j = 0 \text{ and } \psi_j = 270° \; or \; -90° \qquad \text{Eq. 5.1}$$

This input can be commanded to the single active 2-DOF wheel for the tricycle platform as well to all the three active wheels of the other two platforms.

5.1.2 STRAIGHT LINE MOTION WITH ORIENTATION CHANGE

This special motion plan requires that the platform moves in a straight line with a constant velocity v_P while also changing the orientation such that the line joining the two rear wheel attachment points is always directed towards a fixed point in space. Fig. 5.4 shows the motion in discrete steps where the x axis of the body fixed frame passes

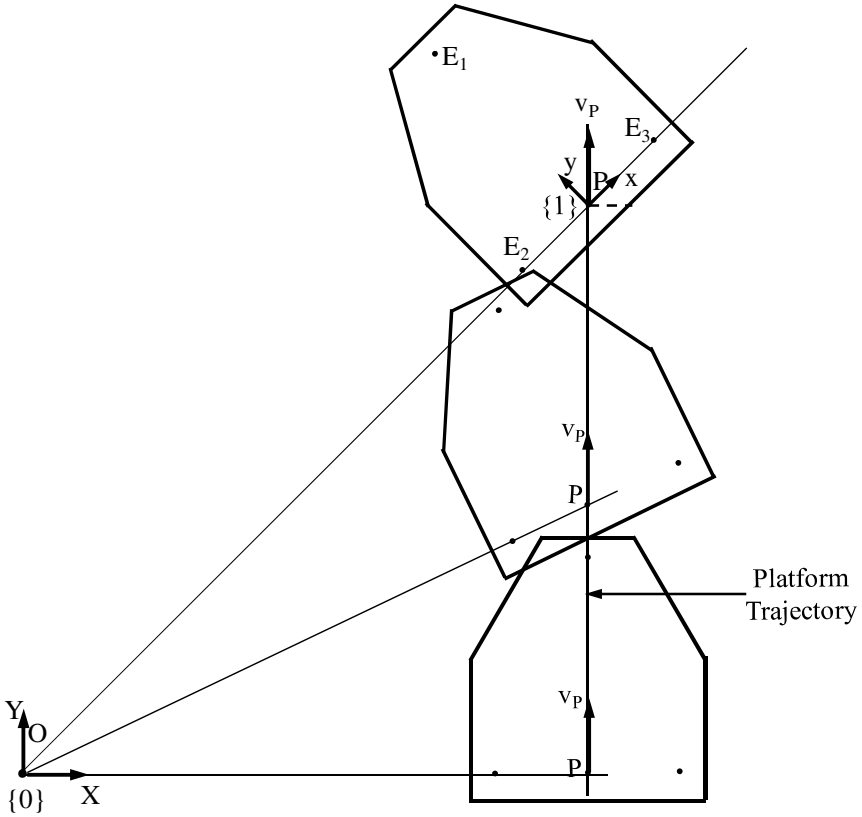

Fig. 5.4: A Straight Line Motion of the Platforms with Orientation Control

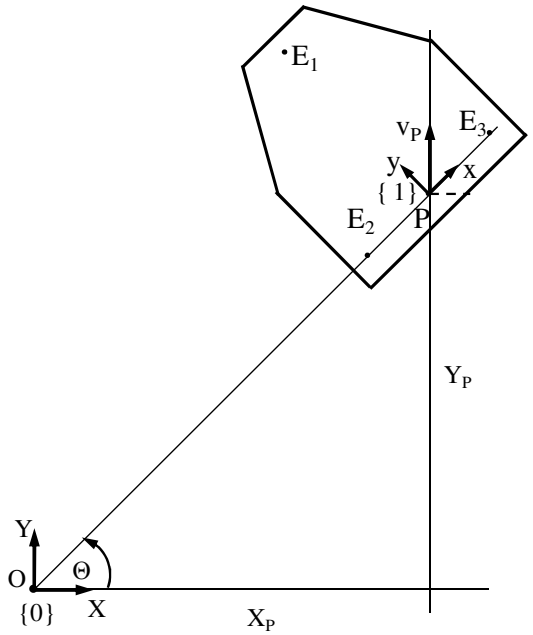

Fig. 5.5: Computation of the Angular Velocity for the Straight Line Motion with Orientation Control

through a fixed point (point O) in space. We have attached an inertial reference frame $\{0\}$ at point O such that its Y axis is oriented in the direction of travel. Thus we have $\dot{Y}_P = v_P$ and $\dot{X}_P = 0$. An example use of this motion plan is a mobile platform traveling in a straight line while a camera mounted on the platform monitors a fixed location in space. Since this motion plan requires a motion along the common axis joining the two rear wheel attachment points E_2 and E_3, the tricycle platform cannot perform this motion. However the two platforms with three active centered wheels and three active caster wheels can accomplish this motion plan. The following section describes the motion synthesis required for this motion.

The motion of the platform is described by the linear velocity v_P of point P and the angular velocity ω of the platform. Fig. 5.5 shows a general mobile platform at a particular instant. The location of point P at the instant is $[X_P, Y_P]$. The orientation of the platform is Θ can be computed as:

$$tan\,\Theta = \frac{Y_P}{X_P} \qquad \text{Eq. 5.2}$$

Differentiating Eq. 5.2, we get:

$$sec^2(\Theta)\,\dot{\Theta} = \frac{\dot{Y}_P}{X_P} \qquad \text{Eq. 5.3}$$

Notice that the *X* component of point P X_P has a constant value at all times. After further simplification we get:

$$\omega = \frac{\dot{Y}_P\,cos^2\,\Theta}{X_P} \qquad \text{Eq. 5.4}$$

The location of the velocity IC is then computed using Eq. 2.5 which is reproduced here:

$$X_{I1} = X_P - \frac{\dot{Y}_P}{\omega}$$
$$Y_{I1} = Y_P + \frac{\dot{X}_P}{\omega} \qquad \text{Eq. 5.5}$$

Substituting the expression for the angular velocity ω (Eq. 5.4), we get:

$$X_{I1} = X_P - \frac{X_P}{cos^2\,\Theta}$$
$$Y_{I1} = Y_P \qquad \text{Eq. 5.6}$$

Eq. 5.6 is a parametric equation of the velocity IC for the motion of a general platform when the platform moves in a straight line such that the x axis of the body fixed frame {1} is directed towards a fixed point in space. The locus of the velocity IC is plotted with the following numerical values for the motion plan:

X_P = 20 ft,

Y_P = *-20 ft* to *20 ft*,

v_P = 4 *ft/s,* Eq. 5.7

b = 2 ft,

d = 2 ft,

l = 2ft.

Due to the range of motion from Y_P = *-20 ft* to *20 ft*, the orientation Θ of the platform changes from -45^o to 45^o. With these values, the locus of the velocity IC is plotted for the

range of motion as shown in Fig. 5.6.

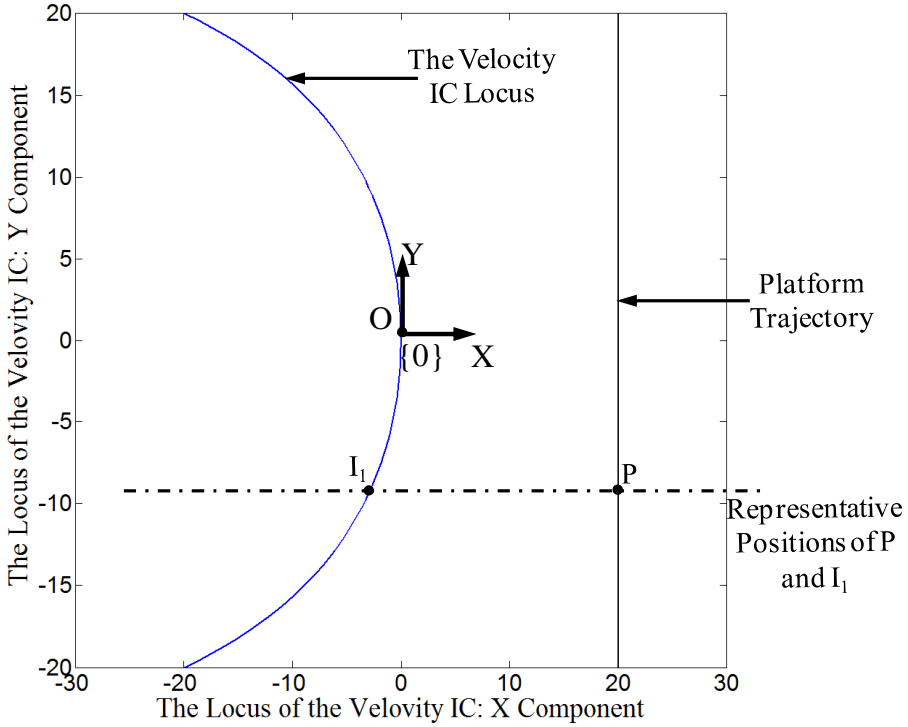

Fig. 5.6: The Locus of the Velocity IC for a Motion of a General Platform Along a Straight Line with Orientation Control

This can be physically verified as follows. As v_P is always directed in Y direction, the velocity IC must be along X direction. The farther away the platform is from point O, the slower the angular velocity will be, shifting the velocity IC away from point P. As an example, an instantaneous location of velocity IC for a representative location of point P is shown in Fig. 5.6.

5.1.2.1 Motion Synthesis: The Platform with Three Centered Wheels

The motion synthesis for the trajectory entails computing the steering angle ψ_j and the driving velocity $\dot{\theta}_j$ for each wheel for the three wheeled mobile platform at each time step based on the location of the velocity IC at that instant. Based on the orientation of the platform and the orientation of the required velocity v_j of the wheel attachment point, the absolute steering angle ψ_j for wheel j can be computed as:

$$\psi_j = \sigma_{1(j)} - \Theta \qquad \text{Eq. 5.8}$$

Where, angle Θ is the orientation of the platform and angle $\sigma_{1(j)}$ is the orientation of wheel velocity v_j in frame {0}. Angle ψ_j is the position input to the steering actuator. The driving input is computed as:

$$v_j = \dot{\theta}_j \frac{d_j}{2}$$
$$\therefore \dot{\theta}_j = 2\frac{v_j}{d_j} \qquad \text{Eq. 5.9}$$

The values of the velocity of the j^{th} wheel subsystem v_j and the velocity orientation angle $\sigma_{1(j)}$ (w.r.t. frame {0}) are computed using the following equations:

$$v_j = \sqrt{\dot{X}_j^{\,2} + \dot{Y}_j^{\,2}}$$

And

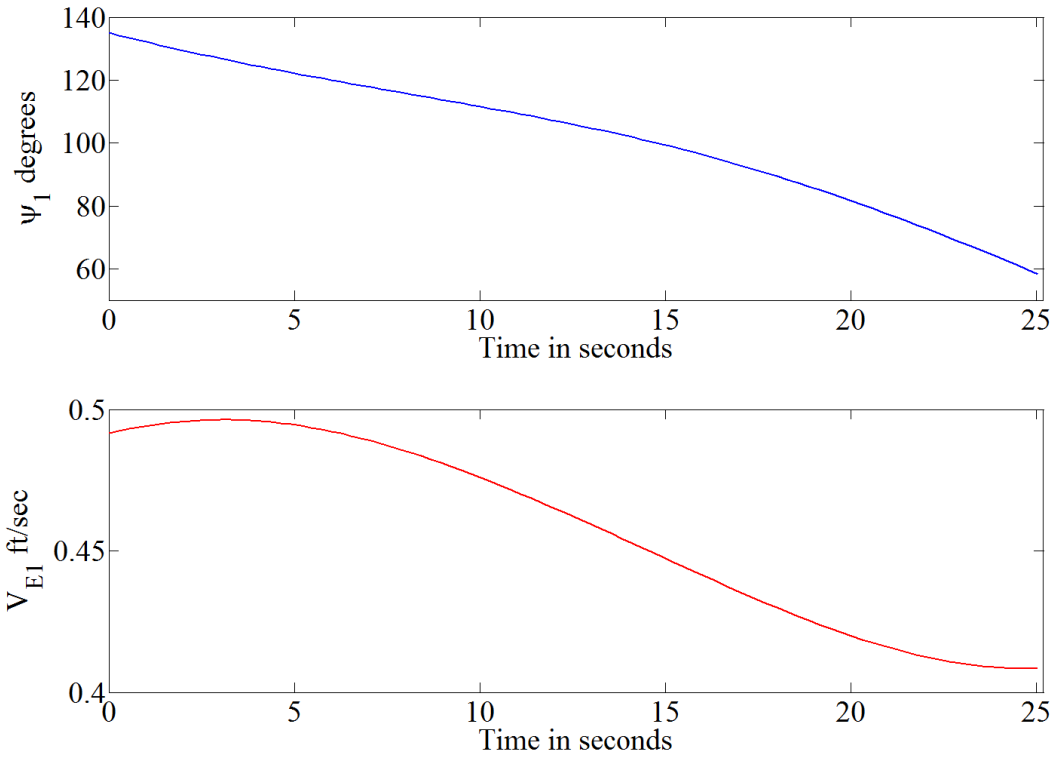

Fig. 5.7: Motion Synthesis for the Front Wheel of the Mobile Platform with Three Active Centered Wheels Undergoing a Straight Line Motion with Orientation Control

$$\sigma_{1(j)} = \tan^{-1}(\frac{\dot{Y}_j}{\dot{X}_j})$$

Where,

$$\dot{X}_{E1} = -Y_{\rho 1}\omega$$

$$\dot{Y}_{E1} = X_{\rho 1}\omega$$

Based on a numerical simulation, the values for the steering and driving inputs for the front wheel (E_1 is the wheel attachment point) of the platform are plotted. Fig. 5.7 shows the plot.

5.1.2.2 Motion Synthesis: The Platform with Three Caster Wheels

The motion synthesis for a mobile platform with active caster wheels requires computing the steering velocity $\dot{\psi}_j$ and the driving velocity $\dot{\theta}_j$ for each wheel j at each time step based on the location of the velocity IC at that instant. To compute the angle at which the total wheel velocity v_j is oriented with respect to the steering link, we use Eq. 4.57 which describes the incremental steering angle $\zeta_{1(j)}$ (Fig. 5.8) as follows

$$\zeta_{1(j)} = \sigma_{1(j)} - \Theta - \psi_j \qquad \text{Eq. 5.10}$$

The driving and steering velocities required are computed using Eq. 4.31 as:

$$v_{jd} = v_j \cos(\zeta_{1(j)})$$
$$v_{js} = v_j \sin(\zeta_{1(j)}) \qquad \text{Eq. 5.11}$$

The driving and steering actuator inputs can then be computed in terms of the respective angular velocities as:

$$\dot{\theta}_j = 2\frac{v_{jd}}{d_j}$$
$$\dot{\psi}_j = \frac{v_{js}}{l_j} \qquad \text{Eq. 5.12}$$

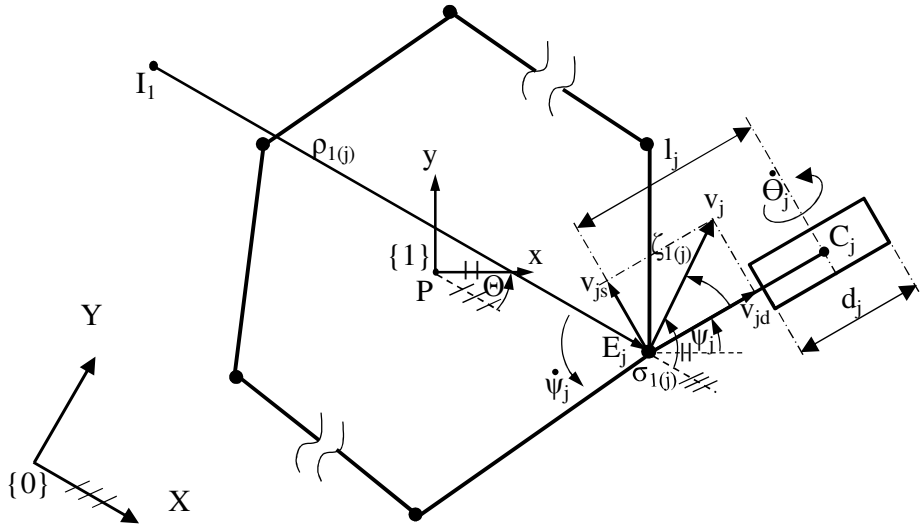

Fig. 5.8: Velocity of Wheel Attachment Point, E_j, Expressed in Terms of the First Order IC.

The values of v_j and $\sigma_{1(j)}$ are computed using the following equations:

$$v_j = \sqrt{\dot{X}_j^{\,2} + \dot{Y}_j^{\,2}}$$

and

$$\sigma_{1(j)} = \tan^{-1}\left(\frac{\dot{Y}_j}{\dot{X}_j}\right) \qquad \text{Eq. 5.13}$$

where

$$\dot{X}_E = -Y_{\rho 1}\omega$$

$$\dot{Y}_E = X_{\rho 1}\omega$$

Using a simulation, the values for the steering and driving inputs $\dot{\psi}_1$ and $\dot{\theta}_1$for the front wheel of the platform are plotted. To compute the incremental steering angle $\zeta_{1(j)}$, we need the initial steering angle for the front wheel. Let it be 225 so that the wheel is facing the Y direction. The plot shown in Fig. 5.9 is generated using a simulation using the numerical values given by on Eq. 5.7.

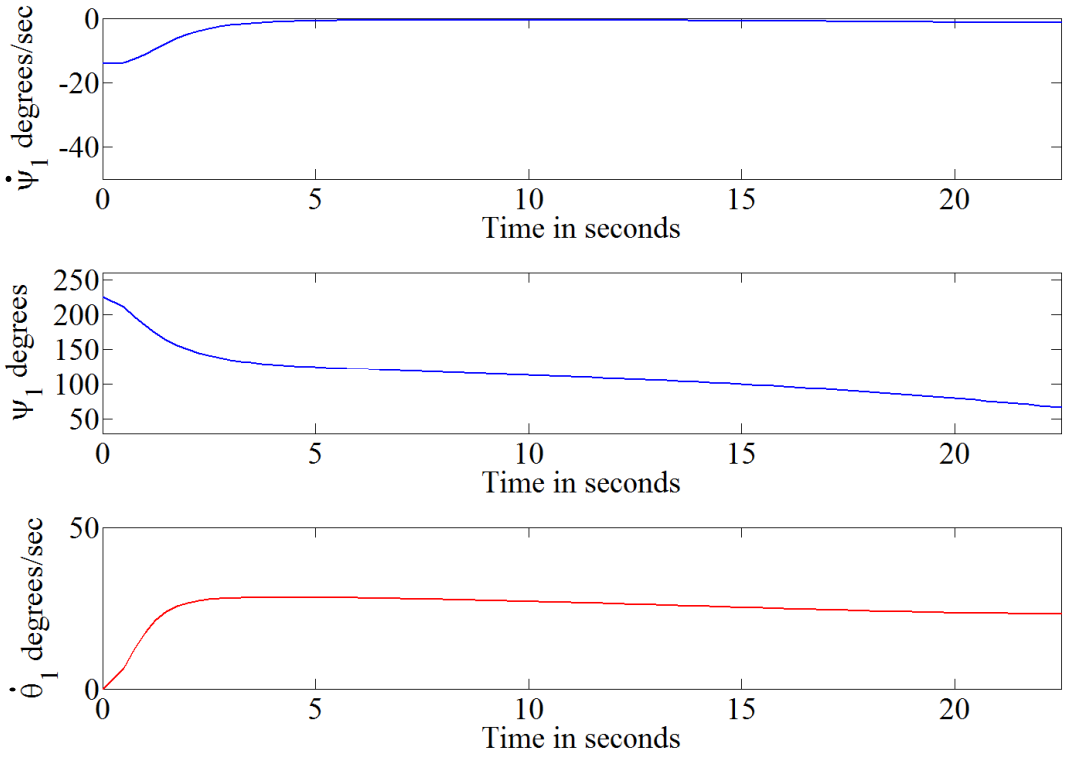

Fig. 5.9: Motion Synthesis for the Front Wheel of the Mobile Platform with Three Active Caster Wheels Undergoing a Straight Line Motion with Orientation Control: Simulation for Initial Steering Angle $\psi_1 = 225^o$

From the simulation plots, we see that there is a large change initially in the steering and driving inputs for the motion synthesis. This is because the initial steering angle ψ_1 was chosen away from the desired chosen angle. This choice resulted in a large incremental steering angle thus requiring large steering input (Note that the steering input is proportional to total velocity by sine of ζ_1). After the initial motion, when the incremental steering angle ζ_1 stabilizes to a small value, we see a steady plot. To show this graphically, a different initial steering angle of 135^o was chosen based on the steering angle value around 2 seconds in the graph shown in Fig. 5.9. This initial steering angle value can also be verified from the motion synthesis for the mobile platform with three centered wheels (Sec. 5.1.2.1) Fig. 5.7. The choice of the initial steering angle results in a smoother plot for steering and driving inputs as shown in Fig. 5.11.

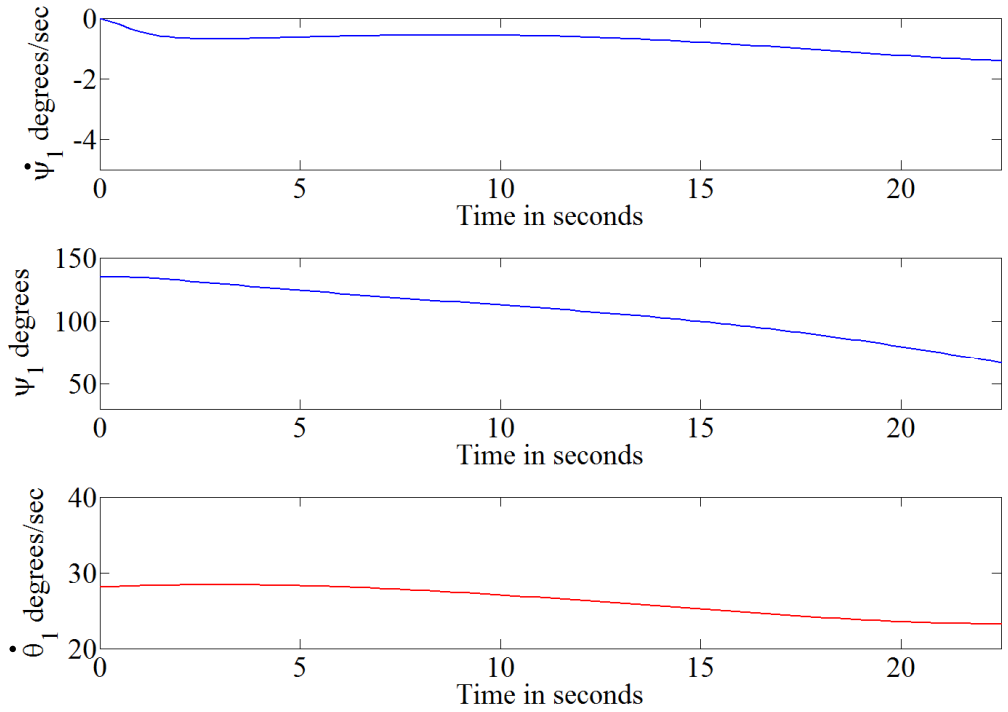

Fig. 5.10: Motion Synthesis for the Front Wheel of the Mobile Platform with Three Active Caster Wheels Undergoing a Straight Line Motion with Orientation Control: Simulation for Initial Steering Angle $\psi_1 = 135^o$

5.2 Circular Motion

Let us consider a scenario in which each of the platforms discussed here travel on a circular path of radius r such that point *P* travels at a constant linear speed v_P.

5.2.1 Circular Motion when Platforms Face the Direction of Travel

When the angular motion of the platform is such that the platform always faces the direction of travel the motion is a 2-DOF motion because the angular velocity of the circular motion is equal to the angular velocity of the platform ω. Thus the motion is achievable by the platform with the fixed trailing wheels as well as by the two platforms with three active 2-DOF wheels. We will examine the dexterity of the three platforms in terms of their motion synthesis options for this motion. Fig. 5.11 shows the three platforms with the fixed trailing wheels undergoing the circular path.

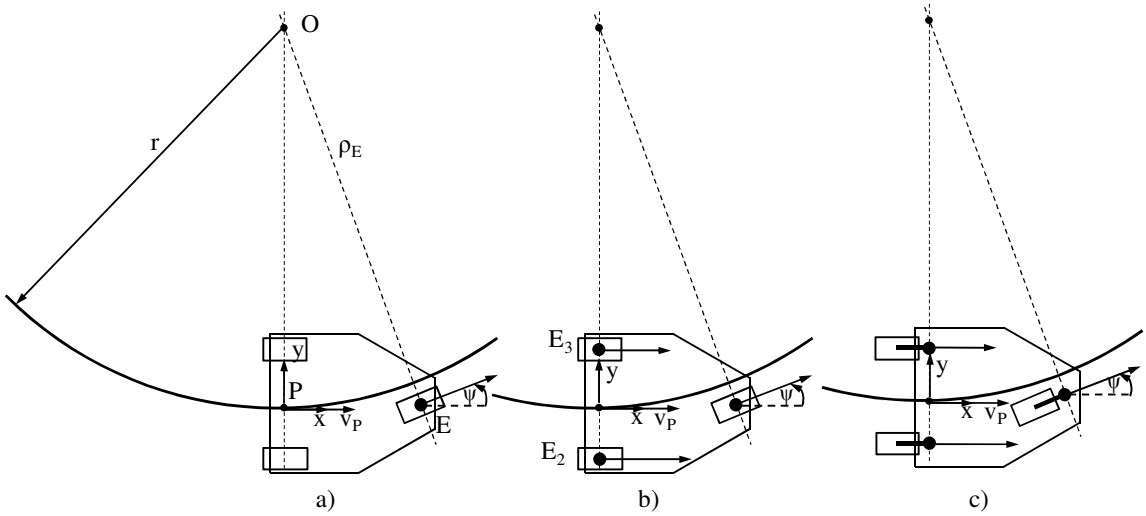

Fig. 5.11: The Mobile Platform with Traveling along a Circular Path

Consider a general mobile platform traversing the circular trajectory as shown as shown in Fig. 5.12. During the course of travel, the angle subtended by corresponding arc is Θ. The initial position of the point of interest, P, on the platform in frame {0} is:

$$X_P = 0$$
$$Y_P = -r \qquad \text{Eq. 5.14}$$

The position of P at the end of the motion in frame {0} is:

$$X_P = r\sin(\Theta)$$
$$Y_P = -r\cos(\Theta) \qquad \text{Eq. 5.15}$$

Differentiating with time, we get:

$$\dot{X}_P = r\cos(\Theta)\,\dot{\Theta}$$
$$\dot{Y}_P = r\sin(\Theta)\,\dot{\Theta} \qquad \text{Eq. 5.16}$$

Thus we can show that the velocity of the point P shown in Fig. 4.12 is computed in frame {1} as:

$$v_P = \dot{x}_P = r\omega$$
$$\dot{y}_P = 0 \qquad \text{Eq. 5.17}$$

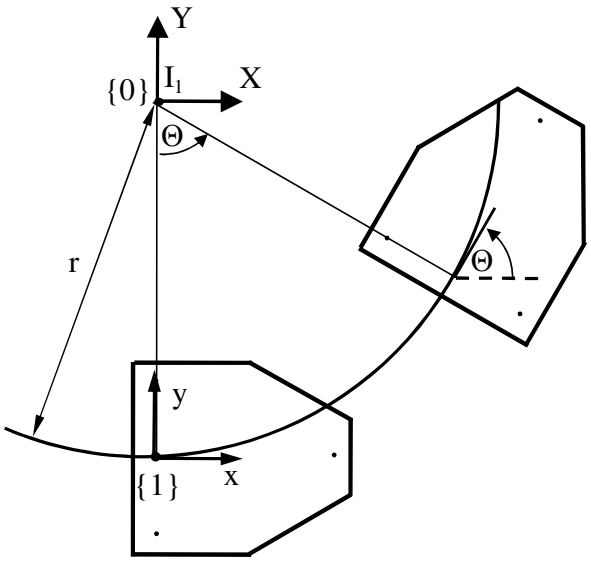

Fig. 5.12: Motion of a General Platform along a a Circular Path when the Mobile Platform Always Faces the Direction of the Motion

The location of the velocity IC depending on the motion requirement in terms of linear velocity, v_P of point P and angular velocity, ω, of the rigid body is computed as (Eq. 2.5):

$$x_{I1} = 0$$
$$y_{I1} = \frac{\dot{x}_P}{\omega} = r \qquad \text{Eq. 5.18}$$

This is also the location of the center of the circle as expressed in frame {1}. Thus the velocity IC is coincident with the center of curvature of the trajectory at all times. Fig. 5.12 shows the location of the velocity IC for a particular instantaneous motion.

In case of the platform with two fixed trailing wheels, the motion is achieved by the 2-DOF active front wheel as shown in Fig. 5.11-a). We can use Eq. 4.9 to compute the steering angle ψ as follows:

$$\psi = \tan^{-1}\left(\frac{3b}{r}\right) \qquad \text{Eq. 5.19}$$

and Eq. 4.10 to compute the driving velocity for the 2-DOF active wheel as follows:

$$v_E = \rho_1 \omega$$
$$\dot{\theta} = \frac{v_E}{d/2}$$
$$where, \rho_1 = \sqrt{{X_{\rho 1}}^2 + {Y_{\rho 1}}^2} \qquad \text{Eq. 5.20}$$
$$X_{\rho 1} = 3b;\ Y_{\rho 1} = -r\,,$$
$$\omega = {v_P}/{r}$$

In case of the platforms with either three active, centered wheels (Fig. 5.11-b)), or three active, caster wheels (Fig. 5.11-c)), the motion synthesis for the front wheel is done in a manner similar to the front wheel in the earlier case. The two wheels in the back are also active and need to perform a coordinated motion. The wheel velocities for these two wheels are computed using Eq. 4.7 and Eq. 4.8 similar to the case of a skid-steer platform as follows:

$$\dot{X}_{E2} = v_P + b\omega$$
$$\dot{Y}_{E2} = 0$$
$$\dot{X}_{E3} = v_P - b\omega \qquad \text{Eq. 5.21}$$
$$\dot{Y}_{E3} = 0$$

The required wheel inputs in terms of wheel angular velocities are:

$$\dot{\theta}_2 = \frac{\dot{X}_{E2}}{d/2}$$
$$\dot{\theta}_3 = \frac{\dot{X}_{E3}}{d/2} \qquad \text{Eq. 5.22}$$
$$\dot{\psi}_2 = \dot{\psi}_3 = 0;\ \psi_2 = \psi_3 = 270°$$

Thus the 2-DOF motion is achieved in this case by motion synthesis in a coordinated manner for the three active wheeled platforms. For the simulation, we used the radius of the circular path r = 20 ft and the angular velocity ω = 8°/sec. The circular path starts at Θ = 0° up to 90°. The definition is angle Θ is shown in Fig. 5.12. With these values the

constant values of steering angle is 17^o and the driving actuator velocity is 2.79 rad/s.

5.2.2 PLATFORMS TRAVELING ON A CIRCULAR PATH WITH FIXED ORIENTATION

In Sec. 5.2.1, we studied a scenario in which each of the platforms discussed here travels on a circular path such that the platform always faces the direction of travel. In this section, we will consider a scenario when the platform travels on the circular path with a fixed orientation. This path requires a *2-DOF* motion that requires motion in the direction of the axis that connects the two rear wheel attachment points. In case of the tricycle platform, this is the fixed rolling axis and any motion along the axis is not possible. Thus the tricycle platform cannot perform this motion. However the other two platform configurations in consideration, namely, the platform with three active centered wheels and the platform with three active caster wheels, are able to perform the motion as shown in Fig. 5.13. We will discuss the motion plan of the two platforms and show a graph generated by a simulation.

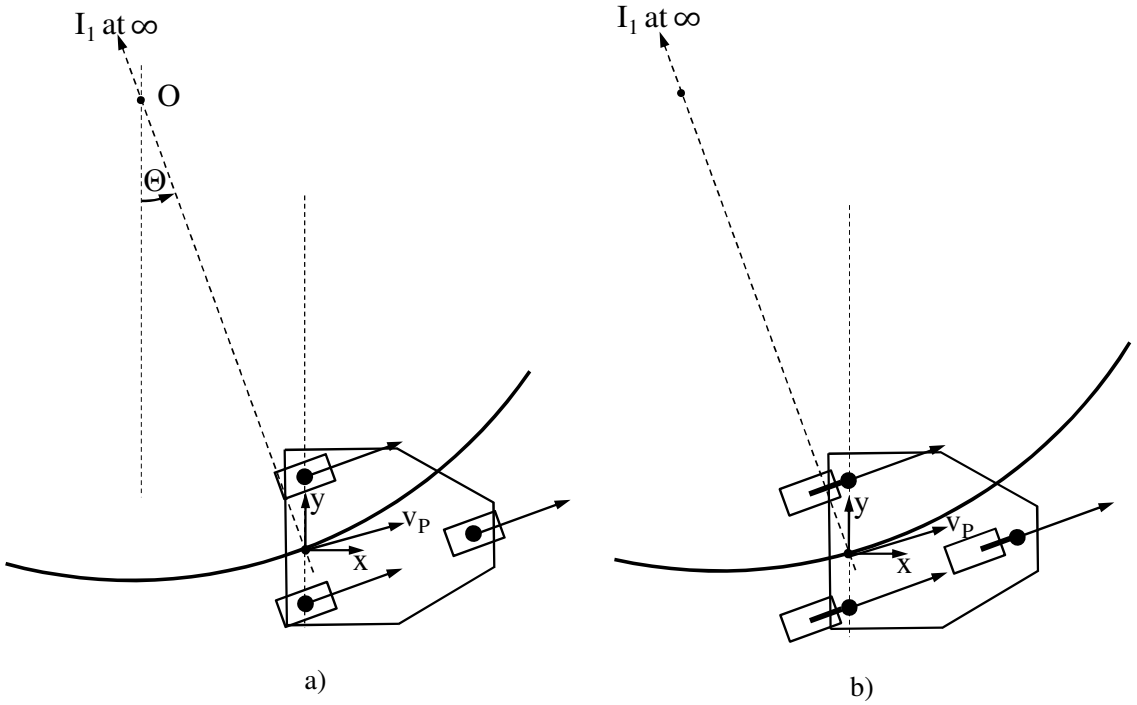

Fig. 5.13: The Mobile Platform with Fixed Wheels Traveling along a Circular Path

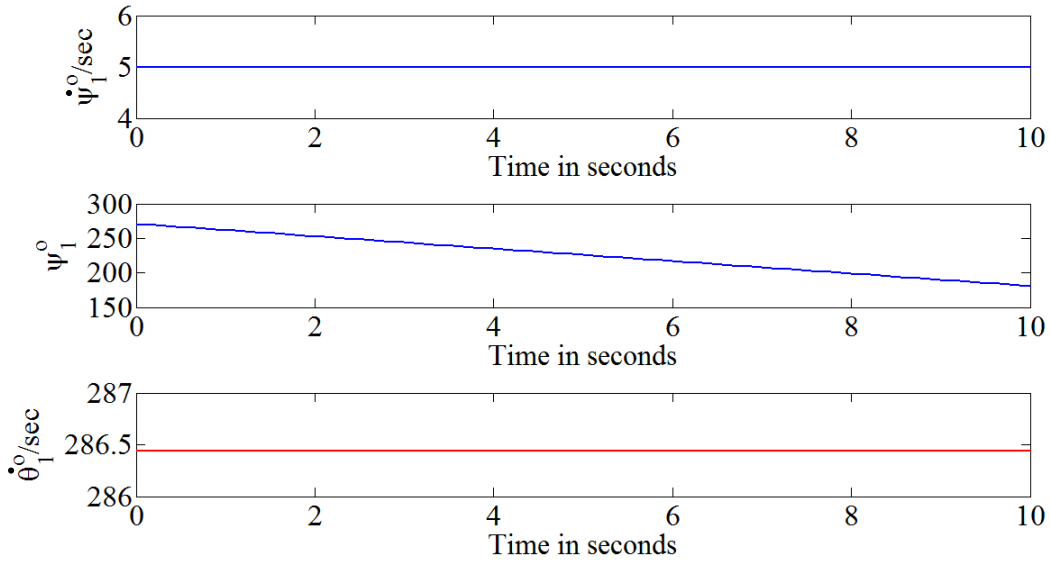

Figure 5.14: Motion Synthesis for the Front Wheel of the Mobile Platform with Three Active Centered Wheels Undergoing a Circular Motion with Fixed Orientation: Simulation

As this is a purely linear motion, the velocity IC is at the infinity at all times during the course of the motion. The simulation was done for the motion of the platform for a quarter of the circular path. The platform starts at the bottom at the circle ($\Theta = 0^o$) and travels counterclockwise for 90^o.

Figure 5.14 shows the plot for the steering actuator velocity $\dot{\psi}_1$, steering angle ψ_1, and driving velocity $\dot{\theta}_1$ for the front wheel for both the platforms, namely, the platform with three centered wheels, and the platform with three caster wheels. Notice that the velocities of the actuators remain constant while the steering angle uniformly changes. The two rear wheels also follow the same motion plan as this is a purely translational motion.

5.3 Discontinuous Path with Straight Lines

So far we have seen the motion of the platforms that involves a smooth and continuous path. In this section, we will discuss the motion synthesis of the platforms that undergo a trajectory that has first order discontinuity i.e., C^1 discontinuity (Farin, G., 2002)

(the curve is continuous in position however the velocity profile along the curve has one or more discontinuities). A typical example of such a path is a path created by two straight line segments at right angles.

5.3.1 C^1 DISCONTINUOUS PATH WITH STRAIGHT LINES WITH ORIENTATION CONTROL

As shown in Fig. 5.15, this motion plan requires the platform to turn by 90^o so that it can always face the direction of travel. All three platform configurations can effectively traverse this path.

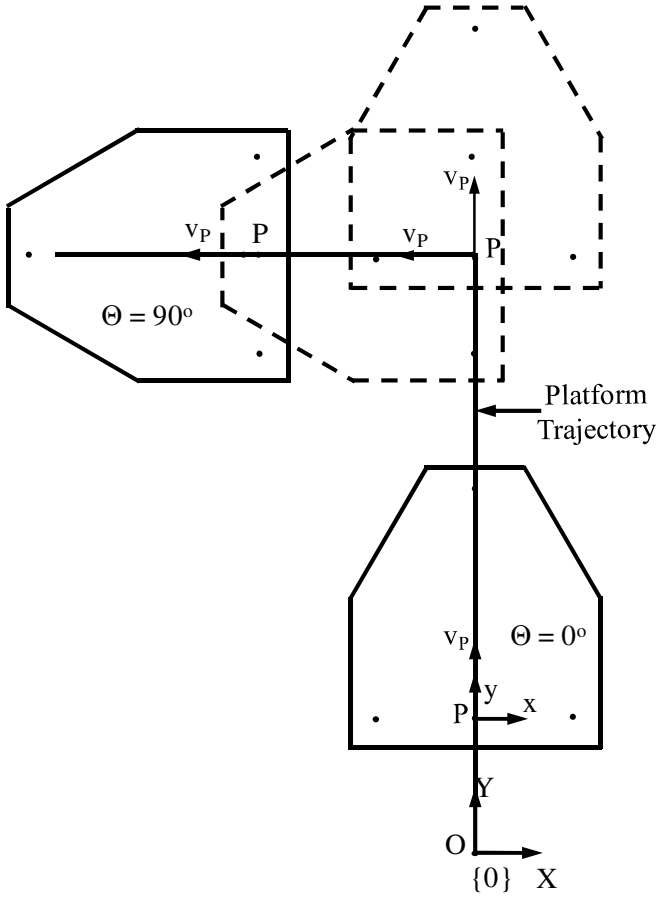

Fig. 5.15: The Mobile Platform Traveling along a Circular Path

For motion synthesis, the description of the trajectory is as follows. Both the straight legs of the path are 15 ft. The path involves a 90^o anti-clock-wise turn. The global frame {0} is oriented such that its Y axis is parallel to the first leg of the path and the negative X

axis is aligned with the second leg. The platform needs to travel at a constant speed of *1.5ft/s* during the straight line motion. Note that this motion plan is just for demonstration purposes and thus does not involve a smooth velocity profile. Generating a smooth motion plan considering the hardware limitations is beyond the scope of this chapter. A simulation is done to show the motion synthesis for the front wheel of the three platforms.

5.3.1.1 Motion Synthesis for the Tricycle Platform or the Platform with Three Active Centered Wheels

Fig. 5.16 shows the motion synthesis parameters for the front wheel of the tricycle platform or the platform with three active centered wheels for a C^1 discontinuous motion (Farin, G., 2002) when the platform faces the direction of the travel. The graph is

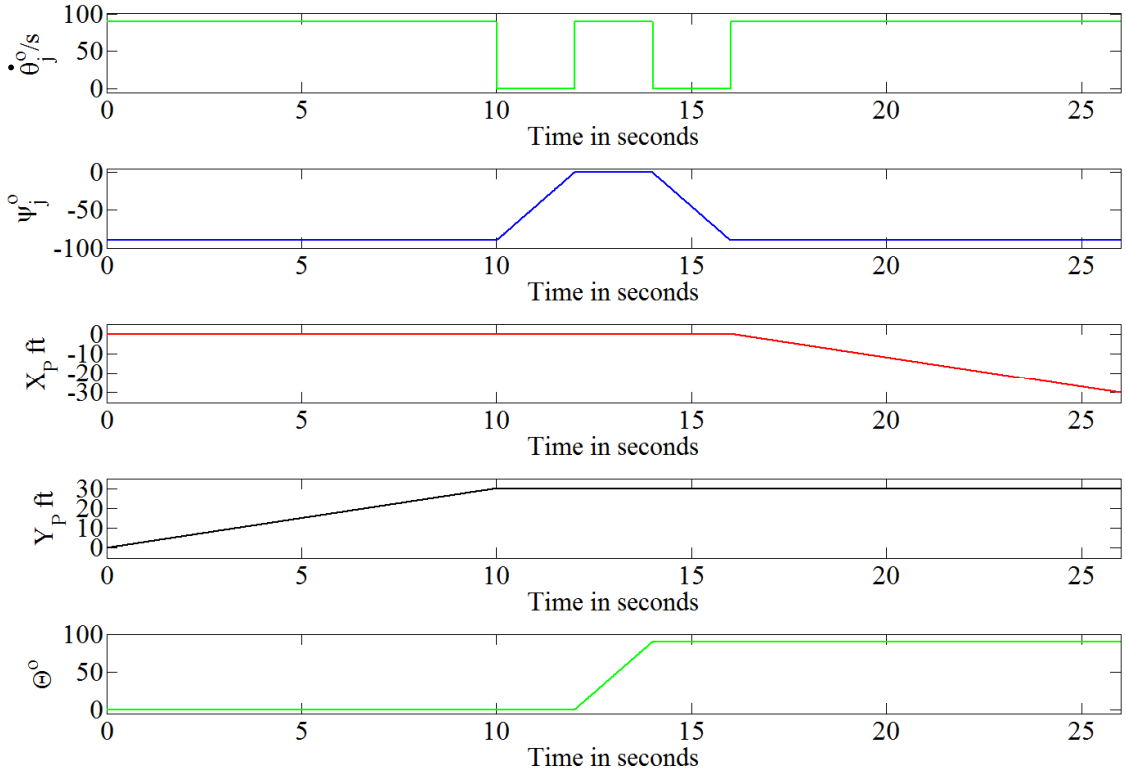

Fig. 5.16: Motion Synthesis for the Front Wheel of the Tricycle Platform or the Platform with Three Active Centered Wheels for a C_1 Discontinuous Motion when the Platform faces the Direction of Travel

identical for the two configurations as this is a 2-DOF motion. The rear wheels of the platform with three active wheels need to do a coordinated motion that is identical to the motion of the passive wheels of the tricycle platform.

The motion is performed as follows. For first 10 seconds, the platform travels in a straight line in Y direction. During the next 2 seconds, the front wheel steers by 90^o such that the front wheel axis passes through point *P* while the platform is stationary. The velocity IC in case of the platform with three active centered wheels is at the intersection of the wheel axes of all the active wheels. In case of a tricycle, the velocity IC is at the intersection of the rolling axis of the active 2-DOF wheel and the common rolling axis for the passive trailing wheels. Thus, in both the cases, the velocity IC is located at point P as shown in Fig. 5.17. For next two seconds, the driving actuator is commanded so that the platform orientation changes by 90^o without change in the platform location. For next two seconds, the front wheel steers back to normal position (-90^o). The platform then moves in –X direction for next 10 seconds to complete the motion.

5.3.1.2 Motion Synthesis for the Platform with Three Active Caster Wheels

Fig. 5.18 shows the motion synthesis for the platform with three active caster wheels.

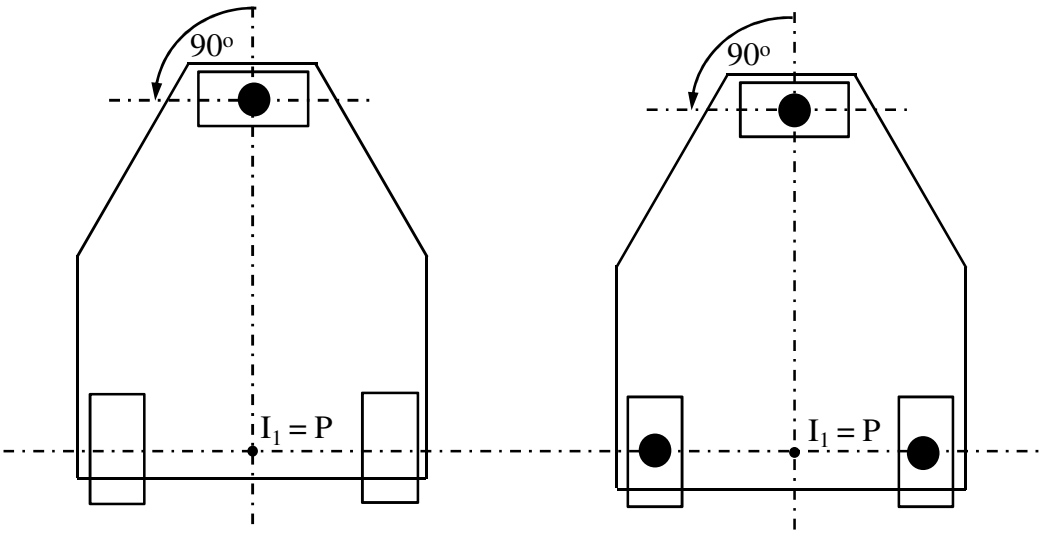

Fig. 5.17: Location of the Velocity IC Coincident with the POI

Here we see that the platform moves for 10 seconds in Y direction, then the orientation control of the platform is done without having to reorient the wheels for next two seconds. At the end of this motion, the caster wheels are at 90 degrees to the travel direction, thus the combination of the steering and driving inputs is used to move the platform in negative X direction for 2 seconds. The rest of the motion in the negative X direction is achieved by the driving actuators of the platform in 8 seconds.

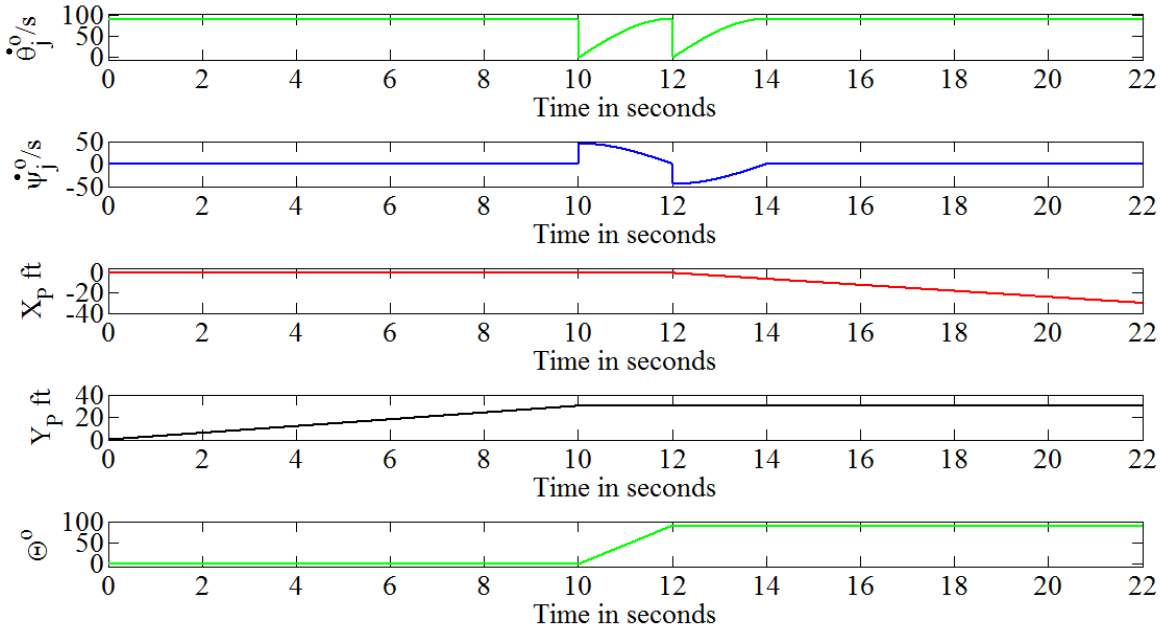

Fig. 5.18: Motion Synthesis for the Front Wheel of the Tricycle Platform or the Platform with Three Active Centered Wheel For a C_1 Discontinuous Motion when the Platform Faces Direction of Travel

5.3.2 PLATFORMS TRAVELING ON A STRAIGHT LINE DISCONTINUOUS PATH WITH FIXED ORIENTATION

Here, the platform moves along the path such that the orientation of the platform does not change similar to Sec. 5.2.2. Fig. 5.19 shows the general mobile platform undergoing the path. As this path requires a lateral motion along the axis connecting the two rear wheel attachment points, it is clear that the tricycle platform cannot perform this motion.

The other two configurations involving three active 2-DOF wheels can perform this motion effectively.

For the motion synthesis, the description of the trajectory is as follows. Both the straight legs of the path are 15 ft at a right angle to each other. The global frame {0} is oriented such that its Y axis is parallel to the first leg of the path. The platform needs to travel at a constant speed of *1.5ft/s* throughout the travel.

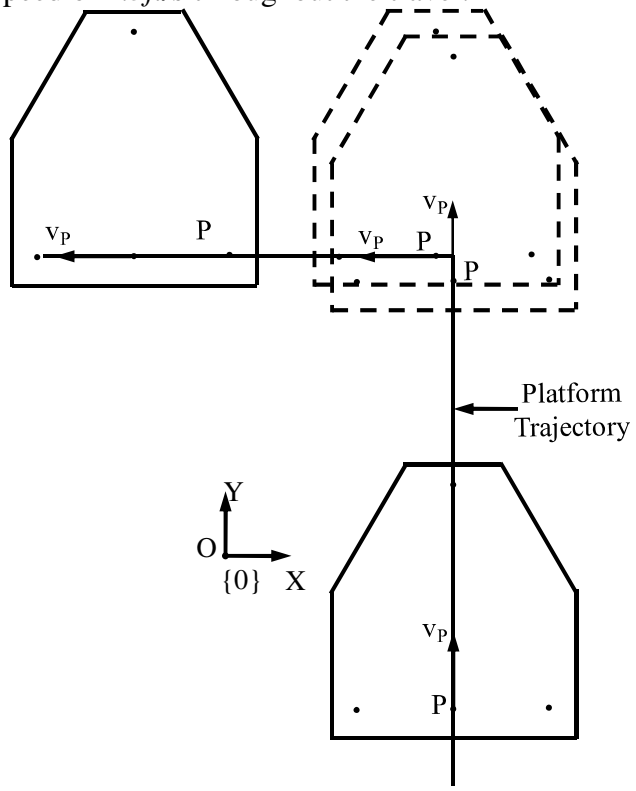

Fig. 5.19: The General Mobile Platform Undergoing the Discontinuous Path Composed of Straight Lines

5.3.2.1 Motion Synthesis for the Platform with Three Active Centered Wheels

We can realize that the platform with centered wheels needs to stop and turn the wheels by 90^o to realign the wheels in the direction of travel to accomplish this motion. Note that this does not change the orientation of the platform as the wheels turn in place. The platform with caster wheels can perform the motion without stopping to turn as the

steering motion also contributes to the wheel linear velocities. The geometrical parameters values given in Eq. 5.7 are used in the simulation for the motion synthesis. The result of the motion synthesis for the platform with the three active centered wheels is shown Fig. 5.20.

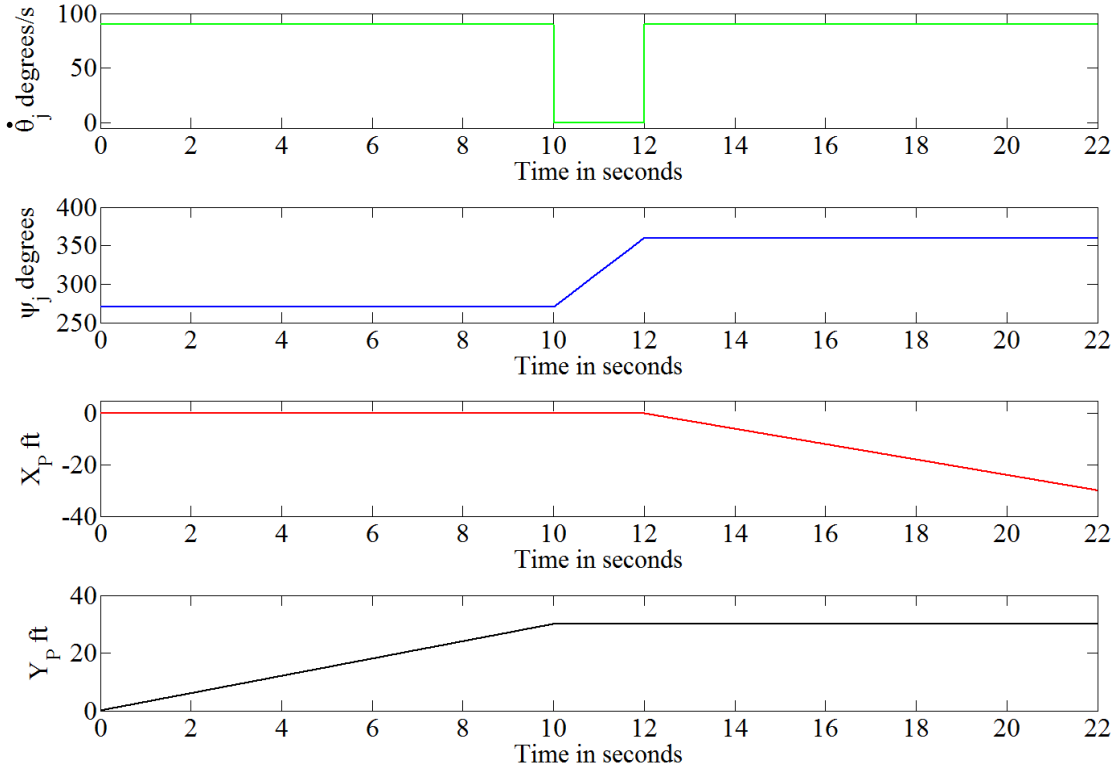

Fig. 5.20: The Motion Synthesis for a Mobile Platform with Three Centered Wheels

Fig. 5.20 shows that at the end of the first straight line motion the steering actuator turned the wheel by 90^o at the rate of 45^o/sec. Thus the platform is stationary for 2 seconds.

5.3.2.2 Motion Synthesis for the Platform with Three Active Caster Wheels

For the same motion requirement, the plot in Fig. 5.21 shows the motion synthesis for the mobile platform with three caster wheels. In the plot, we see that, the steering actuator for the caster wheel contributes to the platform motion in a direction orthogonal to the direction of driving velocity, thus the combined motion of the steering and driving

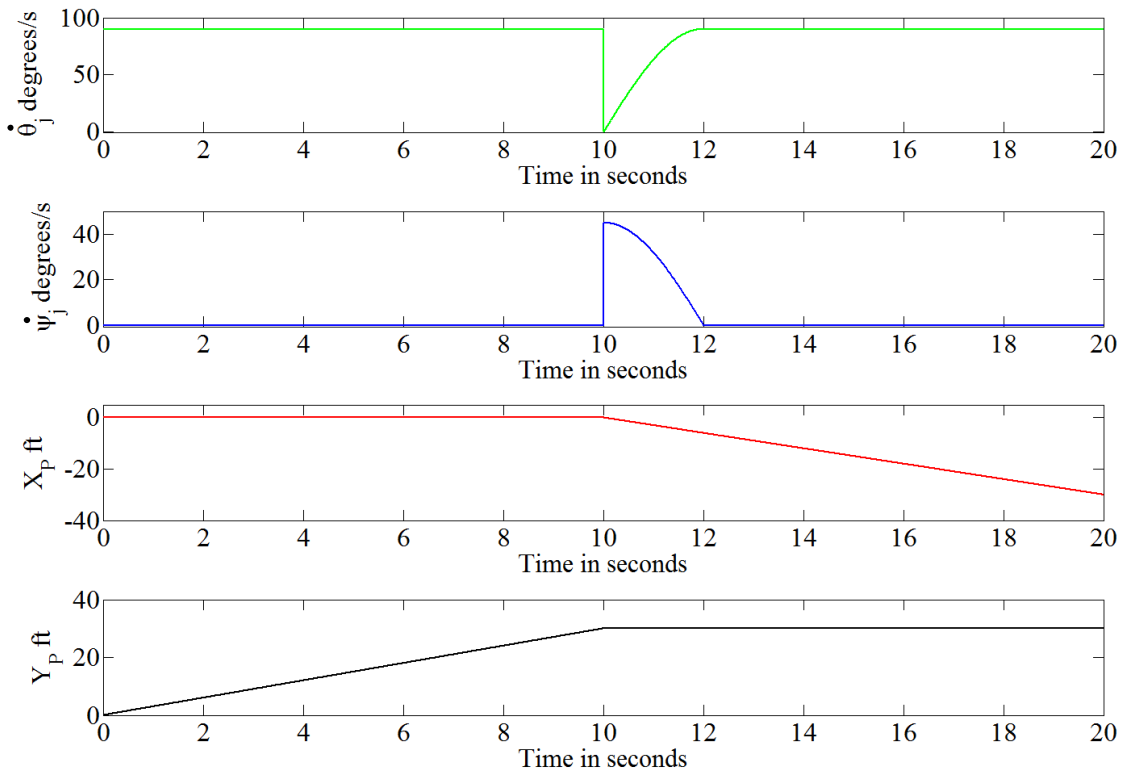

Fig. 5.21: The Motion Synthesis for a Mobile Platform with Three Centered Wheels

actuators contributes to the velocity of the platform in the *–X* direction as required by the second leg. Due to this capability of the steering input, the motion of the platform requires *20* seconds as compared to *22* seconds required by the platform with active centered wheels for the same motion. This is a continuous motion without having to stop to align the wheels. One of the practical limitations in the motion plan may arise due to the velocity limits of the steering actuators. For the simulation, the length of steering link was 2ft (Eq. 5.7) equal to the diameter of the wheel. This enabled us to command the steering actuator to be run at approximately 45^o/sec compared to approximately 90^o/sec for driving actuator. However the driving actuator usually can run much faster than the steering actuator without causing any dynamic instability effects. This limitation may be considered during dynamic motion synthesis.

5.4 Platforms Traveling on a Discontinuous, Curved Path

In Sec, 5.3 we studied motions of the platforms when they travel on discontinuous trajectories composed of straight line segments. In the following section we will study the motion of the three platforms on trajectories that are discontinuous with curved segments. Again there are two different scenarios to be studied, namely, when the platform faces the direction of the travel and when the platform maintains a fixed orientation in space.

5.4.1 Platforms Traveling on a Discontinuous, Curved Path Facing Direction of the Travel

Consider a general mobile platform traveling on a path made up of two quarter circles as shown in Fig. 5.22. As discussed in Sec. 5.2.1, this portion of the motion can be accomplished successfully by all the three platforms. During the travel along the circular path, the velocity IC is coincident with the center of curvature of the trajectory at all times as discussed in Sec. 5.2.1. Thus the motion synthesis for the 2-DOF active front wheel can be done as shown in Fig. 5.11-a). We can use Eq. 4.9 to compute the steering angle ψ as follows:

$$\psi = \tan^{-1}\left(\frac{3b}{r}\right) \qquad \text{Eq. 5.23}$$

and Eq. 4.10 to compute the driving velocity for the 2-DOF active wheel as follows:

$$\begin{gathered} v_E = \rho_1 \omega \\ \dot{\theta} = \frac{v_E}{d/2} \\ where, \rho_1 = \sqrt{{X_{\rho 1}}^2 + {Y_{\rho 1}}^2} \\ X_{\rho 1} = 3b;\ Y_{\rho 1} = -r\,, \\ \omega = {v_P}/{r} \end{gathered} \qquad \text{Eq. 5.24}$$

5.4.1.1 Motion Synthesis for the Tricycle Platform or the Platform with Three Active Centered Wheels

Using this information, the motion synthesis for the platforms with active centered wheels is performed as follows. For the first curved segment, we compute the steering and driving input using Eq. 5.23 and Eq. 5.24. After the 90^o travel on the first segment, the front wheel steers by 90^o such that the front wheel axis passes through point *P* while the platform is stationary. The velocity IC in case of the platform with three active centered wheels is at the intersection of the wheel axes of all the active wheels. In case of a tricycle, the velocity IC is at the intersection of the rolling axis of the active 2-DOF wheel and the common rolling axis for the passive trailing wheels. Thus, in both the cases, the velocity IC is located at point P. Next, the driving actuator is commanded so that the platform orientation changes by 180^o without change in the platform location.

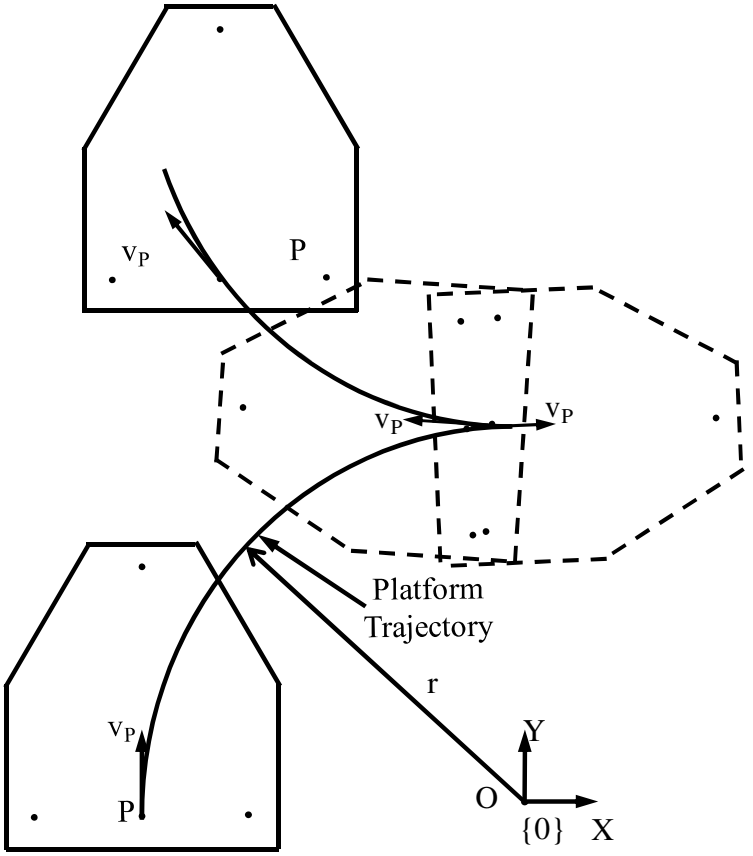

Fig. 5.22: The Mobile Platform with Fixed Wheels Traveling along a Circular Path

Next, the front wheel steers back to normal position (-90^o). The platform then moves along the second curved segment with the steering and driving input using Eq. 5.23 and Eq. 5.24 to complete the motion.

5.4.1.2 Motion Synthesis for the Platform with Three Active Caster Wheels

For the platform with three active caster wheels, the motion synthesis for the two curved segments is done similar to the other two platforms. However, the orientation control of the platform to rotate it by 180^o to align it along the second path is done without having to reorient the wheels. At the end of this motion, the caster wheels are at 180 degrees to the travel direction, thus the combination of the steering and driving inputs is used to move the platform on the second curved segment. The rest of the motion on the second curved segment is achieved with the steering and driving input using Eq. 5.23 and Eq. 5.24.

5.4.2 PLATFORMS TRAVELING ON A DISCONTINUOUS CURVED PATH WITH FIXED ORIENTATION

Here, the platforms need to accomplish the motion along the discontinuous path without a change in orientation in global frame {0} as shown in Fig. 5.23. As discussed earlier, the tricycle platform is unable to move laterally hence it cannot perform the motion. The two platforms with three active wheels perform the motion across the circular segments as discussed in the Sec. 5.2.2. At the discontinuity between the two curved segments, the platform motion synthesis is done as discussed in Sec. 5.3.2.

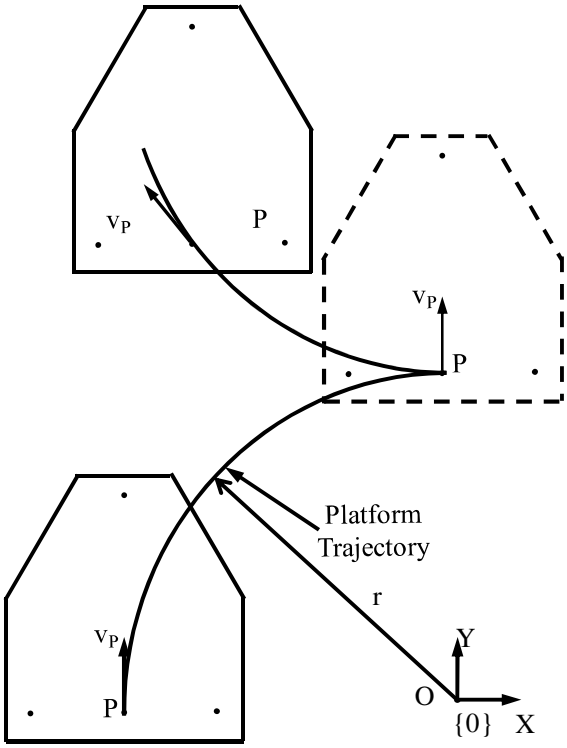

Fig. 5.23: The Mobile Platform with Fixed Wheels Traveling along a Circular Path

5.5 Summary and Discussions

Based on the examples, the following observations may be made:

1. Due to the motion of the steering actuator as a position input and the driving actuator as a velocity input, the time required for the platform with the centered wheels, is *25.05 s* as compared to *22.5 s* for the platform with the caster wheels.
2. For active centered wheel motions, the driving actuator is responsible for the motion of the platform while the steering actuator is used mainly to place the wheel in the appropriate direction. This results in higher motion requirements for the driving actuator.
3. When the wheel is in a direction away from the required direction of motion, the centered wheel configuration needs the steering actuator to align the wheel in the direction first. In case of a caster wheel configuration, this is not needed since the

steering motion also contributes to the useful platform motions. This means that the platform with active caster wheels can instantaneously start moving in an arbitrary direction while the platform with active centered wheels needs to realign the wheels in the direction of travel before doing so.

4. As both the steering and the driving actuators contribute to the platform motions with active caster wheels, the motion requirements from the driving actuator reduce. Although it can be seen that the steering actuators moves less compared to the driving actuator (*s*). For ex., the steering actuator in the range of *0-2 deg/s* compared the driving actuator in the range of *20-30 deg/s* in the case of the motion along a straight line motion with orientation control (Sec. 5.1.2.2).
5. One of the practical limitations in the motion plan may arise due to the velocity limits of the steering actuators. Usually, the driving actuator can run much faster than the steering actuator without causing any dynamic instability effects. This limitation would be considered during the dynamic motion synthesis.

6 DYNAMICS OF MOBILE PLATFORMS

6.1 Introduction

In the previous chapters, we studied the kinematic formulation for various mobile platforms using the instant centers for up to the third order motion. We also presented a generalized formulation that can be used to describe the k^{th} order motion of a planar platform. This chapter presents a dynamic model of a general mobile platform with active caster wheels. The significance of the force analysis of a mobile platform lies in the fact that a mobile platform with redundant actuation provides redundancy in force domain (Yi and Freeman, 1993) just as a redundant manipulator provides redundancy in position domain. The dynamic modeling of mobile platforms has been presented in the literature by various researchers. The dynamic formulation using the Natural Orthogonal Complement algorithm for a skid-steer platform was proposed by Saha and Angeles (1996). Chung et al. (2008) described the dynamic model of an omnidirectional mobile platform with three caster wheels using the Lagrangian dynamics based on the dynamic model presented by Freeman and Tesar (1988). Holmberg and Khatib (2000) presented a dynamic model for an omnidirectional model using Newton-Euler formulation. Li et al. (2006) extended the Newton-Euler based dynamic model of a generalized omnidirectional mobile platform with n caster wheels that accounts for the wheel-ground interaction.

In the following sections, we will present the dynamic model of a general mobile platform with J active caster wheels using the Newton-Euler method as the method provides means to account for/compute the reaction forces in the interacting links/bodies.

6.2 Description of the Mobile Platform

Fig. 6.1 shows a mobile platform with a generic shape. Point E_j is the attachment point of the wheel subsystem j to the platform. The SAE (Society of Automobile Engineers (Wong, 2001) recommends an axis system for description of wheel forces and moments such that the X axis is in the positive rolling direction, the Z axis is vertical and downwards with respect to the ground, and the Y axis makes the frame a right handed frame. However, to be consistent with the notation used in this dissertation, we define the frame $\{j\}$ for the wheel subsystem j such that the x_j axis is in the positive wheel rolling direction, the z_j axis is vertical and upwards with respect to the ground, and the y_j axis makes the frame a right handed frame as shown in Fig. 6.1. Similarly, frame $\{0\}$ is a global inertial frame located in the plane containing the top face of the platform body such that its Z axis is vertical and upwards. Frame $\{1\}$ is a body fixed frame located at

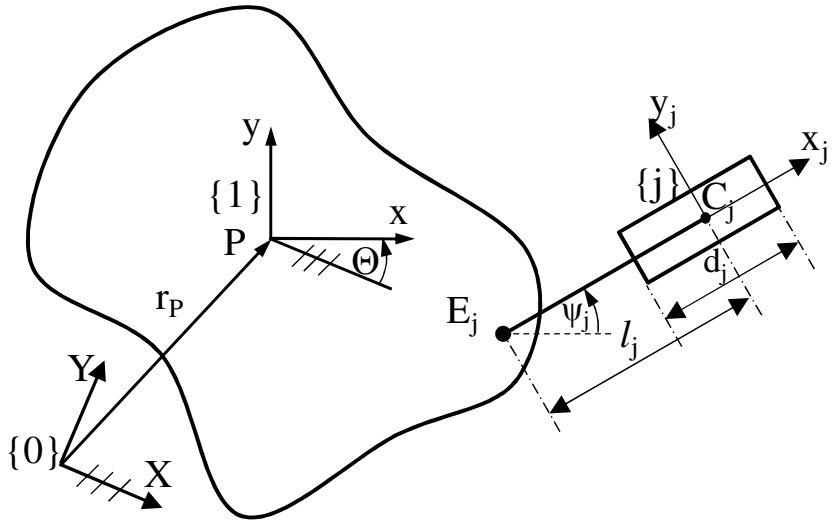

Fig. 6.1: Frame Assignments for Dynamics

the centroid *G* of the top face of the platform body. The orientation of frame {*1*} with frame {*0*} is the platform orientation *Θ*.

With these frame assignments, the dynamic model of the mobile platform is shown in Fig. 6.2. Wong (2001) presented a dynamic model of an automobile tire with an emphasis on the ground interaction forces and moments (Fig. 1.2, pg. 8 in the reference). The dynamic model for the wheel subsystem presented here is derived from the model presented in Wong (2001). We will first describe all the notations and then discuss the force and moment equilibrium as follows.

In Fig. 6.2,

Frame {*1*}: the body fixed frame *xy* located at the POI P,

Frame {*j*}: the frame $x_j y_j$ attached to the wheel subsystem, such that its origin is at the point of contact of the wheel with the ground, the x_j axis is oriented in the

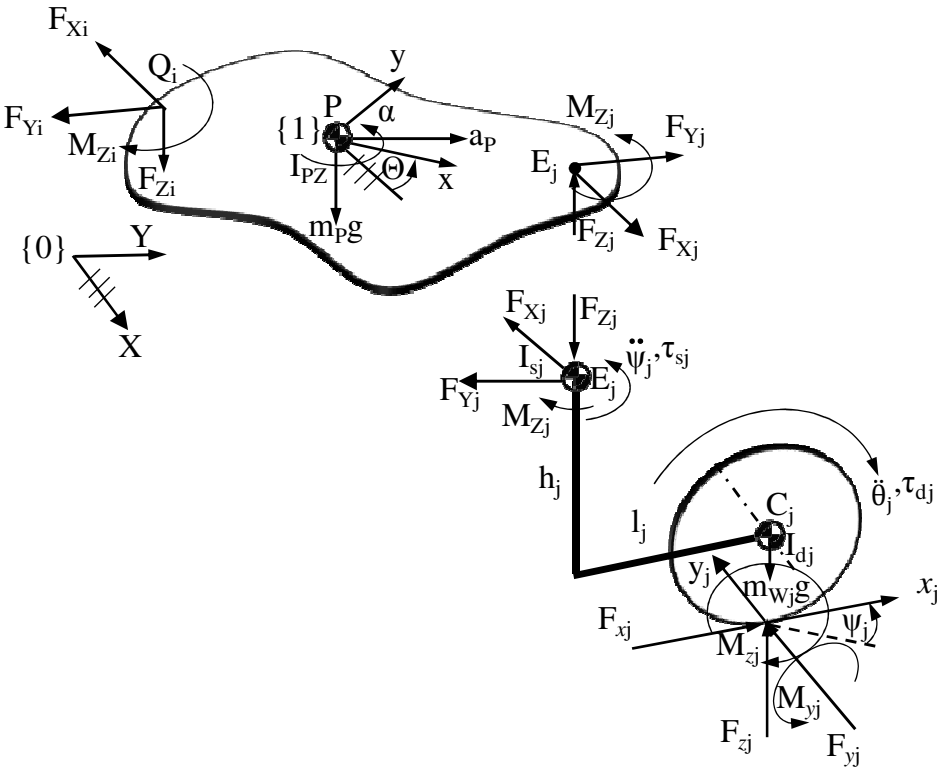

Fig. 6.2: The Free-Body Diagram of a General Mobile Platform with *J* Active 2-DOF Caster Wheels

positive driving direction, the z_j axis vertically upwards and y_j axis is assigned to create a right handed coordinate system.

Angle ψ_j: the steering angle of the wheel subsystem j. The orientation difference between frame $\{1\}$ and frame x_jy_j is ψ_j,

m_P: the mass of the platform body,

I_{PZ}: the moment of Inertia of the platform body about the z axis,

A_P: the total acceleration of point P,

g: the gravitational acceleration constant,

F_{Xj}: the X component of the force at the wheel subsystem attachment point Ej due to the platform-subsystem interaction,

F_{Yj}: the Y component of the force at the wheel attachment point Ej due to the platform-wheel subsystem interaction,

F_{Zj}: the Z component of the force at the wheel attachment point Ej due to the platform-wheel subsystem interaction,

M_{Zj}: the moment acting at E_j due to the inertia and external forces of the platform parallel to the Z axis,

Q_i: a point of application of external forces $[X_{Qi}, Y_{Qi}]$. Point Q_i (i = 1, 2, …, N) could be a manipulator attachment point, a payload placement point, etc.

F_{Xi}: the X component of the external force at Q_i on the platform,

F_{Yi}: the Y component of the external force at Q_i on the platform,

F_{Zi}: the Z component of the external force at Q_i on the platform,

M_{Zj}: the external moment at Q_i on the platform in Z direction,

For the j^{th} wheel subsystem,

m_{Wj}: the mass of the j^{th} wheel subsystem (including the link, actuators etc.),

I_{sj}: the moment of inertia of the wheel subsystem j about the steering axis,

I_{dj}: the moment of inertia of the wheel subsystem j about the driving axis,

d_j: the diameter of wheel j,

l_j: the steering offset of wheel subsystem j,

h_j: the height of wheel attachment point from the wheel rolling axis for the j^{th} wheel subsystem,

τ_{sj}: the torque applied by steering actuator,

τ_{dj}: the torque applied by driving actuator,

F_{xj}: the tractive force due to the wheel/ground interaction,

F_{yj}: the lateral force (resistance to the lateral motion of the wheel due to steering) due to the wheel/ground interaction,

F_{zj}: the vertical reaction force due to the ground,

M_{yj}: the rolling resistance moment,

M_{zj}: the steering resistance moment (aligning torque (Wong, 2001)).

6.3 Force/Moment Equilibrium Equations

Using the description of forces, we derive the equations of force/moment equilibrium in the principle directions for the platform body and the j^{th} wheel subsystem as follows. The body fixed frame $\{1\}$ for the platform body is located at the center of gravity of the platform body. The location of wheel attachment points are at E_1, E_2, …, E_j, …, E_J and the locations of the external force application points are at Q_1, Q_2, …, Q_N. The following are the assumptions for the dynamic behavior of the mobile platform.

1. The platform is capable of planar motions only. Any out of plane motions are reserved for a future development effort.

2. The ground is flat and smooth such that all the J wheels are in constant contact with ground.
3. The platform body and the links are rigid.
4. The wheel is assumed to be vertical at all times with no tilting (zero camber angle (Wong, 2008)).
5. There is no moment M_{xj} (zero overturning moment (Wong, 2008)) acting in the x_j direction.

6.3.1 FORCE AND MOMENT EQUILIBRIUM FOR THE PLATFORM BODY

With the assumptions stated above, we draw the free body diagram of the different rigid bodies as shown in Fig. 6.2.

From Newton's second law,

$$\overline{F}^{i} = \overline{M}a \qquad \text{Eq. 6.1}$$

The inertial resistance forces (D'Alembert's forces) are given as (Tesar, 1992):

$$\overline{F}^{d} \equiv -\overline{M}\ddot{X}\,, -\overline{M}\ddot{Y}, -\overline{I}\ddot{\theta} \qquad \text{Eq. 6.2}$$

Thus we have for the force and moment equilibrium,

$$\overline{F}^{i} + \overline{F}^{d} = 0 \qquad \text{Eq. 6.3}$$

The force and moment equilibrium on the platform body results in the following equilibrium equations.

$\sum F_X$:

$$\sum_{j=1}^{J} F_{Xj} - \sum_{i=1}^{N} F_{Xi} - m_P a_X = 0 \qquad \text{Eq. 6.4}$$

$\sum F_Y$:

$$\sum_{j=1}^{J} F_{Yj} - \sum_{i=1}^{N} F_{Yi} - m_P a_Y = 0$$

$\sum F_Z$:

$$\sum_{j=1}^{J} F_{Zj} - \sum_{i=1}^{N} F_{Zi} - m_P g = 0$$

$\sum M_Z@G$:

$$\sum_{j=1}^{J} M_{Zj} - \sum_{i=1}^{N} M_{Zi} - \sum_{j=1}^{J} F_{Xj} Y_{Ej} + \sum_{j=1}^{J} F_{Yj} X_{Ej} - \sum_{i=1}^{N} F_{Xi} Y_{Pi} + \sum_{i=1}^{N} F_{Yi} X_{Pi} - I_{PZ}\alpha = 0$$

From the equilibrium of forces and moment we can compute the forces that must be collectively provided by the *J* wheel subsystems as follows:

$$\sum_{j=1}^{J} F_{Xj} = \sum_{i=1}^{N} F_{Xi} + m_P a_X$$

$$\sum_{j=1}^{J} F_{Yj} = \sum_{i=1}^{N} F_{Yi} + m_P a_Y$$

$$\sum_{j=1}^{J} F_{Zj} = \sum_{i=1}^{N} F_{Zi} + m_P g \qquad \text{Eq. 6.5}$$

$$\sum_{j=1}^{J} M_{Zj} = \sum_{i=1}^{N} M_{Zi} + \sum_{j=1}^{J} F_{Xj} Y_{Ej} - \sum_{j=1}^{J} F_{Yj} X_{Ej} - \sum_{i=1}^{N} F_{Xi} Y_{Pi} + \sum_{i=1}^{N} F_{Yi} X_{Pi} + I_{PZ}\alpha$$

Note that this is a redundant system of forces that demands a force distribution scheme. Some of the simplest schemes for force distribution include distributing the forces and moments equally among all the wheel subsystems or using a pseudo-inverse technique (Kumar and Waldron, 1988; Li et al., 2006a). However the redundancy in the force domain should be exploited to distribute the forces among the wheel subsystem

based on the performance capabilities of each subsystem in terms of the wheel-ground traction limits, the actuator torque availability, etc (Li et al., 2006b). The redundancy can also be used to operate the system with efficient (energy consumption, minimum inertia, etc.) and stable (rollover stability, limited jerk, etc.) motions. Thus it is important to study the dynamic model of the wheel subsystem which is studied in the following section.

6.3.2 FORCE AND MOMENT EQUILIBRIUM FOR THE J^{TH} WHEEL SUBSYSTEM

The linear acceleration of the wheel subsystem can be expressed in terms of the acceleration of point E_j. Fig. 6.2 shows various forces and moments acting on a representative wheel subsystem j. Point C_j is the center of the wheel while E_j is the attachment point of the steering link to the platform. Considering the forces and moments in the $x_j y_j$ direction, we state the equilibrium equations for the j^{th} wheel subsystem as follows:

$$\sum F_{xj}:$$

$$F_{xj} + F_{Xj}\cos(\psi_j) + F_{Yj}\sin(\psi_j) - m_{Wj}a_{xj} = 0$$

$$\sum F_{yj}:$$

$$F_{yj} + F_{Yj}\cos(\psi_j) - F_{Xj}\sin(\psi_j) - m_{Wj}a_{yj} = 0$$

$$\sum F_{zj}:$$

$$F_{zj} - F_{Zj} - m_{Wj}g = 0 \qquad \text{Eq. 6.6}$$

$$\sum M_{zj}\ @Ej:$$

$$\tau_{s(j)} - F_{yj}l_j - M_{zj} - M_{Zj} - I_{sj}\ddot{\psi}_j = 0$$

$$\sum M_{xj}\ @Cj:$$

$$\tau_{dj} - F_{xj}\frac{d_j}{2} - M_{yj} - \left[F_{Xj}\cos(\psi_j) + F_{Yj}sin(\psi_j)\right]h_j - F_{Zj}l_j - I_{dj}\ddot{\theta}_j = 0$$

Using Eq. 4.45, Eq. 6.6 can be rearranged as follows:

$$F_{xj} + F_{Xj}cos\psi_j + F_{Yj}\sin\psi_j - m_{Wj}\left(\frac{\ddot{\theta}_j d}{2} + l\dot{\psi}_j^{\,2}\right) = 0 \qquad \text{Eq. 6.7-a)}$$

$$F_{yj} - F_{Xj}sin\psi_j + F_{Yj}\cos\psi_j - m_{Wj}\left(\dot{\psi}\dot{\theta}d - l\ddot{\psi}\right) = 0 \quad \text{Eq. 6.7-b)}$$

$$F_{zj} - F_{Zj} - m_{Wj}g = 0 \quad \text{Eq. 6.7-c)}$$

$$\tau_{dj} - F_{xj}\frac{d_j}{2} - M_{yj} - \left[F_{Xj}\cos\psi_j + F_{Yj}sin\psi_j\right]h_j - F_{Zj}l_j - I_{dj}\ddot{\theta}_j = 0 \quad \text{Eq. 6.7-d)}$$

$$\tau_{s(j)} - F_{yj}l_j - M_{zj} - M_{Zj} - I_{sj}\ddot{\psi}_j = 0 \quad \text{Eq. 6.7-e)}$$

Eq. 6.7 is the dynamic equation of the wheel subsystem *j*. In the following sections, we will describe the

In Eq. 6.7-a), -b), and -c), F_{Xj}, F_{Yj}, and F_{Zj} are the forces exerted on wheel subsystem *j* by platform body (Eq. 6.2), and F_{xj}, F_{yj}, and F_{zj} are the wheel-ground contact forces, respectively. It can be realized that the force the wheel subsystem can exert (or conversely sustain) on the platform is limited by these ground contact forces. Similarly, in Eq. 6.7-d), and -e), M_{yj}, M_{zj} are the the rolling resistance moment, and the steering resistance moment, respectively due to the ground-wheel contact.

The numerical values of these contact forces and moments are dependent on the incidental wheel-ground contact conditions dependent on the ground properties (surface quality, wetness, irregularities, etc.), wheel driving and steering velocities and accelerations, inflation pressure in the tire, temperature of the contact as well as internal temperature of the wheel, etc. Thus it is evident that the dynamic capabilities and also the overall performance of the mobile platform are largely influenced by these factors. Note that some of these factors are out of control of the operator (for ex., the surface properties, contact temperature, etc.) and some factors can be actively controlled (for ex., the tire inflation pressure, the wheel velocities, internal temperature (to some extent), etc.). In any case, it is important that the effect of these factors on the contact forces and

moments must be studied and considered for the operation of the platform which is the purpose of the following section.

6.4 Wheel Dynamics

The following sections study the effect of the external factors such as ground properties, inflation pressure in the tire, temperature of the contact as well as internal temperature of the wheel, etc., on the capabilities (and efficiency) of the wheel in terms tractive force availability, resistance to the motion etc.

6.4.1 GROUND CONTACT FORCES

The contact force in z_j direction F_{zj} is the normal reaction of the ground due to the platform interaction forces and weight of the wheel subsystem. The contact force F_{xj} in the x_j direction is known as tractive effort during the acceleration and braking. Note that the direction of F_{xj} reverses for the braking mode of the wheel as compared to the driving (acceleration). Based on the magnitude of F_{zj}, the contact forces in rolling (tractive (braking) force F_{xj}) and lateral direction (F_{yj}) are computed (Li et al., 2006a) as follows:

$$F_{xj} = sgn(\dot{\theta})\mu_{xj}F_{zj}$$
$$F_{yj} = -sgn(\dot{\theta})\mu_{yj}F_{zj} \qquad \text{Eq. 6.8}$$

Where, μ_{xj} and μ_{yj} are the longitudinal and lateral friction coefficients for the j^{th} wheel subsystem, respectively. The numerical values of μ_{xj} and μ_{yj} are dependent on the incidental contact conditions such as ground properties, wheel driving and steering velocities and accelerations, inflation pressure in the tire, temperature of the contact as well as internal temperature, etc. Note that the estimation of the friction coefficient is a vast area of research and is beyond the scope of this dissertation. The brief section here is intended to emphasize the complex and non-linear nature of the problem that is required to estimate the ground-wheel contact forces.

6.4.1.1 Longitudinal Friction Coefficient and Tractive (Braking) Force

Li et al. (2006a) describe a parameter "slip ratio" similar to the slippage factor defined in Sec. 3.4.2. The longitudinal slip (Wong, 2001, Li et al., 2006a, Jazar, 2008) is defined as follows

$$\lambda = 1 - \frac{v_{xj}}{\dot{\theta} d/2} \times 100\% \qquad \text{Eq. 6.9}$$

The variation of the longitudinal friction coefficient μ_x with the slip ratio is shown in Fig. 6.3. The curve has following distinct regions (Wong 2001, Li et al., 2006a):

1. Linear region: Initially, the longitudinal friction coefficient μ_x (and thus the traction force F_x) increases linearly with the longitudinal slip. This is the linear region (region OA) as shown in Fig. 6.3. The magnitude of μ_x at the end of the linear region is approximately ½ of the peak value of the longitudinal friction coefficient (μ_{peak}).
2. Non-linear, stable region: This is the region AB after the linear region till the magnitude of the longitudinal friction coefficient μ_x reaches its peak value) μ_{peak} which is arrived at between 15 to 20% of the longitudinal slip as shown in Fig. 6.3 (according to the typical experimental data (Wong, 2001)).
3. Non-linear, unstable region: The magnitude of the friction coefficient μ_x starts reducing till it reaches the friction coefficient for pure sliding $\mu_{sliding}$.

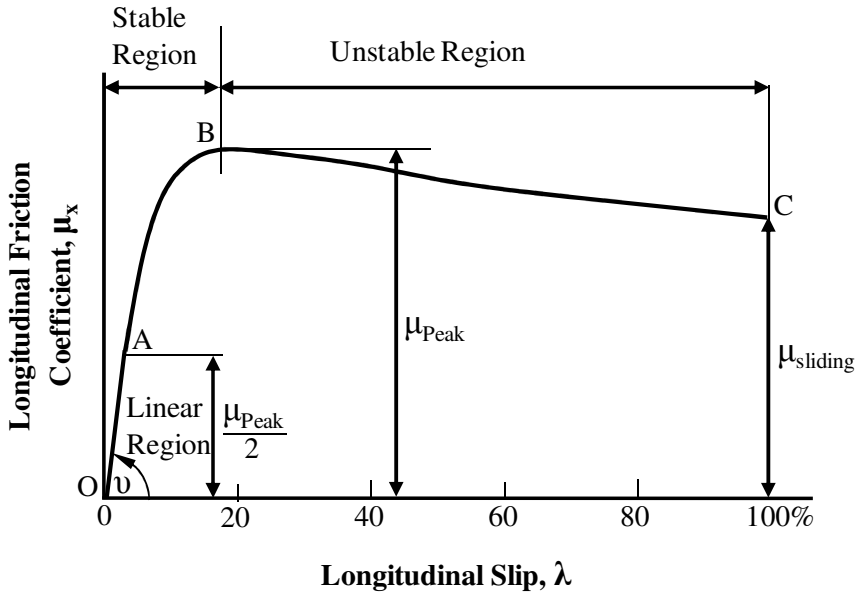

Fig. 6.3:The Variation of Longitudinal Friction Coefficient μ_x with Respect to the Longitudinal Slip λ [Wong, 2001]

Thus, the longitudinal friction coefficient has non-linear characteristics over most of the region of the longitudinal slip. The reader is encouraged to review the portion of Sec 1.3 (pp. 18-23) from the book by Wong (2001) pertaining to this section. According to Wong (2001), the total traction force is composed of two components, traction force due to sliding F_{xs} and traction force due to adhesion F_{xa}. The expression for total traction force is reproduced here without going into the details:

$$Fx = F_{xs} + F_{xa} = \mu_p \dot{\theta} - \frac{\left(\mu_p \dot{\theta}\right)^2}{4\lambda \tan \upsilon} \qquad \text{Eq. 6.10}$$

This expression shows the non-linear behavior of the traction force and the equivalent longitudinal friction coefficient μ_x.

The following section discusses various factors such as speed, and inflation pressure in tires that affect the friction coefficient.

6.4.1.1.1 Effect of Speed on the Friction Coefficient

The longitudinal friction coefficient of a tire is inversely proportional to the speed of the wheel as shown in Fig. 6.4 which shows the effect of the vehicle speed on the braking coefficient. The data is generated for a truck tire running on asphalt (Wong, 2001)

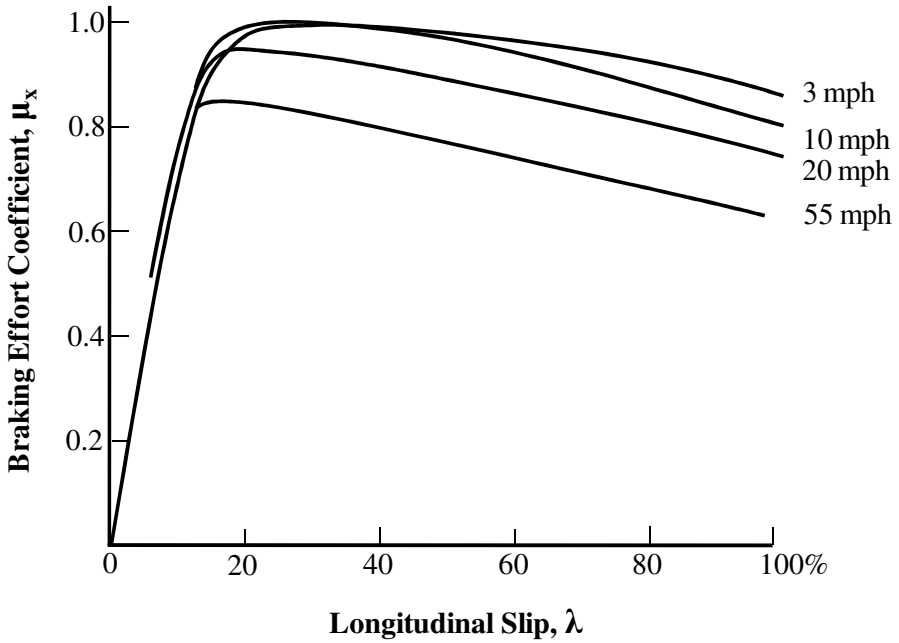

Fig. 6.4: The Magnitude of Braking Friction Coefficient μ_x with Respect to the Vehicle Speed [Wong 2001]

6.4.1.1.2 Effect of Normal Load on the Braking Effort

With the increase in normal load on a tire, the potential braking effort increases significantly (Wong, 2001).

6.4.1.1.3 Effect of Inflation Pressure on the Braking Friction Coefficient

With the increase in inflation pressure of a tire, the peak longitudinal friction coefficient μ_{peak} of a tire increases moderately while the sliding friction coefficient $\mu_{sliding}$ decreases as shown in Fig. 6.5. The data is generated for a bias ply car tire running on dry pavement (Wong, 2001).

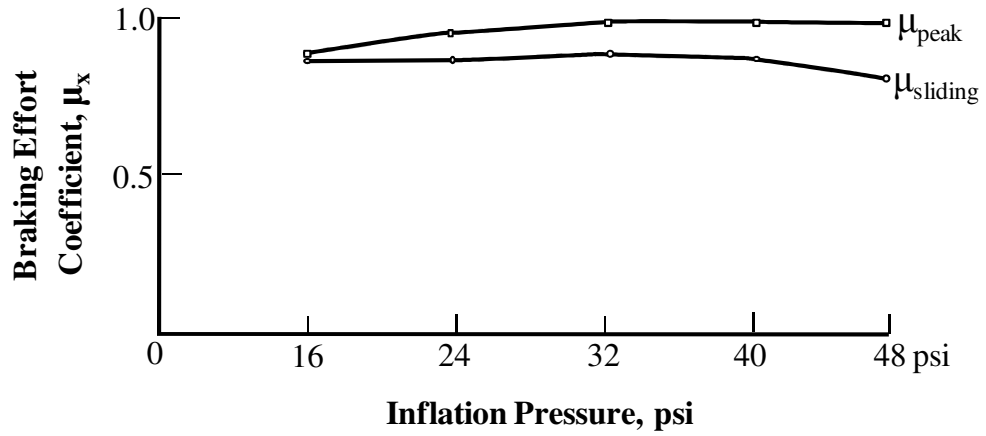

Fig. 6.5: The Magnitude of Braking Friction Coefficient μ_x with Respect to the Tire Inflation Pressure [Wong 2001]

6.4.1.2 Lateral Friction Coefficient and Lateral (Cornering) Force

In case of an active caster wheel, there is significant force F_y in the lateral direction. Also known as cornering force, its magnitude is dependent on the ground-wheel interaction properties and also on other factors such as temperature, inflation pressure, etc. The following section briefly discusses the effect of some of these factors on the lateral forces on a pneumatic wheel. The aim of the discussion is to underscore the dynamic and non-linear nature of the cornering force.

6.4.1.3 Lateral (Cornering) Coefficient and Normal Load

With the increase in normal load on a tire, the lateral friction coefficient significantly decreases as shown in Fig. 6.6 (Wong, 2001).

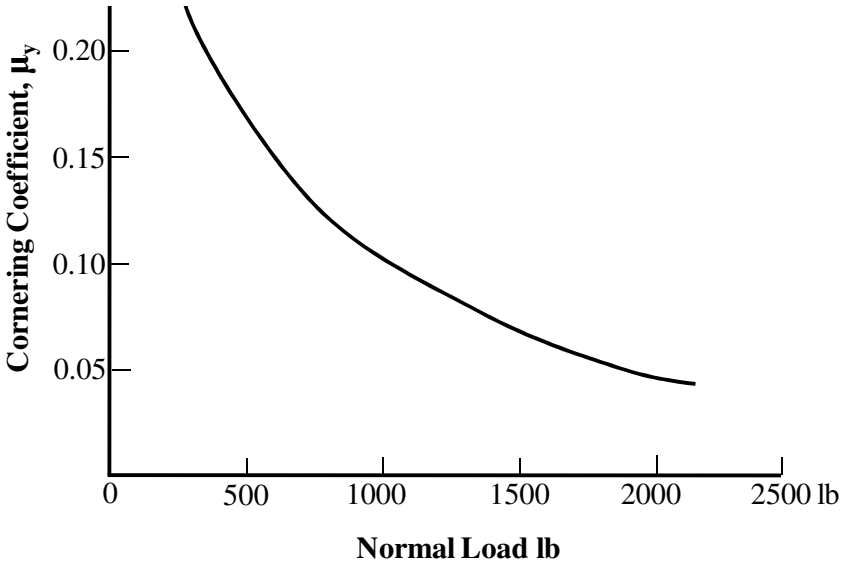

Fig. 6.6: Effect of the Normal Load on the Cornering Coefficient μ_y Wong 2001]

6.4.1.4 Lateral (Cornering) Coefficient and Inflation Pressure

With the increase in inflation pressure of the tire, the lateral friction coefficient increases as shown in Fig. 6.6 (Wong, 2001).

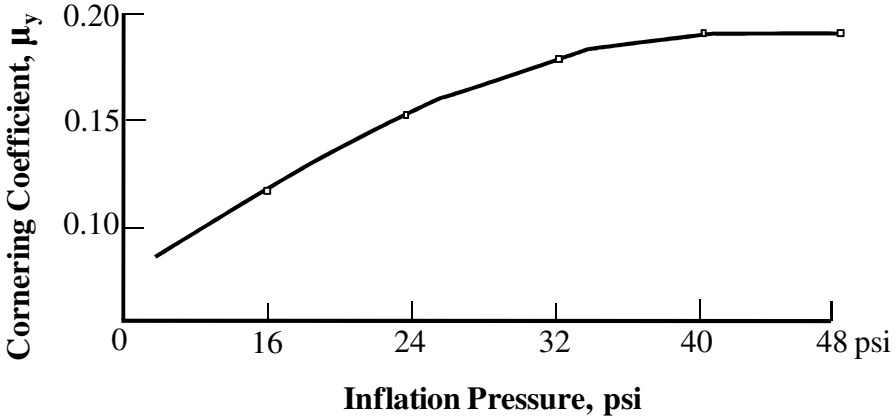

Figure 6.7: Effect of the Tire Inflation Pressure on the Cornering Coefficient μ_y [Wong 2001]

6.4.2 ROLLING RESISTANCE MOMENT

Another unknown in the dynamic equation for the wheel subsystem *j* (Eq. 6.7-d)) is the rolling resistance moment, M_y. The rolling resistance is directed in the opposite direction of the wheel torque and is affected by a number of factors including the design aspects

(material, construction) and the operating conditions (temperature, inflation condition, ground properties, speed, etc.). The following section discusses the effect of some of these factors on the rolling resistance.

6.4.2.1 Tire Pressure

In general, the rolling resistance coefficient decreases with tan increase in the tire pressure for harder surfaces and increases for softer surfaces as shown in Fig. 6.8.

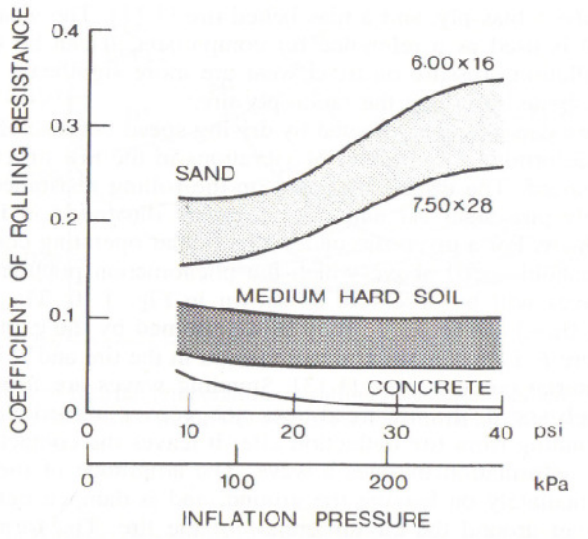

Fig. 6.8: Rolling Resistance Coefficient with respect to the Tire Inflation Pressure on Various Surfaces. (Reproduced from Wong (2001))

6.4.2.2 Temperature

In general, the rolling resistance decreases with temperature as shown in Fig. 6.9. Note that the performance map is quite nonlinear.

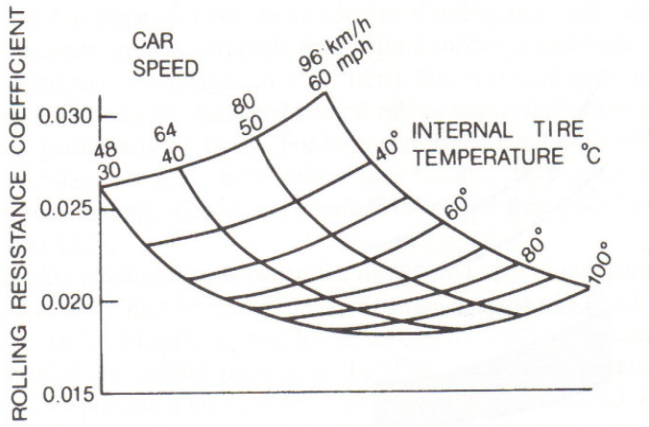

Fig. 6.9: Rolling Resistance Coefficient with respect to the Tire Internal Temperature (Reproduced from Wong (2001))

6.4.2.3 Rolling Resistance Moment and the Vehicle Speed

Rolling resistance increases with speed as shown in Fig. 6.10.

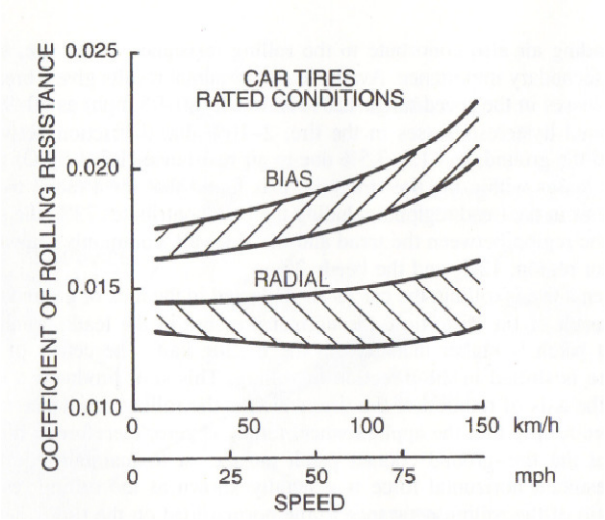

Fig. 6.10: Rolling Resistance Coefficient with respect to the Vehicle Speed (Reproduced from Wong (2001))

6.4.2.4 Rolling Resistance Moment and the Ground Surface Quality

The rolling resistance increases with roughness of the surface. Wet surfaces have higher rolling resistance than dry surfaces.

6.4.3 ACTUATOR LIMITATIONS

Another limiting factor for the platform interaction forces is the limitation of the actuator to exert a finite amount of torque and to run at a finite speed. In short, the forces and moments that a wheel subsystem can exert on the platform body are limited by 1) the wheel-ground interaction and 2) the capability of the driving and steering actuators. Of course, the structural design of the platform is assumed to be designed to withstand the dynamic forces and moments on the system.

6.4.4 PLATFORM PERFORMANCE FACTORS

In summary, the following factors affect the dynamic capabilities and operation performance of the wheel subsystem and also of the mobile platform considering the simplified dynamic model of the wheel subsystem described in Sec. 6.2:

1. Surface qualities such as smoothness, flatness
2. Wetness in terms of the depth of water on surface,
3. Vehicle speed,
4. Tire inflation pressure,
5. Normal load on tire,
6. Actuator limitations such as torque capacity,

Some other factors such as slip angle, camber angle (Wong 2001) are also influential when we consider a more complex dynamic model such as one that has a finite camber angle, slip angle etc. For an intelligent vehicle, all of these maps must be integrated into an operational decision structure. Next, we will provide first level example of where this must go.

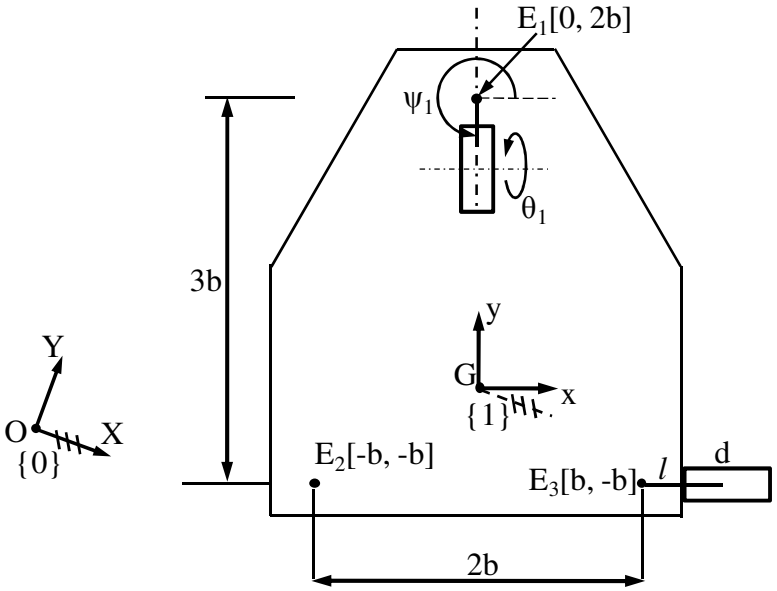

Fig. 6.11: Geometric Description of the Mobile Platform with Three Active Caster Wheels

6.5 Numerical Example

As an illustrative example, we present here a numerical example demonstrating the dynamic motion programming of a mobile platform with active caster wheels. As shown in Fig. 6.11 this is a three wheeled mobile platform with all 2-DOF caster wheels similar to the mobile platform that was studied in Chapter 5 (Fig. 5.1-b).

The geometric and mass properties of the mobile platform are shown in Table 6.1. It is assumed that all the wheel subsystems have identical properties.

Table 6.1: Geometric and Mass Properties of the Mobile Platform with Three Active caster Wheels

$d = 1\ ft$	$l = 1\ ft$	$b = 2\ ft$	$h = 1\ ft$
$m_P = 100\ lb$	$m_W = 10\ lb$	$I_{PZ} = 200\ lb\text{-}ft^2$	$I_d = 10\ lb\text{-}ft^2$
$I_s = 20\ lb\text{-}ft^2$			

To study the dynamic properties of the mobile platforms, consider the trajectory of the platform as shown in Fig. 6.12. The mobile platform is required to travel on the straight

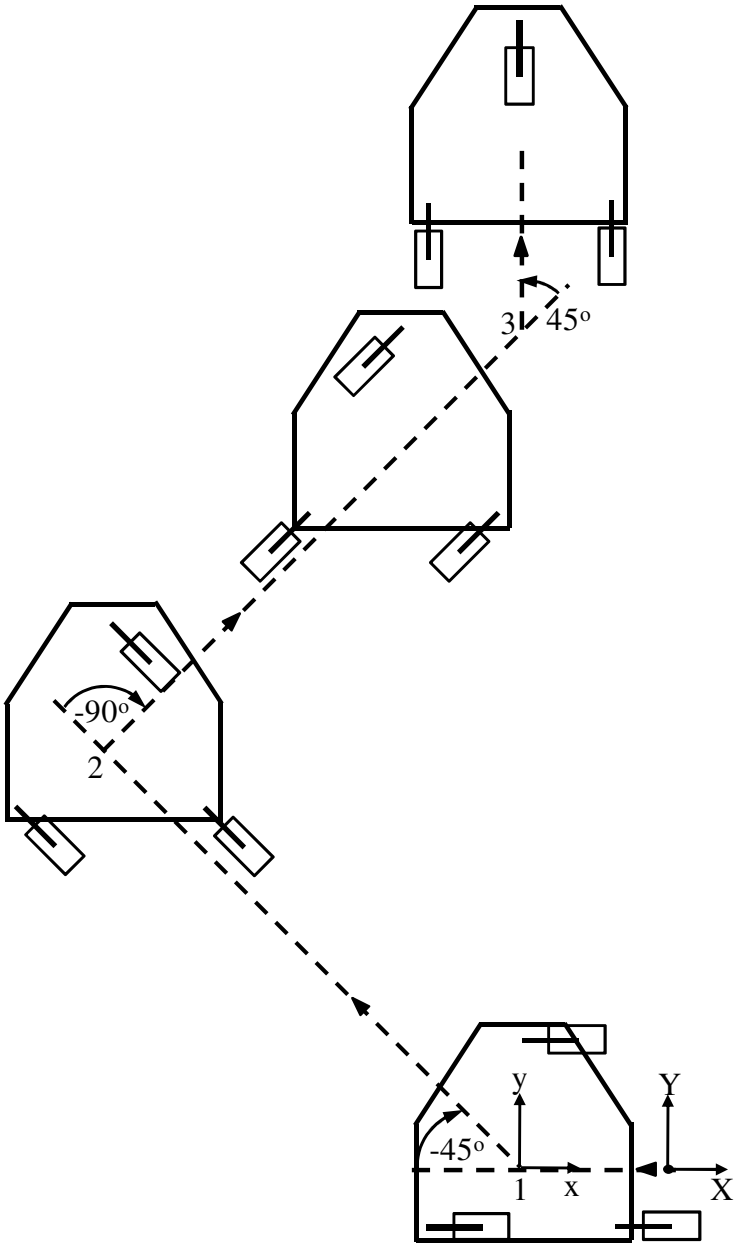

Fig. 6.12: The Path of the Mobile Platform

line segments as shown in Fig. 6.12. The motion of the platform is completed in following steps:

1. At corner 1, the platform travels in *-X* direction and changes direction by *-45^o* to travel in a direction that is *135^o* with *+X* axis for 10 seconds (*t = 0 to10 (s)*),

2. At corner *2*, the platform travels at an angle 135^o with $+X$ axis and changes direction by -90^o to travel in a direction that is 45^o with $+X$ axis for the next *10* seconds (*t = 10 to 20 (s)*),

3. At corner *3*, the platform travels at an angle 45^o with $+X$ axis and changes direction by 45^o to travel in $+Y$ direction for the next 10 seconds (*t = 20 to 30 (s)*).

In order to avoid excessively large inertial forces, the motion plan of the platform is required such that the platform smoothly transitions at each corner and proceeds in the required direction on the next segment.

6.5.1 DYNAMIC MOTION PROGRAMMING

For the required motion plan, the dynamic motion synthesis for the mobile platform with three active caster wheels (Fig. 6.11) is computed in terms of the wheel torques (steering and driving torques) required from each wheel subsystem *j* at each time step. To accomplish this, we need the wheel subsystem input velocities ($\dot{\psi}_j$ and $\dot{\theta}_j$) and the input accelerations ($\ddot{\psi}_j$ and $\ddot{\theta}_j$). Thus, the motion programming of the platform is done for each time step in two stages:

1. Kinematic motion synthesis to compute the input velocities ($\dot{\psi}_j$ and $\dot{\theta}_j$) and accelerations ($\ddot{\psi}_j$ and $\ddot{\theta}_j$), and
2. Dynamic motion synthesis to compute the input joint torques (τ_{sj} and τ_{dj}).

The following sections discuss these two steps in terms of the numerical example. Note that the kinematic motion synthesis for the system involves no uncertainty since there is no redundancy in motion space. However, there are multiple solutions available for the dynamic motion synthesis due to the redundancy in the force domain.

6.5.2 KINEMATIC MOTION SYNTHESIS

The motion of the mobile platform is expressed in terms the linear motion of the Point Of Interest *P* and the rotational motion of the platform. Since this particular motion is purely translational, the linear motion of POI alone describes the motion of the operational space as follows.

6.5.2.1 Operational Space Motion Description

In order to stop and start smoothly at each corner, we plan the motion of the platform along each straight line segment that uses a trapezoid profile for acceleration (March and Tesar, 2008), as shown in Fig. 6.13. The graph in Fig. 6.13 shows the profiles for the magnitudes of the jerk, acceleration, velocity and the position of the POI of the mobile platform with respect to time. This representative motion profile is done for a total of 10 seconds along a path such that the initial and final velocity and acceleration of the platform are zero. This is achieved by using the rectangular profile for the jerk (third order property) of the platform resulting into a trapezoidal profile for the acceleration of

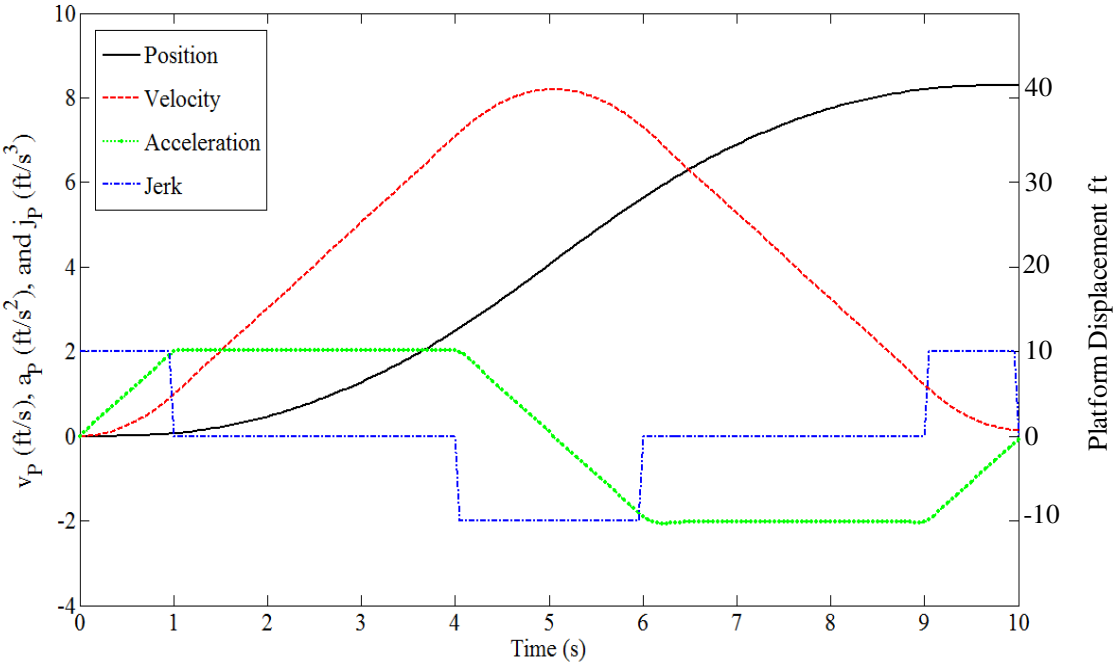

Fig. 6.13: The Motion Plan for Smooth Platform Motions

the platform.

This motion profile is repeated between each corner so that the overall motion of the platform is smooth. In the following section, we will describe the motion synthesis for the three wheel subsystems using this operational space motion profile.

6.5.2.2 Motion Synthesis for the Wheel Subsystems

Since this is a purely translational motion for the platform, the motions (the velocity, acceleration, etc.) of all the wheel attachment points are equal to the motion of the POI (the centroid G in this case). As the geometric parameters for all the wheels are identical, it will suffice to show a common motion synthesis for all wheel subsystems.

The motion along the segment between corners 1 and 2

At corner 1, the initial steering angle ψ (the angle made by the respective steering link with the body fixed frame *xy*) for each of the wheel subsystem is 0^o. Also we chose to keep the orientation of the platform is constant at all times to result in a purely translational motion. Due to the choice of a global inertial frame $\{0\}$ that is initially coincident with the body fixed frame $\{1\}$, we have the platform orientation $\Theta = 0^o$ at all times. Thus the acceleration of wheel attachment point *E*, $\ddot{X}_{Ej}$ and $\ddot{Y}_{Ej}$, is transformed (rotation by -ψ) in the wheel subsystem frame (frame $\{j\}$ as described in Fig. 6.2) as follows:

$$\ddot{X}_{Ej} = \ddot{X}_E \cos\psi + \ddot{Y}_E \sin\psi$$
$$\ddot{Y}_{Ej} = -\ddot{X}_E \sin\psi + \ddot{Y}_E \cos\psi \qquad \text{Eq. 6.11}$$

$\ddot{X}_{Ej}$ and $\ddot{Y}_{Ej}$ are the *X* and *Y* components of the acceleration of point E as expressed in frame {0}.

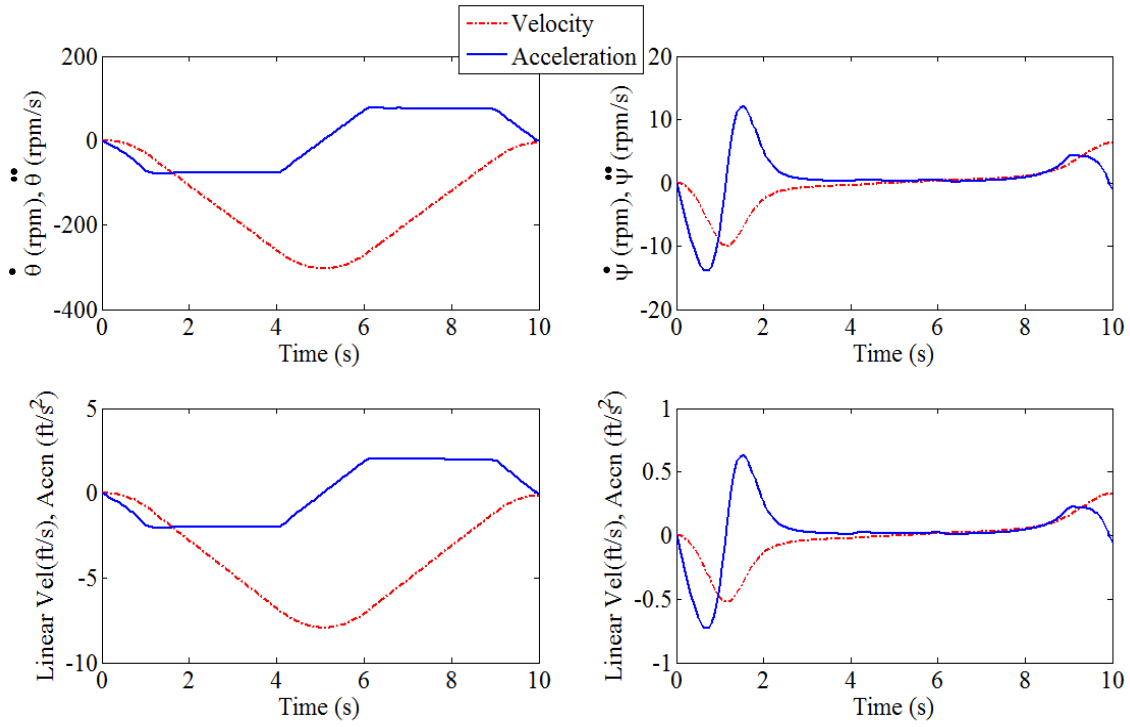

Driving Input Steering Input

Fig. 6.14: Simulation Second Order Input Motion Synthesis for the Mobile Platform with Three caster Wheels when it Travels from Corner 1 to Corner 2 as shown in Fig. 6.12

The angular accelerations of the driving input (denoted by θ) and the steering input (denoted by ψ) of each wheel subsystem is then computed by inverting Eq. 4.45 as follows:

$$\ddot{\theta} = 2\frac{\ddot{X}_{Ej} - l\dot{\psi}^2}{d}$$
$$\ddot{\psi} = \frac{-\ddot{Y}_{Ej} + \dot{\psi}\dot{\theta}d}{l} \qquad \text{Eq. 6.12}$$

Note that the acceleration of point E is expressed in a global frame coincident with the wheel subsystem frame $\{j\}$ as shown in Fig. 4.34. The angular velocity $\dot{\psi}$ and $\dot{\theta}$ of each wheel subsystem is then computed by integrating the angular acceleration $\ddot{\psi}$ and $\ddot{\theta}$. The graph of the motion synthesis result is shown in Fig. 6.14. The graphs shown in the top row are the result of motion synthesis in terms of the joint velocities and

accelerations. The graphs in the bottom row are plotted to show the equivalent linear velocities and accelerations so that we can evaluate the magnitudes in terms of realistic values. The graph for linear acceleration due to driving input shows that the peak acceleration reached is ~ 2 ft /s^2, a modest value compared the gravitational constant (~32.2 ft/s^2).

The motion along the segment between corners 2 and 3

After 10 seconds, the platforms encounters corner 2. The motion of the platform is in the direction that -90^o to the one discussed above. Also the simulation shows that the steering angle at the end of the motion above is ~-18^o. It was expected that the steering link aligns with the direction of travel such that the steering angle in this case should become -45^o. This is the case if we do the first order motion synthesis. However the second order

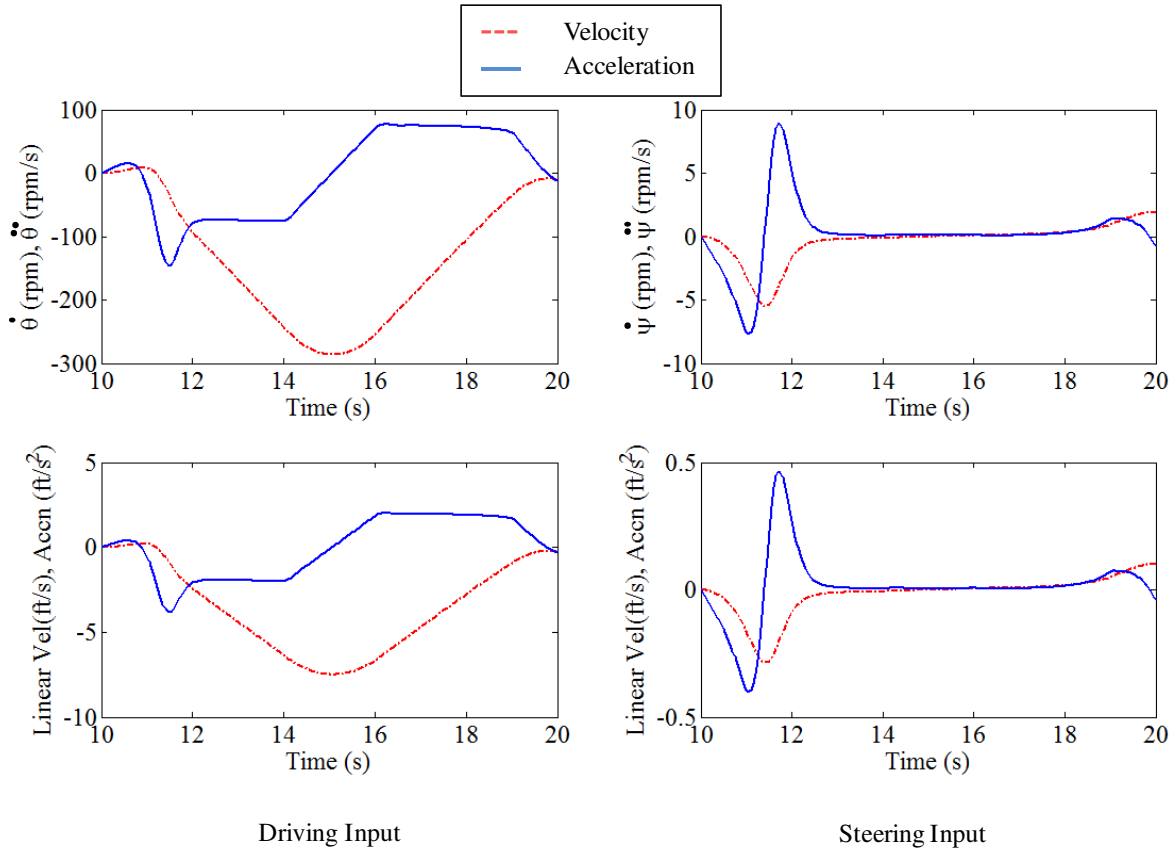

Fig. 6.15: Second Order Input Motion Synthesis for the Mobile Platform with Three caster Wheels when it Travels from Corner 2 to Corner 3 as shown in Fig. 6.12.

motion synthesis such as the one shown here results in the steering angle of -18^o. This is because the combination of tangential acceleration and Coriolis acceleration results in the steering angle away from the stable value (the magnitude of steering angle when the steering link is in the direction of travel such that the driving is the dominant input). With this initial steering angle value, the motion synthesis of the wheel subsystems results in the simulation graph for the two inputs as shown in Fig. 6.15.

The motion along the segment between corners 1 and 3

The combined graph of the motion synthesis shown in Fig. 6.16 shows the motion synthesis from *t = 0 s to 20 s*. Notice that the steering link angular velocity has a jump at t = 10 s.

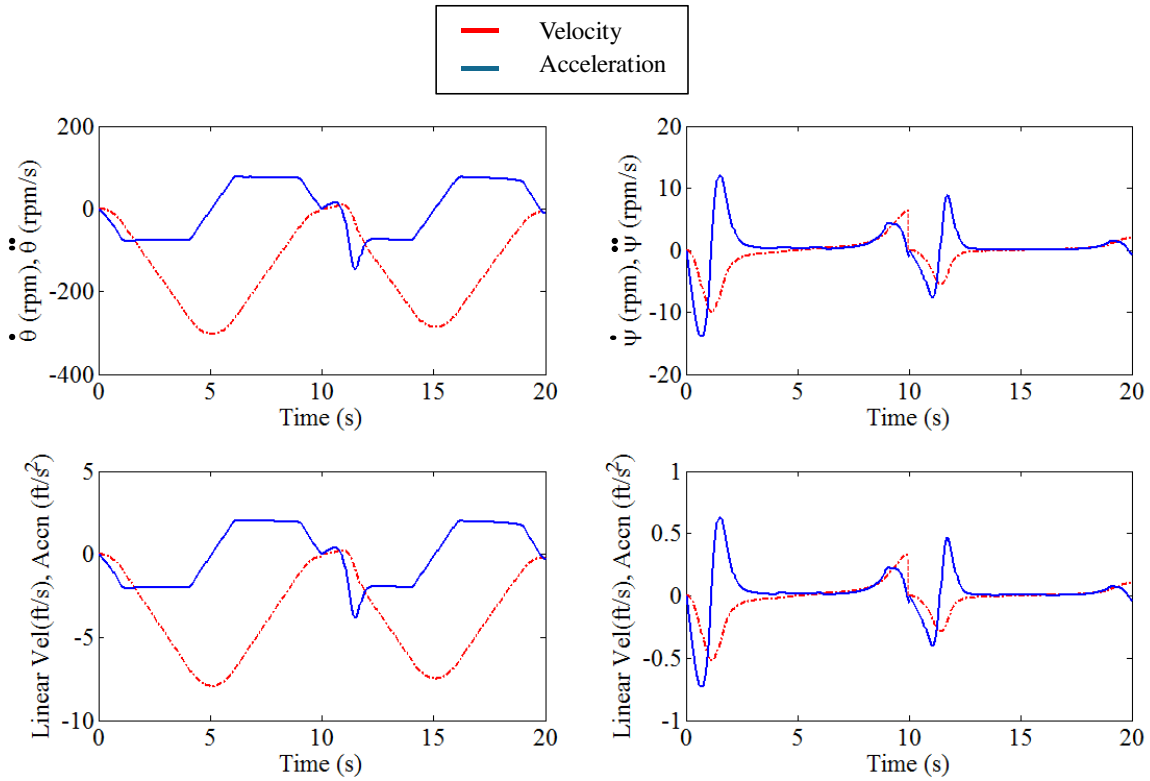

Fig. 6.16: Second Order Input Motion Synthesis for the Mobile Platform with Three caster Wheels when it Travels from Corner 1 to Corner 3 as shown in Fig. 6.12

With the accelerations of the input degrees of freedom known at all times during the

motion of the platform from corner 1 to 3, we can compute the input joint torques by force synthesis as discussed in the following section.

6.5.3 DYNAMIC MOTION SYNTHESIS

The mobile platform has inertial and external forces as shown in Fig. 6.2. For the successful motion of the platform along the required path, these forces should be sustained by the input rotations (steering τ_{sj} and driving τ_{dj} torques) of the platform wheel subsystems. Under the ideal conditions, these external forces are distributed evenly to the wheel subsystems. Here we will show the force synthesis under ideal conditions first and then discuss the case when different wheel subsystems encounter varying circumstances such as different ground conditions (in terms of wet patch, oil spills, pothole, etc.), or temperatures, etc.

6.5.3.1 Platform Body Forces

Fig. 6.17 shows the general schematic of all the forces on the platform body. The directions of all the forces are generic and not in the specific direction and magnitude pertaining to the numerical example. Point Q is a point in the body where the external force and moment is applied. Let the location of Q in the body be [-1, 1.5] in frame {1}.

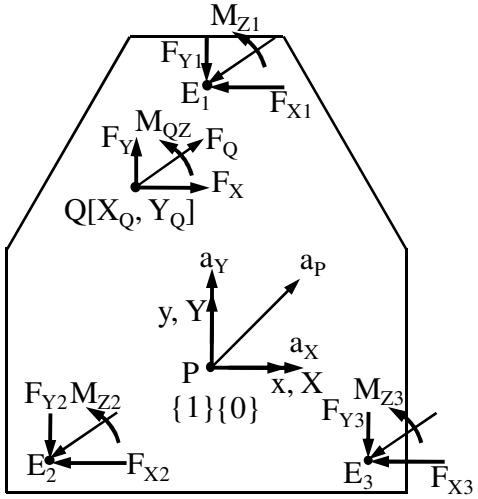

Fig. 6.17: Force Equilibrium for the Platform Body

Let the external force F_Q be *200 lb @ -30°* with the global X axis for *t = 0* to *20 s*. Also the external moment M_{QZ} be *400 lb-ft* for *t = 0* to *20 s*. Note that potentially there can be more than one point of application for the external forces and moments. We restrict ourselves to one point without loss of the generality. Using these conditions, the force equilibrium of the platform (Eq. 6.4) is:

$$\sum_{j=1}^{3} F_{Xj} = -200\cos(-30) + m_P a_X \qquad \text{Eq. 6.13-a)}$$

$$\sum_{j=1}^{3} F_{Yj} = -200\sin(-30) + m_P a_Y \qquad \text{Eq. 6.13-b)}$$

$$\sum_{j=1}^{3} F_{Zj} = m_P g \qquad \text{Eq. 6.13-c)}$$

$$\sum_{j=1}^{3} M_{Zj} = -400 + \sum_{j=1}^{3} F_{Xj} Y_{Ej} - \sum_{j=1}^{3} F_{Yj} X_{Ej} + (200\cos(-30))(1.5) - (200\sin(-30))(-1.0) \qquad \text{Eq. 6.13-d)}$$

Eq. 6.13-a) through Eq. 6.13-d) are the equations for the force and moment equilibrium of the mobile platform body. The aim of the first part of the motion synthesis is to compute the forces and moments that the three wheel subsystems need to sustain for the successful motion of the platform under the influence of the external force F_Q and Moment M_{Qz}. Initially we assume identical dynamic conditions (such as ground contact force availability, torque capacity of the input DOFs, etc.) for each wheel subsystem. We can then distribute the forces equally among the three wheel subsystems as follows:

$$F_{X1} = F_{X2} = F_{X3} = \frac{-200\cos(-30) + m_P a_X}{3} \qquad \text{Eq. 6.14-a)}$$

$$F_{Y1} = F_{Y2} = F_{Y3} = \frac{-200\sin(-30) + m_P a_Y}{3} \quad \text{Eq. 6.14-b)}$$

$$F_{Z1} = F_{Z2} = F_{Z3} = \frac{m_P g}{3} \quad \text{Eq. 6.14-c)}$$

$$M_{Z1} = M_{Z2} = M_{Z3} = \frac{400 - \sum_{j=1}^{3}(F_{Xj}Y_{Ej}) + \sum_{j=1}^{3}(F_{Yj}X_{Ej}) + (200\cos(-30))(1.5) - (200\sin(-30))(-1.0)}{3} \quad \text{Eq. 6.14-d)}$$

Eq. 6.14-a) through Eq. 6.14-d) provide us with the wheel subsystem-platform interaction forces. Note that the expressions on the right hand side of these equations are dictated by the operational space kinematic and dynamic requirements at each time step. Thus the external force F_Q, the platform gravity weight and the platform acceleration computed in Sec. 6.5.3.1 are the inputs to Eq. 6.14-a) through Eq. 6.14-c). The values of the forces on the wheel subsystems computed using these equations along with the external force F_Q and moment M_{QZ} then become inputs to Eq. 6.14-d).

The following numerical example shows how to compute the wheel subsystem forces and moments. For discussion purposes, let at $t = 2s$, the acceleration of the platform be $2\ ft/s^2\ @135^o$ to frame {0}. Using this information, the values of forces F_{Xj} ($j = 1, 2, 3$), F_{Yj}, F_{Zj} and M_{Zj} are computed using Eq. 6.14 as:

$$F_{X1} = F_{X2} = F_{X3} = \frac{-200\,cos(-30) + 100\ \times 2\,cos(135)}{3} = -104.87\ lbf \quad \text{Eq. 6.15-a)}$$

$$F_{Y1} = F_{Y2} = F_{Y3} = \frac{-200\,sin(-30) + 100\ \times 2\,sin(135)}{3} = +80.47\ lbf \quad \text{Eq. 6.15-b)}$$

$$F_{Z1} = F_{Z2} = F_{Z3} = \frac{m_P g}{3} = 1073\ lbf \quad \text{Eq. 6.15-c)}$$

$$M_{Z1} = M_{Z2} = M_{Z3} =$$

$$\frac{-400 - \sum_{j=1}^{3}(F_{Xj}Y_{Ej}) + \sum_{j=1}^{3}(F_{Yj}X_{Ej}) + (200\,cos(-30))(1.5) - (200\,sin(-30))(-1.0)}{3} \quad \text{Eq. 6.15-d)}$$

$$= -13.39\ lb - ft$$

A simulation is created for the motion of the platform from corner 1 to corner 3 in 20 seconds as discussed in the kinematic synthesis section. Fig. 6.18, shows the plot of the subsystem force requirement in terms of X_j and Y_j component for each subsystem to accomplish the dynamic motion of the platform. This requirement is identical to all wheel subsystems under identical external conditions.

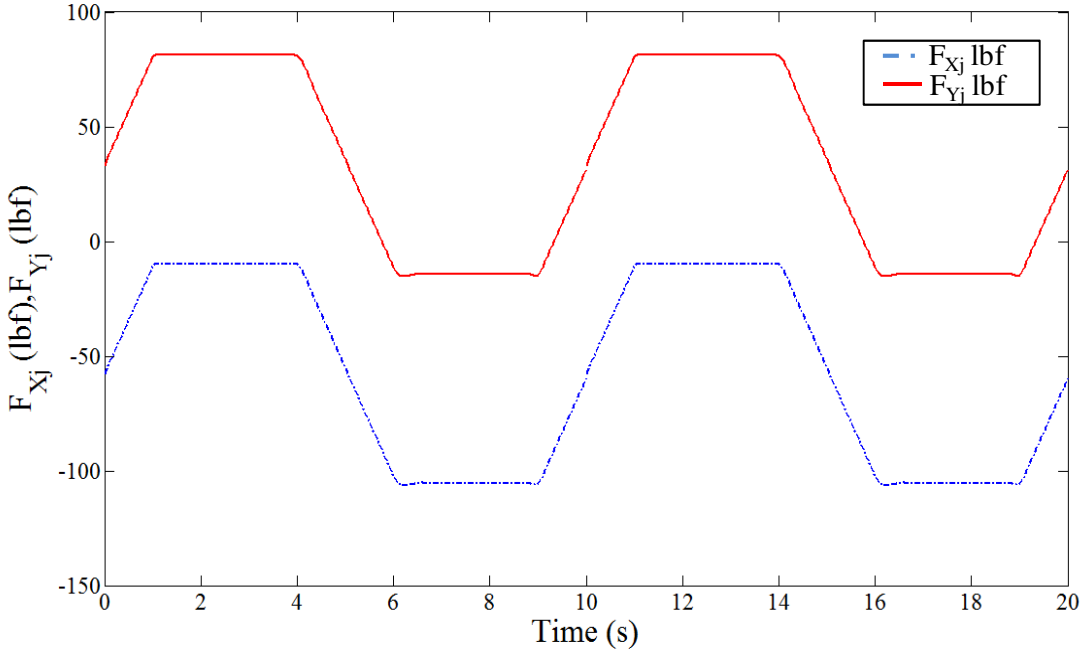

Fig. 6.18: Wheel Subsystem Forces due to Operational Space Dynamic Requirement when the Mobile Platform with Three Caster Wheels Travels From Corner 1 to Corner 3 (*t = 0s* to *20s*)

6.5.3.2 Wheel Subsystem Dynamics

With the wheel subsystem-platform interaction forces and moments known, we can use Eq. 6.7 to compute the ground-wheel contact forces and then the required joint torques as follows:

$$F_{xj} = -F_{Xj}cos\psi_j - F_{Yj}\,sin\,\psi_j + m_{Wj}\left(\frac{\ddot{\theta}_j d}{2} + l\dot{\psi}_j^{\,2}\right) \quad \text{Eq. 6.16-a)}$$

$$F_{yj} = F_{Xj}sin\psi_j - F_{Yj}\,cos\,\psi_j + m_{Wj}\left(\dot{\psi}_j\dot{\theta}_j d - l\ddot{\psi}\right) \quad \text{Eq. 6.16-b)}$$

$$F_{zj} = -F_{Zj} + m_{Wj}g \quad \text{Eq. 6.16-c)}$$

$$\tau_{dj} = F_{xj}\frac{d_j}{2} + M_{yj} + \left[F_{Xj}\,cos\,\psi_j + F_{Yj}sin\psi_j\right]h_j + F_{Zj}l_j + I_{dj}\ddot{\theta}_j = 0 \quad \text{Eq. 6.16-d)}$$

$$\tau_{s(j)} = F_{yj}l_j + M_{zj} + M_{Zj} + I_{sj}\ddot{\psi}_j \quad \text{Eq. 6.16-e)}$$

Note that the driving and steering input velocities ($\dot{\theta}_j$ and $\dot{\psi}_j$) and the accelerations ($\ddot{\theta}_j$ and $\ddot{\psi}_j$) of each wheel subsystems were computed in Sec. 6.5.2.2 (Fig. 6.14-Fig. 6.16). Considering that the rolling resistance moment M_{yj} and the steering resistance moment M_{zj} are small compared to the traction force and lateral force, we neglect them from the computation as the aim of this simulation is to discuss the general procedure of the dynamic synthesis. Using these conditions, we generated a simulation to compute the input torques, namely, driving and steering torques. Fig. 6.19 shows the simulation graph

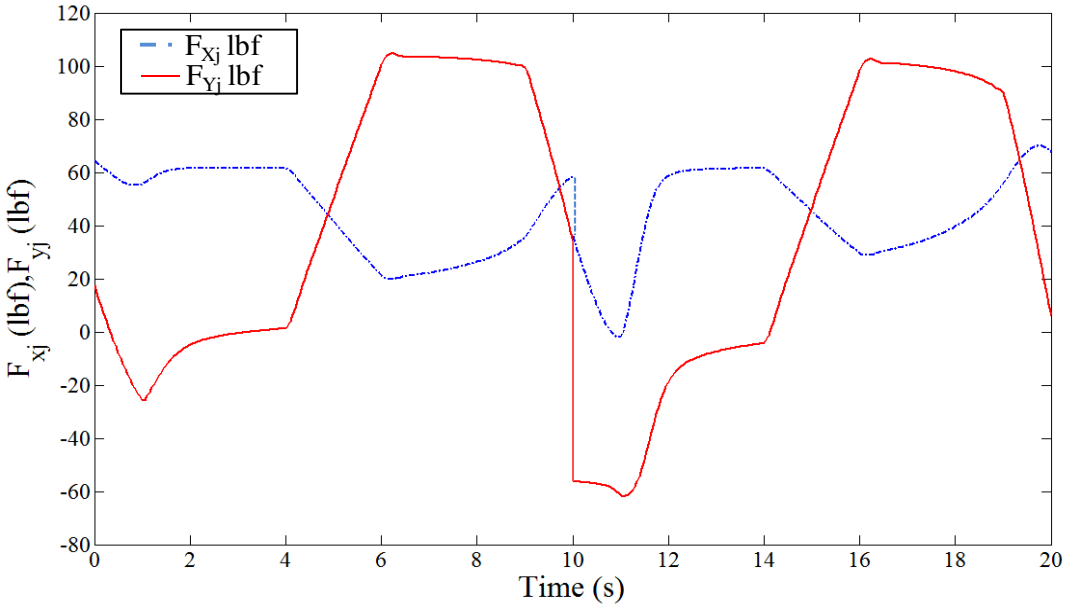

Fig. 6.19: The Tractive Force Fxj and the Lateral Force Fyj for the Platform Dynamic Motion from t= 0 to 20(s)

of the ground-contact forces, namely, the tractive force F_{xj} and the lateral force F_{yj} for the Platform Dynamic Motion from *t= 0 to 20(s)*.

The input torques required to accomplish this motion are shown in Fig. 6.20.

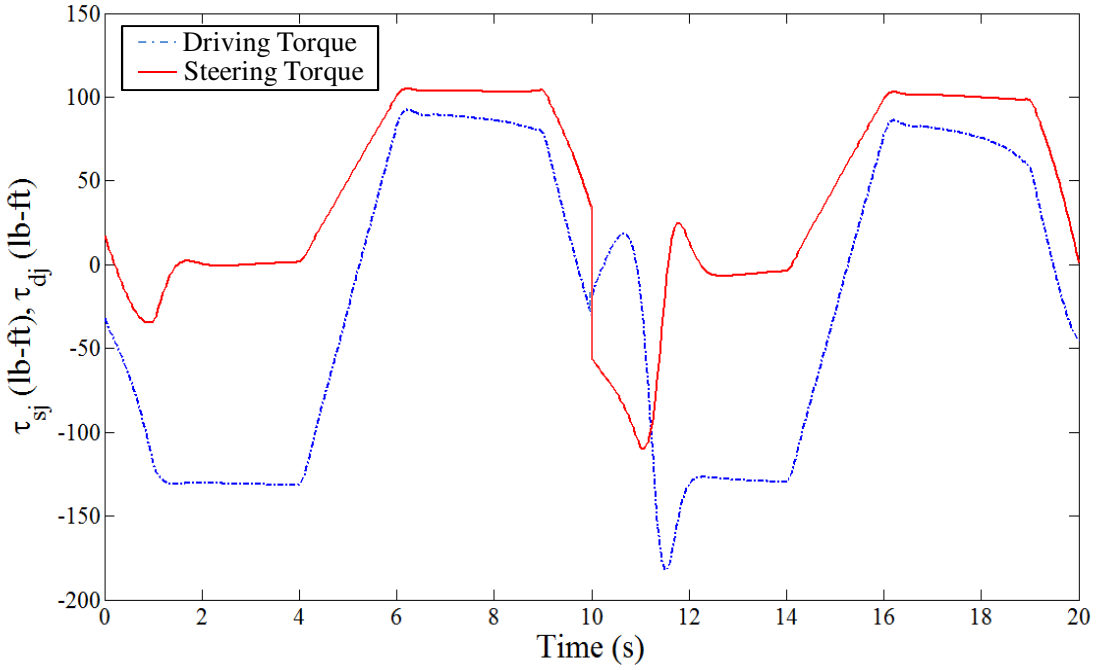

Fig. 6.20: Input Torque Curve for the Dynamic Motion of the Mobile Platform with Three Caster Wheels from *t = 0 to 20 (s)*

6.5.4 DYNAMIC SYNTHESIS UNDER VARYING EXTERNAL CONDITIONS

So far, we discussed the dynamic motion synthesis under ideal conditions. Under these conditions, the platform external forces and moments, and inertial forces and moments were equally distributed among the three wheel subsystems. However, the interaction between wheel and ground is very dynamic and different wheels on the platform may be subjected to different conditions. There are other factors that also influence the performance of a tire thus making wheel (in turn tire) dynamics a very dominant factor in the dynamic synthesis of the mobile platform. Wong (2001) presents a noteworthy effort in presenting a case for the dynamic and non-linear nature of the

wheel-ground interaction forces and moments such as, the tractive effort, rolling resistance, lateral (cornering) force, steering resistance (self-aligning force), etc. these tire-related performance factors are in dependent on a set of operational factors such as: the vehicle speed v_P, normal force F_{zj}, tire inflation pressure p, tire internal temperature t_i, surface temperature t_s, wetness of the surface characterized by water depth (d)). Thus characterizing the performance of the wheel subsystem using the performance factors under the influence of the dynamic operational factors is an important step in successfully operating the mobile platform in general.

To this effect a future study is proposed here to generate a spectrum of performance maps that capture the influence of these operational factors on the performance factors. Another aspect of the dynamic synthesis is to distribute the forces among the wheel subsystems to command the platform efficiently in terms of energy consumption, speed, time required, etc. much in the same way as is done for the manipulators (Tisius et al. 2009; Kapoor and Tesar, 2006).

6.6 Summary

The aim of this chapter was to present a representative dynamic model for a mobile platform that has redundant system of inputs. We showed that the redundancy of input DOF for the mobile platforms results in force redundancy. The force redundancy in this case is beneficial due the dynamic and nonlinear nature of wheel forces that limit the amount of forces and moments the wheel subsystem can sustain from the platform interaction. The wheel-ground interaction forces (such as the tractive effort, rolling resistance, lateral (cornering) force, steering resistance (self-aligning force), etc.) are dependent on various external factors such as the vehicle speed v_P, normal force F_{zj}, tire inflation pressure p, tire internal temperature t_i, surface temperature t_s, wetness of the

surface characterized by water depth (d)), etc. These factors should be considered while devising the force distribution scheme for successful operation of the mobile platforms.

7 SUMMARY AND FUTURE WORK

7.1 Introduction

The goal of this chapter is to highlight the important findings/results of this research report and to lay out a roadmap for the future work. Thus, the chapter is organized into two broad categories, (i) Summary and Conclusions, and (ii) Recommendations for Future Work. The overall organization of the chapter is as follows.

- **Research Summary and Conclusions**
  - **Research Objectives**

    The objectives of this research work are summarized in this section.

  - **Literature Summary**

    This research has presented an opportunity for a literature review in the areas of theory of instantaneous invariants (curvature theory) applied to linkage mechanisms, mobile platform kinematics and dynamics. While a detailed review of the literature was presented in the report, the important literature pertaining to this report is summarized in a tabular form in this section.

  - **Research Results and Discussions**

    This section summarizes the important results and lessons learned through this research.

  - **Primary Contributions**

    A list of the primary contributions of this research is tabulated in this section.

- **Recommendations and Future Work**

Based on the research findings, lessons learned and the literature review, some recommendations for the future work are detailed in this section.

7.2 Research Summary and Conclusions

This section includes a brief review of the report in the form of bulleted lists and/or pertaining discussions.

7.2.1 RESEARCH OBJECTIVES

The overall objective of the research was at two levels, (i) to generalize the theory for the instant centers (also known as curvature theory (Bottema and Roth, 1979) to higher order motions (third and higher) and (ii) to study the mobile platforms and their motion programming in the light of the theory for ICs. Table 7.1 provides a more granulated list of objectives.

Table 7.1: Research Objectives

- Investigate the existing kinematic modeling methodologies for planar mobile platforms.
- Study the first and second order Instant Centers (IC) in the current literature and propose a generalized algebraic formulation to extend the IC based formulation to the higher order planar motion of a general rigid body.
- Study a finite set of special case 1-DOF, 2-DOF motions to understand the properties of the higher order ICs.
- Survey the mobile platform architectures that are capable of planar motions and categorize them based on their IC properties (on the lines similar to Campion et al. (1996) who categorized wheel subsystems based on kinematic constraints).
- Propose the IC based motion synthesis methodology for the set of mobile platforms.
- Study the dynamic model of a representative mobile platform to underscore the influence of input redundancy on the distribution of inertial and external forces among the wheel subsystems.

7.3 Literature Review Summary

This research has presented an opportunity for a literature review in the areas of theory of instantaneous invariants (curvature theory) applied to linkage mechanisms, mobile platform kinematics and dynamics. While a detailed review of the literature was presented in the report, the important literature pertaining to this report is summarized in a tabular form in this Table 7.2.

Table 7.2: Literature Review		
Instantaneous Invariants Theory	Bottema, 1961; Bottema and Roth, 1979	• Introduced the theory of instantaneous invariants • Presented an algebraic formulation to describe planar and spatial rigid body motion using instantaneous invariants
	Tesar et al. 1967, 1968, 1968	• generalized the instantaneous formulation for kinematic motion synthesis in terms of multiply separated positions
	Cowie, 1961	• Vector based formulation for the first and second order IC with physically relevant discussions
Spatial Case Study	Veldkamp, 1969	• studied the acceleration center and acceleration field of the rigid body spatial motion with a study of special cases
	Ridley, 1992	• Used screw and its time derivative to describe the spatial motion of a rigid body for up to the second order
Mobile Platform Kinematics	Muir and Newman, 1989	• Presented a general approach to model mobile platforms on the lines similar to manipulators (Thomas and Tesar, 1982).
	Campion et al., 1996	• Presented a method for kinematic modeling of mobile platforms using kinematic constraints on various wheel configurations
	Yi and Kim, 2002	• Presented inverse kinematics methodology for redundantly actuated mobile platform

Mobile Platform Dynamics	Freeman and Tesar, 1988	• Proposed a generalized dynamic modeling methodology for serial and parallel robotic systems
	Holmberg and Khatib, 2000	• Presented Newton-Euler based dynamic model for mobile platform with caster wheels
	Wong, 2001	• Detailed study of vehicle dynamics with an emphasis on wheel-ground interaction properties

The literature review in the area of instantaneous invariants pointed us to the physical nature of the first and second order IC. However, these results have not been fully applied to the time dependent motion synthesis of mobile platform. Also there was a need of generalizing the theory of instantaneous invariants to the higher order motion such that the higher order motion properties of the platform subsystems could be effectively computed. Moreover, the currently utilized Jacobian based approach to do the inverse kinematics of mobile platforms (proposed by Muir and Newman, 1898, and demonstrated by Yi and Kim, 2002) results in mathematical complexity, an unnecessary result for parallel configurations such as a mobile platform. The current research addresses these shortcomings by generalizing the theory of instantaneous invariants to higher order (Chapters 2 and 3) and applying the results to the mobile platforms there by completely generalizing the motion synthesis of mobile platforms as demonstrated in Chapter 3 through 5 by means of a simple/direct computation.

7.4 Research Results and Discussions

This research emphasized the fact that a mobile platform is a parallel system with a straightforward inverse kinematics. It follows that the kinematic formulation using ICs can result in a simpler and yet physically intuitive motion synthesis of mobile platforms. The following is a summary of the important observations and results of this report. The summary is divided into two distinct areas, (i) the generalized IC based formulation, and

(ii) the mobile platforms.

7.4.1 IC BASED FORMULATION

Chapter 2 and 3 of this report studied the planar motion of a general rigid body without focusing on the mobile platform. The important observations pertaining to the IC based formulation are as follows.

1. The velocity (first order) IC is a unique entity for instantaneous motion of the rigid body in consideration as long as the body has finite angular velocity ω as shown in Sec. 2.4. On the other hand, when $\omega = 0$, the velocity IC lies at ∞ and the body is instantaneously in pure translation.

2. The velocity IC is a geometric property for a 1-DOF constrained planar motion as shown in Sec. 3.2. In case of a 2-DOF and 3-DOF planar motion, the IC is not based entirely on geometry but depends on the instantaneous kinematic properties (translational and rotational velocities) of the rigid body motion (Sec. 2.4).

3. In general, the IC of any order is a unique entity and follows two properties: directionality and proportionality as elaborated in Sec. 2.6 (Eq. 2.48-Eq. 2.54).

   a. Directionality: Every time state (such as velocity, acceleration, etc.) of every point E in the rigid body is at an angle β_k to the radius vector ρ_k that joins the point E with the corresponding IC, I_k. For the first order motion (velocity), the angle β_1 is 90^o.

   b. Proportionality: The magnitude of the time state is proportional to the radius vector, ρ_k.

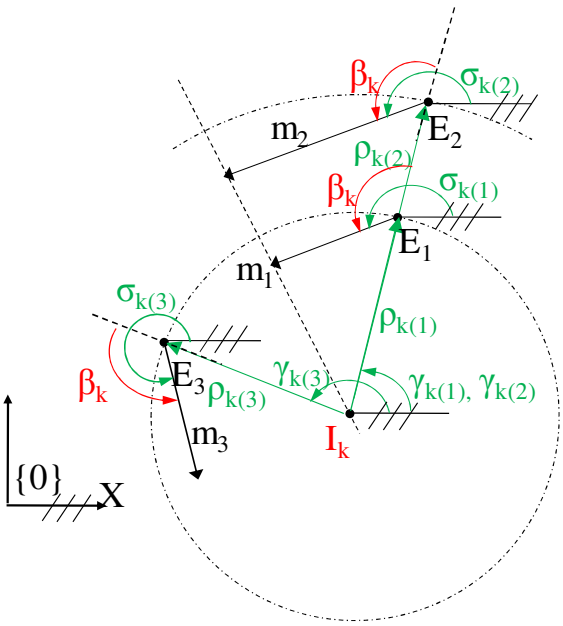

Fig. 7.1: k^{th} Order Kinematics of a General Rigid Body

The general equation for the k^{th} order motion state of any point E in a rigid body under a planar motion can be expressed as follows: $m_k = \left|\frac{M_k}{cos\beta_k}\rho_k\right| e^{i(\gamma_k+\beta_k)}$, where $\left|\frac{M_k}{cos\beta_k}\rho_k\right|$ is the magnitude and $e^{i(\gamma_k+\beta_k)}$ is the direction. Then, the magnitude proportionality can be analytically described as: $m_k \propto \rho_k$. Also the directionality comes from the fact that the angle β_k between two unit vectors for m_k and ρ_k is constant for any point E in the rigid body.

4. As shown in Fig. 7.1, all points on a radial line drawn from the k^{th} order IC (Points E_1 and E_2) will have the same global orientation for respective time states and all points at same radial distance ρ_k (Points E_1 and E_3) will have equal time state magnitudes. This illustrates the geometric nature of the formulation.

Table 7.3 summarizes the analytical formulation for up to the fifth order motion of a general rigid body under 3-DOF planar motion.

Table 7.3: Summary of the IC Based Kinematic Formulation for Mobile Platforms

	IC Location	The Orientation Angle	Times States of a General Point 'E'
First Order	$X_{I1} = X_P - \frac{\dot{Y}_P}{\omega}$ $Y_{I1} = Y_P + \frac{\dot{X}_P}{\omega}$	$\beta_1 = 90^o$	$\dot{X}_E = -\omega . Y_{\rho 1}$ $\dot{Y}_E = \omega . X_{\rho 1}$ $m_1 = \rho_1 . \omega,\ \beta_1 = 90^o$
Second Order	$X_{I2} = X_P + \frac{\ddot{X}_P \omega^2 - \ddot{Y}_P \alpha}{\alpha^2 + \omega^4}$ $Y_{I2} = Y_P + \frac{\ddot{X}_P \alpha + \ddot{Y}_P \omega^2}{\alpha^2 + \omega^4}$	$tan\ \beta_2 = -\frac{\alpha}{\omega^2}$	$\ddot{X}_E = -\omega^2 [X_{\rho 2} - Y_{\rho 2} tan\beta_2]$ $\ddot{Y}_E = -\omega^2 [X_{\rho 2} . tan\beta_2 + Y_{\rho 2}]$ $m_2 = \left\| -\frac{\omega^2}{cos\beta_2} \rho_2 \right\| e^{j(\gamma_2 + \beta_2)}$
Third Order	$X_{I3} = X_P + \frac{X_P^{(3)}(3\omega\alpha) - Y_P^{(3)}(\dot{\alpha} - \omega^3)}{(\dot{\alpha} - \omega^3)^2 + (3\omega\alpha)^2}$ $X_{I3} = Y_P + \frac{X_P^{(3)}(\dot{\alpha} - \omega^3) + Y_P^{(3)}(3\omega\alpha)}{(\dot{\alpha} - \omega^3)^2 + (3\omega\alpha)^2}$	$tan\ \beta_3 = -\frac{\dot{\alpha} - \omega^3}{3\omega\alpha}$	$X_E^{(3)} = -3\omega\alpha [X_{\rho 3} - Y_{\rho 2} tan\beta_3]$ $Y_E^{(3)} = -3\omega\alpha [X_{\rho 3} tan\beta_k + Y_{\rho 3}]$ $m_3 = \left\| -\frac{3\omega\alpha}{cos\beta_3} \rho_3 \right\| e^{j(\gamma_3 + \beta_3)}$
Fourth Order	$X_{I4} = X_P + \frac{X_P^{(4)}(4\omega\dot{\alpha} + 3\alpha^2 - \omega^4) - Y_P^{(4)}(\ddot{\alpha} - 6\omega^2\alpha)}{(\ddot{\alpha} - 6\omega^2\alpha)^2 + (4\omega\dot{\alpha} + 3\alpha^2 - \omega^4)^2}$ $Y_{I4} = Y_P + \frac{X_P^{(4)}(\ddot{\alpha} - 6\omega^2\alpha) + Y_P^{(4)}(4\omega\dot{\alpha} + 3\alpha^2 - \omega^4)}{(\ddot{\alpha} - 6\omega^2\alpha)^2 + (4\omega\dot{\alpha} + 3\alpha^2 - \omega^4)^2}$	$tan\ \beta_4 = -\frac{\ddot{\alpha} - 6\omega^2\alpha}{4\omega\dot{\alpha} + 3\alpha^2 - \omega^4}$	$X_E^{(4)} = -(4\omega\dot{\alpha} + 3\alpha^2 - \omega^4) . [X_{\rho 4} - Y_{\rho 4} tan\beta_4]$ $Y_E^{(4)} = -(4\omega\dot{\alpha} + 3\alpha^2 - \omega^4) . [X_{\rho 4} tan\beta_4 + Y_{\rho 4}]$ $m_4 = \left\| -\frac{4\omega\dot{\alpha} + 3\alpha^2 - \omega^4}{cos\beta_4} \rho_4 \right\| e^{j(\gamma_4 + \beta_4)}$
Fifth Order	$X_{I5} = X_P + \frac{X_P^{(5)}(10\alpha\dot{\alpha} + 3\omega\ddot{\alpha} - 10\omega^3\alpha) - Y_P^{(5)}(\alpha^{(3)} - 10\omega^2\dot{\alpha} - 15\omega\alpha^2 + \omega^5)}{(\alpha^{(3)} - 10\omega^2\dot{\alpha} - 15\omega\alpha^2 + \omega^5)^2 + (10\alpha\dot{\alpha} + 3\omega\ddot{\alpha} - 10\omega^3\alpha)^2}$ $Y_{I5} = Y_P + \frac{X_P^{(5)}(\alpha^{(3)} - 10\omega^2\dot{\alpha} - 15\omega\alpha^2 + \omega^5) + Y_P^{(5)}(10\alpha\dot{\alpha} + 3\omega\ddot{\alpha} - 10\omega^3\alpha)}{(\alpha^{(3)} - 10\omega^2\dot{\alpha} - 15\omega\alpha^2 + \omega^5)^2 + (10\alpha\dot{\alpha} + 3\omega\ddot{\alpha} - 10\omega^3\alpha)^2}$	$tan\ \beta_5 = -\frac{\alpha^{(3)} - 10\omega^2\dot{\alpha} - 15\omega\alpha^2 + \omega^5}{10\alpha\dot{\alpha} + 3\omega\ddot{\alpha} - 10\omega^3\alpha}$	$X_E^{(5)} = -(10\alpha\dot{\alpha} + 3\omega\ddot{\alpha} - 10\omega^3\alpha) . [X_{\rho 5} - Y_{\rho 5} tan\beta_5]$ $Y_E^{(5)} = -(10\alpha\dot{\alpha} + 3\omega\ddot{\alpha} - 10\omega^3\alpha) . [X_{\rho 5} tan\beta_5 + Y_{\rho 5}]$ $m_5 = \left\| -\frac{10\alpha\dot{\alpha} + 3\omega\ddot{\alpha} - 10\omega^3\alpha}{cos\beta_5} \rho_5 \right\| e^{j(\gamma_5 + \beta_5)}$

7.4.1.1 General Discussions

Here, we summarize the first and second order motion parameter choices that the IC based formulation offers for composing a motion plan of a mobile platform. We restrict ourselves to the motion of the POI on the body for this discussion. Consider a rigid body as shown in Figure 7.2.

First Order Motion (Sec. 2.4)

1. If we choose the velocity of POI v_P, it fixes the orientation of ρ_1 (since $\beta_1 = 90$)
   a. We can choose the radius ρ_1 to fix the angular velocity ω of the body and also the first order IC, I_1.
   b. We can choose the angular velocity ω of the body to fix the radius ρ_1 and also the first order IC, I_1.
2. If we choose the radius ρ_1 of POI, it fixes the orientation of v_p (since $\beta_1 = 90$)
   a. We can choose v_P to fix the angular velocity ω of the body and also the first order IC, I_1.
   b. We can choose the angular velocity ω of the body to fix the velocity v_P and also the first order IC, I_1.

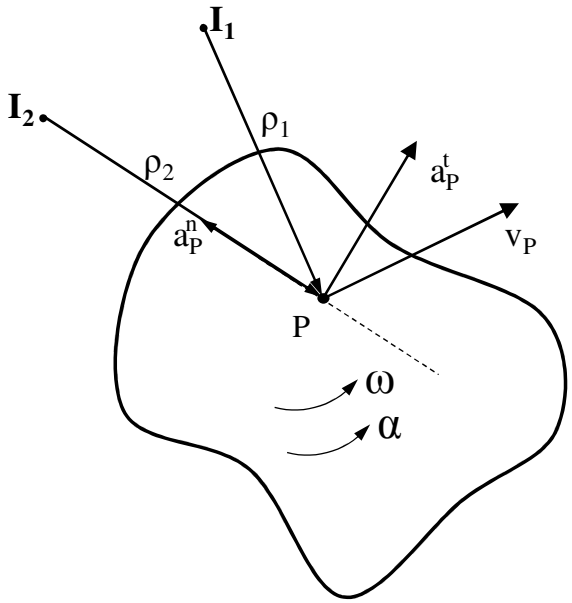

Figure 7.2: Motion Plan for a Rigid Body Using the First and Second Order ICs

Second Order Motion (Sec. 2.5.2)

We know ω from first order motion computation.

1. The normal component of the total acceleration a_p^n of POI fixes the location of I_2 (Fig. 2.9)
   a. Choose the angular acceleration α to fix the tangential component a_p^t
   b. Choose the tangential component a_p^t to fix the angular acceleration α
2. The tangential component of acceleration a_p^t fixes the direction of the radius ρ_2 (Fig. 2.9)
   a. Choose the angular acceleration α to fix the location of I_2. Since angular acceleration is already known, we can compute the normal component of the total acceleration a_p^n (Fig. 2.9)
   b. Choose the radius ρ_2 to fix the location of I_2. Since angular acceleration is already known, we can compute the normal component of the total acceleration a_p^n (Fig. 2.9)

Table 7.4 summarizes some special scenarios for the first and second order ICs that provide user with further guidelines on the consequences of the locations of the ICs.

Table 7.4: Special Case Scenarios for the First and Second Order ICs

Condition	Result/Consequence
$I_1 => \infty$	$\omega = 0, \alpha = 0$: Stationary Translation
	$\omega = 0, \alpha \neq 0$: Instantaneous Translation
$I_1 \equiv I_2$	$\omega \neq 0, \alpha \neq 0$ Instant Centers Coincident; Pure Rotation
$I_1 => I_2$	Going Towards a Condition of Pure Rotation, I_1 is stationary
$I_1 \neq> I_2$	I_2 is going away from I_1 to Give a More Complex Motion
I_2 is Stationary	Accelerating Around a Point acting as the Acceleration Center

7.4.1.2 Numerical Example of Motion Planning

Consider a mobile platform traversing a trajectory that changes from concave to convex at point C so as to make an 'S' shaped curve as shown in Fig. 7.3. In this case, it is always aligned with the direction of travel, such that all the ICs for the velocity, acceleration, jerk, etc., are located at the center of the curvature. When the mobile platform crosses point C, the normal acceleration, jerk etc. instantaneously switch to the opposite direction resulting in shock and motion uncertainty.

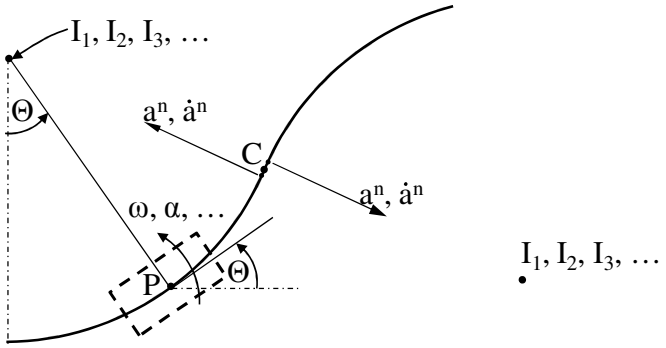

Fig. 7.3: Mobile Platform Traversing an '*S*' Shaped Trajectory

Using IC based motion programming; we can remove this crossover shock and uncertainty with a dexterous platform as follows. To prevent the shock, we put a restriction on the motion whereby point C becomes a stationary inflection point. To accomplish this, we select the IC locations, the instantaneous motion states of point P and

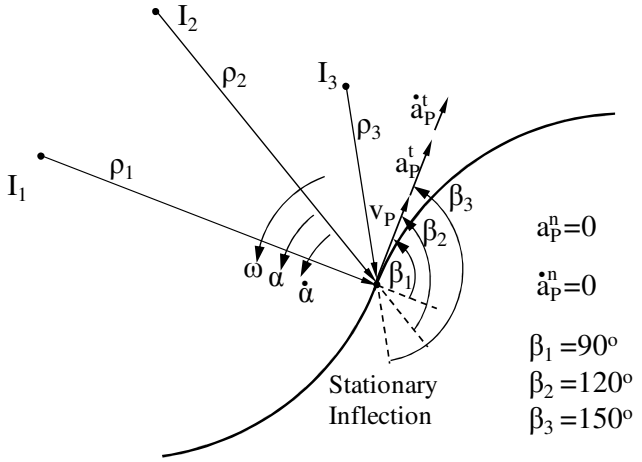

Fig. 7.4: Higher Order Motion Planning for the Mobile Platform Traversing the *S* Shaped Trajectory

the mobile platform such that the velocity, acceleration and the jerk of point P are instantaneously parallel to each other and tangential to the trajectory at point C (see Fig. 7.4) thereby eliminating the normal components for acceleration and jerk.

A numerical example of the required motion plan follows.

Step1: First Order Motion Requirement

Choose the radius, ρ_1 of point P for the first order IC. Based on ρ_1, compute the magnitude of the angular velocity (Sec. 2.4, Eq. 2.12) $\omega = \frac{v_P}{\rho_1}$, where $\beta_1 = \frac{\pi}{2}$ rad. Let the instantaneous linear velocity v_P of point P on the mobile platform be 5 ft/s. Let ρ_1 be 15 ft. Thus the angular velocity, ω, of the platform would be $\omega = \frac{v_P}{\rho_1} = 0.33 \frac{\text{rad}}{\text{s}}$.

Step 2: Second Order Motion Requirement

Choose the tangential acceleration a_P^t of point P. Choose the second order orientation angle β_2 which cannot be $\frac{\pi}{2}$ for a nonzero angular velocity, ω (Sec. 2.5.2). Further, compute the angular acceleration, α, and the radius ρ_2 of P from the second order IC I_2 where $a_P^t = \frac{g}{10} \frac{\text{ft}}{s^2} = 3.22 \frac{\text{ft}}{s^2}$. Note that a large value of β_2 results in a small value of the angular acceleration and a large value for radius ρ_2. Thus, we choose angle β_2 to be $\frac{2\pi}{3}$ radians (120^o). With these numerical values, the instantaneous angular acceleration, α, can be computed (Eq. 2.20) as $\alpha = -\frac{\tan \beta_2}{\omega^2} = 0.19 \frac{\text{rad}}{s^2}$ and the radius ρ_2 can be computed using Eq. 2.52 as $\rho_2 = -\frac{a_P^t \cos \beta_2}{\omega^2} = 14.48\text{ft}$.

Step 3: Third Order Motion Requirement

Choose the tangential jerk, $\dot{a}_P^t$ of point P required with zero normal jerk. Also, choose the third order orientation angle β_3 which cannot be $\frac{\pi}{2}$ radians for nonzero angular velocity, ω and nonzero angular acceleration, α (Eq. 2.40). In this scenario, we have finite values for both of the terms. Further, compute the radius ρ_3 of P for the third order IC I_3 as well as the angular jerk, $\dot{\alpha}$. Let the linear jerk of point P be 1/20th of the gravitational acceleration constant per second, thus $\dot{a}_P^t = 1.61 \frac{\text{ft}}{s^3}$. Again, note that a larger value of β_3

results in a smaller value of the angular jerk and a larger value for radius ρ_3. Here, we choose angle β_3 to be $\frac{5\pi}{6}$ radians (150^o) as we want a small angular jerk. Thus the instantaneous angular jerk can be computed using Eq. 2.40 as $\dot{\alpha} = \omega^3 - 3\omega\alpha \times \tan\beta_3 = 0.15\frac{\text{rad}}{\text{s}^3}$. The radius ρ_3 of P can be computed using Eq. 2.52 as $\rho_3 = -\frac{\dot{a}_P^t \cos\beta_3}{3\omega\alpha} = 7.24\text{ft}$.

The numerical values of all the kinematic parameters are summarized in Table 7.5. With the motion specifications for the first three orders of motion, the mobile platform wheel subsystem requirements can be computed using Eq. 2.12, and Eq. 2.52. This simple example emphasizes the intuitive and yet generalized nature of the IC based formulation.

Guidelines for the Motion Planning

Based on the observations made during this numerical example, we can provide some guidelines to arrive at useful motion planning values as follows:

1. For a given value of v_P, choosing a large ρ_1 results in a small ω. In other words, $\omega \propto 1/\rho_1$.
2. Choosing a small β_2 reduces the size of ω but increases α. Notice that the magnitude of β_2 can vary between $\frac{\pi}{2}$ and π. For a particular value of β_2, a large ω increases α by the square. When $\beta 2 = \frac{\pi}{2}$, ω is zero.
3. Choosing a small β_2 reduces the size of ρ_2.
4. Choosing a small β_3 (between $\frac{\pi}{2}$ and π) reduces the size of α but increases $\dot{\alpha}$. Notice

Table 7.5: Summary of the Numerical Example Result

	m_K	Angular Motion	ρ_K	β_K
1st Order	$5\frac{\text{ft}}{\text{s}}$	$0.33\frac{\text{rad}}{\text{s}}$	15 ft	$\frac{\pi}{2}$ rad
2nd Order	$3.22\frac{\text{ft}}{\text{s}^2}$	$0.19\frac{\text{rad}}{\text{s}^2}$	14.48ft	$\frac{2\pi}{3}$ rad
3rd Order	$1.61\frac{\text{ft}}{\text{s}^3}$	$0.15\frac{\text{rad}}{\text{s}^3}$	7.24ft	$\frac{5\pi}{6}$ rad

that the magnitude of β_3 can vary between 0 and π. For a particular value of β_3, a large ω decreases $\dot{\alpha}$ by the cube.

5. Choosing a small β_3 (between $\frac{\pi}{2}$ and π) reduces the size of ρ_3.

7.4.1.3 Study of Classical Motions to Understand Physical Meaning of ICs

In Table 7.3, we see that the IC based formulation for the third and higher order motion contains highly coupled terms (such as $(3\omega\alpha)$ for the third order, $(\ddot{\alpha} - 6\omega^2\alpha)$ for the fourth order, etc.). To understand the physical nature of the higher order ICs, Chapter 3 studied some well represented 1-DOF and 2-DOF rigid body (simplified as geometric

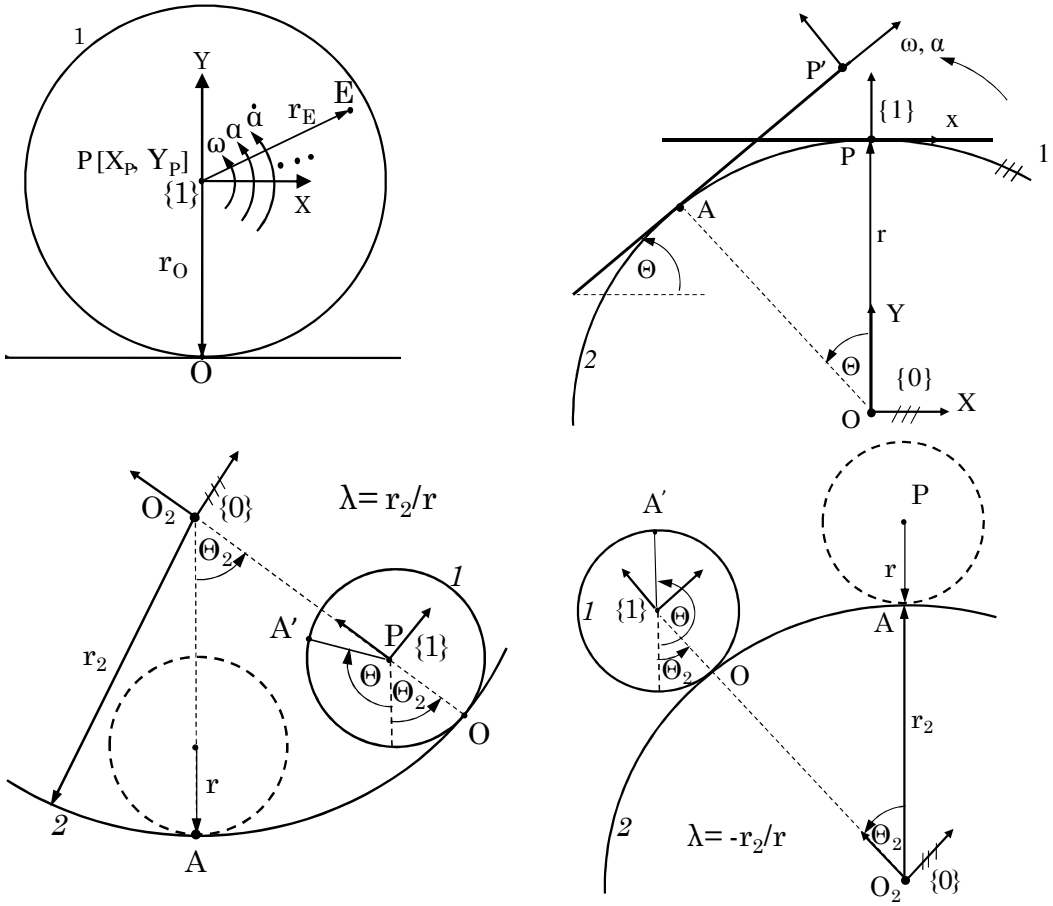

Figure 7.5: The Schematic Representations of the Classical Motions. Clockwise From Top Left: (i) A circle Rolling on a Straight Line (with or without Slipping), (ii) A Line Rolling on a Circle without Slipping, (iii) A Circle Rolling Outside Another Circle, and (iv) a Circle Rolling Inside another circle

shapes) motions as follows:

- A circle rolling on a straight line without slipping (Sec. 3.2)
- A circle rolling on the inside of another circle without slipping (Sec. 3.3)
- A circle rolling on the outside of another circle without slipping (Sec. 3.3)
- A line rolling on a circle without slipping (Sec. 3.5)
- A circle rolling on a line with slipping (Sec. 3.4)

Following are the important observations and results of the study:

1. Though the locus of the k^{th} order IC in case of a general planar 3-DOF motion is dependent on the instantaneous kinematic states of the rigid body (such as the angular motion of the rigid body (ω, α, etc.), and the linear motion of the Point of Interest P (such as v_P, a_P, etc.)), the locus of a general k^{th} order IC for special case 1DOF motions (such as a cylindrical body rolling without slipping on a flat surface or on another cylindrical body, etc.), that locus is dependent on geometry of the interacting rigid bodies (Sec. 3.2, Sec. 3.3, and Sec. 3.4).

2. The velocity IC for the 1-DOF motions is always located at the point of contact of the two bodies rolling without slip.

3. The locus of the acceleration IC in case of the 1DOF motions (rolling without slip) is a circle coincident with the corresponding inflection circle (Fig. 3.20).

4. The third and fourth order ICs for 1-DOF motions are purely geometric in nature. The study of further special cases of instantaneous kinematic states resulted in certain analytical shapes such as a straight line or a circle which are shown in Table 3.1 to Table 3.5. Table 7.7 shows an example summary of special case scenario for the fourth order motion of a circle rolling on a straight line.

    a. For example, if at an instant in time, if a circle of unity radius is rolling on a straight line with zero angular jerk $\dot{\alpha}$, and the angular velocity ω with non-zero

the angular acceleration α and the derivative of angular jerk α̈, the locus of the fourth order IC becomes a circle with radius of ½. The constant orientation angle for all points in the rigid body (represented as a circle) for the fourth order is $\beta_4 = tan^{-1}(-\frac{\ddot{\alpha}}{3\alpha^2})$ as shown Sec. 3.2.5.2, Case 3.

b. When the angular jerk α̇ of the rolling circle is instantaneously zero, the location of the fourth order IC is always located at the center *P* of the circle regardless of the state of the angular velocity ω, the angular acceleration α, and the angular jerk α̇. However the fourth order orientation angle β_4 varies based on the states of these kinematic states as shown in Table 7.6 (a detailed discussion in Sec. 3.2.5.2, Case 2).

Table 7.6: The Fourth Order Motion for a Circle Rolling on a Straight Line: Special Case Scenario when $\ddot{\alpha} = 0$, and $\omega \neq 0$ or $\alpha \neq 0$. The Fourth Order IC is at point P [0, 0]

$\dot{\alpha}$	α	ω	β_4
Does not affect the outcome	1	0	0^o
0	0	1	180^o
1	0	1	0^o if $(4\omega\dot{\alpha} - \omega^4) > 0$ 180^o if $(4\omega\dot{\alpha} - \omega^4) < 0$

Table 7.7: Summary of the Fourth Order Motion Properties for Special Case Scenarios for a Circle Rolling on a Straight Line

$\ddot{\alpha}$	$\dot{\alpha}$	α	ω	*IC Location*	β_4
0	No Effect	0	0	∞	90°
0	0	0	$\neq 0$	*P [0, 0]*	0°
0	No Effect	$\neq 0$	0	*P [0, 0]*	180°
0	No Effect	$\neq 0$	$\neq 0$	*P [0, 0]*	$\tan^{-1}\left(\frac{6\omega^2\alpha}{4\omega\dot{\alpha}+3\alpha^2-\omega^4}\right)$
0	$\neq 0$	0	$\neq 0$	*P [0, 0]*	0° or 180°
$\neq 0$	No Effect	0	0	*O [0, -r]*	90°
$\neq 0$	0 or nonzero	0	$\neq 0$	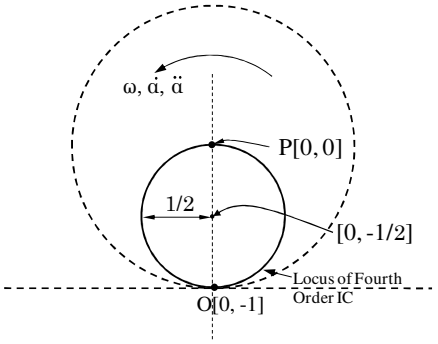	$\dot{\alpha} \neq 0$: $\tan^{-1}\left(-\frac{\ddot{\alpha}}{4\omega\dot{\alpha}-\omega^4}\right)$ $\dot{\alpha} = 0$: $\tan^{-1}(\frac{\ddot{\alpha}}{\omega^4})$
$\neq 0$	No Effect	$\neq 0$	0	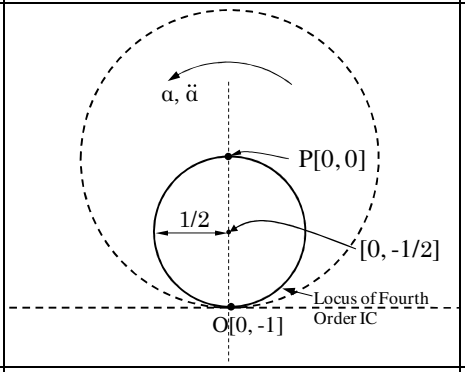	$\tan^{-1}(-\frac{\ddot{\alpha}}{3\alpha^2})$
$\neq 0$	$\neq 0$	$\neq 0$	$\neq 0$	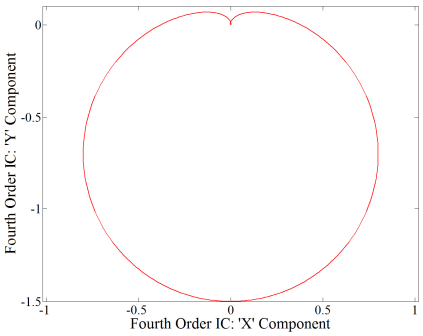	$\tan^{-1}\left(\frac{-(\ddot{\alpha}-6\omega^2\alpha)}{4\omega\dot{\alpha}+3\alpha^2-\omega^4}\right)$

5. For the 2-DOF case of a circle rolling on a straight line with slipping, we defined the slipping, skidding and sliding as shown in Figure 7.6. Section 3.4 discussed the motion of a circle rolling with slipping/sliding. As the skidding resulted in the out of plane motion (the motion of the wheel was simplified by using a circle to represent it), this study is restricted to the slipping and sliding only. The slippage factor ε that measured the amount of slipping and sliding was defined such that:

$$V_P = -(1-\varepsilon)r\omega$$
$$\varepsilon = 1 - \frac{V_P}{r\omega} \qquad \text{Eq. 7.1}$$

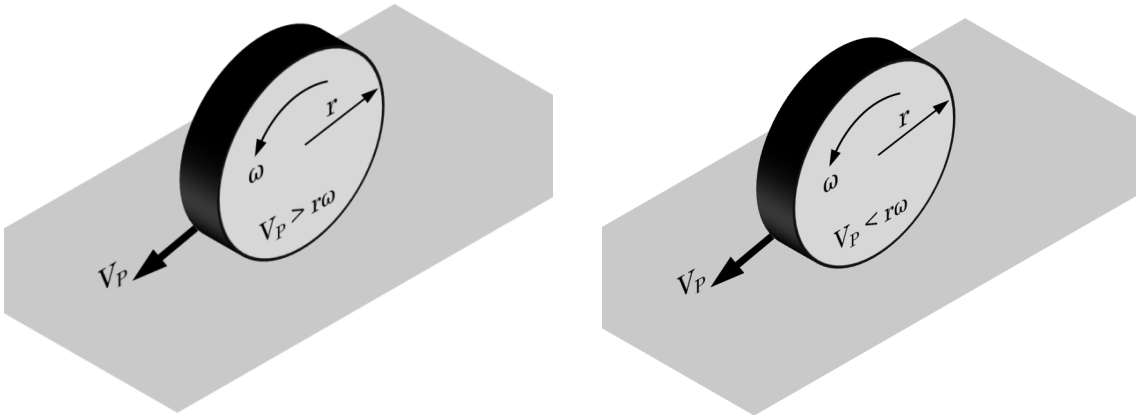

Slipping Condition $|V_P| = |\dot{X}_P| < |r\omega|$ Condition for Sliding $|V_P| = |\dot{X}_P| > |r\omega|$

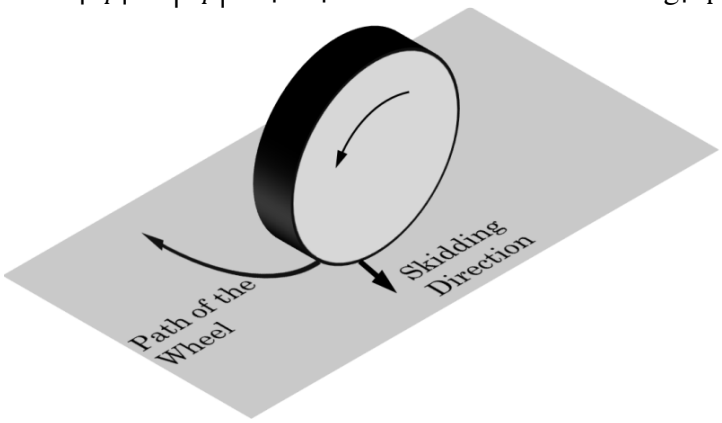

Skidding (Lateral Direction), Condition $\dot{Y}_P \neq 0$

Figure 7.6:The Schematic Representation of Wheel Slipping, Sliding and Skidding

The range of value of slippage factor is:

$$slipping: \varepsilon \in (0, 1]$$
$$sliding: \varepsilon \in (0, -\infty] \qquad \text{Eq. 7.2}$$

Using this definition, the analysis of the first four orders of the motion for a circle rolling on a straight line with slipping was performed in Sec. 3.4 which summarized in Table 7.8. Table 7.8 summarizes the loci for the first four orders of the IC with a representative case of a circle (representing the cylindrical rigid bodies such as a wheel) of unity radius rolling on a straight line (representing the planar rigid bodies such as a flat and smooth ground) in case of the rolling without slipping and rolling with slipping conditions.

The following is the summary of the result of the analysis:

a. The first order IC for a circle rolling on a straight line without slipping is coincident with the point of contact (*O*) of the circle with the line. In case of the circle rolling with slipping (as measured by the slippage factor ε) the IC is shifted along the line joining the center of the circle (*P*) and the point of contact (*O*) by the slippage factor as shown in Table 7.8.
b. The locus of the second order IC for a circle rolling on a straight line is a circle with half the radius of the rolling circle as shown in Table 7.8. When the circle rolls with slipping, the locus of the second order IC is still a circle but the radius is scaled by the amount of slippage factor so that the radius is (1-ε)/2 for a rolling circle radius of unity.
c. Similarly, the loci of the third or fourth order ICs for a circle rolling on a straight line with slipping were scaled by the slippage factors as compared to the loci of the third or fourth order ICs for a circle rolling on a straight line without slipping as shown in Table 7.8.

Table 7.8: Summary of the IC Loci for a Circle Rolling on a Straight Line

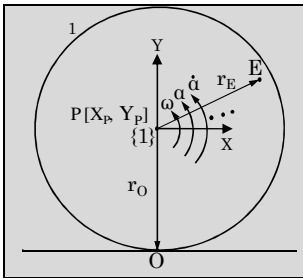	**Rolling Without Slip** **1-DOF Motion**	**Rolling With Slip (ε)** **2-DOF Motion**
First Order IC Location, I_1	Point *O [0, -1]*	*[0, -(1-ε)]*
Locus of Second Order IC, I_2	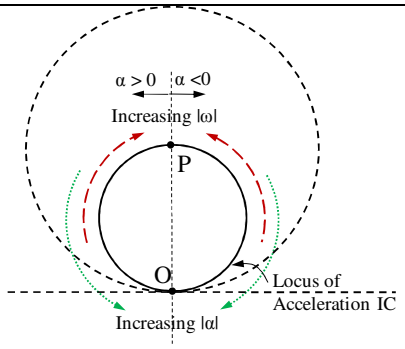	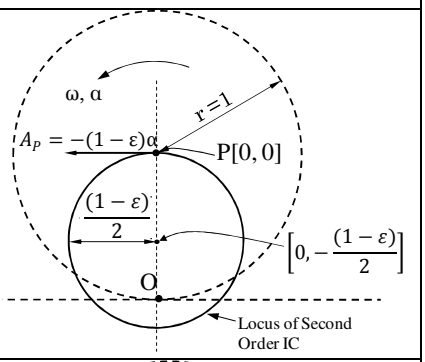
Locus of the Third Order IC	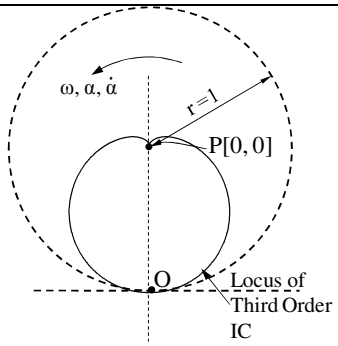	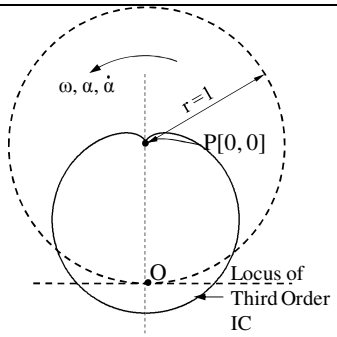
Locus of the Fourth Order IC	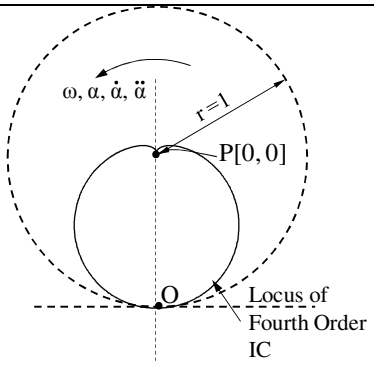	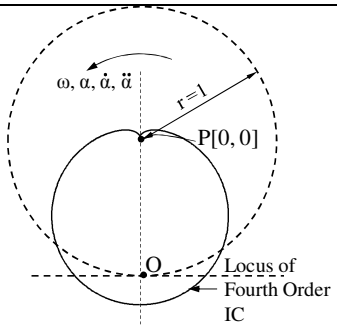

7.4.2 MOBILE PLATFORM KINEMATICS AND DYNAMICS

Chapter 4 studied various mobile platform configurations that are limited to planar motions. We categorized the mobile platform into four distinct categories:

1. Platforms that have one or more fixed wheels (or tracks) on both sides (Sec. 4.1),
2. Platforms with two or more active 2-DOF caster wheels (Sec. 4.2),
3. Platforms with two or more active 2-DOF centered wheels (Sec. 4.3), and

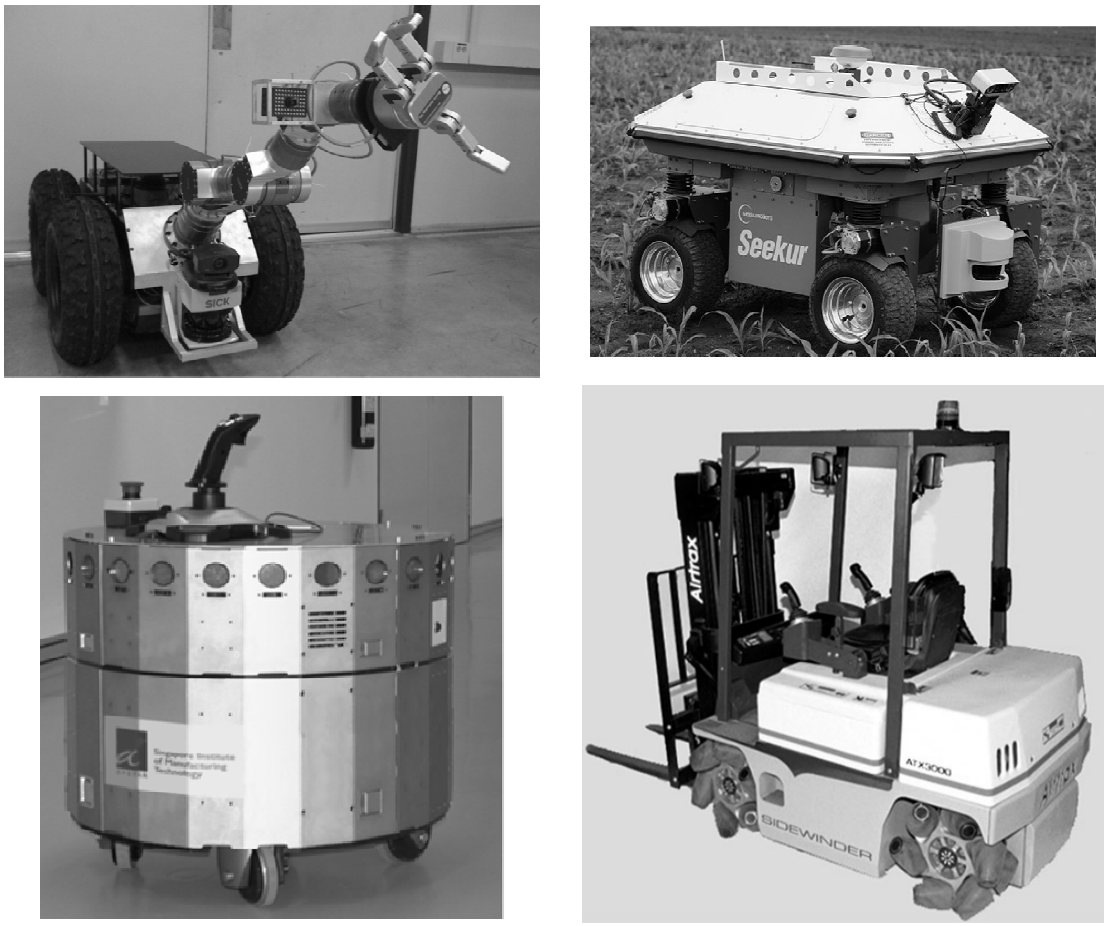

Figure 7.7: Examples of Planar Mobile Platforms. Clockwise from Top Left, (i) a Four Wheeled, Skid-Steer Platform (RMP400 from Segway Inc., Picture shows the Mobile Manipulation System at RRG), (ii) An Example of Centered Wheel Omnidirectional Robot (Seekur from Mobile Robots Inc., Picture Reproduced from http://robotika.cz/competitions/fieldrobot2009/cs). A Mobile Platform with Four Active Centered Wheels, (iii) A Forklift with Four Mecanum Wheel from Airtrax (Picture Reproduced from News Site http://www.forkliftaction.com/upload/news/1913-1.jpg), and (iv) An Example of the Mobile Platform with Active Caster Wheels (Picture Reproduced from Low and Leow [2006a])

4. Platforms with specially designed omnidirectional wheels (Sec. 4.4).

We showed that the platforms with fixed wheels on both sides are capable of motions that require the platforms to face the direction of travel at all times. We also showed that for these platforms, all the ICs are constrained to lie on the common rolling axis of the fixed wheels at all times.

The platforms with active caster wheels are truly omnidirectional; i.e., they have ability to move in any direction instantaneously. This allows for all ICs to be arbitrarily placed providing the user with a wide range of choices as shown in the demonstrative example (Sec. 4.1.5). Both the steering and driving inputs in this case are used as rate inputs.

The platforms with active centered wheels are also omnidirectional; however before

Table 7.9: Qualitative Comparison of the Four Categories of Planar Mobile Platforms

Platform Configs / *Attributes*	**Fixed Wheels on Both Sides**	**Active Centered Wheels**	**Active Caster Wheels**	**Omnidirectional Wheels**
Dexterity	Low Dexterity	Good Dexterity	High Dexterity	High Dexterity
Ruggedness	High Ruggedness	Good Ruggedness	Moderate Ruggedness	Low Ruggedness
Efficiency	Moderate Efficiency	High Efficiency	High Efficiency	Low Efficiency
Sensitivity to Ground Quality	Least Sensitive	Moderately Sensitive	Sensitive	Most Sensitive
Fault Tolerance	Low Fault Tolerance	No Fault Tolerance (when Steering Actuator Fails)	High Fault Tolerance	Low Fault Tolerance (No Fault Tolerance for up to the Four Wheeled Configurations)
Number of Actuators per wheel	1	2	2	1

traveling in a direction, the wheels must be steered into the direction of travel first (Sec. 4.3.2). This is because the steering input is used as a position input here. Again due to omnidirectional capability, locations of all ICs can be arbitrarily chosen providing the user a wide range of choices.

The platforms with omnidirectional wheels (Sec. 4.4) are also truly omnidirectional for more than three active omnidirectional wheels. However as shown in Appendix A, they are complex, have low load capacity, low maintainability, and lack standardization. Table 7.9 compares the four categories of platforms on a qualitative basis.

Chapter 5 presented a comparative study of a set of platforms summarized in Table 7.9, representative of the platforms with conventional wheels from dexterity standpoint using a set of numerical examples. Based on these examples, the following observations were made:

1. The mobile platforms with fixed wheels on both sides have limited dexterity as they cannot travel in lateral direction (direction along the common rolling axis of the fixed wheels). This constraint limits them from performing certain motion plans such as motion along a straight line so that the platform is always directed towards a fixed point in space (Sec. 5.1.2), motion along a curved path with fixed orientation (Sec. 5.2.2), etc. Fig. 7.8 shows the example of such a motion that requires the mobile platforms to move in a straight line while controlling orientation such that the body fixed x axis is always directed towards a fixed point in space.
2. When the wheel is in a direction away from the required direction of motion, the centered wheel configuration needs the steering actuator to align the wheel in the direction first. In case of a caster wheel configuration, this is not needed since the steering motion also contributes to the useful platform motions. This means that the platform with active caster wheels can instantaneously start moving in an arbitrary

direction while the platform with active centered wheels needs to realign the wheels in the direction of travel before doing so.

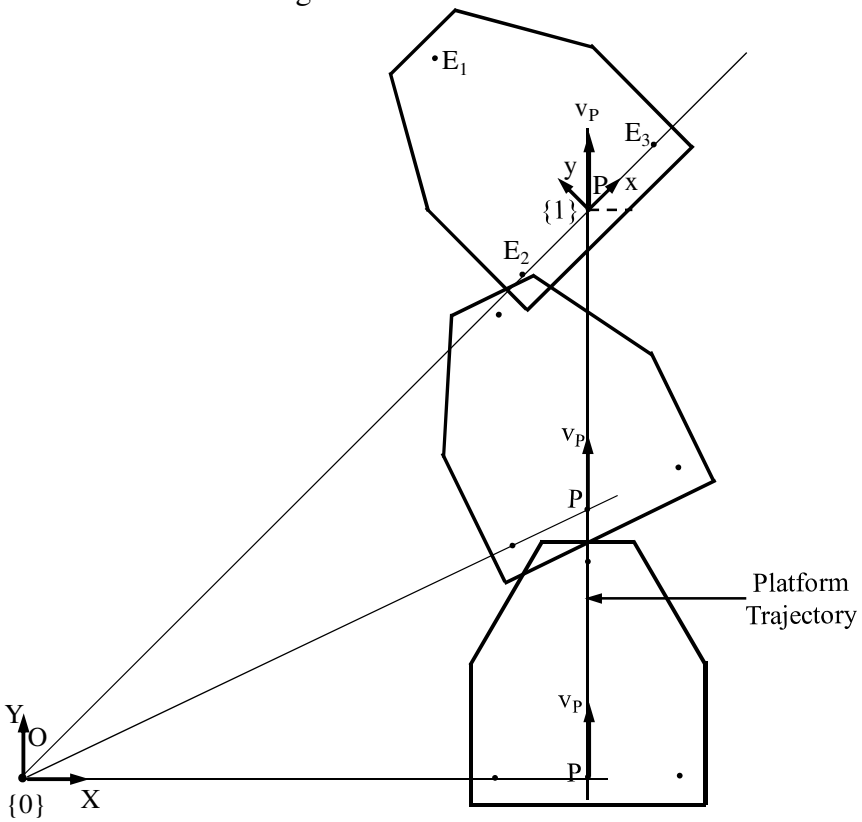

Fig. 7.8: A Straight Line Motion of the Platforms with Orientation Control

Due to this property of the platform with centered wheels, more time is required to carry out a complex motion scenario for the platform with the centered wheels than for the platform with the caster wheels. For ex., in Sec. 5.3, the motion plan required that the platforms make a right turn instantaneously (Fig. 7.9). Since the platform with three active centered wheels completed the motion by stopping at the corner and turning the wheels by 90^o before continuing motion, the total motion time was computed as approximately *22s*. In contrast, the platform with three active caster wheels could negotiate the 90^o turn without stopping and thus required approximately *20s* for the motion completion (Sec. 5.3).

3. For active centered wheel motions, the driving actuator is responsible for the dynamic motion of the platform while the steering actuator is used mainly to place the wheel in the appropriate direction needed for the programmed motion. This results in higher motion requirements for the driving actuator in case of platform with active centered wheels. In contrast, as both the steering and the driving actuators contribute to the platform motions with active caster wheels, the motion demands on the driving actuator are reduced for the platforms with caster wheels. (Sec. 5.1.2.2).

4. One of the practical limitations in the motion plan may arise due to the velocity limits of the steering actuators. This limitation should be considered during the dynamic motion synthesis. For example, for a platform with active centered wheel to accomplish the motion plan shown in Fig. 7.9, the steering actuator theoretically needs to move at infinite speed for the wheel to rotate by 90^o instantaneously. However, for this motion plan, we used a maximum angular speed of 45^o/s for the steering actuator.

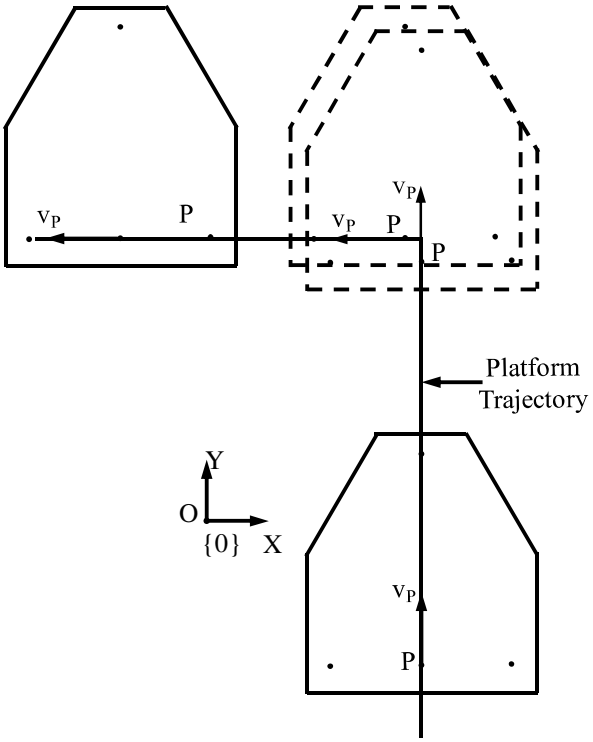

Fig. 7.9: Mobile Platform Undergoing the Discontinuous Path Composed of Straight Lines

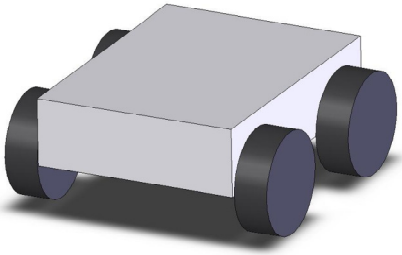

Skid-Steer Platform with no Steerable Wheels

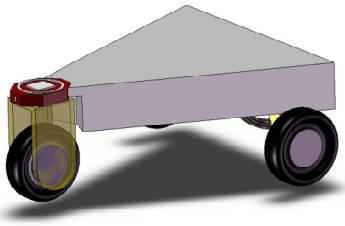

Platform with Single Steerable Wheel

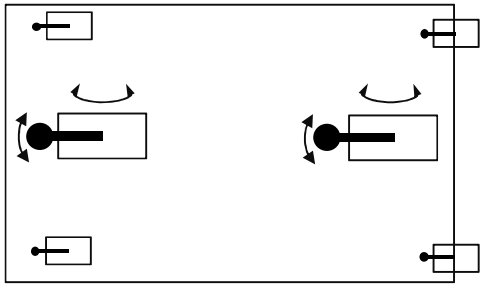

Platform with Two Steerable Wheels

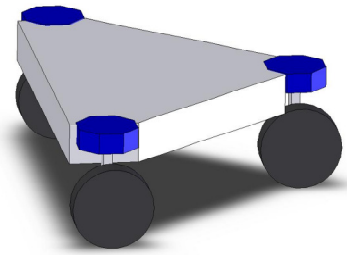

Platform with Three Steerable Wheels

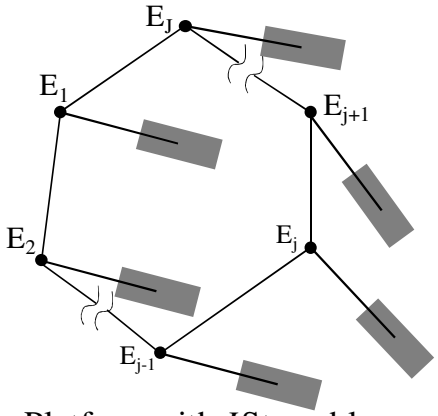

Platform with *J* Steerable Wheels

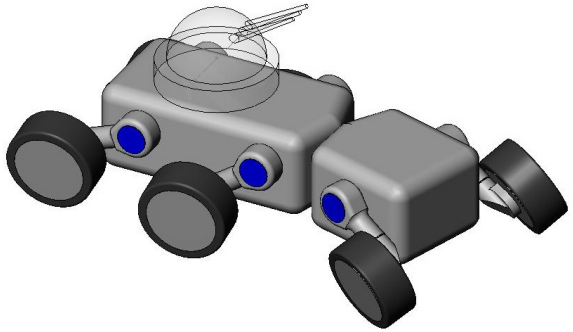

Unique Embodiment

Figure 7.10: Array of Open Architecture Mobile Platforms ((Emphasis on Steerable Centered/Caster Wheels)

7.4.2.1 Dynamic Motion Synthesis for Mobile Platforms

Chapter 4 presented a systematic approach to perform dynamic motion synthesis of a general mobile platform with *J* caster wheels such that it has a redundant system of inputs. Fig. 7.11 shows the free body diagram of the platform rigid body and a general j^{th} wheel subsystem with two actuator inputs, one for steering and the other for driving. The dynamic model for the wheel subsystem presented here is derived from the model presented in Wong (2001). The notations used in the diagram are explained in detail in Sec. 6.2. The following assumptions were made for the dynamic behavior of the mobile platform:

1. The platform is capable of planar motions only. Any out of plane motions are reserved for a future development effort.

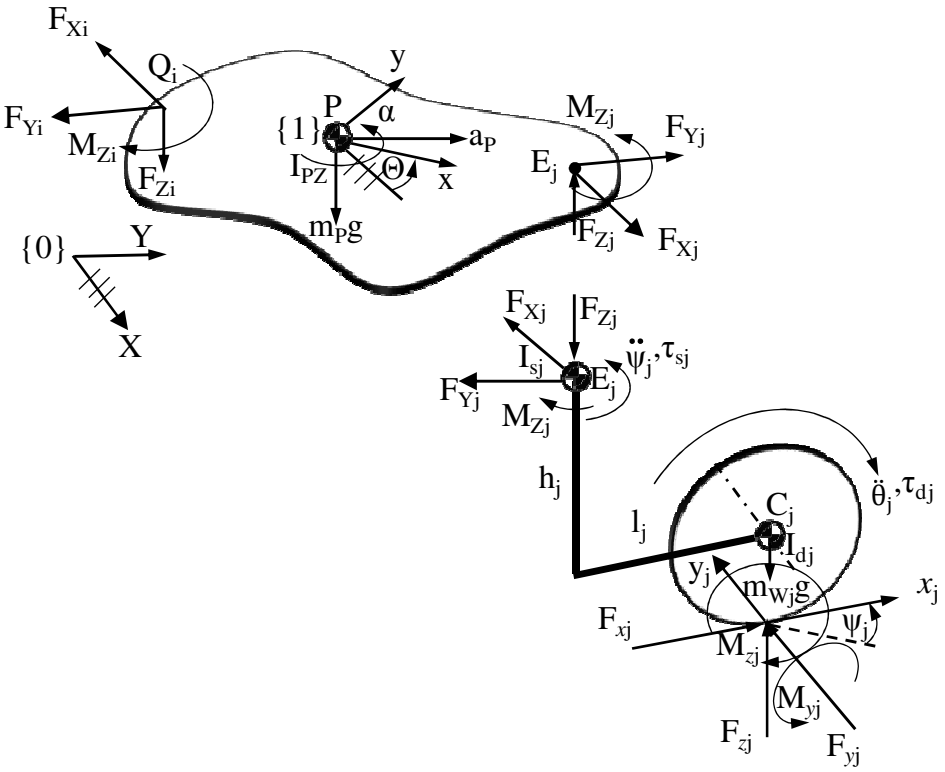

Fig. 7.11: The Free-Body Diagram of a General Mobile Platform with *J* Active 2-DOF Caster Wheels

2. The ground is flat and smooth such that all the J wheels are in constant contact with ground.
3. The platform body and the links are rigid.
4. The wheel is assumed to be vertical at all times with no tilting (zero camber angle Wong, 2001).
5. There is no moment M_{xj} (zero overturning moment (Wong, 2008)) acting in the x_j direction.

With these assumptions, the force/moment equilibrium (according to frame {0}) for the platform body is given as:

$$\sum_{j=1}^{J} F_{Xj} = \sum_{i=1}^{N} F_{Xi} + m_P a_X$$
$$\sum_{j=1}^{J} F_{Yj} = \sum_{i=1}^{N} F_{Yi} + m_P a_Y$$
$$\sum_{j=1}^{J} F_{Zj} = \sum_{i=1}^{N} F_{Zi} + m_P g \qquad \text{Eq. 7.3}$$

$$\sum_{j=1}^{J} M_{Zj} = \sum_{i=1}^{N} M_{Zi} + \sum_{j=1}^{J} F_{Xj} Y_{Ej} - \sum_{j=1}^{J} F_{Yj} X_{Ej} - \sum_{i=1}^{N} F_{Xi} Y_{Pi} + \sum_{i=1}^{N} F_{Yi} X_{Pi} + I_{PZ}\alpha$$

The force and moment equilibrium for the j^{th} subsystem expressed in frame $x_j y_j$ is given as follows:

$$F_{xj} + F_{Xj} cos\psi_j + F_{Yj} \sin\psi_j - m_{Wj}\left(\frac{\ddot{\theta}_j d}{2} + l\dot{\psi}_j^{\,2}\right) = 0 \qquad \text{Eq. 7.4-a)}$$

$$F_{yj} - F_{Xj} sin\psi_j + F_{Yj} \cos\psi_j - m_{Wj}\left(\dot{\psi}\dot{\theta} d - l\ddot{\psi}\right) = 0 \qquad \text{Eq. 7.4-b)}$$

$$F_{zj} - F_{Zj} - m_{Wj} g = 0 \qquad \text{Eq. 7.4-c)}$$

$$\tau_{dj} - F_{xj}\frac{d_j}{2} - M_{yj} - \left[F_{Xj}\cos\psi_j + F_{Yj}sin\psi_j\right]h_j - F_{Zj}l_j - I_{dj}\ddot{\theta}_j = 0 \qquad \text{Eq. 7.4-d)}$$

$$\tau_{s(j)} - F_{yj}l_j - M_{zj} - M_{Zj} - I_{sj}\ddot{\psi}_j = 0 \qquad \text{Eq. 7.4-e)}$$

7.4.2.1.1 Numerical Example

To demonstrate the steps in the dynamic motion synthesis, a numerical example was provided in Chapter 6 (Sec. 6.5) using a three wheeled platform as shown in Fig. 7.12. The geometric and mass properties of the platform are shown in Table 7.10.

Table 7.10: Geometric and Mass Properties of the Mobile Platform with Three Active caster Wheels

$d = 1\ ft$	$l = 1\ ft$	$b = 2\ ft$	$h = 1\ ft$
$m_P = 100\ lb$	$m_W = 10\ lb$	$I_{PZ} = 200\ lb\text{-}ft^2$	$I_d = 10\ lb\text{-}ft^2$
$I_s = 20\ lb\text{-}ft^2$			

The platform was required to travel smoothly on a path as shown in Fig. 7.13 with the presence of external force/moment (shown in Fig. 7.11). The goal of the overall motion synthesis was (i) to compute the input velocities ($\dot{\psi}_j$ and $\dot{\theta}_j$) and accelerations ($\ddot{\psi}_j$ and $\ddot{\theta}_j$)

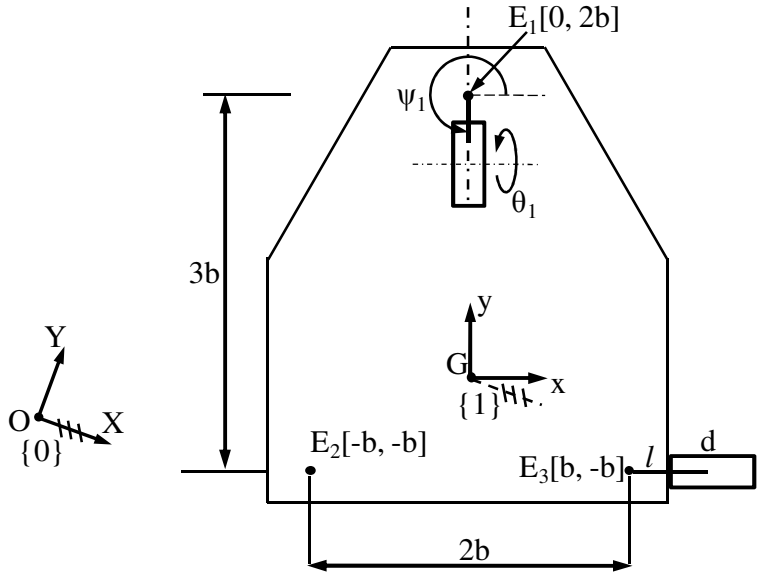

Fig. 7.12: Geometric Description of the Mobile Platform with Three Active Caster Wheels

required for the platform to complete the motion, and (ii) to compute the input joint torques (τ_{sj} and τ_{dj}) required to sustain the applied and inertia forces/moments acting on the platform during the motion.

The motion programming for the platform is done in using the following steps:

1. Formulate the motion plan for the platform in terms of the linear motion of the Pont Of Interest (POI, in this case is the centroid of the platform body) and the angular motion of the platform body. Since this motion plan is purely translational, the linear

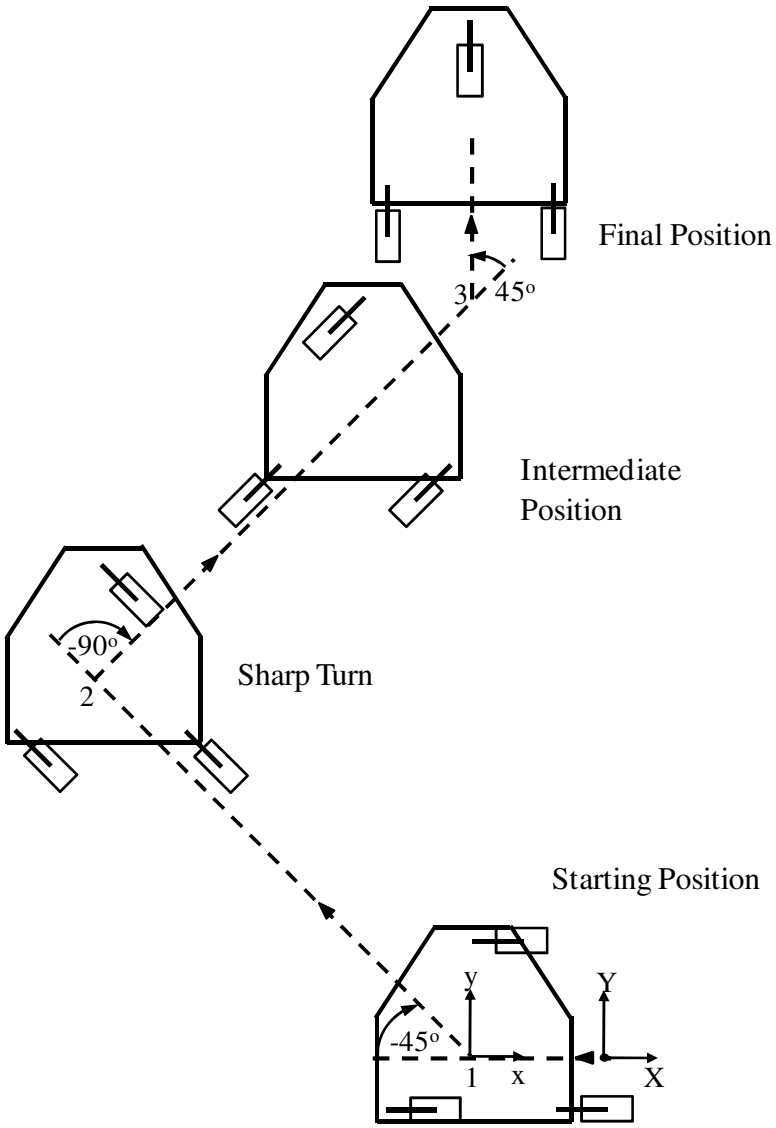

Fig. 7.13: The Path of the Mobile Platform

motion of POI completely describes the motion of the platform. A smooth motion plan such as trapezoidal shape for the acceleration profile is used for the motion (Sec. 6.5.2.1, Fig. 6.13). In this case, the velocity and acceleration of point G is computed for the complete motion plan.

2. Compute the first and second order IC locations for the whole spectrum of the motion plan. In this case, as the motion is purely translational, the first and second order ICs are at infinity during the complete motion. However, in general, this step can provide the user with valuable information as discussed in Chapters 2 and 3.
3. Compute the velocities and accelerations for the three wheel attachment points, E_1, E_2, and E_3, respectively. This should be done using the IC based formulation summarized in Table 7.3 (Sec. 2.4 and Sec. 2.5).
4. Compute the velocities and accelerations of input DOF for each wheel in terms the steering and driving velocities and accelerations, using the methodology described in Sec. 4.2.2 and Sec. 4.2.3 (specifically Sec. 4.2.3.1), respectively. This completes the kinematic motion synthesis.
5. Next, compute the platform body forces in terms of the applied forces/moments and inertia forces using the free body diagram shown in Fig. 7.11. The applied forces are a result of the payload on the platform as well as the interaction of the platform body with the world as depicted in Eq. 7.3.
6. The platform body forces are to be sustained by the set of wheel subsystems. Thus the next step is to distribute these forces among the wheel subsystems (Eq. 7.3). For the numerical example, the forces and moments are distributed evenly among the three wheel subsystems (Sec. 6.5.3.2).

7. The next step is to compute the traction force requirements (in longitudinal direction, $F_{xj,}$ and lateral direction F_{yj}) from the ground using Eq. 7.4-a) and Eq. 7.4-b). These

forces must be met by the wheel-ground interaction in order for the wheel to move without slipping/skidding.

8. The last step is to compute the wheel input torques, namely, the driving torque, τ_{sj} and the steering torque τ_{dj} for each wheel subsystem j using Eq. 7.4-d) and Eq. 7.4-e).

Following section summarizes the complete dynamic synthesis process.

Kinematic Motion Synthesis

Using the kinematic motion synthesis methodology described in Chapter 4 (Sec. 4.2.3), the wheel input accelerations are computed as shown in Fig. 7.14.

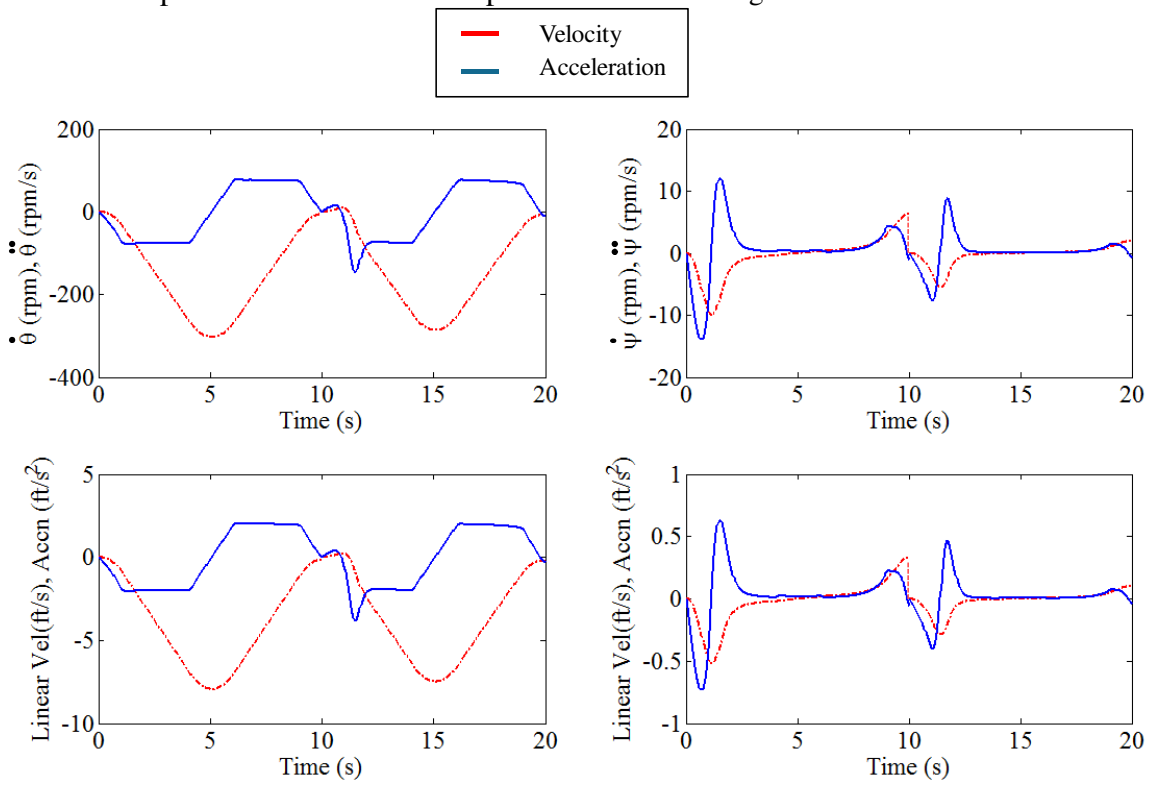

Driving Input ***Steering Input***

Fig. 7.14: Second Order Input Motion Synthesis for the Mobile Platform with Three caster Wheels when it Travels from Corner 1 to Corner 3

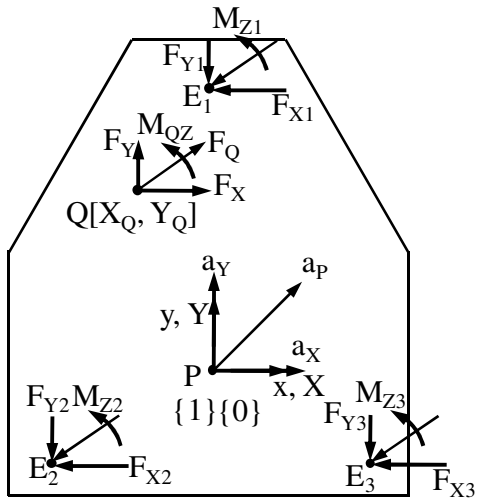

Fig. 7.15: System of Forces and Moments for the Platform Body

Dynamic Motion Synthesis

For the dynamic motion synthesis, the free body diagram of the platform body is shown in Fig. 7.15**.** Point Q ([-1, 1.5] in frame {1}) is a point in the body where the external force and moment is applied. The external force F_Q was a constant *200 lb @ -30*^{o} with the global X axis and the external moment M_{QZ} was *400 lb-ft*.

Note that, the redundancy of input DOF for the mobile platform in this case results in

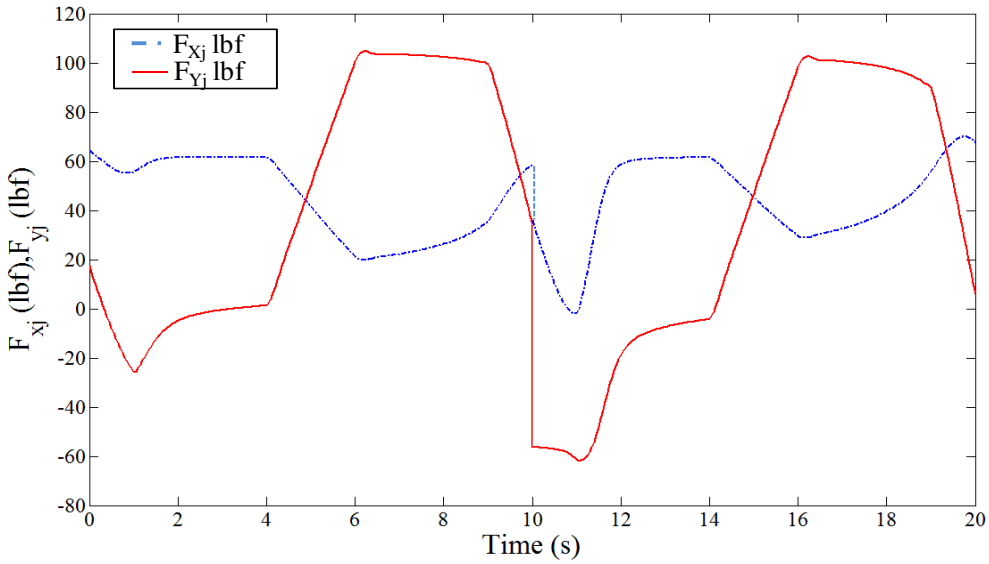

Fig. 7.16: The Tractive Force F_{xj} and the Lateral Force F_{yj} for the Platform Dynamic Motion from t= 0 to 20(s)

force redundancy since these system of forces on the platform body may be distributed among the three wheel subsystem in more than one ways. This redundancy in force is beneficial due the dynamic and nonlinear nature of wheel forces that limit the amount of forces and moments the wheel subsystem can sustain from the platform interaction. However, in this numerical demonstration we distribute the forces evenly among all the wheel subsystems.

In Eq. 7.4-a), -b), and -c), F_{Xj}, F_{Yj}, and F_{Zj} are the forces exerted on wheel subsystem j by platform body, and F_{xj}, F_{yj}, and F_{zj} are the wheel-ground contact forces, respectively. It can be realized that the force the wheel subsystem can exert (or conversely sustain) on the platform is limited by these ground contact forces. Similarly, in Eq. 6.7-d), and -e), M_{yj}, M_{zj} are the the rolling resistance moment, and the steering resistance moment, respectively due to the ground-wheel contact.

In this numerical example, the tractive force requirements in the longitudinal (F_{xj}) and longitudinal (F_{yj}) directions are computed by using Eq. 7.4-a) and Eq. 7.4-a), respectively, as shown in Fig. 7.16. The input torque requirement for the jth wheel in terms of the driving and steering actuator torque is then computed using Eq. 7.4-d) and Eq. 7.4-e) as shown in Fig. 7.17.

In general, the wheel-ground interaction forces (such as the tractive effort, rolling resistance, lateral (cornering) force, steering resistance (self-aligning force), etc.) are dependent on various external factors such as the vehicle speed v_P, normal force F_{zj}, tire inflation pressure p, tire internal temperature t_i, surface temperature t_s, wetness of the surface characterized by water depth (d)), etc. Fig. 7.18 demonstrates the effect of various operating factors (vehicle speed v_P, normal force F_{zj}, and tire inflation pressure p) on the wheel-ground interaction forces (in terms of the friction coefficient in driving and steering directions). These curves further emphasize that these external factors influence

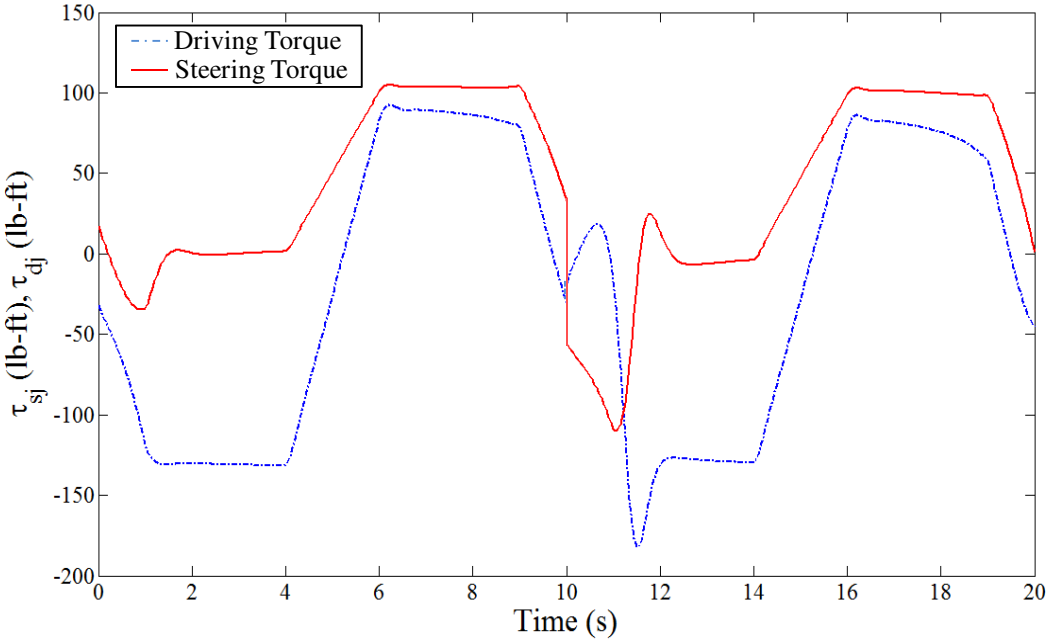

Fig. 7.17: Input Torque Curve for the Dynamic Motion of the Mobile Platform with Three Caster Wheels from t = 0 to 20 (s)

the performance of the mobile platforms and should be accounted for while devising the force distribution scheme for successful operation of mobile platforms.

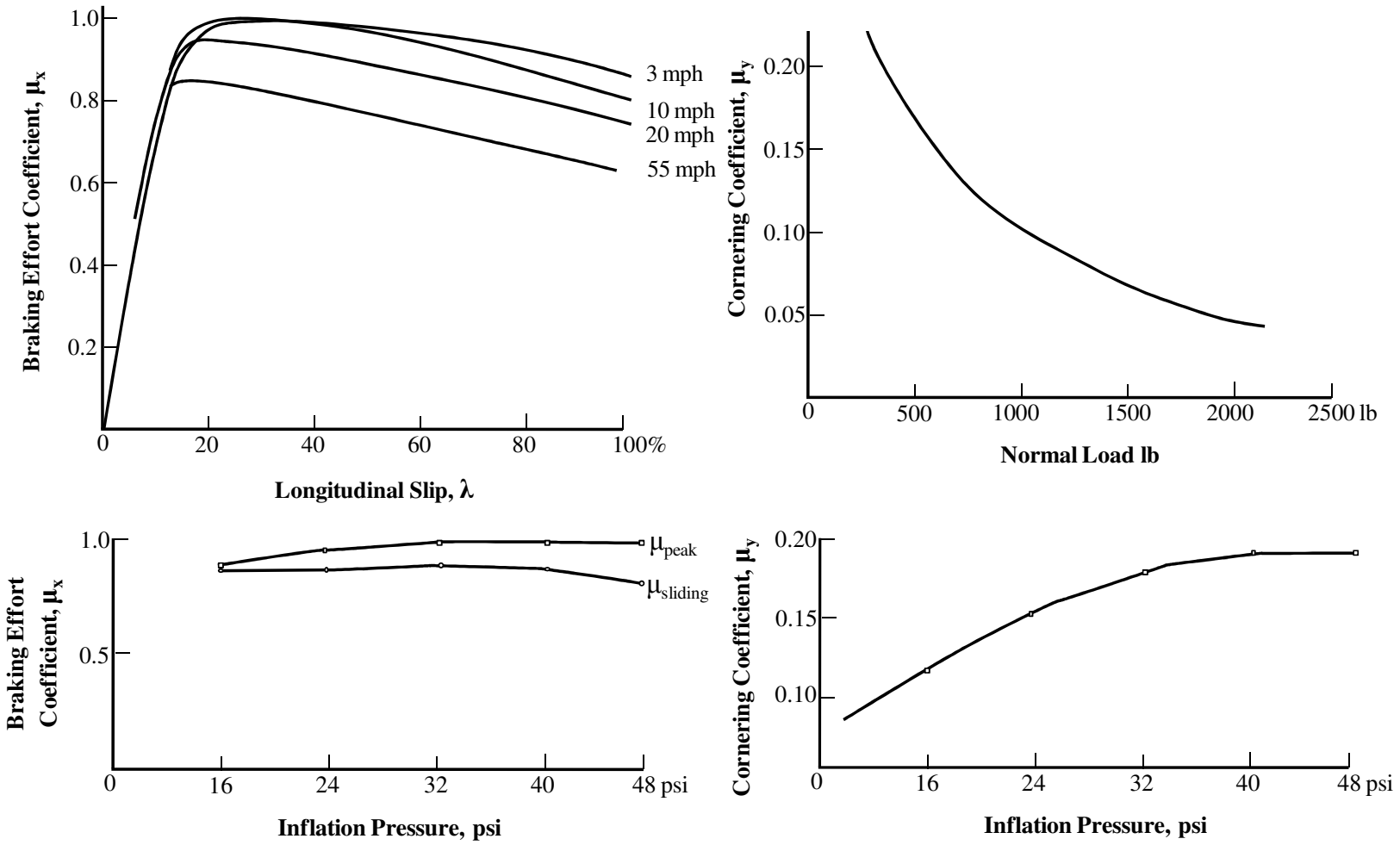

Longitudinal Friction Coefficient, μ_x Lateral Friction Coefficient, μ_y

Fig. 7.18: Nonlinear Nature of the Wheel-Ground Contact (Wong, 2001)

7.4.3 PRIMARY CONTRIBUTIONS

Table 7.11 enumerates the important contributions made by this research effort. The original contributions are highlighted by bold and italic typeset.

Table 7.11: Primary Contributions

- A generalized notation was proposed to describe motion of a general k^{th} order, planar 3DOF motion of a rigid body. (Sec. 2.3)
- ***Using algebraic formulation, an analytic method was presented (Sec. 2.6) to compute the higher order ICs (the third and higher order) similar to first (Sec. 2.4) and second order (Sec. 2.5) ICs.***
- ***An analytic method to compute the higher order motion state of a general point in the rigid body based on its location with respect to the corresponding IC location was presented***
    - ***While the formulation showed the motion states of a general point up to the fifth order motion, the formulation was presented for a general k^{th} order motion of a general point in the body. (Sec. 2.6)***
- A study of classical 1-DOF and 2-DOF motions (Such as a cylindrical body rolling on a flat surface without slipping (1-DOF), and with slipping (2-DOF)) was performed to understand and characterize the higher order ICs (up to the fourth order IC).
    - ***The locus of particular IC in case of a completely general motion for each special case was studied.(Sections 3.2, 3.3, 3.4, and 3.5)***
    - ***The locus (sometimes unique location) of a particular IC in case of special case instantaneous kinematic states (such as zero angular velocity ω of the rigid body, zero linear acceleration a_P of POI) was studied. (Sections 3.2.3.1, 3.2.4.2, 3.2.5.2, 3.3.3.2, 3.3.4.2, 3.3.5.2, 3.4.4.1, 3.4.5.2, and 3.4.6.2)***
- The different architectures of planar mobile platforms were studied and characterized into four categories (Platforms with fixed wheels on both sides, Platforms with active caster wheels, Platforms with active centered wheels, and Platforms with omnidirectional wheels.). (Sections 4.1.1, 4.1.2, 4.1.3, 4.2.1, 4.3.1, and 4.4.1)
- ***The motion syntheses of these platforms for the first three orders of motion were discussed.(Sec. 4.1.4, 4.2.2, 4.2.3, 4.3.2, and 4.4.2)***
    - The motion syntheses can be generalized such that one analytic description is

sufficient for motion programming, dynamic analysis, and wheel commands that can be computed in parallel (separately) from all wheels in the system.

- The dexterity of the different configurations of mobile platforms involving conventional wheels is discussed through a set of demonstrative examples. (Chapter 5)
- The dynamic force model of a general mobile platform with caster wheels is discussed (Sections 6.2, 6.3, and 6.4) with a numerical example involving caster wheel actuator demand torques for a three wheeled platform configuration. (Sec. 6.5)

7.5 Recommendations and Future Work

Based on the research findings, lessons learned and the literature review, recommendations for applying this research elsewhere will be made. Also to advance the research further, the scope of the future work will be detailed in this section.

The roadmap for future work is categorized into two groups, namely, a short term i.e., one to two years plan and a long term plan as follows.

7.5.1 SHORT TERM PLAN

The following section discusses the scope for future work to extend the current research in a near term basis (1-2 years).

7.5.1.1 Studying Wheel Dynamics

Once the platform dynamic motion synthesis has been achieved (which is now generalized in terms of J caster wheels), then all the rest of the problem to be treated has to do with the response/performance of the wheels and the parametric variability of the contact surface. Here we identify a set the external parameters associated with the wheel/surface contact as the following:

Speed (v)	Normal Force (F_z)	Surface Temperature (t)
Slip Angle (α)	Tire Pressure (p)	Water Depth (d)

There have been studies done (as summarized in Wong, 2001) to understand and document the effect of these external (tire/surface contact parameters) parameters on the operational parameters such as the following 10 effects:

Rolling Resistance Moment $M_y(v,t,fn)$	Self-Aligning Torque M_z (p, fn, α) (Steering Resistance Moment)
Longitudinal Friction Coefficient μ_x (v,t,fn) (braking, traction)	Tire Deflection (p, fn, t)
Cornering Force F_y (p,α ,fn)	Lateral Stiffness (fn, p, t)
Hydro-planing Speed (p, d, fn)	Vertical Stiffness (fn, p, t)
Lateral Friction Coefficient μ_y (v, t, fn)	Damping Coefficient (v, p, t)

The general surface can be represented by a finite number of experimental maps (20 (+) for each of 8 classes of surfaces) where sensors provide data to locate actual performance from these in real time. Similar maps exist for each (two) wheel actuators. Contact force demands come from the vehicles motion plan, inertia forces, active systems (say a manipulator), or from load shifting (for ex. liquid in a vessel), etc. All of this must be made into a decision process responding to human set criteria to enhance overall performance. Criteria must be established through extensive testing and analytical verification. These criteria then would be embedded in operator commands such as: watch out!, be efficient, accelerate, its rough, its icy, etc. Sensors of the condition of the contact surface and performance sensors on-board the vehicle can continue to give a full situational awareness of the vehicle's capability to carry on a desired maneuver. The operator must then be trained to use these criteria effectively to get the best vehicle performance based on the combination of the human and machine intelligence. This is a complex objective of which we are only starting. The analytics developed here simplify/structure only the first step: the motion plan and the required caster wheel dynamics/forces.

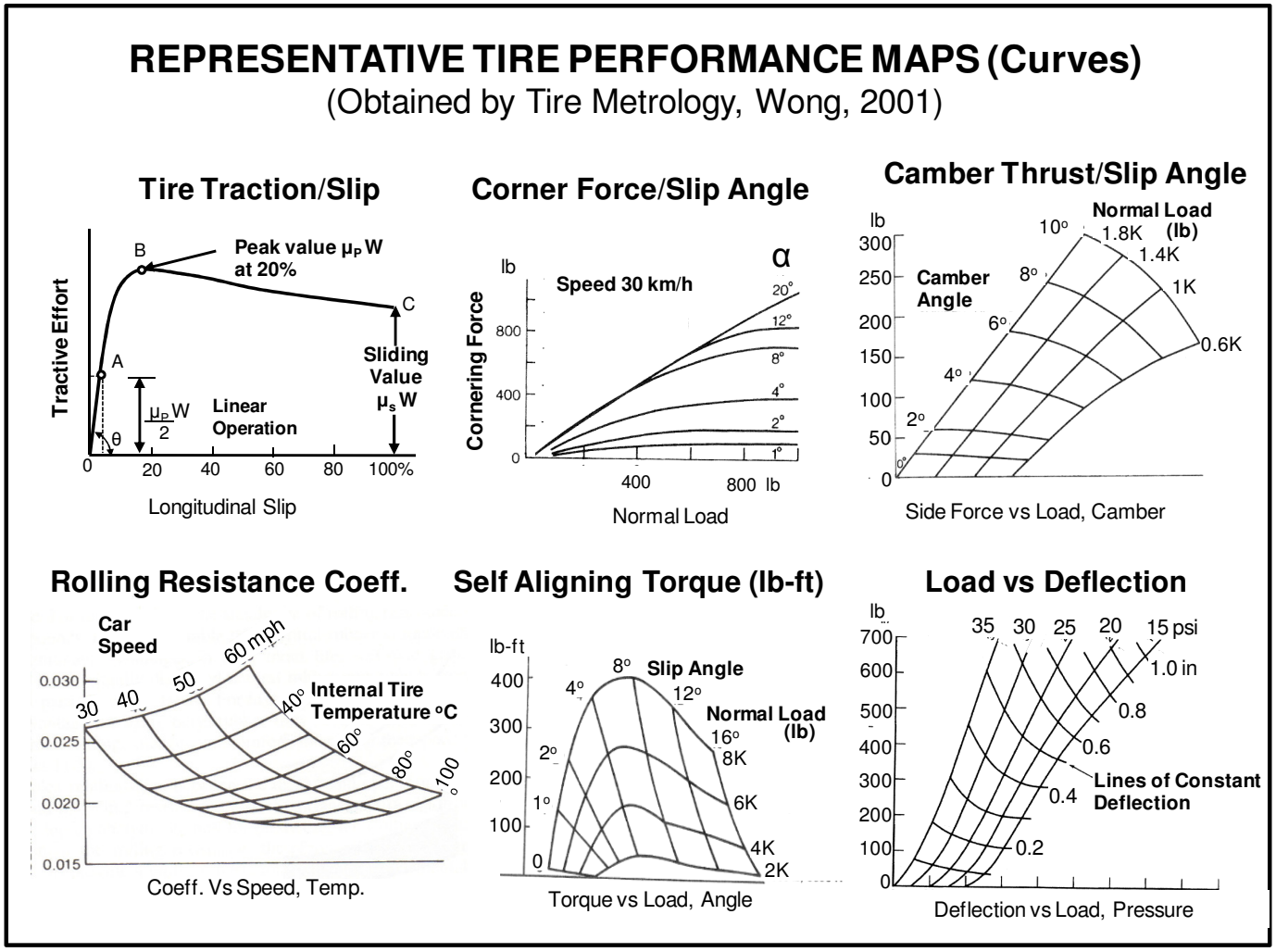

Fig. 7.19: Tire Performance Maps Depicting the Influence of Wheel/Ground Contact (External) Parameters on the Operating (Performance) Parameters of Vehicles (Reproduced from Tesar, 2009)

7.5.1.2 Wheel Dynamics Based Performance

In the numerical example provided in Chapter 6 (Sec. 6.5), we assumed ideal and evenly distributed conditions for the operational parameters for all the wheel subsystems. This resulted in even force distribution among all the wheels. However, the redundancy of wheel input DOF can be more effectively used by employing the aforementioned performance maps towards a force distribution scheme. This requires two levels of effort: (i) defining the performance of the platforms as discussed in Sec. 7.5.1.1 and (ii) distributing the external and inertial forces/moments among the redundant system of inputs (J wheel subsystems) based on the performance requirements.

The performance of the platform can be defined in terms of the performance maps and also in terms of operational criteria such as actuator torque availability, efficiency (energy consumption, minimum inertia, etc.), stability (rollover stability, limited jerk, etc.) etc.

With the knowledge of the current state of the system (in terms of the external parameters defined in Sec. 7.5.1.1) with the help of sensing and operator input, we should then use the redundancy of the system inputs to distribute the forces/moments among the wheel subsystems. Unfortunately, for vehicles (and generalized mobile platforms), the distribution of resources at each of the wheel subsystems must be accomplished within milliseconds to respond to operator commands, to ensure that the best performance is achieved at each wheel subsystem, that the system best achieves it motion program, and that an internal supervisory intelligence ensures safety, achieves efficiency, evaluates performance limits, accommodates faults (partial failures), provides condition awareness and recommends repair or even refreshment in terms of available updated subsystem modules.

7.5.1.3 Payload Interaction

In the numerical example from Chapter 6, we considered an applied force and moment structure that had constant magnitudes and directions (as expressed in a planar frame). However, that is a very simplified scenario. The external forces/moments acting on a platform will have dynamic nature as evident from several scenarios such as:

- A mobile platform carrying a liquid container. In this case, the directions and magnitudes of the force and moment change due to the inertia and vorticity of the liquid.
- A battlefield mobile platform carrying firearms may have an instant increase in the external payload due to the release of ammunition. This dynamic nature of the external payload must be sustained by the mobile platform while on the move.
- A mobile platform may have varying gravity loads when it is moving over an incline. This results in a varying payload on the system.
- A mobile manipulation system may have one or more manipulators attached to a mobile platform for active manipulation or sensing of the environment, added dexterity, excavation arms, loading subsystems, etc. This is a more active (and controllable) form of the payload and should be closely integrated in the dynamic model of the system (Kulkarni et al. 2008).
- A mobile platform with one or more passive trailers has a dynamic payload due to the interaction among bodies.
- Two or more cooperating mobile platforms that are performing a manipulation task among themselves create a dynamic system of external forces and moments acting on the platforms.

Clearly, the field of vehicle intelligence under human control is only in the early stages of its development. This report developed a body of analytics to give physical meaning to

the motion plan, to simplify the use this analytic process, eliminate any uncertainty in the synthesis (i.e., there is no pseudo-inverse), and shows how to directly derive motion commands for each wheel subsystem (in parallel). Previous literature left this process in the hands of specialists in math inversion which would be a permanent barrier to a single valued computation for the required motion planning of generalized mobile platforms.

7.5.1.4 Spatial Mobile Platforms

In this research we studied the mobile platforms capable of planar motions only. A further study is needed to extend this IC based formulation to the class of mobile platforms that are capable of 6-DOF spatial motions. From the kinematic synthesis point of view, the IC based formulation is extendible to spatial motions. Note that in order to achieve the motion plan in this case, we need a responsive and accurate wheel subsystem. Thus, we can define a set of criteria to assess the fidelity of the wheel subsystems to follow the motion plan in order to enable a closed decision structure to enhance actual performance and to advise the operator what is working and not working. (for ex., how to recognize an incipient rollover).

7.5.2 LONG TERM PLAN

The following section discusses a more expansive research scope for future work to extend the current research for a longer term basis (5 years).

7.5.2.1 Uneven Terrain

We assumed a flat and smooth terrain for this research. This restricted problem definition has real value in structured environments like factories, warehouses, hospitals, homes, etc. However, on the other end of the spectrum (construction sites, the battlefield, farming, etc.) the mobile platform will face a wide range of surface conditions. A study of the mobile platform operation over such surfaces is an important issue that must be

tackled (Chakraborty and Ghosal, 2004). Especially, Automated Guided Vehicles (AGVs) often used for outdoor and off-road applications must operate on a wide range of surfaces such as the following (Wong, 2001; Tesar, 2009):

Concrete	Hard Soil	Gravel	Ice/Snow
Asphalt	Soft Soil	Sand	Standing Water

The redundancy in the inputs should be effectively used to respond to the true non-linear and dynamic nature of tire/vehicle operation (traction, slip, cornering, efficiency, stability, etc.) on such a wide range of surfaces. Uncontrolled cornering can occur in ice conditions or water on road surfaces. Rollovers can occur because of a combination of high tire slip in cornering and high turning velocities (high slip angles). These conditions can best be met by real time operation of the vehicle (priorities set by the operator) and a significant expansion of operator set control parameters (velocity, tire pressure, slip angle, etc.). This expansion of priorities and choices is what is meant by intelligent vehicle operation.

The operational parameters defined in Sec. 7.5.1.2 should be associated with each of these surface classes. As discussed earlier, these operational parameters influence the performance of the vehicle in terms of the wheel-ground interaction forces and moments (categorized as performance parameters). The performance maps proposed in Sec. 7.5.1.1 capture this relationship between the operational parameters and performance parameters and should be used for operation of the platforms (or UGVs).

7.5.2.2 Necessary Mobile Platform Decision Theory/Software Development

For 3 decades, the Robotics Research group at the University of Texas at Austin has pursued the science for complex decision making combining numerous performance criteria, subsystem performance capabilities (maps, envelopes), multi-level operational

software, and human interaction (operator set criteria, objectives). This effort was initially applied to the highly coupled and nonlinear serial (and parallel) robot manipulators. There the math framework is deterministic, even though the criteria (up to 100) are highly coupled and frequently have uncertain physical meaning. During the past decade, this decision process has been applied to intelligent electro-mechanical actuators where the physical meaning is clear but the math framework is weakly defined analytically (mostly derived from extensive testing and metrology) to result in decision uncertainty. Fortunately, here the motion synthesis problem for the parallel mobile platform is much more direct than it is for serial robot manipulators. The uncertainty enters where the wheel meets the surface. Sensors on the platform, in the wheel actuators, at the task interface, etc. can provide a rather clean description of these subsystem and system operations. The "road" surface is another matter. Look-ahead sensors must define the surface (ice, water, gravel, slope, rocks, potholes, etc.). Clearly, at this time, we can only begin to obtain some of the necessary real time data (real rime situational awareness). This complexity is now left to the experienced judgment of the operator. Here, we wish to do much better. The system must provide choices and what those choices mean (say for mission planning). If one of the subsystems is failing, what choices remain? Can the systems operate at 90% or does it go down to 50% of its performance according to operator set criteria? What are the lessons learned (in achieving a useful tool for future development)? How can we better train the operator? All of this suggests a depth of technology similar to that now embedded in our military aircraft; battlefield (and commercial) vehicles must move in this direction to not only enhance performance but also to reduce life cycle cost.

7.5.2.3 Development Forecast

This report presents a complete analytic framework for mobile platform planar motion. It outlines a preliminary structure for dynamic motion planning. It needs to be extended to spatial motions (velocity, acceleration, forces, moments) and to provide a formal analytic/decision process to outline the demands on the actuators for all the wheel subsystems in contact with a wide range of parameters associated with the contact surface. The better it does all of this, the better will be the planar model. *I.e., systems criteria will come from the difference between the ideal planar model and the actual spatial model.* Each wheel subsystem will function under these system criteria to best meet the demands that come from the system performance goals. Hence there will be motion criteria, task criteria, wheel subsystem criteria, surface maps, etc. all to be combined into a logical decision process (envelopes as decision surfaces) by an ever expanding (and open) platform operational software. It is clear that for more electric vehicles having an open architecture, these new choices (i.e. new technologies) are just emerging. It will take the best of several technologies (mechanical, electrical, computational decisions, operational software, human and machine intelligence, etc.) to do so.

This open architecture, extended physical and operational choices, operational software, etc. is a complete breakaway from past vehicle development. Wong gives an exceptional description of the past approach. It is also an excellent foundation for the future. In the past, the vehicle dynamics was studied in detail and parametric design decisions were made to improve the dynamics (safety, comfort, efficiency, etc.) in a given application paradigm (racing, highway driving, off-road operation, heavy transport, etc.). Unfortunately, once the vehicle existed, this solution as a set of embedded compromises left almost no choices to adapt to new combinations of dynamic criteria and

road/surface conditions. I.e., the vehicle was largely passive (in its drive train and suspension). If the operator over committed the vehicle, safety was compromised. Here we wish to embed new choices available to the operator, provide guidance to improve safety, efficiency, responsiveness, etc. by creating a new science of vehicle intelligence at all levels for the vehicle operation.

APPENDIX

Appendix A

COMPARISON BETWEEN TWO BASIC DRIVE WHEEL CONCEPTS

1 HYPOTHESIS:

Standard orientable powered wheels are better than Mecanum wheels from an operational perspective for a rectangular mobile platform with four wheels for mobile manipulation applications in a cluttered indoor setting.

2 INTRODUCTION:

Wheeled Mobile Robots (WMRs) are a class of mechanical systems which have wheels for their mobility and possess some autonomous behavior. The research in this area is widely sought after for decades due to its application in various areas like manufacturing, service robotics, defense, space research, nuclear plants, locomotion, and reconnaissance (Pastore et al., 1999).

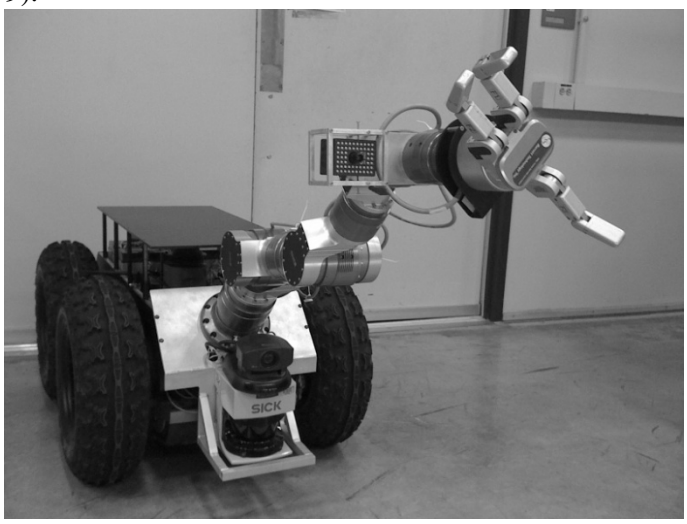

Fig. A.1: The Mobile Manipulation System at RRG

One of the emerging application areas of WMRs is Mobile Manipulation. A typical mobile manipulation system consists of one or more manipulators mounted on a WMR as shown in Fig. A.1 (http://www.robotics.utexas.edu/rrg/research/mobilemp/). It offers

many advantages over a fixed base manipulator due to added dexterity and potentially infinite workspace. However it has non-linear properties due to rolling and skidding (Campion et al., 1996) adding significant uncertainty to control algorithms. A solution to this problem is making the WMR omnidirectional. Omnidirectional capability is also useful for working in a cluttered and narrow space.

There are various ways in which we can provide omnidirectional capability. One is to design innovative omnidirectional wheels which will allow you to move in any direction (Byun et al., 2003; Pin and Mori, 1994; Borenstein and Evans, 1997; West and Asada, 1992). Another way is to use a standard wheel with two actuators, one for driving and the other for steering (Yi and Kim, 2002; Campion et al., 1996). These designs are dealt in some detail in the Sections 3 and 4.

Thus we have two different mainstream approaches; one of them uses innovative design while the other uses conventional design with standard parts. The question that arises is "*is the innovation for omnidirectional wheels justified when the alternative solution with all standardized parts already exists?*"

This paper will study the two approaches of design in detail and compare them from operational perspective. The rest of paper is organized as follows. The omnidirectional wheel and standard wheel mechanisms will be discussed. For comparison, the scope will be defined. Based on the scope, the important criteria will be arrived at. The evaluation of the alternative designs will be done based on the criteria which will be summarized in a metric analysis. The analysis will then be used to make the decision on the better suitability of the solutions for the defined scope. At the end, the important findings will be summarized along with a conclusion.

3 OMNIDIRECTIONAL WHEEL MECHANISMS:

A typical design of an omnidirectional wheel has the ability to actively move in rotational direction while it is unconstrained in the direction normal to the plane of the wheel. These designs are sought after because they are intuitive, they require minimum actuation and thus are easy to control (Ferriere, et al. 1996).

One of the most widely used designs is called a Mecanum wheel (Byun, et al., 2003). This wheel was invented in 1973 by Bengt Ilon from Mecanum AB, a Swedish company. It has a circular wheel with rollers placed at an angle circumferentially as shown in Figure A.2.

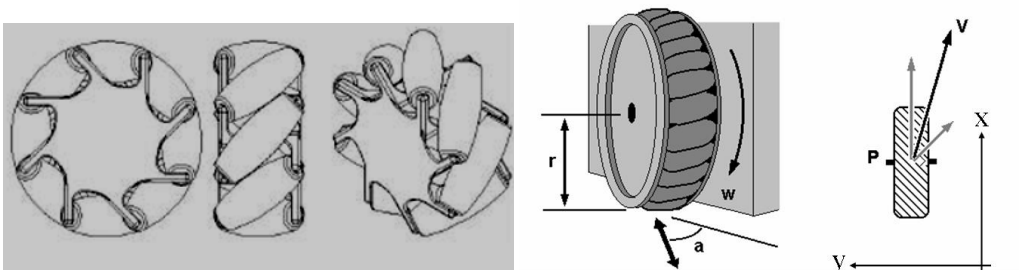

Fig. A.2: An illustrative Mecanum wheel

Typically the rollers are passively driven and transmit a portion of the force applied in the rotational direction to the normal direction of wheel's forward travel. The combination of the forces from all wheels results in a direction of force which moves the platform in that direction. The initial designs had problems such as having a gap in the two successive rollers which caused noise and vibration, inability to negotiate uneven surfaces, inefficiency due to the fact that the rollers transmit a portion of force in normal direction, all of which have been alleviated to some extent by subsequent efforts (Byun et al., 2003; , Diegel et al., 2002).

STANDARD WHEEL WITH ORIENTATION CAPABILITY:

To date many efforts have been done to achieve the omnidirectional capability with many conventional wheels (Yi and Kim, 2003; Campion et al. 1996). Conventional wheel

designs have been researched and improved for years now and it is a proven efficient and safe way for mobility. The omnidirectional design has the wheels driven and steered so that they are able to move in any direction by orienting themselves in that direction. The set of such wheels on a wheeled mobile robot should allow the platform to move in any direction. Figures 3-a and 3-b illustrate the concept.

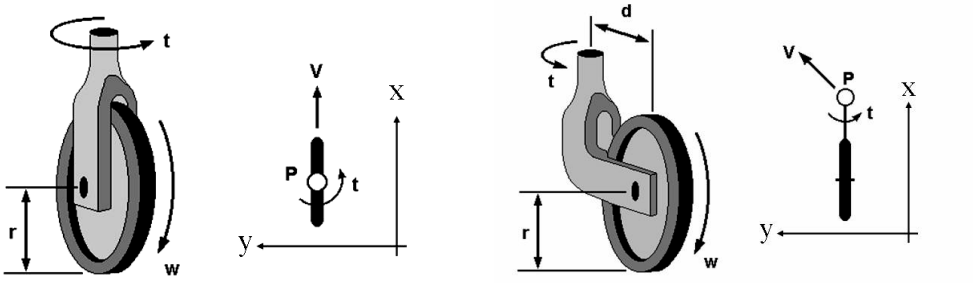

Figure 3-a: Centered orientable wheel *le (caster) wheel*

Note that there are two possible wheel configurations for such mechanism. The first has the wheel centered with respect to the orientation axis (Figure 3-a) [8]. The other design has the wheel placed offset from the orientation axis (Figure 3-b) [Campion et al., 1996]. The two designs differ from kinematics point of view as discussed in Section 7.1.

4 SCOPE OF THE COMPARISON:

For the comparison it is important that we define the context which is discussed here.

1. **The Platform**: The mobile platform being analyzed here will be a four wheeled platform with a rectangular shaped base for enhanced stability. 2. **Environment**: We intend to use this platform in an indoor setting which is cluttered like a manufacturing facility or a nuclear facility. The indoor space is assumed rigid, planar. The floor will have some small bumps due to door sills or electrical wirings. 3. **Task**: One of the important application areas of mobile manipulator is in the area of decontamination and decommissioning. For this application, the task we would aim at is to open a door given its location with respect to the system's current position or absolute position with respect

to an already defined inertial reference frame. 4. **The Control**: We assume that we would open the door using coordinated motion of both the WMR and the manipulator. 5. **Wheel Designs**: For the comparison we will restrict to the Mecanum wheel design as an omniwheel, as it is the most widely used design. In the standard wheel category, we would use caster wheel as it is most general case. 6. **Material**: The wheels are assumed to be made up of polyurethane which is the most widely used material for commercially available Mecanum wheels and casters.

5 CRITERIA SELECTION AND RANKING: One of the important steps in a comparison is to define parameters on which the alternative solutions are to be evaluated [13]. In our case, the desired configuration and the task to be accomplished dictate clearly the requirement of the system. They are listed below.

5.1 Omnidirectional capability: The capability of robot to navigate through a cluttered environment is enhanced greatly with omnidirectional tasks. For the given task of door opening and to do a coordinated motion, omnidirectional capability is vitally important.

5.2 Load capacity: The mobile robot in question has to carry the power source required to drive everything onboard. It has to carry the manipulator, the sensory suit for mobile robot and the manipulator, onboard computer and communication device. So there is already an overhead on its payload capacity. For doing manipulation and mobility tasks it needs additional payload.

5.3 Ability to negotiate bumps: In an indoor setup, which has comparatively planar floor, there still are obstacles in the form of bumps due to door sills or electrical cables.

5.4 Efficiency: The onboard power source needs to power all systems onboard. The power source is limited, thus the energy efficiency is important.

5.5 Accuracy: The accuracy of the WMR is also an important factor though very accurate WMRs would add to cost. Also if we have very good external sensing, we can compensate for accuracy limitations.

5.6 Sensory capability: The ability of the platform to integrate good sensing is a key to be able to perform the highly demanding coordinated task of door opening.

5.7 Controllability: For an efficient handling of the system, it is beneficial if the system is designed such that it is responsive to commands.

5.8 Singularity: Singularity reduces the degree of freedom of the systems.

5.9 Re-configurability: Re-configurability is important for effective flexible automation. Though lack of it doesn't necessarily stop you from doing the task the system is designed for, having re-configurability makes the system useful in many other tasks making the design more viable.

5.10 Operation speed: The normal speed of operation is important in a large setup like a nuclear power plant. Faster systems will be more efficient and may help reduce the number of systems required thereby reducing the overall cost.

5.11 Control loop speed: Speed of control loop is a key to a good performance because with high speed of the loop the inaccuracies of WMR can be compensated by the manipulator during the prehensile door opening operation.

5.12 Cost: The overall cost involved for the operation includes many costs. It is a key factor in the success or failures of many designs.

5.13 Reliability: An important criterion for evaluation of success of a design is its reliability. We want the design to perform normally with minimum interruptions.

5.14 Maintainability: In the event the design fails, we want the system to be easily maintainable so that there is a minimum downtime and required skilled labor.

5.15 Manufacturability: The design should be easy to manufacture.

For comparison, the criteria are ranked as follows:

1 The criteria are given weights based on their importance for successful completion of the task (of door opening) in particular and for the mobile manipulation system in general

2 The evaluation of designs are done as follows:

a. If the two designs perform equally on a criterion, they are scored 1 each.

b. If design 'A' proves to be inferior to 'B' (for instance) for the same size but can match the performance with increased size or modification of design parameters, A is scored as 0.5 and B as 1.

c. If 'A' proves to be inferior to 'B' and it can not perform equivalently even with increased size or other design parameters, 'A' is scored as 0.25 and B as 1.

d. If 'A' lacks completely on a criterion, it is scored 0.

6 DESIGN EVALUATION

This section will compare the designs based on each criterion at a time. A detailed treatment is given to criteria that need some discussion in this Section first. The design evaluation based on rest of the criteria is summarized in Table 2.1. The overall comparison is also tabulated concisely in Table 2.1.

7.1 Omnidirectional capability: To evaluate omnidirectional capability, we would summarize the notable work by Campion et al. (1996). The robot position can be described by x, y, θ as shown in the Figure 5. We define a vector ξ and a rotation matrix R(θ) such that,

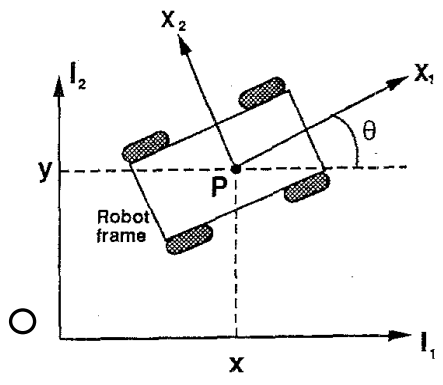

Figure 5: The Robot Position

$$\xi = \begin{pmatrix} x \\ y \\ \theta \end{pmatrix} \quad \& \quad R(\theta) = \begin{pmatrix} \cos\theta & \sin\theta & 0 \\ -\sin\theta & \cos\theta & 0 \\ 0 & 0 & 1 \end{pmatrix}$$

(1) The paper identifies four different types of wheel configurations; a fixed conventional wheel, a centered conventional wheel, an

offcentered conventional wheel (caster wheel) and a Swedish wheel. Of our interest are the later three configurations. Under ideal conditions a conventional wheel is constrained by no slipping (velocity of point of contact with ground is zero) and no skidding (velocity in the direction of wheel axis is zero). While a Swedish wheel is constrained only in the rolling direction. These constraints are formulated as below.

- *Centered conventional wheel*

As shown in Figure 6, a centered conventional wheel is described by constants l, α *and* r *(wheel radius)* and variables $\varphi(t)$ and $\beta(t)$. Thus the constraints are defined as:

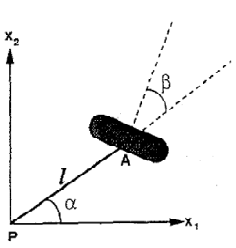

Figure 6: centered wheel

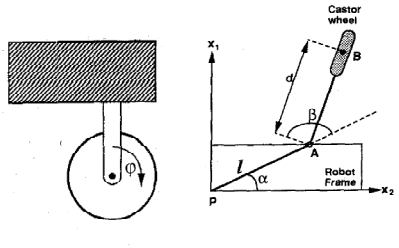

Figure 7: Caster wheel

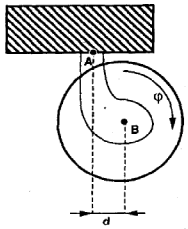

Figure 8: Swedish Wheel

$$\left[-\sin(\alpha+\beta)\ \cos(\alpha+\beta)\ l\cos\beta\right] R(\theta)\dot{\xi} + r\,\dot{j} = 0 \tag{2}$$

$$\left[\cos(\alpha+\beta)\ \sin(\alpha+\beta)\ l\sin\beta\right] R(\theta)\dot{\xi} = 0 \tag{3}$$

- *Offcentered conventional wheel (caster wheel)*

As shown in Figure 7, a caster wheel is described by constants l, α, r and d and variables $\varphi(t)$ and $\beta(t)$. Thus the constraints are defined as:

$$\left[-\sin(\alpha+\beta)\ \cos(\alpha+\beta)\ l\cos\beta\right] R(\theta)\dot{\xi} + r\,\dot{j} = 0 \tag{4}$$

$$\left[\cos(\alpha+\beta)\sin(\alpha+\beta)\,d + l\sin\beta\right] R(\theta)\dot{\xi} + d\dot{\beta} = 0 \tag{5}$$

- *Swedish wheel*

The Swedish wheel is described by l, α, r, β and variable γ which is the direction of the zero component of velocity with respect to the wheel plane. Thus the constraint is defined as:

$$\left[-\sin(\alpha+\beta+\gamma)\cos(\alpha+\beta+\gamma)\, l\cos(\beta+\gamma)\right] R(\theta)\dot{\xi} + r\cos\gamma\, \dot{j} = 0 \tag{6}$$

With these constraints defined, a general 'N' wheeled mobile robot with any combination of four types of wheel is denoted as $N = N_f + N_c + N_{oc} + N_{sw}$. It is fully described by vectors of posture coordinates $\xi(t)$ (from (1)), angular coordinates $\beta_c(t)$ (for centered wheel) and $\beta_{oc}(t)$ (for caster wheel), and rotational coordinates $\varphi(t)$.

Thus the general constraint equations can be written as:

$$J_1(\beta_c, \beta_{oc})R(\theta)\dot{\xi} + J_2\,\dot{j} = 0 \tag{7}$$

$$C_1(\beta_c, \beta_{oc})R(\theta)\dot{\xi} + C_2\,\dot{\beta}_{oc} = 0. \tag{8}$$

Where,

$$J_1(\beta_c, \beta_{oc}) \equiv \begin{pmatrix} J_{1f} \\ J_{1c}(\beta_c) \\ J_{1oc}(\beta_{oc}) \\ J_{1sw} \end{pmatrix},\ C_1(\beta_c, \beta_{oc}) \equiv \begin{pmatrix} C_{1f} \\ C_{1c}(\beta_c) \\ C_{1oc}(\beta_{oc}) \end{pmatrix} \text{ and } C_2 \equiv \begin{pmatrix} 0 \\ 0 \\ C_{2oc} \end{pmatrix}$$

From (8) the constraints for N_c and N_f are written separately as,

$$C_{1f}R(\theta)\dot{\xi} = 0, \qquad C_{1c}(\beta_c)R(\theta)\dot{\xi} = 0 \quad \text{and} \quad C_1^*(\beta_c) \equiv \begin{pmatrix} C_{1f} \\ C_{1c}(\beta_c) \end{pmatrix} \tag{9, 10 and 11}$$

Thus R(θ) belongs to the null space of C1*(βc).

Hence the degree of mobility is defined as

$$\delta_m = 3 - rank\left[C_1^*(\beta_c)\right]. \tag{12}$$

This clearly tells us that if there are no conventional fixed or centered wheels the degree of mobility of the robot is 3 which is a true omnidirectional case.

Thus both the designs are truly omnidirectional as long as the standard wheel is offcentered. From omnidirectional capability aspect, the two designs are equivalent.

Another parameter called degree of steerability is defined as:

$$\delta_s = rank\left[C_{1c}(\beta_c)\right]. \tag{13}$$

Physically it means the steering capacity of the robot which is denoted by the number of centered wheels that are steered independently. Thus the degree of freedom of a robot with all centered wheels is = δm + δs which is more than 3.

Thus an omnidirectional behavior can be achieved by using even a centered wheel mechanism.

7.2 Load Bearing Capacity: The load bearing capacity in a standard wheel is dependent on the wheel size (the radius) while for a Mecanum wheel it is dictated by roller size.

Ideally the contact between the wheel and floor is assumed to be a point or a line depending on the geometry. However in practice there develops a contact area which according to Hertz's theory is an ellipse (Dukkapati, 2000). Based on Hertz's theory, the load bearing capacity is calculated as following:

The size of ellipse is calculated as:

$$a = m\left[3\pi N(K_1 + K_2)/4K_3\right]^{1/3} \text{ and } b = n\left[3\pi N(K_1 + K_2)/4K_3\right]^{1/3} \tag{14}$$

Where N is the total normal force and

$$K_1 = \frac{1 - \nu_w^2}{\pi E_w}\ ,\ K_2 = \frac{1 - \nu_g^2}{\pi E_g} \text{ and } K_3 = \frac{1}{2}\left[\frac{1}{R_1} + \frac{1}{R_1'} + \frac{1}{R_2} + \frac{1}{R_2'}\right] \tag{15}$$

Where, R1 = Wheel rolling radius at point of contact (or roller),

R1' = Transverse radius of curvature for wheel (or roller),

R2 = Rolling radius for floor at point of contact (in our case, ∞),

R2' = Transverse radius of curvature for floor (in our case, ∞),

ν_w, ν_g = Poisson's ratio for the wheel and floor, respectively,

E_w, E_g = Young's modulus for wheel and floor, respectively,

m, n are calculated from table (Waterman and Ashby, 1997) based on value of θ where,

$\theta = \cos^{-1}(K4/K3)$ where,

$$K_4 = \frac{1}{2}\left[\left[\frac{1}{R_1}+\frac{1}{R_1'}\right]^2+\left[\frac{1}{R_2}+\frac{1}{R_2'}\right]^2+2\left[\frac{1}{R_1}-\frac{1}{R_1'}\right]\left[\frac{1}{R_2}-\frac{1}{R_2'}\right]cos2\psi\right]^{1/2} \quad (16)$$

Maximum normal stress is given as

$$\sigma_z = \frac{3}{2}\left[\frac{N}{\pi ab}\right] \quad (17)$$

Thus we can find out the maximum load that is within the strength of the material being used.

Polyurethane is the widely used material for the wheels; the material properties are,

Yield strength = 25 MPA, Young's modulus = 0.7 GPA, Poisson's ratio = 0.42

Assuming the wheel radius as 0.1 mm and roller radius as 0.01 m, the ratio of load capacity of standard wheel to a Mecanum wheel is calculated as 96.83.

Thus the standard wheel is better than Mecanum wheel for load capacity.

Note that as long as wheel radius is larger than roller radius, for same material this is always true.

7.3 Ability to negotiate bumps

In order to compare the designs on this criterion we will calculate the maximum bumps

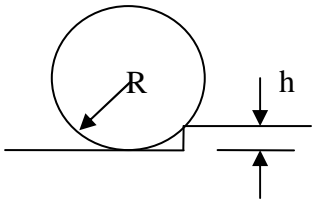

Figure 9 a: A step parallel to wheel axis

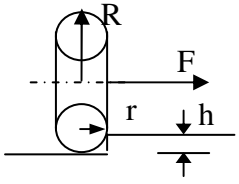

Figure 9 b: A step parallel to roller axis

that can be negotiated by the wheels.

For a standard wheel the bump is modeled as a step as shown in the Figure 9 a. According to European Federation of Handling Industry, the bump should

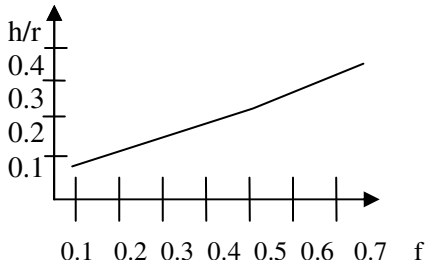

Figure 10: Maximum value of h/r for h/R = 0.06

be smaller than 6 percent of the wheel radius, thus h / R = 0.06 is the limiting value. For a Mecanum wheel however there are two scenarios, as described in Figure 9-a and 9- b. In the second scenario the bump is negotiable if the force F is high enough and the roller does not slide back. Thus the condition depends on roller diameter as well as friction coefficient. Figure 10 (reproduced from Dukkapati, 2000) describes the relation. For an average friction coefficient of 0.5 the value of h/r is approximately 0.2. The ratio of wheel diameter to roller diameter is typically is 8-10 (Byun et al., 2003). Thus the ratio of h in first scenario (Figure 9-a) and that in the best of second scenario (Figure 9-b) is 2.5.

Thus the standard wheel is better than Mecanum wheel for negotiating bumps.

7.4 The Metric Analysis:

The summary of the comparison in Table 1 as follows.

Criteria	Weight	Mecanum Wheel	Standard wheel	Analysis
Omnidirectional Capability	10	1	1	As discussed in 6.1, the degree of mobility for an offcentered standard wheel and a Mecanum wheel is 3 i.e. they are omnidirectional. For a centered wheel, though it is not kinematically omnidirectional, with steering ability you have the required degrees of freedom (in the case of redundant actuation, DOF is greater than 3 in the input space)
Load Capacity	5	0.5	1	As discussed in Section 6.2 The ratio of Load Capacity of Standard wheel to

				Mecanum wheel is approximately 2.5.
Ability to Negotiate Bump	3	0.25	1	As discussed in Section 6.3, the ratio of maximum height of obstacle (bump) that is allowed in a standard wheel to that of a Mecanum wheel is 3.64.
Efficiency	3	0.5	1	Mecanum wheel translates a component of force exerted in radial direction to normal direction. There is loss of energy due to that in addition to the losses due to slippage like standard wheel. Thus the efficiency of Mecanum wheel is less than the standard wheel.
Singularity	6	1	1	The Mecanum wheel design is singular free by nature as long as the axis of rollers is at some angle to axis of wheel. The standard wheel configurations are singular free as well.
Accuracy	8	0.25	1	Mecanum wheels cause slippage due the passive rollers, which causes loss of accuracy.
Controllability	7	1	1	One of the major benefits according to research community for choosing a Mecanum wheel (or an omnidirectional wheel) design is the minimum

				actuation requirement. Extra degrees of freedom due to redundancy and less slippage in the case of standard wheel result in more choices for enhanced control.
Sensory Capability	8	0.5	1	Mecanum wheels cause slippage due the passive rollers. Most of the onboard sensors are based on odometry which cause errors due to slippage.
Control Loop Speed	5	0.5	1	The simplicity of criteria in standard wheel configuration yields higher speed of control loops.
Re-configurability	8	0.25	1	Due to standardization, the re-configurability aspect of the conventional wheel design is greatly enhanced. With a careful design of the WMR it is entirely possible to change the configuration of a WMR with remarkable speed just like what you can do with a modular arm like PowerCube (http://www.amtec-robotics.com/robotersysteme_en.html)
Operation Speed	6	0.5	1	Mecanum wheel cause uneven ride due to intermittent roller contact and slippage due to their passive rolling.

				Thus their speed has to be low for a smoother operation.
Cost	6	0.5	1	Standardization reduces cost due to mass production, lower cost of replacement parts and lower cost of labor.
Reliability	8	0.5	1	Reliability is better due to standardized and well designed parts. Performance maps help predict the reliability better.
Maintainability	5	0.5	1	Condition based maintenance can be used to better the maintainability. Also the highly certified electromechanical actuators make maintenance easier. Standardized parts are easier to replace.
Manufacturability	6	0.5	1	Standards parts can be mass produced due to their wide applicability.
Total = weight * score		**53.75**	**92**	

7.5 CALCULATING THE BETTER DESIGN

From the comparison chart, it is clear that the standardized design with a conventional wheel is better than Mecanum wheel.

8 SUMMARY

The goal of this paper was to evaluate the two basic drive wheel designs viz. the Mecanum wheel design and the standard orientable wheel design. For comparison the scope was identified and a set of important criteria was defined. A systematic study based on those criteria showed that the standard wheel design has advantages over Mecanum

wheel design due to their simplicity, higher load capacity and standardization. The standardized design is further beneficial due to the fact that it is highly reconfigurable. Hence the hypothesis is proved.

REFERENCES

Alexander, J., and Maddocks, J, 1989, "On the kinematics of wheeled mobile robots," The International Journal of Robotics Research, v 8, n 5, pp. 15–27

Alleivi, L., 1895, Cinematica Della Biella Piana, Gianni, Naples

Ambike, S., and Schmiedeler, J, 2008, "A methodology for implementing the curvature theory approach to path tracking with planar robots," Mechanism and Machine Theory 43, pp. 1225–1235

Beggs J., 1983, *Kinematics*, Hemisphere

Borenstein J., 1995, "Control and Kinematic Design of Multi-Degree-of-Freedom Mobile Robots with Compliant Linkage", IEEE Transactions on Robotics and Automation, vol. 11(1), pp. 21-35

Borenstein, J., and Evans, J., 1997, "The OmniMate Mobile Robot –Design, Implementation, and Experimental Results", Proc. of Inter. Conf. on Robotics and Automation, pp. 3505-3510

Bottema, O, 1961, "Some Remarks on Theoretical Kinematics I. On Instantaneous Invariants," Proc. Of the Int. Conf. Teachers of Mechanisms p. 159-164

Bottema, O., and Roth, B., 1979, *Theoretical Kinematics*, North Holland Publishing Company, Amsterdam, 1979

Byun, K., and Song, J., April 2003, "Design and Construction of Continuous Alternate Wheels for an Omnidirectional Mobile Robot" Journal of Robotic Systems 20(9), pp. 569–579

Campion, G., Bastin, G., and D'Andrea-Novel, B., 1996, "Structural properties and classification of kinematic and dynamic models of wheeled mobile robots," IEEE Trans Robotics Automation 12(1), pp. 47–62,

Cowie, A., 1961, *Kinematics and Design of Mechanisms*, International Textbook Company

Chakraborty N., and Ghosal, A., 2004, "Kinematics of wheeled mobile robots on uneven terrain," Mechanism and Machine Theory 39 pp. 1273–1287

Chung, J., Yi, B., Kim, W., and Han, S., 2008, "Singularity-Free Dynamic Modeling Including Wheel Dynamics for an Omni-Directional Mobile Robot with Three Caster Wheels," International Journal of Control, Automation, and Systems, 6, (1), pp. 86-100

Denavit, J., and Hartenberg, R., 1955, "A Kinematic Notation for Lower Pair Mechanisms Based on Matrices," J. Applied Mechanics, vol. 22, pp. 139-144

Diegel, O., Badve, A., Bright, G., Potgieter, J., and Tlale, S., 2002, "Improved Mecanum Wheel Design for Omni-directional Robots", Proc. Australian Conference on Robotics and Automation, PP 117-121

Farin, G., 2002, Curves and Surfaces for CAGD: A Practical Guide, Morgan-Kaufman, 5th edition.

Ferriere, L., Raucent, B. and, Campion G., 1996, "Design of Omnimobile Robot Wheels", Proc. of International Conference on Robotics and Automation, pp 3664-3670

Freeman, R., and Tesar, D., 1988, "Dynamic modeling of serial and parallel mechanisms/ robotic systems, Part I-Methodology, Part II Applications," Proc. of the 20th Conf. ASME Biennial Mechanism, pp. 7-27

Gallardo-Alvarado, J., and Rico-Martínez, J., 2001, "Jerk influence coefficients, via screw theory, of closed chains," Meccanica 36 (2), pp. 213–228

Gracia, L. and Tornero, J., 2008, "Kinematic models and isotropy analysis of wheeled mobile robots," Robotica, v 26, pp. 587-599

Goehler, C., Stanisic, M., and Perez, V, 2004 "A Generalized Parameterization of T1 Motion and its Application to the Synthesis of Planar Mechanisms," Mechanism and Machine Theory, 39, pp. 1223-1244

Halftrack Vehicle Picture from Wikimedia Commons**:** http://en.wikipedia.org/wiki/File:Halftrack_Cromer_Mai_1993.JPG

Hirschhorn, J., 1962, Kinematics and Design of Plane Mechanisms, McGraw-Hill Book Company

Holmberg, R., and Khatib, O., 2000, "Development and control of a holonomic mobile robot for mobile manipulation tasks," Intl. J. Robotics Research, 19(11):1066-1074

Hong, J., 2002, "Method and device for estimating a friction coefficient between a tire and a road surface," US Patent No. 6601435

Jazar, R., 2008, *Vehicle Dynamics Theory and Application*, Springer 1st edition

Kapoor, C, and Tesar, D, 2006, "Integrated Teleoperation and Automation for Nuclear Facility Cleanup," J. Ind. Robot, 33 (6), pp. 469-484

Kumar, V. and Waldron, K., 1988 "Force distribution in closed kinematic chains", J. Robotics and Automation, Vol. 4(6), pp. 657-664

Kumar, V, and Gardner, J., 1989, "Kinematics of redundantly actuated closed chains," IEEE Transaction of Robotics and Automation, Vol. 6(2), pp.269-274

Lorenc, S., and Stanisic, M., and Hall, A., 1995 "Application of instantaneous invariants to the path tracking control problem of planar two degree-of-freedom systems: a singularity-free mapping of trajectory geometry," Mechanism and Machine Theory 30 (6) 883–896.

Li, Y., Zielinska, T., Ang, M, and Lin, W, 2006a, "Vehicle dynamics of redundant mobile robots with powered caster wheels,"

Li, Y., Zielinska, T., Ang, M, and Lin, W, 2006b, “Wheel-Ground Interaction Modelling and Torque Distribution for a Redundant Mobile Robot,” Proc. of IEEE Int. Conf. on Robotics and Automation, pp. 3362-3367

Low, K., and Leow, Y., 2005, “Kinematic modeling, mobility analysis and design of wheeled mobile robots,” Advanced Robotics, v 19, pp. 73–99

Low, K., Loh, W., Wang, H., and Angeles J, 2005, “Motion Study of an Omni-Directional Rover for Step Climbing,” Proc. of the IEEE International Conference on Robotics and Automation, pp. 1585-1590

Mandow, A., Martinez, J., Morales, J., Blanco, J.L., Garcia-Cerezo, A., and Gonzalez, J., 2007, "Experimental kinematics for wheeled skid-steer mobile robots," IEEE/RSJ International Conference on Intelligent Robots and Systems, pp.1222-1227

Martinez, J., and Duffy, J., 1998 “Determination of the acceleration center of a rigid body in spatial motion,” European Journal of Mechanics - A/Solids, Volume 17 (6), pp. 969-977

Mueller R., 1960, “Papers on Geometrical Theory of Motion,” translated by Tesar, D., et al., Special report No. 21 Kansas Engineering Experiment Station

Muir, P., and Newman, C., 1987, “Kinematic modeling of wheeled mobile robots,” J. Robotic Systems 4(2), pp. 281– 340

Myklebust, A., and Tesar, D., 1975, “The Analytical Synthesis of Complex Mechanisms for Combinations of Specified Geometric or Time Derivatives up to the Fourth Order,” Engineering for Industry, 96, pp. 714-722

Oetomo, D., and Ang, M., 2008, “Singularity-Free Joint Actuation in Omnidirectional Mobile Platforms with Powered Offset Caster Wheels,” Mechanical Design 130(5)

Oleska, S., and Tesar, D., 1971, “Multiply Separated Position Design of the Geared Five-Bar Function Generator,” Engineering for Industry, 92, pp. 74-84

Papadopoulos, E. and Poulakakis, J., “Planning and Model-Based Control for Mobile Manipulators,” Proceedings of IROS 2000 Conference on Intelligent Robots and Systems, Takamatsu, Japan.

Pennock, G., 2008, “Curvature Theory for a Two-Degree-of-Freedom Planar Linkage,” Mechanism and Machine Theory, 43, pp. 525-548

Pastore, T, Everett, H., and Bonner, K., April 1999, "Mobile Robots for Outdoor Security Applications," ANS 8th International Topical Meeting on Robotics and Remote Systems (ANS'99), Pittsburgh, PA,

Pin, F.G., and Mori, S., 1994, “A new family of Omni-directional and holonomic wheeled platforms for mobile robots”, IEEE Trans. on Robotics and Automation, 10(4): pp. 480-489.

Pholsiri, C. and Tesar, D., 2004, “Task-Based Decision Making and Control of Robotic

Manipulators," Ph. D. Dissertation, University of Texas at Austin.

Raheman, H., and Singh, R, 2004, "Steering forces on undriven tractor wheel," Journal of Terramechanics, 40 (2004), pp. 161–178

Reister, D., 1991, "A New Wheel Control System for the Omnidirectional HERMIES-III Robot", Proc. of the IEEE International Conference on Robotics and Automation, pp. 232-237

Ridley, P., Bokelberg, E., and Hunt, K., 1992, "Spatial Motion — II. Acceleration and the differential geometry of screws," Mechanism and Machine Theory 27, pp. 17–35.

Saha, S., and Angeles, J., "Kinematics and dynamics of a three-wheeled 2-dof AGV," Proc. of IEEE Int. Conf. on Robotics and Automation, Vol. 3, pp. 1572-1577, (1989)

Saha, K, Ángeles, J., and Darcovich, J, 1995, "The design of Kinematically Isotropic Rolling Robots with Omnidirectional Wheels," Mech. and Machine Theory, v 30, n 8, pp. 1127–1137

Soh, G., and McCarthy, J, 2008, "Parametric Design of a Spherical Eight-Bar Linkage based on a Spherical Parallel Manipulator," Mechanisms and Robots

Spragg, D., and Tesar, D., 1971, "Generalized Cycloidal Motion," Engineering for Industry, 92, pp. 131-139

Sreenivasan, S.V., and Nanua, P., 1999, "Kinematic geometry of wheeled vehicle systems," Mechanical Design, V (121:11), pp 50-56,

Tesar, D., 1967, "The generalized concept of three multiply separated positions in coplanar motions," Mechanisms, 2, pp. 461-474

Tesar, D., 1968, "The generalized concept of four multiply separated positions in coplanar motions," Mechanisms, 3, pp. 11-23

Tesar, D., and Anderson, H., 1968, "Generalized Cardon Motion," Engineering for Industry, 89, pp. 135-142

Tesar, D., and Sparks, J., 1968, "The generalized concept of five multiply separated positions in coplanar motions," Mechanisms, 3, pp. 25-33

Tesar, D., and Tosunoglu, S., 1992, *Robotics & Automation: An Introduction to Cams, Mechanisms and Robotics*, University of Texas at Austin.

Tisius, M., Pryor, M., Kapoor, C., and Tesar, D., 2009, "An Empirical Approach to Performance Criteria for Manipulation," accepted J. Mech. and Robots

Uicker, J., Pennock, G, and Shigley, J, 2003, Theory of Machines and Mechanisms, Oxford University Press

Veldkamp, G., 1963, Curvature Theory in Plane Kinematics, Groningen

Veldkamp, G., 1967, "Canonical Systems and Instantaneous Invariants in Spatial Kinematics," Mechanisms, pp. 329-388

Veldkamp G., 1969, "Acceleration axes and acceleration distribution in spatial motion," Engineering for. Industry, 89, pp. 147-151

Vidosic, J., and Tesar, D., 1967, "The Selection of Four-Bar Mechanisms Having Required Approximate Straight-Line Outputs-Part I: The General Ball-Burmester Point," Journal of Mechanisms, Vol. 2, pp. 23-44

Wang, D., Low, C., 2006, "Modeling Skidding and Slipping in Wheeled Mobile Robots: Control Design Perspective," International Conference on Intelligent Robots and Systems, pp. 1867-1872

Wang, L., Liu, J, and Xiao, Z., 1997, "Kinematic Differential Geometry of a Rigid Body in Spatial Motion - III. Distribution of characteristic lines in the moving body in spatial motion," Mechanism and Machine Theory, v 32, p 445-457

Waarsing, B., Nuttin, M., and Brussel, H., 2003, "Behaviour-based mobile manipulation: the opening of a door", Proc. 1st Inter. Workshop on Advances in Service Robotics, pp. 168-175

Waterman, N., and Ashby, M, 1997, "The Materials Selector", Chapman and Hall, Second

Edition, V 3

West, M, and Asada, H., 1992, "Design of Holonomic Omnidirectional Vehicle" Proc. of Inter. Conf. on Robotics and Automation, pp. 97-103

Williams, J., 1995, *Fundamentals of Applied Dynamics*, J. Wiley

Wong, J, 2001, *Theory of Ground Vehicles*, John Wiley and Sons, Inc., 3rd edition

Yi, B.-J., and Freeman, R., 1993, "Geometric analysis of antagonistic stiffness in redundantly actuated parallel mechanisms," J Robotic Systems v 10, pp. 581–603.

Yi, B. J., and Kim, W., 2002, "The Kinematics for Redundantly Actuated Omni-directional Mobile Robots," Robotic Systems 19(6), pp. 255–267

Yu, H., Spenko, M., and Dubowsky, S., September 2004, "Omni-Directional Mobility Using Active Split Offset Castors", Journal of Mechanical Design, 126 (5), pp. 822-829

Zaw, M., Oetomo, D., M.H.A. Jr. and Ng, T., 2003, "Kinematics and dynamics of an omni-directional mobile platform with powered caster wheels", Int. Symposium Dynamics and Control Hanoi, Vietnam, pp. 15-20

VITA

Amit Vijay Kulkarni was born in Beed, Maharashtra, India, to Vinaya Kulkarni and Vijay Kulkarni. He received his undergraduate degree (B.Engg.) in Mechanical Engineering from Jawaharlal Nehru Engineering College, Aurangabad, India and master's degree (M.Tech.) in Design Engineering from the Indian Institute of Technology, Delhi, India. During his master's studies he received the DAAD fellowship to pursue his master's thesis at the Technical University of Karlsruhe, Karlsruhe, Germany. Prior to his doctoral studies, he worked with Goodyear Tires and Siemens PLM Solutions in the area of Manufacturing and Software Development for about four years. During his doctoral studies, he interned at Idaho National Lab in Idaho Falls, Idaho.

Permanent Address: Vakil Colony
Kaij, District Beed, Maharashtra 431123
India

This dissertation was typed by Amit Vijay Kulkarni